

Rowan University

Rowan Digital Works

Theses and Dissertations

4-16-2019

Investigations of novel strategies to treat bacterial infection and development of new reaction methodology

Shane Philippi
Rowan University

Follow this and additional works at: <https://rdw.rowan.edu/etd>



Part of the [Pharmacy and Pharmaceutical Sciences Commons](#)

Recommended Citation

Philippi, Shane, "Investigations of novel strategies to treat bacterial infection and development of new reaction methodology" (2019). *Theses and Dissertations*. 2644.
<https://rdw.rowan.edu/etd/2644>

This Thesis is brought to you for free and open access by Rowan Digital Works. It has been accepted for inclusion in Theses and Dissertations by an authorized administrator of Rowan Digital Works. For more information, please contact graduateresearch@rowan.edu.

**INVESTIGATIONS OF NOVEL STRATEGIES TO TREAT BACTERIAL
INFECTION AND DEVELOPMENT OF NEW REACTION METHODOLOGY**

by

Shane Philippi

A Thesis

Submitted to the
Department of Chemistry and Biochemistry
College of Science and Mathematics
In partial fulfillment of the requirement
For the degree of
Master of Science in Pharmaceutical Sciences
at
Rowan University
February 12, 2019

Thesis Chair: Lark Perez

© 2019 Shane Vincent Philippi

Dedications

I dedicate this thesis to my mother and father for their continued support of my educational career. Without their love and support I would not have been able to complete my undergraduate or graduate programs. Every step of the way I had support to fall back on whenever I needed it.

I also dedicate this thesis to my fiancé Alyssa for being there for me each and every day and providing the unconditional support that I needed. She was always just as busy as me through her own graduate program but found the time to support my education.

Acknowledgments

I first would like to acknowledge Dr. Lark Perez for his support in the research laboratory over the last three years. He was an amazing mentor and made my learning experience exciting, comfortable, and extremely informative. Even before he took on this role in my education he served as a fantastic organic chemistry instructor and altered my course of education from initially finding physical chemistry the most interesting, to my eventual interest of organic chemistry coming to fruition.

I would also like to acknowledge the many members of the Perez Group for all of their contributions to my research career. Without their continuous positive attitude to learn new things or serve as a helping hand, my research would have not have been as successful.

Abstract

Shane Philippi

INVESTIGATIONS OF NOVEL STRATEGIES TO TREAT BACTERIAL
INFECTION AND DEVELOPMENT OF NEW REACTION METHODOLOGY

2018-2019

Lark Perez

Master of Science in Pharmaceutical Sciences

Quorum Sensing (QS), a form of bacteria communication mediated through chemical signaling, was investigated in the bacterial pathogen *Pseudomonas aeruginosa*. QS has the ability to regulate when a bacterial pathogen is infective or benign. LasR is the main regulator in this system and is also the receptor targeted for inhibition. A Structure Activity Relationship was produced for the system along with the binding pocket being explored.

A new reaction methodology was developed inspired by the Haloform reaction. The reaction was optimized based on solvent, stoichiometry, and conditions. Changing the initial electrophile and the reagent nucleophile created the scope of the reaction.

A series of molecules were prepared as Narrow Spectrum Antibiotics against both *Pseudomonas aeruginosa* and *Acinetobacter baumannii*. A Structure Activity Relationship was created for these molecules testing three key positions of the structure with steric and electronic changes. Optimization of the molecule leads to a potentially new lead compound in the series. Future directions for the molecule are discussed in order to further expand the SAR while also increasing stability of the molecules, and possibly reducing toxicity.

Table of Contents

Abstract	v
List of Figures	viii
List of Tables	x
Chapter 1A: Development of Agonist and Antagonist of LasR	1
Introduction to Quorum Sensing.....	1
Library Synthesis	3
Library Design and SAR.....	5
Conclusions.....	20
Chapter 1B: Experimental Data for LasR Discussion	21
General Experimental	21
Computational Modeling – Ligand Preparation	43
Protein Structure Preparation.....	44
Ligand Docking	44
Binding Energy Calculations and Decomposition Methods.....	44
Supplemental Figures.....	45
¹ H-NMR and ¹³ C-NMR Sepctra for all Final Compounds and Key Intermediates...48	
Chapter 2A: New Reaction Methodology.....	116
Introduction to New Reaction Development	116
Reaction Optimization	118
Conclusion	121
Chapter 2B: Experimental Data for New Reaction Methodology	122

Table of Contents (Continued)

General Experimental Data.....	122
¹ H-NMR and ¹³ C-NMR Sepctra for all Final Compounds and Key Intermediates ...	123
Chapter 3A: Narrow Spectrum Antibiotic Development.....	154
Introduction.....	154
Reaction Mechanism.....	154
Structure Activity Relationship.....	156
Biological Data Overview.....	159
Future Directions	163
Conclusions.....	163
Chapter 3B: Experimental Data for Narrow Spectrum Antibiotic Development	164
General Experimental	164
¹ H-NMR and ¹³ C-NMR Sepctra for all Final Compounds and Key Intermediates ...	165
Bioassay Procedure.....	225
References.....	227

List of Figures

Figure	Page
Figure 1. Top - the structures of the native agonist of the QS receptor	4
Figure 2. Computational binding contributions of individual amino acids in LasR.....	11
Figure 3. Key residues in LasR shown with 3 docked.....	12
Figure 4. The effect of amide bond orientation on activity of selected LasR ligands	16
Figure 5. Computational binding contributions of individual amino acids in LasR.....	17
Figure 6. Comparison of docking poses for LasR agonist 3 (panel A).....	18
Figure 7. The 3-pyridine analog is a LasR agonist	19
Figure 8. Hybrid analogs combining optimized structural features.....	19
Figure 9. Comparison of the crystal pose and the Glide XP docked pose of 3-	45
Figure 10. Correlation plot between the experimental binding free energy	46
Figure 11. Key Residues contributing to the binding energy for the 3 C ring analogs ...	47
Figure 12. The superimposed ligands 33 (red) and 39 (black) in the binding pockets....	48
Figure 13. Percent conversion was calculated based on H ¹ NMR.....	119
Figure 14. Scope of the Nucleophile.....	120
Figure 15. Scope of the Electrophile.....	120
Figure 16. Heterocycle Synthesis	121
Figure 17. Arrow pushing mechanism of this multicomponent coupling reaction.....	155
Figure 18. Scope of the ketone or aldehyde portion of the molecule	157
Figure 19. Scope of the hydrazine portion of the molecule	158
Figure 20. Scope of the hydrazine portion of the molecule	159
Figure 21. Bioassay data against <i>Acinetobacter baumannii</i> for Molecule 1.....	160

List of Figures (Continued)

Figure	Page
Figure 22. Bioassay data against <i>Acinetobacter baumannii</i> for Molecule 2.....	160
Figure 23. Bioassay data against <i>Acinetobacter baumannii</i> for Molecule 10.....	161
Figure 24. Bioassay data against <i>Acinetobacter baumannii</i> for Molecule 13.....	162

List of Tables

Table	Page
Table 1. Structure-activity relationships of “A-ring” analogs	7
Table 2. Calculated binding energies for “A-Ring” analogs	9
Table 3. Structure-activity relationships of “C-ring” analogs	14
Table 4. Optimization of the reaction changing stoichiometry and solvents.....	118

Chapter 1A

Development of Agonist and Antagonist of LasR

Introduction to Quorum Sensing

Due to the array of medically relevant cellular processes that are under the control of LuxR-type quorum sensing circuits, significant effort has been directed toward the identification of antagonist and agonist molecules in several different bacterial pathogens.¹⁻³ These efforts have led to the identification of antagonists and agonists of quorum sensing from natural sources,⁴ diversity-oriented compound libraries,^{5,6} and focused library synthesis.^{7,8} The most broadly explored class of LuxR-type receptor ligands are based on the structural features found in the native HSLs (e.g. **1**, **Figure 1**). The wealth of studies in this area, maintaining the homoserine lactone while changing the functionality of the acyl-tail is facilitated by ready synthesis of the HSL compound libraries. Together these investigations targeting the modulation of quorum sensing in Gram-negative bacteria have yielded numerous promising results and insightful structure activity relationships.^{9,10}

The inhibition of quorum sensing with small molecules offers a unique strategy for the treatment and prevention of a number of acute and chronic bacterial infections, a fact that is of particular significance given the rapid and ongoing spread of antimicrobial-resistant bacteria.^{2,11,12} Through the inhibition of quorum sensing, control over expression of virulence factors and biofilm formation is achieved, rendering the bacteria benign while not directly affecting viability. This anti-infective approach is conceptually distinct from traditional approaches for the treatment of bacterial infection that typically utilize bactericidal or bacteriostatic molecules, targeting critical cellular processes. As

exemplified by the spread of bacterial resistance, these treatments provide a considerable growth advantage to bacteria that can resist the drug. Contrasting this approach, the inhibition of quorum sensing does not affect cellular viability, decreasing the growth advantage of resistance.¹³ Rather, this approach targets cellular signaling, inhibiting the expression of virulence factors necessary for successful infection, rendering the bacteria benign until the hosts immune system can clear the pathogen.^{2,14-16}

Major challenges that remain in the development of an anti-quorum sensing strategy targeting the development of antagonists of LasR and other LuxR-type receptors is ligand potency and the complications of hydrolytic liability in HSL-based antagonists.¹⁷ Here we advance a strategy to overcome the limitation of inhibitor potency through the exploration of a novel, non-natural triaryl series of LasR quorum sensing ligands. Further, many of the analogs examined in this study are anticipated to overcome the limitations of the HSL-based agonists and antagonists by removing the physiologically labile homoserine lactone functionality.¹⁸

Recently a highly potent agonist of quorum-sensing in *P. aeruginosa* was identified from a high-throughput screen (**2**, **Figure 2**).⁵ While the activation of virulence factor expression in this bacterial pathogen is not therapeutically desirable our rationale to obtain the desired inhibitory function for this potent agonist through analog synthesis is based on precedent. Most notably, a large number of inhibitors have been discovered by systematic modification of HSLs, molecules which serve as natural QS activators. The agonist discovered (**2**) bears many structural and pharmacological properties that potentially make it superior to HSLs as a lead compound for the development of an anti-virulence therapy, including the absence of the metabolically labile homoserine lactone. Additionally, the potency of this molecule for activation of LasR is comparable to the

potency of the natural signaling molecule; however, compounds of this structure type have never been systematically analyzed for the effect of their structure-activity relationships (SARs).^{5,19} Here we describe the first systematic evaluation of the structure-activity relationships of this novel class of LasR QS modulators. Our studies reveal critical details of the activity profile of this new ligand class for LasR activity and using computational modeling we provide insight into the molecular interactions with LasR that contribute to agonist and antagonist activity.

Library Synthesis

Challenging our efforts toward the goal of identifying inhibitors of LasR based on the structure of **2** is the number of synthetic steps required for its assembly (Figure 1).¹⁹ Previous studies had described an eight step synthesis of **2**, however, to prepare a library of molecules related to **2** ideally required a more efficient synthetic route. Identification of an alternative scaffold to target for structure-activity relationship studies was informed by examination of the recently published crystal structure of the QS receptor in *P. aeruginosa*, LasR, in the presence of **2**.²⁰ Analysis of the binding pocket for the ligand suggested that a subtle structural change in the orientation of the amide bond in **2** (**Figure 1**, highlighted in blue) may be tolerated. Indeed, examination of the scaffold resulting from the inversion of the amide linker between the “B-ring” and “C-ring” (highlighted in red, **3**) more closely maps onto the orientation of this structure in the native LasR agonist, 3-oxo-C12HSL (**1**).

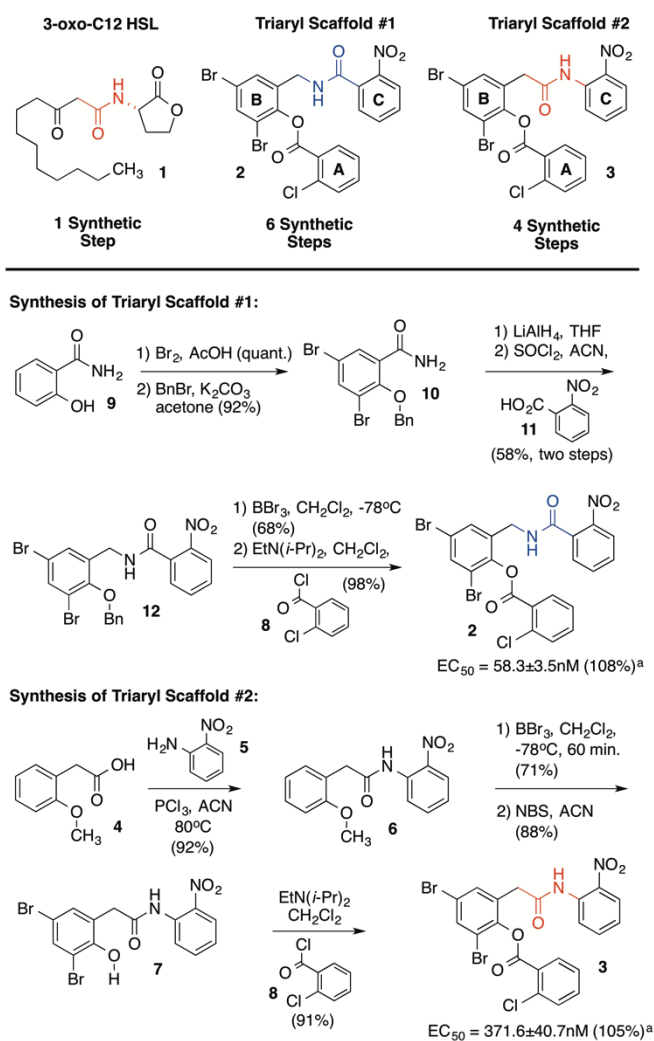


Figure 1. Top - the structures of the native agonist of the QS receptor, LasR, 3-oxo-C12HSL and the triaryl scaffolds evaluated as LasR agonists and antagonists in this study. Bottom; a description of the modular chemical synthesis pathways for library assembly.

Based on these target scaffolds, we have successfully identified two efficient and modular synthetic routes (Figure 1) to analogs containing the core scaffold as in **2** (Scaffold #1) analogs containing the core scaffold as in **3** (Scaffold #2). In our optimized six step synthesis of **2** and analogs of this structure, bromination and benzyl protection of salicylamide is followed by reduction of the amide and introduction of the “C-ring” through amidation with **11**. Final incorporation of the “A-ring” is achieved through

deprotection of the phenol and esterification with **8**. This route is modular, enabling ready diversification of the “A-ring” and “C-ring” of the ligand and proceeds in 35% yield overall from salicylamide. The synthesis of **3** and related analogs involves initial coupling of **4** and 2-nitro aniline (**5**). Deprotection of the phenol and bromination of the more electron rich “B-ring” proceeds smoothly to provide **7** which can be directly esterified with **8**. Overall, this route allows rapid diversification of the “A-ring” and “C-ring” of **3**, proceeding in four steps with 52% overall yield from **4**.

Library Design and SAR

Analysis of the crystal structure of LasR complexed to **2**²⁰ suggests that the two terminal aromatic rings (Figure 1, labeled “A” and “C”) play an important role by interacting with LasR whereas the central ring appears to play primarily a scaffolding role in ligand binding. Therefore, we have focused our initial efforts on identifying the structure activity correlations of the pendant ring structures (“A-ring” and “C-ring”) while maintaining the structure of the central ring (“B-ring”). Our strategy involved initial broad investigation of structure-activity relationships in the more readily synthesized ligand series (Scaffold #2, e.g. **3**) before returning to investigate key analogs prepared based on Scaffold #1. While the two scaffolds differ only in the orientation of one amide bond, we have observed some notable differences in biological activity for analogs prepared on the two different scaffolds.

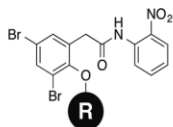
Our initial investigations of the structure activity relationships involved modulation of the structure of the “A-ring” in Scaffold #2. From this series of structural analogs, we observe a consistent dependence of substitution in this ring structure on the potency of the molecules (Table 1). We discovered that substitution in the *ortho*-position of the arene (entries 1, 4, 7, 9, 10, and 13-14) is critical for agonist activity. Interestingly,

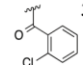
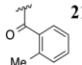
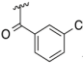
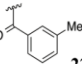
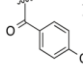
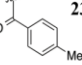
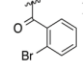
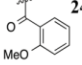
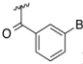
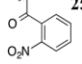
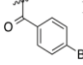
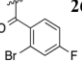
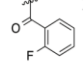
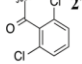
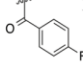
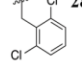
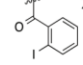
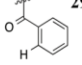
the activity of the analogs bearing *ortho*-substitution appears to be largely independent of the nature of the substituent. Analogs with electron-withdrawing substituents (halogen, nitro, trifluoromethyl) and electron-donating groups (methyl, methoxy) in the *ortho*-position all are agonists with EC₅₀ values between 2.4 and 15.8 μM. By contrast to substitution in the *ortho*-position of the “A-ring”, substitution in the *meta*- or *para*-position of the “A-ring” (entries 2-3, 5-7 and 11-12) leads to the complete loss of activity. In support of the significance of *ortho*-substitution, an analog was prepared containing chlorine atoms at both of the *ortho*-positions of the “A-ring” (entry 16) fully retains the activity of the mono-*ortho*-chloro LasR agonist **3**. We additionally find that the carbonyl of the ester is not significant for agonist activity as an analog removing this functionality, linking the “A-ring” through an ether linker (**28**, entry 17) retains full agonist activity.

Table 1

Structure-activity relationships of “A-ring” analogs.

EC₅₀ values are reported as the mean of triplicate analysis with the range defining the standard deviation. The native LasR agonist (**1**) was used as a control with an EC₅₀=72.9±24.6nM. ^b Maximal percent activation of GFP at 50 μM with respect to 3-oxo-C12 HSL (**1**) as a positive control for LasR agonism, set at 100% activation.



Entry	Structure	EC ₅₀ (μM) ^a	% Max ^b	Entry	Structure	EC ₅₀ (μM) ^a	% Max ^b
1	 3	0.372±0.041	105	10	 21	0.757±0.065	85
2	 13	>50.0	0	11	 22	>50.0	24
3	 14	>50.0	0	12	 23	>50.0	33
4	 15	0.271±0.022	82	13	 24	0.246±0.012	45
5	 16	>50.0	44	14	 25	0.489±1.28	37
6	 17	>50.0	35	15	 26	0.436±0.550	100
7	 18	1.29±0.598	76	16	 27	0.313±0.149	95
8	 19	>50.0	39	17	 28	0.161±0.101	56
9	 20	1.58±0.046	50	18	 29	>50.0	0

Generally we find that analogs with substituents in the *ortho*-position are potent agonists whereas the *meta*- or *para*-substituted analogs are universally not active. This may suggest that the binding pocket in LasR for this portion of the molecule is not able to accommodate substituents in either the *meta*- or *para*-position. Further, the comparable activities of the analogs containing electronically and sterically diverse substituents in the *ortho*-position suggests that this substitution does not have a direct role interacting with the receptor (no specific hydrogen-bonding or electronic interactions with the receptor) but rather may simply play an anchoring role for the overall positioning of the “A-ring”. In support of this hypothesis, analog **26**, containing an *ortho*-bromo substituent and a *para*-fluoro substituent is active as a LasR agonist (entry 15), while the analog containing the *para*-fluoro substituent alone is inactive (entry 8). Further supporting the significance of maintaining an *ortho*-substituent on the “A-ring” is the lack of agonist activity found in analog **29** (entry 18) that possesses an unsubstituted phenyl ring at this position.

The ligands that were inactive as agonists in this series were further evaluated as antagonists and were found to have no antagonist activity. This observation suggests that the presence of minimally one *ortho* substituent on the “A-ring” of ligands in this series is required for ligand binding to LasR in the cell.

To further investigate the strict requirement for the presence of an *ortho*-substituent on the “A-ring” for LasR agonist activity we performed computational binding studies using the Schrodinger Drug Discovery Suite. We were pleased to find that the MMGBSA scores (measure of binding affinity) from this computational binding

analysis for the full series of compounds in Table 1 was strongly correlated to the observed biological activity of the analogs with the *ortho*-substituted analogs showing the strongest binding and the unsubstituted phenyl “A-ring” analog (**29**) predicted to be a poor LasR ligand (Table 2).

Table 2

Calculated binding energies for “A-ring” analogs.

Average calculated binding energy of analogs **3**, **15**, **18**, **20**, **21**, **24** and **25**.^b Average calculated binding energy of analogs **13**, **16** and **22**.^c Average calculated binding energy of analogs **14**, **17**, **19** and **23**.^d MMGBSA is reported as the average binding energy with the error representing standard deviation.

	MMGBSA Binding Energy (kcal/mol)
Ortho-Substituted Analogs ^a	-87.12±20.87 ^d
Meta-Substituted Analogs ^b	-37.35±6.15 ^d
Para-Substituted Analogs ^c	-18.86±27.79 ^d
Unsubstituted Phenyl Analog 29	-11.05

Building on this result we computationally investigated the relative contributions for each of the amino acids within the LasR binding pocket that, in sum, contribute to the overall MMGBSA score for the compound. We hypothesized that this analysis may enable the identification of key residues in LasR that contribute to ligand binding rationalizing that the *meta*- and *para*- substituted “A-ring” analogs would lack these stabilizing interactions or would display destabilizing interactions. We identified several individual amino acids that showed variations in their extracted contribution to the computational binding energies (**Figure 2**).

Generally, amino acids residues proximal to the 2-nitro aniline “C-ring” of the analog, not varied in this series of analogs, displayed similar binding energies to each of the ligands, irrespective of the substitution pattern on the “A-ring”. For example, W60 and F101 (Figure 3, light blue) independently contribute stabilizing binding interactions to all of the analogs evaluated (**Figure 2**).

Some variations in the extracted binding energies are noted in the amino acid residues responsible for interactions with the amide linker between the “C-ring” and “B-ring” of the analogs. Amino acid residues which are highly conserved among soluble HSL-binding proteins, Y56 and D73 (**Figure 3**, yellow), display different patterns of binding between the analogs dependent on the substitution of the “A-ring”. While Y56 shows strongly stabilizing interactions with all analogs, by virtue of a hydrogen bond to the carbonyl oxygen of the linker amide, this stabilizing interaction appears to be slightly weakened in the binding of the *para*-substituted ligands (**Figure 2**). In contrast, the

interactions between the ligand and D73 are calculated to be generally low in energy with *ortho*- and *meta*-substituted analogs however becomes significantly destabilizing in interactions with ligands bearing a *para*-substituent in the “A-ring”. Apparently, substitution in the *para*-position of the distant “A-ring” is effectively propagated through the ligand to disrupt the hydrogen bonding interactions between LasR and the linker amide of the ligand.

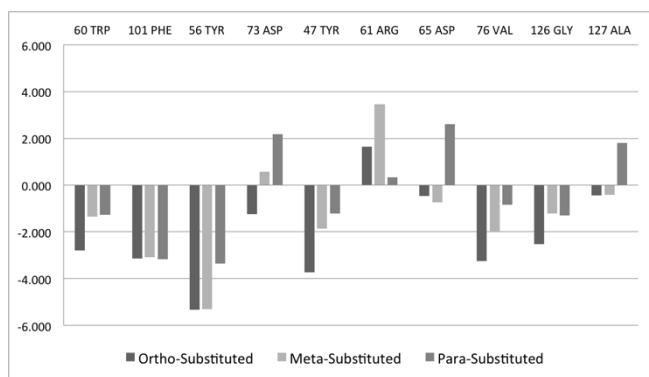


Figure 2. Computational binding contributions of individual amino acids in LasR, with the ligands in Table 1. Energies are described in kcal/mol.

Not surprisingly, a series of amino acids in the binding pocket proximal to the “A-ring” were found to be most significantly influenced by the structural changes investigated in this ligand series. While much of this large portion of the HSL binding pocket in LasR is hydrophobic, key amino acids displaying significant differences in binding to the structural variations in the “A-ring” include Y47, R61, D65, V76, G126 and A127 (Figure 3, magenta). Two primary trends are noted in the binding contribution of amino acids in this region of LasR. Firstly, in stabilizing interactions the *ortho*-substituted analogs show greater stabilization than *meta*- or *para*-substituted analogs.

This trend is exemplified in the binding contributions of Y47, V76 and G126 (Figure 2). Secondly, two residues show strong destabilizing interactions uniquely with the *para*-substituted analogs, D65 and A127 (Figure 3). These residues are located on opposing sides of the binding pocket possibly suggesting that a steric clash on one side of the ligand binding pocket pushes the ligand toward the opposing side of the binding pocket resulting in destabilizing interactions with these two spatially separated amino acids. Lastly, it should be noted that not all amino acids showed a preference for the *ortho*-substituted analogs. One residue analyzed, R61 shows significant destabilizing interactions with both *ortho*- and *meta*-substituted analogs that is alleviated in the *para*-substituted series of compounds.

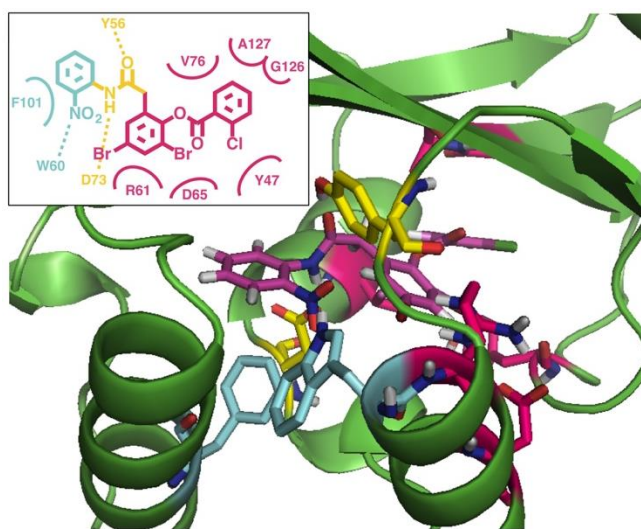


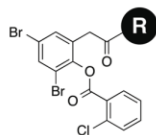
Figure 3. Key residues in LasR shown with 3 docked. W60 and F101 are shown in light blue, Y56 and D73 are shown in yellow and Y47, R61, D65, V76, G126 and A127 are shown in magenta. Inset: a schematic representation highlighting these amino acids in proximity to three regions of the ligand.

While most analogs that we have analyzed with changes in the structure of the “A-ring” were found to be either agonists or to have no activity, analogs with structural changes in the “C-ring” have both changes in potency and changes in function (agonism vs. antagonism). We first assessed the impact of the position of the nitro-substituent on the activity of the molecules (Table 3, entries 1-3), revealing the importance of an *ortho*-nitro substituent. We then prepared a series of analogs in which the *ortho*-nitro group on the “C-ring” of the parent compound (**3**) was exchanged for functionality that had been previously found to be a suitable bioisostere of an aromatic nitro group.²¹ While the 2-pyridine was observed to have no agonist activity (entry 4) the di-fluoro bioisostere was found to show enhanced activity as a LasR agonist (entry 5). Introducing additional electron-withdrawing substituents onto the ring (entry 6) had minimal effect on activity however, interestingly, the pyrimidine analog (entry 7) was found to be active as an agonist. Combining the 2-nitro substitution with a ring nitrogen at the 4-position (entry 8) also provided an agonist of comparable activity to the parent compound. Therefore, within the series of aromatic and hetero-aromatic analogs of this ring highest agonist activity was noted with the di-fluoro analog (entry 5) and the 2-pyridine and *meta*- and *para*-nitro analogs were found to be inactive. Based on published crystal-structure analysis from which the *ortho*-nitro ring serves the role of a mimic of the homoserine lactone characteristic of this class of signaling molecules having direct interactions with a conserved tryptophan (W60) in the LasR binding pocket. Accordingly, we replaced the 2-nitro aniline “C-ring” with a homoserine lactone (**37**). Notably, this analog displays significantly enhanced activity to **3** and the native LasR signaling agonist, 3-oxo-C12-HSL, with an EC₅₀ value of 0.9 nM (Entry 9).

Table 3

Structure-activity relationships of “C-ring” analogs.

EC₅₀ values are reported as the mean of triplicate analysis with the range defining the standard deviation. The native LasR agonist (**1**) was used as a control with an EC₅₀=72.9±24.6nM. ^b Maximal percent activation of GFP at 50 μM with respect to 3-oxo-C12 HSL (**1**) as a positive control for LasR agonism, set at 100% activation.



Entry	Structure	EC ₅₀ (μM) ^a	% Max ^b
1		0.372±0.041	105
2		<50.0	0
3		<50.0	0
4		<50.0	0
5		0.0456± 0.0038	116
6		0.335±0.194	89
7		0.601±0.464	92
8		0.446±0.257	112
9		0.000896± 0.0021	105

We next turned our attention to an evaluation of selected analogs identified as significant in our investigation of the SAR of Scaffold #2 as described in Tables 1 and 2. Accordingly we prepared a series of analogs based on Scaffold #1, maintaining the *ortho*-chloro substituent on the “A-ring” and incorporating three selected “C-ring” motifs. We selected the new 2-pyridine, di-fluoro and pyrimidine “C-ring” analogs for this analysis as these analogs displayed a range of agonist activities in our initial library. Therefore, we evaluated analogs **32**, **33**, **35** and **38-40** for both their agonist and antagonist activity in the LasR quorum sensing reporter strain (Figure 4). In our analysis, we found that 2-pyridine analog **32**, earlier observed to show no agonist activity against LasR (Table 3, entry 4) possessed potent antagonist activity with an IC₅₀ of 42μM. We additionally prepared this analog with the amide linker between the “B-ring” and the “C-ring” reversed and observed that this analog (**38**) had similarly high LasR antagonist activity (Figure 4). We next prepared an analog containing a reversed amide corresponding to the potent difluoro arene full LasR agonist **33** (Figure 4, EC₅₀ = 46nM). To our surprise, the analog containing the reversed amide as in Scaffold #1 (**39**) was not an agonist of LasR, instead it displayed a change in *function*, instead acting as a partial antagonist of LasR QS with an IC₅₀ of 65uM (80% maximal inhibition). In contrast to this finding, when we prepared the reversed amide analog of the weak agonist pyrimidine **34** (EC₅₀ = 0.6μM) we found the new analog (**40**) to similarly be a weak agonist of LasR with an EC₅₀ of 1.6 μM. Therefore, while in most cases we evaluated changing the orientation of the amide linker results in small (2-3 fold) changes in the potency of the analog, in certain cases simply reversing this amide linkage appears to result in a shift from LasR agonism to antagonism.

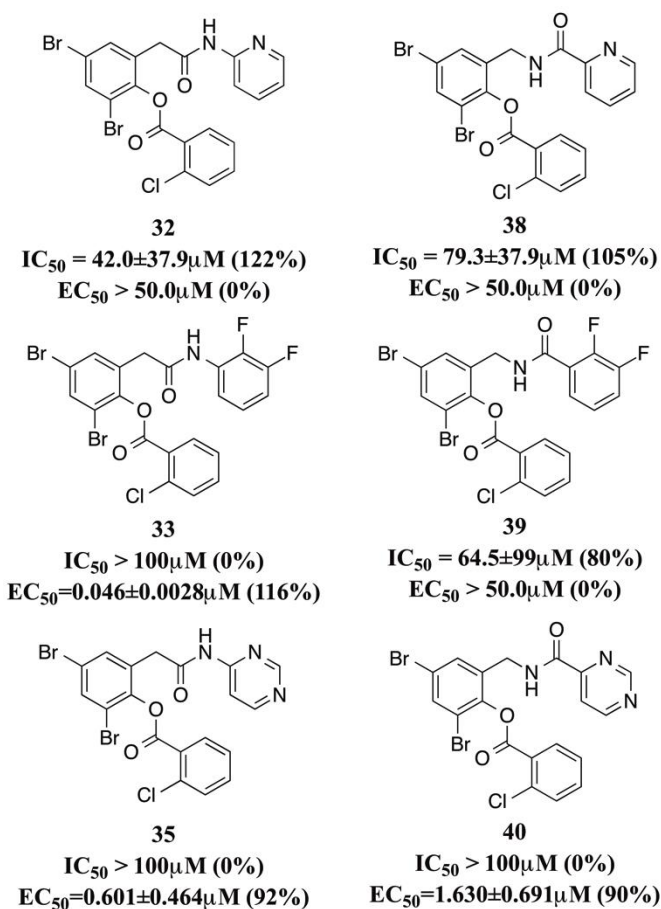


Figure 4. The effect of amide bond orientation on activity of selected LasR ligands. Bioassay and data fitting was performed according to the standard procedure. EC_{50} and IC_{50} values are reported as the mean of triplicate analysis with the range defining the standard deviation.

We turned to computational modeling in an effort to further investigate these observations. In contrast to the ligands in Table 1, where a clear binding preference was noted for *ortho*-substituted “A-ring” analogs based on MMGBSA scores, in this analysis the ligands shown in Figure 5 are universally predicted to have show comparable binding to LasR. As before, we therefore evaluated the independent contributions of amino acid residues within the LasR binding pocket (Figure 5). Importantly, all of the residues that are proximal to the “A-ring” and “B-ring”, which are unchanged in this series of ligands

show minimal changes in their binding energies (e.g. Y47, R61, D65, V76, G126 and A127, Figure 5). One significant change in binding energies at the individual amino acid level is noted and occurs with a residue predicted to be close to the “C-ring” of the ligand. The pyridine analog **32**, an antagonist, shows a stronger binding interaction with Y56 along with diminished binding to W60 when compared to **3** and **33**, two agonists. Evaluation of the docking poses for these ligands reveals a notable reorganization of the ligand which likely leads to the above changes in the binding energies for Y56 and W60 (Figure 6). In these poses there is a clear shift in protein binding involving rotation of the “C-ring” from interaction between the 2-nitro substituent of the agonist **3** with W60 (light blue, Figure 6A) to an interaction between the 2-pyridine of the antagonist **32** with Y56 (yellow, Figure 6B).

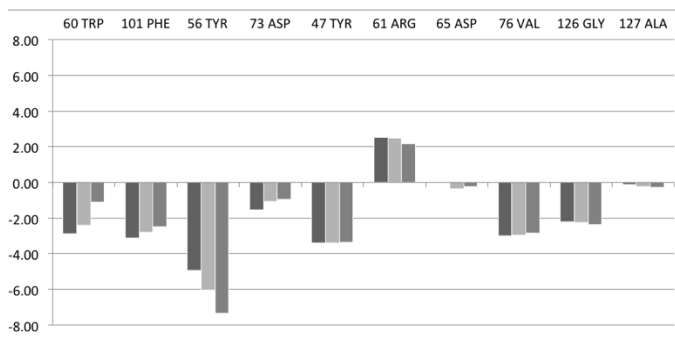


Figure 5. Computational binding contributions of individual amino acids in LasR, with agonist ligands **3** (dark grey) and **33** (light grey) and the antagonist ligand **32** (medium grey).

We hypothesized that this subtle change in protein binding may represent a novel trigger to shift LasR from an agonized to an antagonized state. To test this hypothesis we prepared an analog containing a 3-pyridine ring in lieu of the 2-pyridine ring contained in

the antagonist **32**. Due to the placement of the ring nitrogen, the pyridine should be prevented from interacting with Y56 and we hypothesized would therefore lose its antagonist activity. We accordingly evaluated **41** (**Figure 7**) and found this analog to show no antagonist activity, in striking contrast to the 2-pyridine antagonist (**32**), this analog acts as an agonist of LasR.

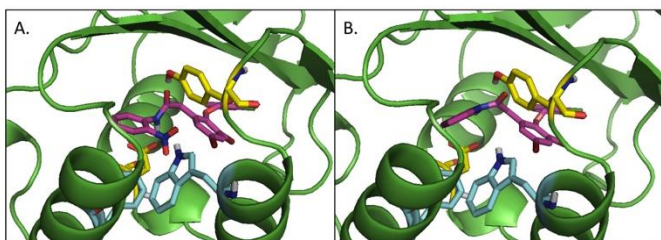


Figure 6. Comparison of the docking poses for LasR agonist **3** (panel A) and LasR antagonist **32** (panel B).

We had previously identified a novel series of potent maleimide containing LasR antagonists that act to irreversibly inhibit LasR through covalent modification of Cys79 in the LasR binding pocket.²² Structurally, the maleimide functionality we identified as being central to the LasR antagonist activity maps onto the “A-ring” of the current ligand series. Accordingly we investigated a series of hybrid analogs containing a 2-pyridine or a homoseriene lactone in the “C-ring” position and a pendant maleimide as the “A-ring” structure (Figure 9). Upon analysis of this series of compounds we found that all fully antagonized LasR, however with considerably different levels of activity (Figure 9). Analog **42**, combining the 2-pyridine “C-ring” with a pendant maleimide was found to be a weak antagonist of LasR. It appears that combining the two structural features we had identified to independently lead to LasR antagonism, through two distinct mechanisms of

interaction with LasR, do not work together in this ligand in an additive manner. Analogs **43** and **44** both containing a homoseriene lactone in place of the 2-nitro aniline “C-ring” display a striking dependence of activity on the linker length to the maleimide. Consistent with our previous studies for ligands containing this amide isomer²², the maleimide linker containing two methylene units (**44**) was more potent with an IC₅₀ of 23.8μM. This analog represents one of the most potent antagonists of LasR discovered, being comparable in activity to the most potent analogs we had previously identified.²²

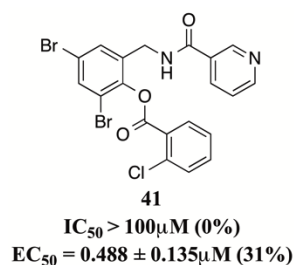


Figure 7. The 3-pyridine analog is a LasR agonist. Bioassay and data fitting was performed according to the standard procedure. EC₅₀ and IC₅₀ values are reported as the mean of triplicate analysis with the range defining the standard deviation.

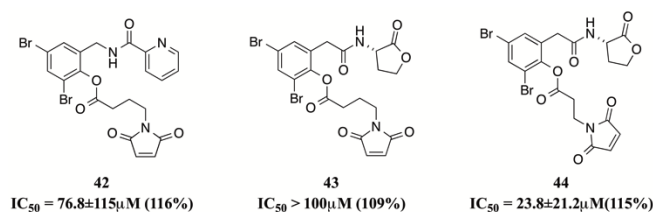


Figure 8. Hybrid analogs combining optimized structural features identified, which in this study with a maleimide for LasR irreversible inhibition. Bioassay and data fitting was performed according to the standard procedure. EC₅₀ and IC₅₀ values are reported as the mean of triplicate analysis with the range defining the standard deviation.

Conclusions

We have evaluated a series of synthetic libraries of non-natural modulators of LasR-mediated QS in *P. aeruginosa*. The compounds prepared are significant as they represent a novel drug-like scaffold for the preparation of inhibitors of bacterial virulence. We have identified several notable structure-activity relationships and in so doing have paved the way for the rational design of potent drug-like inhibitors of LasR QS. Using a combination of experimental and computational investigations, our studies have unveiled a new potential strategy for inducing LasR antagonism and have defined critical structural features of this novel ligand class for receptor binding.

Chapter 1B

Experimental Data for LasR Discussion

General Experimental

Unless otherwise noted, all reactions were performed in flame-dried glassware under an atmosphere of nitrogen or argon using dried reagents and solvents. All chemicals were purchased from commercial vendors and used without further purification. Anhydrous clean solvents were purchased from commercial vendors.

Flash chromatography was performed using standard grade silica gel 60 230-400 mesh from SORBENT Technologies or was performed using a Biotage Flash Purification system equipped with Biotage SNAP columns. All purifications were performed using gradients of mixtures of ethyl acetate and hexanes. Analytical thin-layer chromatography was carried out using Silica G TLC plates, 200 μm with UV₂₅₄ fluorescent indicator (SORBENT Technologies), and visualization was performed by staining and/or by absorbance of UV light.

NMR spectra were recorded using a Varian Mercury Plus spectrometer (400 MHz for ^1H -NMR; 100 MHz for ^{13}C -NMR). Chemical shifts are reported in parts per million (ppm) and were calibrated according to residual protonated solvent. Mass spectroscopy data was collected using an Agilent 1100-Series LC/MSD Trap LC-MS or a Micromass QuattroMicro with a Waters 2795 Separations Module LC-MS with acetonitrile containing 0.1% formic acid as the mobile phase in positive ionization mode. Purity was determined on a Agilent 1100 series equipped with a Phenomenex Kinetex 2.6 μm C18-UPLC column using a gradient of water to acetonitrile with 0.1% TFA.

All final compounds were evaluated to be of greater than 90% purity by analysis of $^1\text{H-NMR}$, $^{13}\text{C-NMR}$, and analytical HPLC. Full $^1\text{H-NMR}$ and $^{13}\text{C-NMR}$ spectra are included below.

2-(Benzyloxy)-3,5-dibromobenzamide, 10.

Salicylamide (10.0 g, 72.9 mmol) was dissolved in glacial acetic acid (146 mL, 0.5 M) and Br_2 (11.2 mL, 218.7 mmol) was added dropwise. The reaction stirred overnight at room temperature and then was quenched with water (500 mL). Product was filtered and washed with a small amount of water and then dried in a desiccator, affording 20.2 g of the desired product, which was used crude in the subsequent step, 93.5% yield. 3,5-Dibromo-2-hydroxybenzamide (10.0 g, 33.7 mmol) was dissolved in acetone (337 mL, 0.1 M) and K_2CO_3 (5.58 g, 40.4 mmol) was added, followed by benzyl bromide (4.80 mL, 40.4 mmol) dropwise. The mixture was stirred at reflux overnight and then was cooled to room temperature. Potassium carbonate was filtered off (filtrate was washed with more acetone) and the solvent was removed in vacuo. The product was recrystallized in acetone, affording 11.3 g of the desired product, 87.1% yield. Spectral data was consistent with previous report.²²

N-(2-(Benzyloxy)-3,5-dibromobenzyl)-2-nitrobenzamide, 12.

2-(Benzyloxy)-3,5-dibromobenzamide (1.0 g, 2.58 mmol) was dissolved in $\text{BH}_3\cdot\text{THF}$ (13.24 mL, 13.24 mmol) under N_2 and the mixture was heated to reflux. The reaction stirred for 48 h at 75 °C and was monitored by TLC (10 mL additional $\text{BH}_3\cdot\text{THF}$ was added at 30 h). Methanol (10 mL x 2) was added dropwise to quench the reaction, and then the solvent was removed in vacuo. The product was used crude in the subsequent step without purification. $^1\text{H NMR}$ (400 MHz, $\text{DMSO-}d_6$) δ 7.95 (d, $J = 2.5$ Hz, 1H), 7.91 (s, 1H), 7.74 (s, 1H), 7.60 (d, $J = 2.4$ Hz, 1H), 7.48 – 7.42 (m, 2H), 7.40 – 7.29 (m, 3H),

4.95 (s, 2H), 4.36 (t, 2H). ^{13}C NMR (101 MHz, DMSO- d_6) δ 151.79, 136.32, 136.20, 134.68, 131.19, 128.40, 128.39, 119.03, 116.67, 60.79, 29.25. 2-Nitrobenzoic acid (534.8 mg, 3.20 mmol) was dissolved in CH_2Cl_2 and the solution was cooled to 0 °C under N_2 . Oxalyl chloride (0.550 mL, 6.40 mmol) was added dropwise, followed by DMF (1 drop). The reaction was allowed to warm to room temperature as it stirred for 2 h. Solvent and excess oxalyl chloride was removed in vacuo and then the residue was resuspended in CH_2Cl_2 . This acid chloride was added dropwise to a solution of (2-(benzyloxy)-3,5-dibromophenyl)methanamine (655 mg, 1.60 mmol) in CH_2Cl_2 (32 mL, 0.1 M). Triethylamine (1.56 mL, 11.2 mmol) was added, followed by DMAP (cat.) and the mixture stirred overnight at room temperature. After quenching the reaction with water (25 mL), more CH_2Cl_2 was added (50 mL) and the organic layer was washed with HCl (50 mL, 1 M), sat. NaHCO_3 (50 mL) and then brine (50 mL), and then was dried over Na_2SO_4 . Purification via silica-gel column chromatography (product elutes around 30% EtOAc) afforded 354 mg of the desired product, 42.5% yield. ^1H NMR (400 MHz, CDCl_3) δ 8.04 (dd, 1H), 7.69 (d, $J = 2.4$ Hz, 1H), 7.66 – 7.59 (m, 1H), 7.59 – 7.53 (m, 2H), 7.44 – 7.40 (m, 2H), 7.37 – 7.29 (m, 3H), 7.26 – 7.20 (m, 1H), 5.81 (t, $J = 6.1$ Hz, 1H), 5.05 (s, 2H), 4.46 (d, $J = 6.1$ Hz, 2H). ^{13}C NMR (101 MHz, CDCl_3) δ 166.46, 153.03, 146.43, 136.07, 135.70, 134.99, 133.83, 132.54, 132.45, 130.73, 129.03, 128.89, 128.87, 128.75, 124.72, 118.29, 117.99, 75.85, 39.21.

2,4-Dibromo-6-((2-nitrobenzamido)methyl)phenyl 2-chlorobenzoate, 2.

N-(2-(Methoxy)-3,5-dibromobenzyl)-2-nitrobenzamide (354 mg, 0.681 mmol) was dissolved in CH_2Cl_2 (4.54 mL, 0.15 M) and cooled to -78 °C in a dry ice/acetone bath. BBr_3 (65 μL , 0.681 mmol) was added dropwise and the mixture stirred for 3 h while the temperature was kept between -20 and -60 °C. The reaction was quenched with sat.

NaHCO₃ (25 mL) and was extracted with CH₂Cl₂ (50 mL). This organic layer was washed with brine and then dried over Na₂SO₄. Purification via silica-gel column chromatography (product elutes around 40% EtOAc) afforded 129.5 mg of the desired product, 30.2% yield. ¹H NMR (400 MHz, DMSO-*d*₆) δ 9.25 (t, *J* = 6.2 Hz, 1H), 7.99 (d, *J* = 8.0 Hz, 1H), 7.75 (t, *J* = 7.5 Hz, 1H), 7.70 – 7.56 (m, 3H), 7.34 (d, *J* = 2.2 Hz, 1H), 4.37 (d, *J* = 5.1 Hz, 2H). ¹³C NMR (101 MHz, DMSO-*d*₆) δ 166.33, 151.20, 147.18, 133.78, 133.02, 131.85, 131.14, 130.27, 130.03, 129.20, 124.28, 112.36, 110.97, 38.51. ESI-MS calculated for C₁₄H₁₁Br₂N₂O₄ 428.9 [M+H], observed 428.9. This product was reacted with 2-chlorobenzoyl chloride following the procedure for 2,4-dibromo-6-(2-((2-nitrophenyl)amino)-2-oxoethyl)phenyl 2-chlorobenzoate to provide the desired product, 72.1 mg (92% yield). Spectral data was consistent with previous report.¹⁹

2,4-Dibromo-6-(2-((2-nitrophenyl)amino)-2-oxoethyl)phenyl 2-chlorobenzoate, 3.

To 2-(3,5-dibromo-2-hydroxyphenyl)-*N*-(2-nitrophenyl)acetamide²² (53.0 mg, 0.123 mmol) in CH₂Cl₂ (2.46 mL, 0.05 M) under N₂ was added 2-chlorobenzoyl chloride (19 μL, 0.148 mmol), followed by Et₃N (41 μL, 0.295 mmol) and then DMAP (1.5 mg, 0.0123 mmol). The mixture was allowed to stir overnight at room temperature and then was diluted with CH₂Cl₂ (50 mL) and washed with HCl (25 mL, 1 M), sat. NaHCO₃ (25 mL) and then brine (25 mL). After drying over Na₂SO₄, the material was purified via silica-gel flash chromatography, affording 12.4 mg of the desired product (55% yield). ¹H-NMR (500MHz, CDCl₃) δ 10.32 (s, 1H), 8.67 (dd, *J* = 8.5, 1.1 Hz, 1H), 8.17-8.10 (m, 2H), 7.81 (d, *J* = 2.2 Hz, 1H), 7.63-7.56 (m, 2H), 7.50-7.45 (m, 2H), 7.36-7.30 (m, 1H), 7.16 (ddd, *J* = 8.5, 7.3, 1.3 Hz, 1H), 3.78 (s, 2H). ¹³C-NMR (125MHz, CDCl₃) δ 169.8, 162.2, 146.6, 136.6, 136.2, 135.9, 135.1, 134.5, 134.2, 133.8, 132.6, 131.7, 130.7, 127.6,

127.1, 125.9, 123.9, 122.4, 120.6, 118.9, 40.8. ESI-MS calculated for C₂₁H₁₄Br₂ClN₂O₅, 566.89 [M+H], observed 566.82. HPLC purity 90.1%.

2,4-Dibromo-6-(2-((2-nitrophenyl)amino)-2-oxoethyl)phenyl 3-chlorobenzoate, 13.

Prepared according to the procedure provided for 2,4-dibromo-6-(2-((2-nitrophenyl)amino)-2-oxoethyl)phenyl 2-chlorobenzoate using the appropriate acid chloride, affording 11.7 mg of the desired product (52% yield). ¹H-NMR (500MHz, CDCl₃) δ 10.35 (s, 1H), 8.68 (d, *J* = 8.4 Hz, 1H), 8.15 (dd, *J* = 8.5, 1.3 Hz, 1H), 8.09-8.05 (m, 1H), 8.02 (d, *J* = 7.9 Hz, 1H), 7.79 (d, *J* = 2.2Hz, 1H), 7.63 (ddd, *J* = 8.5, 7.2, 1.0 Hz, 1H), 7.60-7.54 (m, 2H), 7.39 (t, *J* = 7.9 Hz, 1H), 7.18 (ddd, *J* = 8.4, 7.3, 1.1 Hz, 1H), 3.71 (s, 2H). ¹³C-NMR (125MHz, CDCl₃) δ 167.8, 162.6, 146.6, 136.4, 136.3, 135.8, 135.2, 134.6, 134.5, 133.8, 130.8, 130.6, 130.3, 129.7, 128.8, 126.0, 123.9, 122.2, 120.6, 118.8, 41.0. ESI-MS calculated for C₂₁H₁₄Br₂ClN₂O₅, 566.89 [M+H], observed 566.90. HPLC purity 92.2%.

2,4-Dibromo-6-(2-((2-nitrophenyl)amino)-2-oxoethyl)phenyl 4-chlorobenzoate, 14.

Prepared according to the procedure provided for 2,4-dibromo-6-(2-((2-nitrophenyl)amino)-2-oxoethyl)phenyl 2-chlorobenzoate using the appropriate acid chloride, affording 15.8 mg of the desired product (70% yield). ¹H-NMR (500MHz, CDCl₃) δ 10.33 (s, 1H), 8.67 (dd, *J* = 8.5, 1.1 Hz, 1H), 8.15 (dd, *J* = 8.5, 1.5 Hz, 1H), 8.08-8.03 (m, 2H), 7.79 (d, *J* = 2.2 Hz, 1H), 7.62 (ddd, *J* = 8.6, 7.2, 1.4 Hz, 1H), 7.57 (d, *J* = 2.2 Hz, 1H), 7.43-7.37 (m, 2H), 7.18 (ddd, *J* = 8.5, 7.2, 1.2 Hz, 1H), 3.71 (s, 3H). ¹³C-NMR (125MHz, CDCl₃) δ 167.9, 163.0, 146.7, 141.2, 136.4, 136.2, 135.8, 134.5, 133.7,

132.0, 130.8, 129.4, 126.4, 126.0, 123.9, 122.2, 120.5, 118.8, 41.0. ESI-MS calculated for $C_{21}H_{14}Br_2ClN_2O_5$, 566.89 [M+H], observed 566.80. HPLC purity 91.7%.

2,4-Dibromo-6-(2-((2-nitrophenyl)amino)-2-oxoethyl)phenyl 2-bromobenzoate, 15.

Prepared according to the procedure provided for 2,4-dibromo-6-(2-((2-nitrophenyl)amino)-2-oxoethyl)phenyl 2-chlorobenzoate using the appropriate acid chloride, affording 14.3 mg of the desired product (63% yield). 1H -NMR (500MHz, $CDCl_3$) δ 10.32 (s, 1H), 8.68 (dd, $J = 8.5, 1.0$ Hz, 1H), 8.17-8.11 (m, 2H), 7.81 (d, $J = 2.2$ Hz, 1H), 7.71-7.66 (m, 1H), 7.63-7.57 (m, 2H), 7.41-7.36 (m, 2H), 7.16 (ddd, $J = 8.5, 7.2, 1.2$ Hz, 1H), 3.79 (s, 2H). ^{13}C -NMR (125MHz, $CDCl_3$) δ 167.8, 162.7, 146.6, 136.6, 136.1, 135.9, 135.1, 134.5, 134.1, 133.8, 132.7, 130.7, 129.5, 127.6, 126.0, 123.9, 123.1, 122.4, 120.6, 118.8, 40.8. ESI-MS calculated for $C_{21}H_{14}Br_3N_2O_5$, 610.84 [M+H], observed 610.79. HPLC purity 91.2%.

2,4-Dibromo-6-(2-((2-nitrophenyl)amino)-2-oxoethyl)phenyl 3-bromobenzoate, 16.

Prepared according to the procedure provided for 2,4-dibromo-6-(2-((2-nitrophenyl)amino)-2-oxoethyl)phenyl 2-chlorobenzoate using the appropriate acid chloride, affording 16.3 mg of the desired product (67% yield). 1H -NMR (500MHz, $CDCl_3$) δ 10.35 (s, 1H), 8.68 (dd, $J = 8.5, 1.0$ Hz, 1H), 8.22 (t, $J = 1.0$ Hz, 1H), 8.15 (dd, $J = 8.4, 1.0$ Hz, 1H), 8.06 (d, $J = 8.5$ Hz, 1H), 7.79 (d, $J = 2.2$ Hz, 1H), 7.75-7.71 (m, 1H), 7.64-7.61 (m, 1H), 7.57 (d, $J = 2.1$ Hz, 1H), 7.33 (t, $J = 8.7$ Hz, 1H), 7.18 (t, $J = 8.6$ Hz, 1H), 3.71 (s, 2H). ^{13}C -NMR (125MHz, $CDCl_3$) δ 167.8, 162.5, 146.6, 137.5, 136.3, 135.8, 134.5, 133.8, 133.5, 130.8, 130.5, 129.9, 129.3, 126.0, 124.0, 123.0, 122.2, 120.6,

118.7, 41.0. ESI-MS calculated for $C_{21}H_{14}Br_3N_2O_5$, 610.84 [M+H], observed 610.81. HPLC purity 98.1%.

2,4-Dibromo-6-(2-((2-nitrophenyl)amino)-2-oxoethyl)phenyl 4-bromobenzoate, 17.

Prepared according to the procedure provided for 2,4-dibromo-6-(2-((2-nitrophenyl)amino)-2-oxoethyl)phenyl 2-chlorobenzoate using the appropriate acid chloride, affording 15.1 mg of the desired product (62% yield). 1H -NMR (500MHz, $CDCl_3$) δ 10.34 (s, 1H), 8.68 (dd, $J = 8.5, 0.9$ Hz, 1H), 8.16 (dd, $J = 8.4, 1.0$ Hz, 1H), 7.98 (d, $J = 8.5$ Hz), 7.79 (d, $J = 2.3$ Hz, 1H), 7.65-7.54 (m, 3H), 7.18 (t, $J = 8.4$ Hz, 1H), 3.71 (s, 2H). ^{13}C -NMR (125MHz, $CDCl_3$) δ 167.9, 163.1, 146.7, 136.3, 135.8, 134.5, 133.7, 132.4, 132.1, 130.8, 130.0, 126.8, 126.0, 123.9, 122.2, 120.6, 118.8, 41.0. ESI-MS calculated for $C_{21}H_{14}Br_3N_2O_5$, 610.84 [M+H], observed 610.82. HPLC purity 93.6%.

2,4-Dibromo-6-(2-((2-nitrophenyl)amino)-2-oxoethyl)phenyl 2-fluorobenzoate, 18.

Prepared according to the procedure provided for 2,4-dibromo-6-(2-((2-nitrophenyl)amino)-2-oxoethyl)phenyl 2-chlorobenzoate using the appropriate acid chloride, affording 15.4 mg of the desired product (70% yield). 1H -NMR (500MHz, $CDCl_3$) δ 10.32 (s, 1H), 8.67 (dd, $J = 8.4, 0.9$ Hz, 1H), 8.15 (dd, $J = 8.5, 1.0$ Hz, 1H), 8.06 (dt, $J = 8.4, 0.9$ Hz, 1H), 7.79 (d, $J = 2.2$ Hz, 1H), 7.64-7.55 (m, 2H), 7.24-7.11 (m, 2H), 3.75 (s, 2H). ^{13}C -NMR (125MHz, $CDCl_3$) δ 167.8, 163.7, 161.6, 161.2, 161.1, 136.3, 136.2, 136.2, 135.8, 134.5, 133.7, 133.0, 130.7, 125.9, 124.5, 124.5, 123.9, 122.4, 120.5, 118.8, 117.6, 117.4, 116.7, 116.6, 40.8. ESI-MS calculated for $C_{21}H_{14}Br_2FN_2O_5$, 550.93 [M+H], observed 550.91. HPLC purity 95.8%.

2,4-Dibromo-6-(2-((2-nitrophenyl)amino)-2-oxoethyl)phenyl 4-fluorobenzoate, 19.

Prepared according to the procedure provided for 2,4-dibromo-6-(2-((2-nitrophenyl)amino)-2-oxoethyl)phenyl 2-chlorobenzoate using the appropriate acid chloride, affording 12.7 mg of the desired product (58% yield). ¹H-NMR (500MHz, CDCl₃) δ 10.33 (s, 1H), 8.67 (d, *J* = 8.3 Hz, 1H), 8.20-8.11 (m, 2H), 7.79 (d, *J* = 1.9 Hz, 1H), 7.62 (t, *J* = 8.4 Hz, 1H), 7.57 (d, *J* = 1.8 Hz, 1H), 7.18 (t, *J* = 8.4 Hz, 1H), 7.14-7.07 (m, 2H), 3.71 (s, 2H). ¹³C-NMR (125MHz, CDCl₃) δ 167.9, 167.8, 165.7, 162.8, 146.7, 136.5, 136.2, 135.7, 134.5, 133.7, 133.5, 133.4, 130.8, 126.0, 124.2, 123.9, 122.2, 120.5, 118.8, 116.4, 116.2, 40.9. ESI-MS calculated for C₂₁H₁₄Br₂FN₂O₅, 550.93 [M+H], observed 550.90. HPLC purity 92.0%.

2,4-Dibromo-6-(2-((2-nitrophenyl)amino)-2-oxoethyl)phenyl 2-iodobenzoate, 20.

Prepared according to the procedure provided for 2,4-dibromo-6-(2-((2-nitrophenyl)amino)-2-oxoethyl)phenyl 2-chlorobenzoate using the appropriate acid chloride, affording 9.5 mg of the desired product (77% yield). ¹H NMR (400 MHz, CDCl₃) δ 10.33 (s, 1H), 8.70 (dt, *J* = 8.5, 1.2 Hz, 1H), 8.23 – 8.13 (m, 2H), 8.05 (dt, *J* = 7.9, 1.2 Hz, 1H), 7.82 (dd, *J* = 2.4, 1.1 Hz, 1H), 7.65 – 7.57 (m, 2H), 7.47 – 7.39 (m, 1H), 7.26 – 7.13 (m, 2H), 3.80 (d, *J* = 1.0 Hz, 2H). ¹³C NMR (101 MHz, CDCl₃) δ 167.72, 162.75, 142.23, 141.98, 136.02, 135.78, 135.03, 134.46, 134.11, 133.74, 132.34, 132.11, 130.68, 129.74, 128.30, 125.88, 123.80, 122.38, 120.54, 118.79, 40.81. ESI-MS calculated for C₂₁H₁₄Br₂IN₂O₅, 658.83 [M+H], observed 658.90. HPLC purity 96.8%.

2,4-Dibromo-6-(2-((2-nitrophenyl)amino)-2-oxoethyl)phenyl 2-methylbenzoate, 21.

Prepared according to the procedure provided for 2,4-dibromo-6-(2-((2-nitrophenyl)amino)-2-oxoethyl)phenyl 2-chlorobenzoate using the appropriate acid chloride, affording 16.0 mg of the desired product (61% yield). ¹H-NMR (500MHz, CDCl₃) δ 10.33 (s, 1H), 8.68 (d, *J* = 8.4 Hz, 1H), 8.16 (d, *J* = 8.4 Hz, 1H), 8.13 (dd, *J* = 8.4, 0.9 Hz, 1H), 7.80 (d, *J* = 2.0 Hz, 1H), 7.60 (t, *J* = 8.2 Hz, 1H), 7.57 (d, *J* = 1.9 Hz, 1H), 7.44 (t, *J* = 8.2 Hz, 1H), 7.27-7.13 (m, 2H), 3.73 (s, 2H), 2.53 (s, 3H). ¹³C-NMR (125MHz, CDCl₃) δ 168.0, 163.9, 147.0, 142.4, 136.5, 136.1, 135.7, 134.5, 133.7, 133.7, 132.3, 131.8, 130.9, 126.8, 126.2, 125.9, 123.8, 122.2, 120.2, 119.1, 41.0, 22.1. ESI-MS calculated for C₂₂H₁₇Br₂N₂O₅, 546.95 [M+H], observed 546.89. HPLC purity 96.4%.

2,4-Dibromo-6-(2-((2-nitrophenyl)amino)-2-oxoethyl)phenyl 3-methylbenzoate, 22.

Prepared according to the procedure provided for 2,4-dibromo-6-(2-((2-nitrophenyl)amino)-2-oxoethyl)phenyl 2-chlorobenzoate using the appropriate acid chloride, affording 15.8 mg of the desired product (72% yield). ¹H-NMR (500MHz, CDCl₃) δ 10.33 (s, 1H), 8.70 (dd, *J* = 8.4, 0.8 Hz, 1H), 8.13 (dd, *J* = 8.4, 0.9 Hz), 7.94-7.89 (m, 2H), 7.78 (d, *J* = 2.1, Hz, 1H), 7.61 (t, *J* = 8.2 Hz, 1H), 7.56 (d, *J* = 2.1 Hz, 1H), 7.43-7.37 (m, 1H), 7.30 (t, *J* = 8.4 Hz, 1H), 7.16 (t, *J* = 8.4 Hz, 1H), 3.71 (s, 2H), 2.33 (s, 3H). ¹³C-NMR (125MHz, CDCl₃) δ 167.9, 163.9, 146.9, 138.9, 136.4, 136.2, 135.7, 135.4, 134.6, 133.7, 131.1, 130.9, 128.8, 127.9, 127.8, 125.9, 123.8, 122.2, 120.3, 118.9, 40.9, 21.4. ESI-MS calculated for C₂₂H₁₇Br₂N₂O₅, 546.95 [M+H], observed 546.96. HPLC purity 94.4%.

2,4-Dibromo-6-(2-((2-nitrophenyl)amino)-2-oxoethyl)phenyl 4-methylbenzoate, 23.

Prepared according to the procedure provided for 2,4-dibromo-6-(2-((2-nitrophenyl)amino)-2-oxoethyl)phenyl 2-chlorobenzoate using the appropriate acid chloride, affording 17.1 mg of the desired product (78% yield). $^1\text{H-NMR}$ (500MHz, CDCl_3) δ 10.32 (s, 1H), 8.69 (dd, $J = 8.4, 0.9$ Hz, 1H), 8.13 (dd, $J = 8.4, 0.9$ Hz, 1H), 8.00 (d, $J = 8.5$ Hz, 2H), 7.78 (d, $J = 2.1$ Hz, 1H), 7.61 (t, $J = 8.3$ Hz, 1H), 7.56 (d, $J = 2.1$ Hz, 1H), 7.20 (d, $J = 8.5$ Hz, 2H), 7.17 (t, $J = 8.4$ Hz, 1H), 3.71 (s, 2H), 2.40 (s, 3H). $^{13}\text{C-NMR}$ (125MHz, CDCl_3) δ 168.0, 163.8, 146.9, 145.6, 136.4, 136.2, 135.7, 134.6, 133.6, 131.0, 130.8, 129.6, 125.9, 125.1, 123.8, 122.3, 120.2, 118.9, 40.9, 22.1. ESI-MS calculated for $\text{C}_{22}\text{H}_{17}\text{Br}_2\text{N}_2\text{O}_5$, 546.95 [M+H], observed 546.92. HPLC purity 91.7%.

2,4-Dibromo-6-(2-((2-nitrophenyl)amino)-2-oxoethyl)phenyl 2-methoxybenzoate, 24.

Prepared according to the procedure provided for 2,4-dibromo-6-(2-((2-nitrophenyl)amino)-2-oxoethyl)phenyl 2-chlorobenzoate using the appropriate acid chloride, affording 10 mg of the desired product (65.6% yield). $^1\text{H NMR}$ (400 MHz, CDCl_3) δ 10.29 (s, 1H), 8.70 (dd, $J = 8.5, 1.3$ Hz, 1H), 8.15 (dd, $J = 8.4, 1.6$ Hz, 1H), 8.02 (dd, $J = 7.8, 1.8$ Hz, 1H), 7.80 (d, $J = 2.3$ Hz, 1H), 7.66 – 7.47 (m, 3H), 7.21 – 7.11 (m, 1H), 7.03 – 6.91 (m, 2H), 3.86 (s, 3H), 3.80 (s, 2H). $^{13}\text{C NMR}$ (101 MHz, CDCl_3) δ 168.09, 162.72, 160.18, 146.93, 136.61, 135.95, 135.60, 135.16, 134.51, 133.54, 132.69, 130.81, 125.82, 123.71, 122.36, 120.40, 120.06, 119.02, 117.52, 112.24, 56.10, 40.65. ESI-MS calculated for $\text{C}_{22}\text{H}_{17}\text{Br}_2\text{N}_2\text{O}_6$, 562.94 [M+H], observed 563.07. HPLC purity 89.9%.

2,4-Dibromo-6-(2-((2-nitrophenyl)amino)-2-oxoethyl)phenyl 2-nitrobenzoate, 25.

Prepared according to the procedure provided for 2,4-dibromo-6-(2-((2-nitrophenyl)amino)-2-oxoethyl)phenyl 2-chlorobenzoate using the appropriate acid chloride, affording 14.4 mg of the desired product (19.1% yield). ^1H NMR (400 MHz, CDCl_3) δ 10.35 (s, 1H), 8.68 (dd, $J = 8.6, 1.3$ Hz, 1H), 8.13 (dd, $J = 8.5, 1.2$ Hz, 1H), 8.10 (dd, $J = 7.4, 1.6$ Hz, 1H), 8.01 (dd, $J = 7.8, 1.4$ Hz, 1H), 7.79 (d, 1H), 7.77 – 7.69 (m, 2H), 7.63 (d, 1H), 7.62 – 7.56 (m, 1H), 7.20 – 7.12 (m, 1H), 3.96 (s, 2H). ^{13}C NMR (101 MHz, CDCl_3) δ 167.90, 162.39, 147.98, 145.87, 136.78, 135.86, 135.52, 134.37, 134.16, 133.47, 132.80, 131.18, 130.53, 126.30, 125.74, 124.55, 123.71, 122.51, 120.82, 118.26, 39.85. ESI-MS calculated for $\text{C}_{21}\text{H}_{14}\text{Br}_2\text{N}_3\text{O}_7$, 577.92 [M+H], observed 577.79. HPLC purity 91.1%.

2,4-Dibromo-6-(2-((2-nitrophenyl)amino)-2-oxoethyl)phenyl 2,6-dichlorobenzoate, 27.

Prepared according to the procedure provided for 2,4-dibromo-6-(2-((2-nitrophenyl)amino)-2-oxoethyl)phenyl 2-chlorobenzoate using the appropriate acid chloride, affording 18.6 mg of the desired product (78% yield). ^1H -NMR (500MHz, CDCl_3) δ 10.32 (s, 1H), 8.70 (d, $J = 8.4$ Hz, 1H), 8.16 (dd, $J = 8.4, 1.0$ Hz, 1H), 7.83 (d, $J = 2.1$ Hz, 1H), 7.64-7.57 (m, 2H), 7.41-7.31 (m, 2H), 7.16 (t, $J = 8.4$ Hz, 1H), 3.98 (s, 2H). ^{13}C -NMR (125MHz, CDCl_3) δ 167.9, 161.9, 146.1, 136.6, 136.3, 136.2, 134.5, 134.1, 133.0, 132.2, 131.2, 130.5, 128.9, 126.0, 123.9, 122.3, 121.1, 118.6, 40.5. ESI-MS calculated for $\text{C}_{21}\text{H}_{12}\text{Br}_2\text{Cl}_2\text{N}_2\text{O}_5$, 600.86 [M+H], observed 600.99. HPLC purity 91.2%.

2-(3,5-Dibromo-2-((2,6-dichlorobenzyl)oxy)phenyl)-N-(2-nitrophenyl)acetamide, 28.

Prepared according to the procedure provided for 2,4-dibromo-6-(2-((2-nitrophenyl)amino)-2-oxoethyl)phenyl 2-chlorobenzoate using the appropriate acid

chloride, affording 33.26 mg of the desired product (13.7% yield). ^1H NMR (400 MHz, CDCl_3) δ 10.13 (s, 1H), 8.62 (dd, $J = 8.6, 1.3$ Hz, 1H), 8.13 (dd, $J = 8.5, 1.6$ Hz, 1H), 7.68 (d, $J = 2.4$ Hz, 1H), 7.59 – 7.51 (m, 1H), 7.34 (d, $J = 2.4$ Hz, 1H), 7.25 – 7.21 (m, 2H), 7.17 – 7.07 (m, 2H), 5.45 (s, 2H), 3.54 (s, 2H). ^{13}C NMR (101 MHz, CDCl_3) δ 168.67, 153.71, 137.34, 136.56, 136.06, 135.91, 134.66, 133.49, 132.13, 131.17, 131.00, 128.81, 125.79, 123.52, 122.35, 118.51, 117.84, 70.16, 39.81. ESI-MS calculated for $\text{C}_{21}\text{H}_{15}\text{Br}_2\text{Cl}_2\text{N}_2\text{O}_4$, 586.87 [M+H], observed 586.76. HPLC purity 90.1%.

2,4-Dibromo-6-(2-((2-nitrophenyl)amino)-2-oxoethyl)phenyl benzoate, 29.

Prepared according to the procedure provided for 2,4-dibromo-6-(2-((2-nitrophenyl)amino)-2-oxoethyl)phenyl 2-chlorobenzoate using the appropriate acid chloride, affording 7.3 mg of the desired product (62.1% yield). ^1H NMR (400 MHz, CDCl_3) δ 10.34 (s, 1H), 8.70 (dd, $J = 8.5, 1.3$ Hz, 1H), 8.18 – 8.12 (m, 3H), 7.81 (d, $J = 2.2$ Hz, 1H), 7.67 – 7.57 (m, 3H), 7.49 – 7.41 (m, 2H), 7.22 – 7.15 (m, 1H), 3.74 (s, 2H). ^{13}C NMR (101 MHz, CDCl_3) δ 167.85, 163.71, 136.07, 135.65, 134.50, 134.45, 133.57, 130.85, 130.64, 128.87, 127.94, 125.86, 123.76, 122.23, 120.28, 40.83. ESI-MS calculated for $\text{C}_{21}\text{H}_{14}\text{Br}_2\text{N}_2\text{O}_5$, 532.93 [M+H], observed 532.98. HPLC purity 90.0%.

2,4-Dibromo-6-(2-((2-nitrophenyl)amino)-2-oxoethyl)phenyl 2-bromo-4-fluorobenzoate, 26.

Prepared according to the procedure provided for 2,4-dibromo-6-(2-((2-nitrophenyl)amino)-2-oxoethyl)phenyl 2-chlorobenzoate using the appropriate acid chloride, affording 9.5 mg of the desired product (11% yield). ^1H NMR (400 MHz, CDCl_3) δ 10.34 (s, 1H), 8.69 (dd, $J = 8.5, 1.3$ Hz, 1H), 8.17 (dd, $J = 8.5, 1.5$ Hz, 1H), 7.99 – 7.92 (m, 1H), 7.83 (d, $J = 2.3$ Hz, 1H), 7.63 – 7.58 (m, 2H), 7.45 – 7.30 (m, 2H), 7.22 – 7.15 (m, 1H), 3.81 (s, 2H). ^{13}C NMR (101 MHz, CDCl_3) δ 167.64, 161.84, 146.40,

138.59, 136.55, 136.08, 135.85, 134.37, 133.80, 131.53, 130.52, 128.88, 128.80, 127.94, 125.89, 123.88, 122.26, 120.84, 120.60, 118.68, 40.80. ESI-MS calculated for $C_{21}H_{12}Br_3FN_2O_5$, 628.84 [M+H], observed 629.18. HPLC purity 87.6%.

2-(3,5-Dibromo-2-((2-chlorobenzoyl)oxy)phenyl)acetic acid.

To a solution of methyl 2-(3,5-dibromo-2-hydroxyphenyl)acetate (2.902g, 8.96mmol) in CH_2Cl_2 (59mL) at room temperature was added Et_3N (2.99mL, 21.49mmol), 2-chlorobenzoyl chloride (1.248g, 9.85mmol) and DMAP (0.109g, 0.896mmol). The mixture was allowed to react overnight and was diluted with CH_2Cl_2 , quenched with 1M HCl, washed with sat. $NaHCO_3$ and brine, dried over Na_2SO_4 , concentrated and purified by flash column chromatography to provide 2,4-dibromo-6-(2-methoxy-2-oxoethyl)phenyl 2-chlorobenzoate (2.91g, 70%). 1H NMR (400 MHz, $CDCl_3$) δ 8.19-8.16 (m, 1H), 7.74 (d, $J = 2.2$ Hz, 1H), 7.56-7.72 (m, 2H), 7.50-7.48 (m, 1H), 7.44-7.39 (m, 1H), 3.64 (s, 3H), 3.62 (s, 2H). The above methyl ester, 2,4-dibromo-6-(2-methoxy-2-oxoethyl)phenyl 2-chlorobenzoate (1.823g, 3.94mmol) was dissolved in 1,2-dichloroethane (39.4mL) and was treated with trimethyltinhydroxide (1.425g, 7.88mmol). The mixture was heated to 80°C and was monitored by TLC to confirm the consumption of the starting material. After 2h the reaction was diluted with $CHCl_3$, washed with 1M HCl and sat. NaCl, dried over Na_2SO_4 , concentrated and purified by flash column chromatography using a gradient of 20% EtOAc/hexanes to 100% EtOAc to provide 2-(3,5-dibromo-2-((2-chlorobenzoyl)oxy)phenyl)acetic acid as a white solid (1.045g, 59%). 1H NMR (400 MHz, $CDCl_3$) δ 8.18-8.14 (m, 1H), 7.76 (d, $J = 2.3$ Hz, 1H), 7.55-7.52 (m, 2H), 7.50 (d, $J = 2.2$ Hz, 1H), 7.40 (ddd, $J = 7.8, 5.6, 3.0$ Hz, 1H), 3.65 (s, 2H).

2,4-Dibromo-6-(2-((3-nitrophenyl)amino)-2-oxoethyl)phenyl 2-chlorobenzoate, 30.

To a solution of 2-(3,5-dibromo-2-((2-chlorobenzoyl)oxy)phenyl)acetic acid (0.181g, 0.4035mmol) in ACN (8.07mL) was added 3-nitroaniline (0.0613g, 0.4439mmol) followed by EDC (0.1423g, 0.807mmol) and DMAP (0.0049g, 0.0403mmol). The resulting mixture was allowed to react at room temperature overnight and was concentrated to dryness. The residue was suspended in CHCl_3 , washed with 1M HCl, sat. NaHCO_3 and brine, dried over Na_2SO_4 and concentrated. The residue was purified by flash column chromatography using a gradient of hexanes to EtOAc, affording 1.1 mg of the desired product (0.5% yield). ^1H NMR (400 MHz, CDCl_3) δ 8.41 (t, $J = 2.2$ Hz, 1H), 8.26 (d, $J = 7.4$ Hz, 1H), 8.02 (s, 1H), 7.93 (d, $J = 8.2$ Hz, 1H), 7.86 (d, $J = 8.1$ Hz, 1H), 7.81 (d, $J = 2.3$ Hz, 1H), 7.62 (d, $J = 2.3$ Hz, 1H), 7.60 – 7.53 (m, 2H), 7.51 – 7.38 (m, 2H), 3.74 (s, 2H). ^{13}C NMR (101 MHz, CDCl_3) δ 167.29, 164.52, 148.63, 145.90, 138.97, 135.78, 135.38, 134.75, 133.24, 132.76, 131.92, 131.08, 129.80, 127.30, 127.00, 125.52, 121.07, 119.13, 118.63, 114.70, 39.55. ESI-MS calculated for $\text{C}_{21}\text{H}_{14}\text{Br}_2\text{ClN}_2\text{O}_5$, 566.89 [M+H], observed 566.95. HPLC purity 91.3%.

2,4-Dibromo-6-(2-((4-nitrophenyl)amino)-2-oxoethyl)phenyl 2-chlorobenzoate, 31.

Prepared according to the procedure provided for 2,4-dibromo-6-(2-((3-nitrophenyl)amino)-2-oxoethyl)phenyl 2-chlorobenzoate using the appropriate amine, affording 3.5 mg of the desired product (1.4% yield). ^1H NMR (400 MHz, CDCl_3) δ 8.26 (dd, $J = 8.1, 1.5$ Hz, 1H), 8.20 – 8.15 (m, 2H), 8.14 (s, 1H), 7.81 (d, $J = 2.3$ Hz, 1H), 7.74 – 7.67 (m, 2H), 7.64 – 7.54 (m, 3H), 7.50 – 7.42 (m, 1H), 3.74 (s, 2H). ^{13}C NMR (101 MHz, CDCl_3) δ 167.37, 164.71, 145.84, 143.77, 143.73, 135.85, 135.35, 134.81, 133.17,

132.76, 131.93, 130.93, 127.32, 127.00, 125.08, 121.14, 119.31, 118.63, 39.64. ESI-MS calculated for $C_{21}H_{14}Br_2ClN_2O_5$, 566.89 [M+H], observed 566.86. HPLC purity 94.8%.

2,4-Dibromo-6-(2-oxo-2-(pyridin-2-ylamino)ethyl)phenyl 2-chlorobenzoate, 32.

Prepared according to the procedure provided for 2,4-dibromo-6-(2-((3-nitrophenyl)amino)-2-oxoethyl)phenyl 2-chlorobenzoate using the appropriate amine, affording 24.9 mg of the desired product (22% yield). 1H NMR (400 MHz, $CDCl_3$) δ 8.27 – 8.19 (m, 2H), 8.19 – 8.10 (m, 2H), 7.77 (d, $J = 2.3$ Hz, 1H), 7.70 – 7.64 (m, 1H), 7.58 (d, $J = 2.3$ Hz, 1H), 7.53 – 7.48 (m, 2H), 7.40 – 7.32 (m, 1H), 7.05 – 6.99 (m, 1H), 3.73 (s, 2H). ^{13}C NMR (101 MHz, $CDCl_3$) δ 167.23, 162.64, 151.12, 147.96, 146.34, 138.49, 135.47, 135.01, 134.05, 133.44, 132.56, 131.66, 131.15, 127.73, 127.03, 120.48, 120.20, 118.56, 114.21, 39.73. ESI-MS calculated for $C_{20}H_{14}Br_2ClN_2O_3$, 522.91 [M+H], observed 522.97. HPLC purity 98.3%.

2,4-Dibromo-6-(2-((2,3-difluorophenyl)amino)-2-oxoethyl)phenyl 2-chlorobenzoate, 33.

Prepared according to the procedure provided for 2,4-dibromo-6-(2-((3-nitrophenyl)amino)-2-oxoethyl)phenyl 2-chlorobenzoate using the appropriate amine, affording 24.9 mg of the desired product (41% yield). 1H NMR (400 MHz, Acetone- d_6) δ 9.17 (s, 1H), 8.11 (dd, $J = 7.9, 1.6$ Hz, 1H), 7.80 (t, $J = 7.4$ Hz, 1H), 7.76 (d, $J = 2.3$ Hz, 1H), 7.65 (d, $J = 2.3$ Hz, 1H), 7.57 – 7.46 (m, 2H), 7.38 – 7.31 (m, 1H), 7.03 – 6.94 (m, 1H), 6.94 – 6.85 (m, 1H), 3.86 (s, 2H). ^{13}C NMR (101 MHz, $CDCl_3$) δ 167.08, 162.99, 146.01, 135.52, 135.05, 134.31, 133.18, 133.15, 132.57, 131.73, 131.12, 127.83, 127.46, 127.13, 124.21, 120.63, 118.48, 117.08, 112.62, 112.45, 39.66. ESI-MS calculated for $C_{21}H_{13}Br_2ClF_2NO_3$, 557.89 [M+H], observed 558.09. HPLC purity 92.3%.

2,4-Dibromo-6-(2-((4,5-difluoro-2-nitrophenyl)amino)-2-oxoethyl)phenyl 2-chlorobenzoate, 34.

Prepared according to the procedure provided for 2,4-dibromo-6-(2-((3-nitrophenyl)amino)-2-oxoethyl)phenyl 2-chlorobenzoate using the appropriate amine, affording 36.7 mg of the desired product (16% yield). ¹H NMR (400 MHz, CDCl₃) δ 10.41 (s, 1H), 8.74 (dd, *J* = 12.6, 7.5 Hz, 1H), 8.14 (dd, *J* = 7.9, 0.9 Hz, 1H), 8.07 (dd, *J* = 10.1, 7.9 Hz, 1H), 7.85 (d, *J* = 2.3, 0.7 Hz, 1H), 7.59 (d, 1H), 7.55 – 7.49 (m, 2H), 7.41 – 7.35 (m, 1H), 3.81 (s, 2H). ¹³C NMR (101 MHz, CDCl₃) δ 167.90, 162.12, 146.58, 136.02, 135.00, 134.18, 133.71, 132.55, 131.71, 130.14, 127.47, 127.05, 120.64, 118.93, 115.14, 114.93, 111.01, 110.76, 40.75. ESI-MS calculated for C₂₁H₁₂Br₂ClN₃O₅, 602.88 [M+H], observed 602.77. HPLC purity 97.0%.

2,4-Dibromo-6-(2-oxo-2-(pyrimidin-4-ylamino)ethyl)phenyl 2-chlorobenzoate, 35.

Prepared according to the procedure provided for 2,4-dibromo-6-(2-((3-nitrophenyl)amino)-2-oxoethyl)phenyl 2-chlorobenzoate using the appropriate amine, affording 15.2 mg of the desired product (13% yield). ¹H NMR (400 MHz, CDCl₃) δ 8.83 (s, 1H), 8.61 (s, 1H), 8.34 (s, 1H), 8.21 – 8.14 (m, 1H), 8.10 (dd, *J* = 5.8, 1.2 Hz, 1H), 7.80 (d, *J* = 2.4 Hz, 1H), 7.57 (d, *J* = 2.4 Hz, 1H), 7.55 – 7.52 (m, 2H), 7.42 – 7.36 (m, 1H), 3.76 (s, 2H). ¹³C NMR (101 MHz, CDCl₃) δ 168.19, 162.98, 158.59, 158.49, 156.87, 146.25, 135.79, 135.03, 134.27, 133.32, 132.57, 131.73, 130.43, 127.54, 127.12, 120.67, 118.71, 110.42, 39.79. ESI-MS calculated for C₁₉H₁₃Br₂ClN₃O₃, 523.90 [M+H], observed 523.92. HPLC purity 94.4%.

2,4-Dibromo-6-(2-((3-nitropyridin-4-yl)amino)-2-oxoethyl)phenyl 2-chlorobenzoate, 36.

Prepared according to the procedure provided for 2,4-dibromo-6-(2-((3-nitrophenyl)amino)-2-oxoethyl)phenyl 2-chlorobenzoate using the appropriate amine, affording 4.1 mg of the desired product (5.8% yield). ¹H NMR (400 MHz, CDCl₃) δ 10.50 (s, 1H), 9.33 (s, 1H), 8.67 (s, 2H), 8.13 (dd, 1H), 7.86 (d, *J* = 2.2 Hz, 1H), 7.59 (d, *J* = 2.3 Hz, 1H), 7.56 – 7.47 (m, 2H), 7.41 – 7.34 (m, 1H), 3.84 (s, 2H). ¹³C NMR (101 MHz, CDCl₃) δ 168.31, 162.10, 156.31, 155.69, 136.16, 134.22, 133.69, 132.54, 131.72, 129.85, 129.27, 128.07, 127.41, 127.06, 120.70, 118.99, 114.62, 40.90. ESI-MS calculated for C₂₀H₁₃Br₂ClN₃O₅, 567.89 [M+H], observed 567.82. HPLC purity 89.8%.

(S)-2,4-Dibromo-6-(2-oxo-2-((2-oxotetrahydrofuran-3-yl)amino)ethyl)phenyl 2-chlorobenzoate, **37**.

Prepared according to the procedure provided for 2,4-dibromo-6-(2-((3-nitrophenyl)amino)-2-oxoethyl)phenyl 2-chlorobenzoate using the appropriate amine, affording 27.9 mg of the desired product (81% yield). ¹H NMR (400 MHz, CDCl₃) δ 8.21 (dd, *J* = 7.9, 1.2 Hz, 1H), 7.77 (dd, *J* = 2.3, 1.2 Hz, 1H), 7.59 – 7.53 (m, 3H), 7.47 – 7.40 (m, 1H), 6.18 (s, 1H), 4.55 – 4.35 (m, 2H), 4.29 – 4.14 (m, 1H), 3.61 (s, 2H), 2.76 – 2.61 (m, 1H), 2.16 – 1.99 (m, 1H). ¹³C NMR (101 MHz, CDCl₃) δ 174.76, 169.16, 135.45, 135.02, 134.32, 133.47, 132.70, 131.78, 131.23, 127.48, 127.21, 120.57, 118.45, 66.07, 49.53, 38.19, 29.81. ESI-MS calculated for C₁₉H₁₅Br₂ClNO₅, 529.90 [M+H], observed 529.85. HPLC purity 94.9%.

2,4-Dibromo-6-(picolinamidomethyl)phenyl 2-chlorobenzoate, **38**.

The required phenol, *N*-(3,5-dibromo-2-hydroxybenzyl)picolinamide was prepared in two steps from (2-(benzyloxy)-3,5-dibromophenyl)methanamine and pyridine-2-carboxylic acid as described for *N*-(3,5-dibromo-2-hydroxybenzyl)-2-nitrobenzamide, providing the desired product (0.10g, 35%, two steps). ¹H NMR (400 MHz, Chloroform-d) δ 9.88 (s,

1H), 8.84 – 8.79 (m, 1H), 8.55 (d, $J = 4.7$ Hz, 1H), 8.20 (d, $J = 7.8$ Hz, 1H), 7.87 (dt, $J = 7.7, 1.7$ Hz, 1H), 7.59 (d, $J = 2.4$ Hz, 1H), 7.47 (ddd, $J = 7.6, 4.7, 1.2$ Hz, 1H), 7.29 (d, $J = 2.4$ Hz, 1H), 4.55 (d, $J = 6.8$ Hz, 2H). This product was reacted with 2-chlorobenzoyl chloride according to the procedure provided for 2,4-dibromo-6-((2-nitrobenzamido)methyl)phenyl 2-chlorobenzoate, affording 11.4 mg of the desired product (38% yield). ^1H NMR (400 MHz, CDCl_3) δ 8.54 (dd, $J = 4.7, 1.4$ Hz, 1H), 8.45 (s, 1H), 8.21 (dd, $J = 7.8, 1.1$ Hz, 1H), 8.15 (dd, $J = 7.8, 1.1$ Hz, 1H), 7.84 (td, $J = 7.8, 1.8$ Hz, 1H), 7.74 (d, $J = 2.3$ Hz, 1H), 7.58 (d, $J = 2.3$ Hz, 1H), 7.54 (d, 2H), 7.46 – 7.39 (m, 2H), 4.66 (d, $J = 6.1$ Hz, 2H). ^{13}C NMR (101 MHz, CDCl_3) δ 164.56, 162.48, 149.41, 148.35, 145.84, 137.52, 135.04, 134.94, 133.99, 132.61, 131.78, 131.65, 127.89, 127.00, 126.59, 122.51, 120.33, 118.12, 38.74. ESI-MS calculated for $\text{C}_{20}\text{H}_{14}\text{Br}_2\text{ClN}_2\text{O}_5$, 522.91 [M+H], observed 523.04. HPLC purity 97.7%.

2,4-Dibromo-6-((2,3-difluorobenzamido)methyl)phenyl 2-chlorobenzoate,
39.

Prepared according to the procedure provided for 2,4-dibromo-6-((2-nitrobenzamido)methyl)phenyl 2-chlorobenzoate from 2-chlorobenzoyl chloride and *N*-(3,5-dibromo-2-hydroxybenzyl)-2,3-difluorobenzamide, affording 7.9 mg of the desired product (18% yield). ^1H NMR (400 MHz, CDCl_3) δ 8.21 (dd, 1H), 7.81 – 7.73 (m, 2H), 7.62 (d, $J = 2.3$ Hz, 1H), 7.57 – 7.53 (m, 2H), 7.46 – 7.40 (m, 1H), 7.36 – 7.27 (m, 1H), 7.21 – 7.14 (m, 1H), 7.04 (t, $J = 11.4$ Hz, 1H), 4.66 (s, 2H). ^{13}C NMR (101 MHz, CDCl_3) δ 162.73, 162.47, 145.94, 135.36, 134.98, 134.44, 134.12, 132.55, 132.25, 131.69, 127.75, 127.09, 126.60, 126.57, 124.78, 124.72, 120.83, 120.65, 120.43, 118.16, 39.40. ESI-MS calculated for $\text{C}_{21}\text{H}_{13}\text{Br}_2\text{ClF}_2\text{NO}_3$, 557.89 [M+H], observed 557.77. HPLC purity 90.0%.

2,4-Dibromo-6-((pyrimidine-4-carboxamido)methyl)phenyl 2-chlorobenzoate, 40.

The required phenol, *N*-(3,5-dibromo-2-hydroxybenzyl)pyrimidine-4-carboxamide was prepared in two steps from (2-(benzyloxy)-3,5-dibromophenyl)methanamine and pyrimidine-4-carboxylic acid as described for *N*-(3,5-dibromo-2-hydroxybenzyl)-2-nitrobenzamide, providing the desired product (0.082g, 32%, two steps). ¹H-NMR (400 MHz, Chloroform-d) δ 9.22 (s, 1H), 8.99 (d, *J* = 5.0 Hz, 1H), 8.82 – 8.74 (m, 1H), 8.10 (dd, *J* = 5.0, 1.4 Hz, 1H), 7.56 (d, *J* = 2.4 Hz, 1H), 7.32 (d, *J* = 2.4 Hz, 1H), 4.59 (d, *J* = 6.7 Hz, 2H). This product was reacted with 2-chlorobenzoyl chloride according to the procedure provided for 2,4-dibromo-6-((2-nitrobenzamido)methyl)phenyl 2-chlorobenzoate, affording 7.7 mg of the desired product (7.0% yield). ¹H NMR (400 MHz, Chloroform-d) δ 9.22 (d, *J* = 1.4 Hz, 1H), 8.96 (d, *J* = 5.0 Hz, 1H), 8.38 (t, 1H), 8.20 (d, 1H), 8.06 (d, 1H), 7.76 (d, *J* = 2.3 Hz, 1H), 7.61 – 7.52 (m, 2H), 7.48 – 7.38 (m, 1H), 4.66 (d, *J* = 6.3 Hz, 2H). ¹³C NMR (101 MHz, Chloroform-d) δ 162.91, 162.64, 159.41, 157.96, 155.96, 146.08, 135.49, 134.27, 134.21, 132.72, 132.17, 131.77, 127.84, 127.15, 126.84, 120.46, 118.87, 118.39, 39.10. ESI-MS calculated for C₁₉H₁₃Br₂ClN₃O₃, 523.90 [M+H], observed 523.67. HPLC purity 92.4%.

2,4-Dibromo-6-(nicotinamidomethyl)phenyl 2-chlorobenzoate, 41.

The required phenol, *N*-(3,5-dibromo-2-hydroxybenzyl)nicotinamide was prepared in two steps from (2-(benzyloxy)-3,5-dibromophenyl)methanamine and nicotinic acid as described for *N*-(3,5-dibromo-2-hydroxybenzyl)-2-nitrobenzamide, providing the desired product (0.048g, 17%, two steps). ¹H-NMR (400 MHz, Chloroform-d) δ 9.03-8.91 (m, 1H), 8.81-8.71 (m, 1H), 8.15 (d, *J* = 8.1 Hz, 1H), 7.61 (d, *J* = 2.3 Hz, 1H), 7.42 (dd, *J* = 7.8, 5.0 Hz, 1H), 7.31 (d, *J* = 2.4 Hz, 1H), 7.03 (bs, 1H), 4.59 (d, *J* = 6.4 Hz, 2H). This

product was reacted with 2-chlorobenzoyl chloride according to the procedure provided for 2,4-dibromo-6-((2 nitrobenzamido)methyl)phenyl 2-chlorobenzoate, affording 4.2 mg of the desired product (6.5% yield). ¹H NMR (400 MHz, CDCl₃) δ 8.97 (s, 1H), 8.71 (s, 1H), 8.21 (dd, 1H), 8.07 (d, *J* = 8.1 Hz, 1H), 7.77 (d, *J* = 2.3 Hz, 1H), 7.62 (d, *J* = 2.3 Hz, 1H), 7.58 – 7.50 (m, 2H), 7.47 – 7.39 (m, 1H), 7.39 – 7.33 (m, 1H), 6.80 (t, 1H), 4.63 (s, 2H). ¹³C NMR (101 MHz, CDCl₃) δ 165.40, 163.37, 152.55, 148.24, 146.10, 135.58, 135.21, 135.00, 134.32, 132.79, 132.64, 131.74, 127.52, 127.17, 123.63, 120.52, 118.19, 39.50. ESI-MS calculated for C₂₀H₁₄Br₂ClN₂O₅, 522.91 [M+H], observed 522.97. HPLC purity 89.5%.

2,4-Dibromo-6-(picolinamidomethyl)phenyl 4-(2,5-dioxo-2,5-dihydro-1H-pyrrol-1-yl)butanoate, 42.

Prepared according to the procedure provided for 2,4-dibromo-6-((2 nitrobenzamido)methyl)phenyl 2-chlorobenzoate from *N*-(3,5-dibromo-2-hydroxybenzyl)picolinamide, affording 35.7 mg of the desired product (25.1% yield). ¹H NMR (400 MHz, CDCl₃) δ 8.53 (dd, *J* = 4.8, 1.3 Hz, 1H), 8.41 (s, 1H), 8.19 (dd, *J* = 7.8, 1.2 Hz, 1H), 7.86 (td, *J* = 7.7, 1.7 Hz, 1H), 7.66 (d, *J* = 2.3 Hz, 1H), 7.53 (d, *J* = 2.3 Hz, 1H), 7.47 – 7.39 (m, 1H), 6.72 (s, 2H), 4.59 (d, *J* = 6.4 Hz, 2H), 3.68 (t, *J* = 6.7 Hz, 2H), 2.70 (t, *J* = 7.3 Hz, 2H), 2.10 – 1.98 (m, 2H). ¹³C NMR (101 MHz, CDCl₃) δ 170.94, 170.02, 164.39, 149.49, 148.32, 146.02, 137.56, 134.94, 134.82, 134.31, 132.05, 126.56, 122.53, 119.96, 118.15, 38.75, 36.98, 31.20, 23.79. ESI-MS calculated for C₂₁H₁₈Br₂N₃O₅, 549.96 [M+H], observed 549.92. HPLC purity 89.7%.

(S)-2-(3,5-Dibromo-2-hydroxyphenyl)-N-(2-oxotetrahydrofuran-3-yl)acetamide.

To a solution of 2-(3,5-dibromo-2-hydroxyphenyl)acetic acid (0.750g, 2.42mmol) and L-Homoserine lactone hydrobromide (0.881g, 4.84mmol) in DMF (12.1mL) was added HATU (1.103g, 2.90mmol) followed by *i*-Pr₂NEt (1.3mL, 7.26mmol). The resulting mixture was allowed to stir at room temperature overnight, was diluted with EtOAc, washed with water, 1M HCl and brine, dried over Na₂SO₄ and concentrated to dryness. The residue was purified by flash column chromatography using a gradient from hexanes to EtOAc to provide the desired product (0.430g, 45%). ¹H-NMR (400 MHz, Chloroform-d) δ 8.68 (s, 1H), 7.55 (d, J = 2.3 Hz, 1H), 7.21 (d, J = 2.3 Hz, 1H), 6.92 (d, J = 6.1 Hz, 1H), 4.61-4.52 (m, 1H), 4.48 (t, J = 9.1 Hz, 1H), 4.36-4.25 (m, 1H), 3.62 (ABq, Δ_{VAB} = 11.3 Hz, J_{AB} = 12.3 Hz, 2H), 2.85-2.75 (m, 1H), 2.25-2.11 m, 1H).

2,4-Dibromo-6-(2-oxo-2-((2-oxotetrahydrofuran-3-yl)amino)ethyl)phenyl 4-(2,5-dioxo-2,5-dihydro-1H-pyrrol-1-yl)butanoate, 43.

Prepared according to the procedure provided for 2,4-dibromo-6-(2-((2-nitrophenyl)amino)-2-oxoethyl)phenyl 2-chlorobenzoate from (*S*)-2-(3,5-dibromo-2-hydroxyphenyl)-*N*-(2-oxotetrahydrofuran-3-yl)acetamide, affording 12.5 mg of the desired product (61% yield). ¹H NMR (400 MHz, Chloroform-d) δ 7.67 (d, J = 2.3 Hz, 1H), 7.58 (d, J = 2.3 Hz, 1H), 7.14 (s, 1H), 6.77 (s, 2H), 4.59 – 4.48 (m, 1H), 4.44 (t, 1H), 4.32 – 4.21 (m, 1H), 3.77 – 3.64 (m, 2H), 2.89 – 2.79 (m, 1H), 2.84 – 2.67 (m, 2H), 2.20 – 2.01 (m, 2H). ¹³C NMR (101 MHz, Chloroform-d) δ 175.30, 171.77, 170.42, 169.82, 134.90, 134.56, 134.06, 131.72, 120.02, 66.36, 49.73, 37.50, 36.68, 31.16, 30.62, 30.51, 23.69. ESI-MS calculated for C₂₀H₁₉Br₂N₂O₇, 556.96 [M+H], observed 556.81. HPLC purity 92.5%.

2,4-Dibromo-6-(2-oxo-2-((2-oxotetrahydrofuran-3-yl)amino)ethyl)phenyl 3-(2,5-dioxo-2,5-dihydro-1H-pyrrol-1-yl)propanoate, 44.

Prepared according to the procedure provided for 2,4-dibromo-6-(2-((2-nitrophenyl)amino)-2-oxoethyl)phenyl 2-chlorobenzoate from (S)-2-(3,5-dibromo-2-hydroxyphenyl)-N-(2-oxotetrahydrofuran-3-yl)acetamide, affording 1.8 mg of the desired product (17% yield). ¹H NMR (400 MHz, Chloroform-d) δ 7.68 (d, J = 2.2 Hz, 1H), 7.53 (d, J = 2.2 Hz, 1H), 6.75 (s, 1H), 4.60 – 4.48 (m, 1H), 4.46 (t, J = 9.1 Hz, 1H), 4.33 – 4.21 (m, 1H), 4.15 – 3.91 (m, 2H), 3.62 – 3.47 (m, 2H), 3.12 – 2.97 (m, 2H), 2.83 – 2.71 (m, 0H), 2.75 (s, 1H), 2.25 – 2.09 (m, 1H), 1.38 – 1.23 (m, 2H), 0.89 (d, J = 12.6 Hz, 1H). ¹³C NMR (101 MHz, Chloroform-d) δ 175.23, 170.84, 169.52, 168.71, 146.18, 135.12, 134.60, 133.71, 131.50, 120.34, 118.19, 66.27, 49.62, 37.96, 33.58, 32.69, 31.85, 30.08, 29.87. ESI-MS calculated for C₁₉H₁₇Br₂N₂O₇, 542.94 [M+H], observed 542.92. HPLC purity 91.8%.

1.1. *LasR* Bioassay

The *LasR* reporter strain bioassay was performed as described previously with modifications.²³ Briefly, the assays were performed in *E. coli* strain BL21 DE3 Gold (Agilent) carrying a plasmid containing *lasR* (maintained with 100 µg/mL ampicillin) and a plasmid containing the *rsaL* promoter-driving expression of *gfp* (maintained with 50 µg/mL of kanamycin.) The reporter strain described above was kindly supplied by Bonnie L. Bassler (Princeton University). This *E. coli* strain was grown overnight at 37°C in Luria broth (LB) (Fisher) with the appropriate antibiotics. The overnight culture was subcultured 1:40 for bioassay analysis. The native *LasR* agonist, *N*-3-oxo-dodecanoyl-L-homoseriene lactone was used as a positive control for all agonist assays (EC₅₀=72.9±24.6nM) and was employed at a constant concentration of 50nM for all antagonist assays. For agonists assays, maximal % activation is reported with respect to *N*-3-oxo-dodecanoyl-L-homoseriene lactone set as 100% activation. For antagonism

assays, the previously described antagonist, (*S*)-2-(4-bromophenyl)-*N*-(2-oxotetrahydrofuran-3-yl) acetamide was used as the positive control for antagonism with an IC₅₀ of 26.31±15.7 μM.⁸ Maximal % inhibition is reported with respect to (*S*)-2-(4-bromophenyl)-*N*-(2-oxotetrahydrofuran-3-yl) acetamide set as 100% inhibition. Compounds were added to the diluted overnight reporter strain in 96-well black microplates with clear bottoms (Corning) at the starting concentrations described and titrated by serial dilution. Plates were incubated with shaking at 37°C for 4-6h and were evaluated for fluorescence (ex485/em538) and absorbance (A₆₀₀) using a Molecular Devices SpectraMax M5 microplate reader, or a FlexStation II 384 Molecular Devices for fluorescence and a MultiSkan Spectrum for absorbance measurements. Dose-response curves were fit to the data using standard nonlinear regression data fitting settings in GraphPad Prism 6, no corrections for compound purity were made. All data points are reported as mean with error describing the standard deviation.

Computational Modeling - Ligand Preparation

The triaryl series of ligands were prepared using first Maestro Elements then Maestro 10.3. The 2D structures were drawn using the 2D sketcher function in Maestro Elements. The templates for the ligands were obtained from the Perez Lab. The 2D sketches were then converted to 3D structures. Epik (an empirical pKa prediction program) was utilized to determine the charge of the molecule at pH 7.²⁴ Finally, the 3D structures were uploaded into the Maestro 10.3 and restrained minimization was run. This function is used to relax and optimize the ligand structure.

Protein Structure Preparation

The LasR crystal structure (PDB 3IX3) was prepared using the protein preparation wizard function in Maestro. The charge state of preprocessed protein was optimized at pH=7. Finally restrained minimization was performed to relax the protein structure using OPLS3 force field.²⁵

Ligand Docking

The individual ligands were docking using glide docking with extra precision (XP) and default parameters.^{26,27} The receptor grid required for docking process was generated using Van der Waals scaling factor of 1 and partial charge cutoff 0.25. Docking was performed using a ligand-centered grid using OPLS3 force field. The Glide XP Dock function performs a comprehensive systematic search for the best receptor conformations and orientations to fit the ligand. To validate the docking method, the crystal ligand of 3-OXO-C12-HSL was docked back to the pocket. The small heavy atom RMSD of 0.6Å between the docked pose and the crystal pose indicates the validity of the docking method (see online supporting information, Figure S1).

Binding Energy Calculations and Decomposition Methods

Molecular Mechanism-General Born Surface Area (MM-GBSA) binding energies were calculated on the complexes from the docking. OPLS3 force field²⁵, VSGB 2.0 solvation model²⁸ and the default Prime procedure was used for the MM-GBSA calculation. The default procedure consists of three steps: Receptor alone (minimization), Ligand alone (minimization), Receptor-ligand complex (minimization). The total binding energy equation is: $\Delta G_{(\text{bind})} = E_{\text{complex}(\text{minimized})} - (E_{\text{ligand}(\text{minimized})} + E_{\text{receptor}(\text{minimized})}$. The docked complex with the MM-GBSA binding energy is listed in Figure S2 of the online supporting information. The residue breakdown of the $\Delta G_{(\text{bind})}$ were then used in

combination with 2D interaction diagrams to identify and compare key residues within the binding pocket. Note that since the binding entropy is not included in our analysis, the binding energies by MMGBSA may over-estimate the binding free energy (i.e. the binding affinity). But when the entropic term of different ligands are comparable, the relative MMGBSA binding energies can be used to estimate the relative binding free energy for ranking ligands.²⁹ The correlation coefficient between the experimental binding free energy (calculated from the EC₅₀) and the MMGBSA binding energies is 0.5572, which is reasonable (see online supporting information, Figure S3).

Supplemental Figures

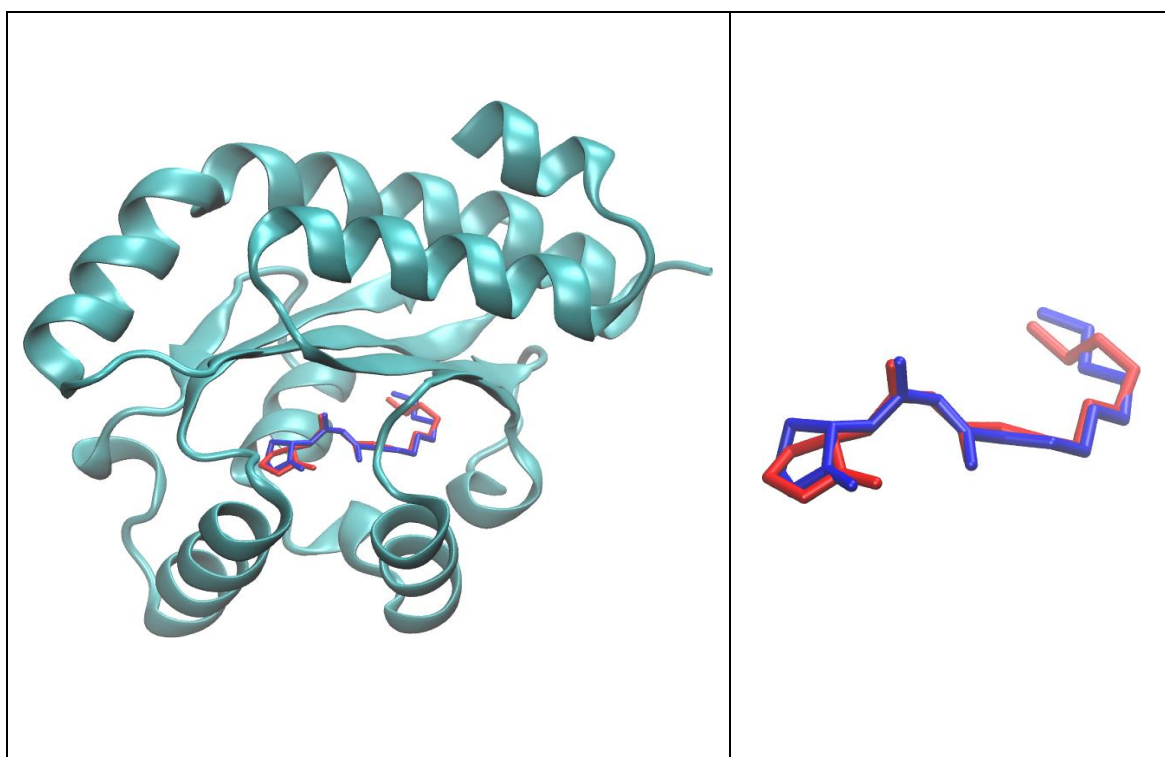


Figure 9. Comparison of the crystal pose and the Glide XP docked pose of 3-OXO-C12-HSL.

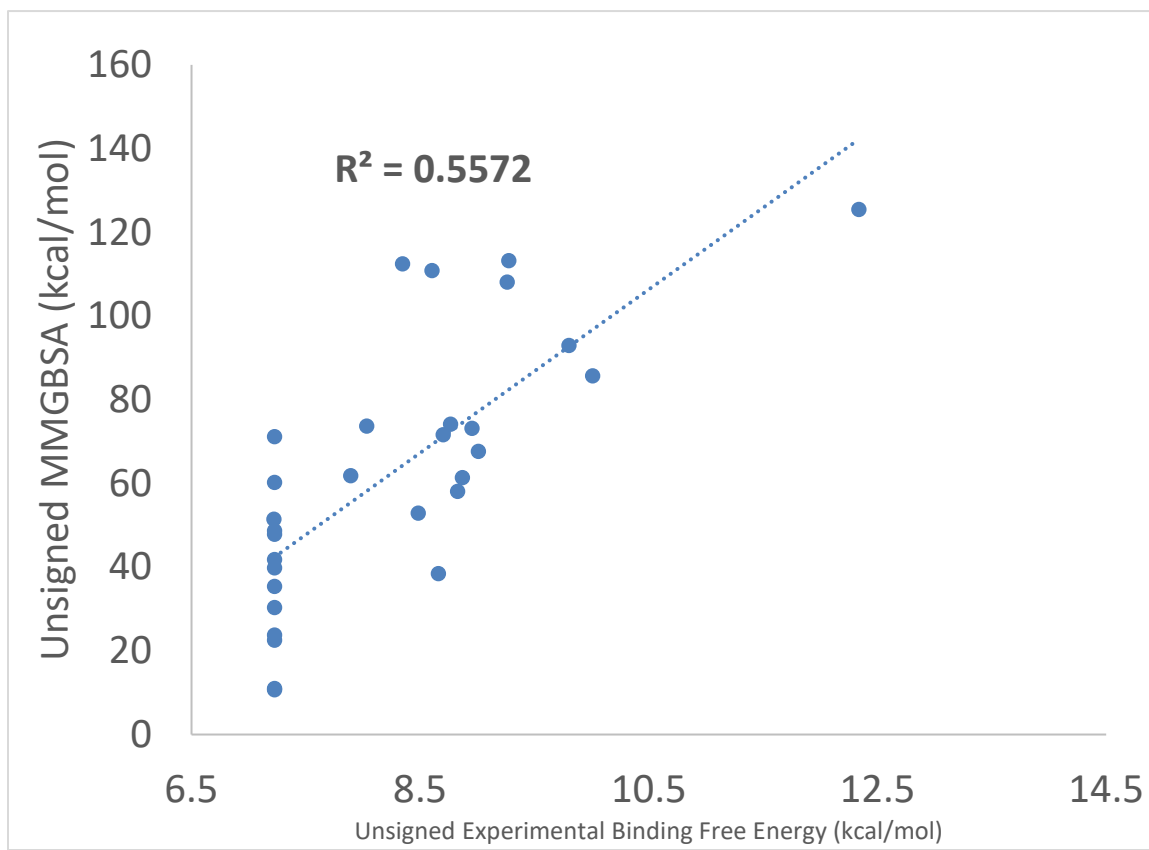


Figure 10. Correlation plot between the experimental binding free energy, and the calculated MMGBSA binding energy for the ligands in Figure S2.

	3	32	33
	Nitro Group	Nitrogen	Florine
	(kcal/mol)	(Kcal/mol)	(kcal/mol)
56 TYR	-4.9	-7.3	-6.0
60 TRP	-2.9		-2.4
64 TYR	-2.8		-3.9
73 ASP			-1.1
88 TRP		-5.8	
101 PHE	-3.1		-2.8
105 ALA			-0.6
110 LEU	-2.0		-2.1
MMGBSA	-74.2	-80.5	-85.6
Experimental Value	-8.8	-7.2	-10.0

Figure 11. Key residues contributing to the binding energy for the 3 C ring analogs (3, 32 and 33).

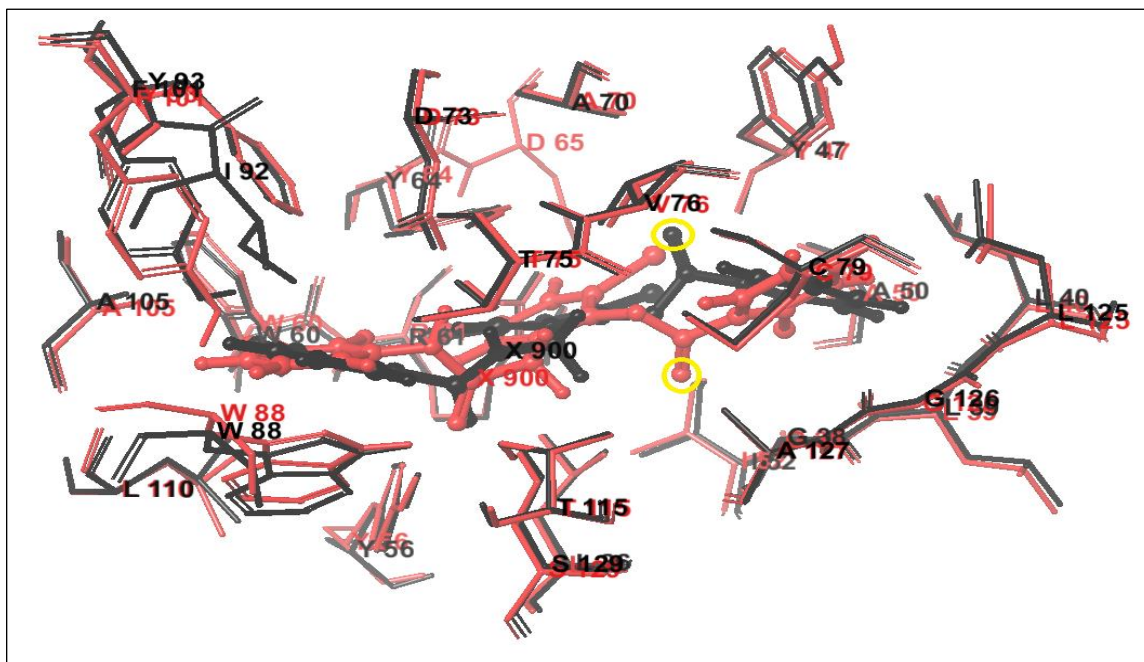
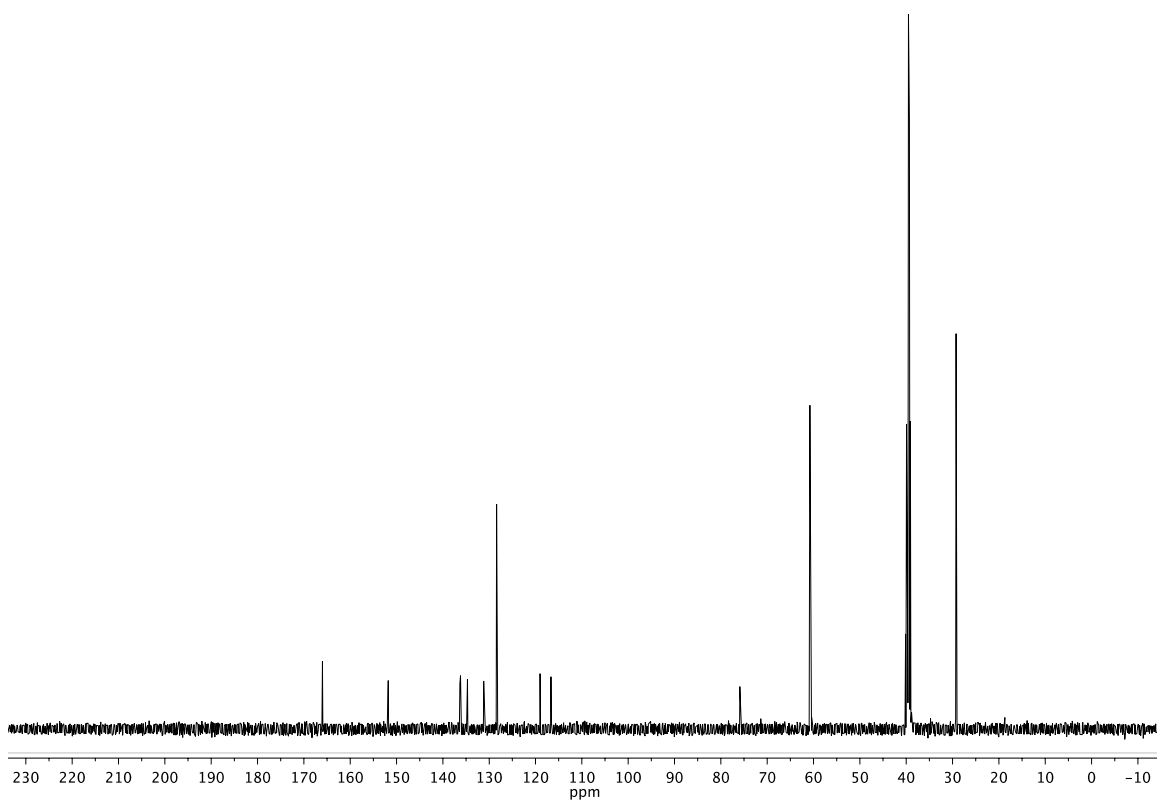
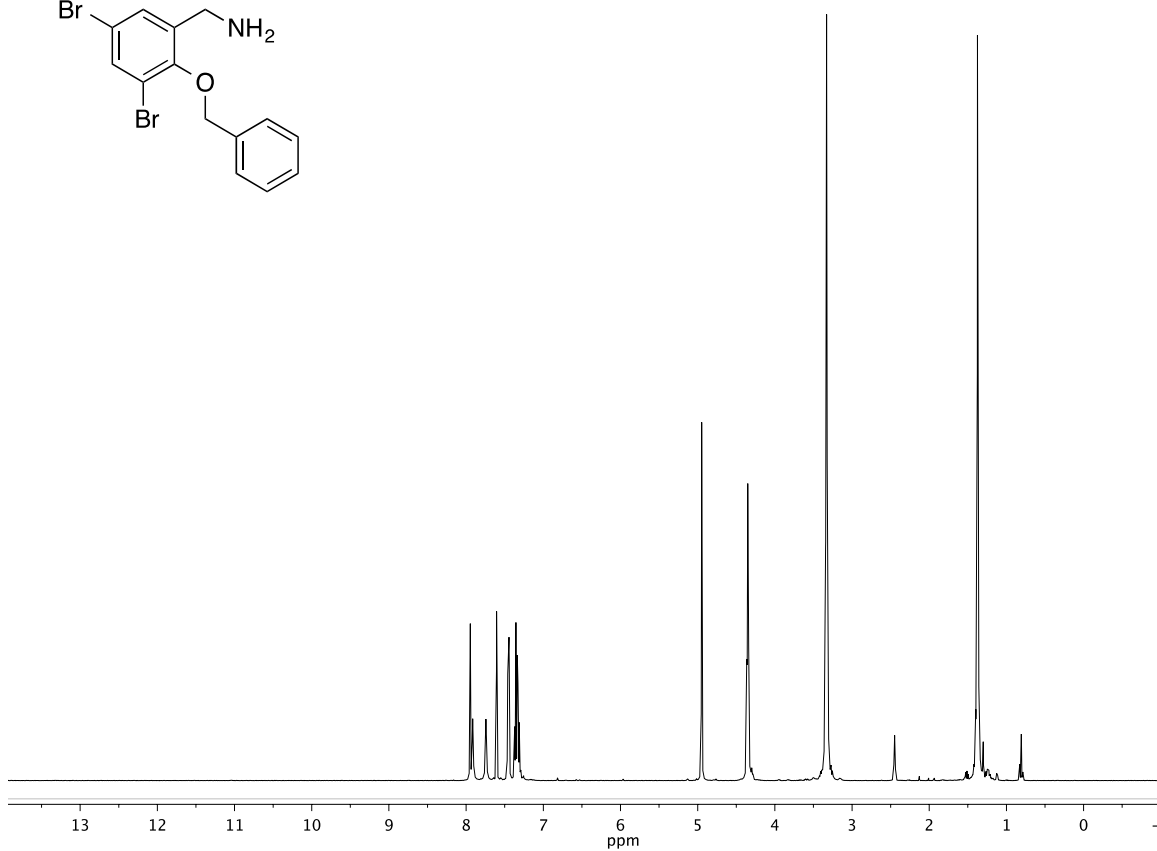
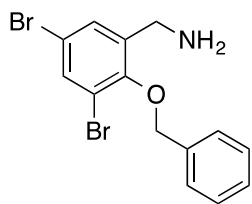


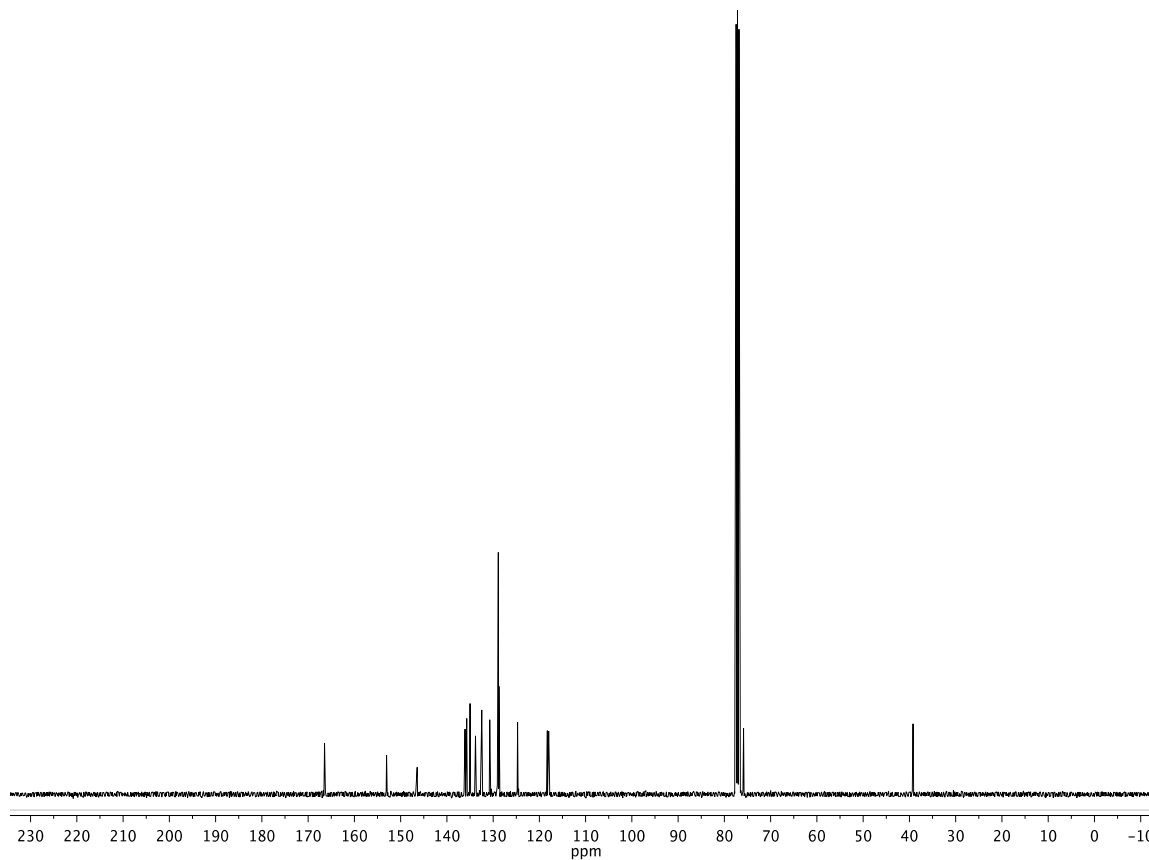
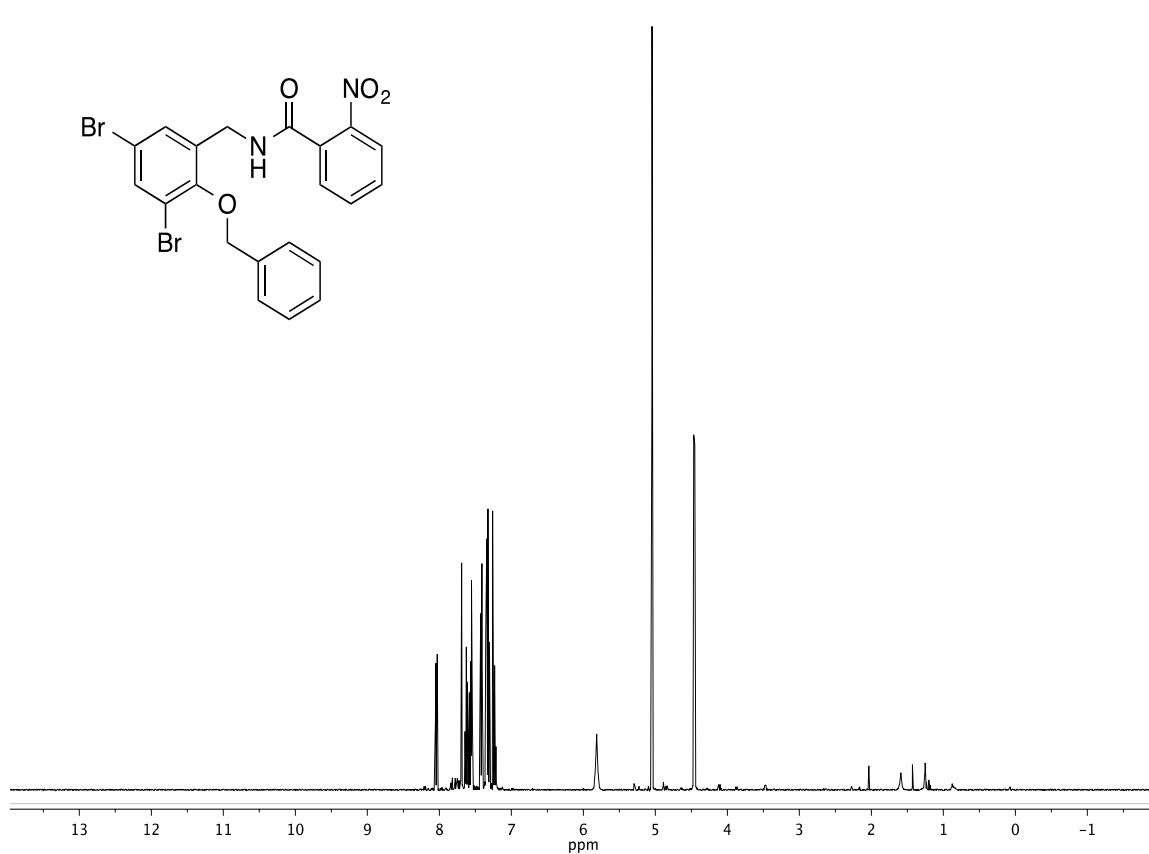
Figure 12. The superimposed ligands **33** (red) and **39** (black) in the binding pockets. The bonding poses were very similar, except for the oxygen (yellow) within the amide which showed a 180° flip.

¹H-NMR and ¹³C-NMR Spectra for all Final Compounds and Key Intermediates

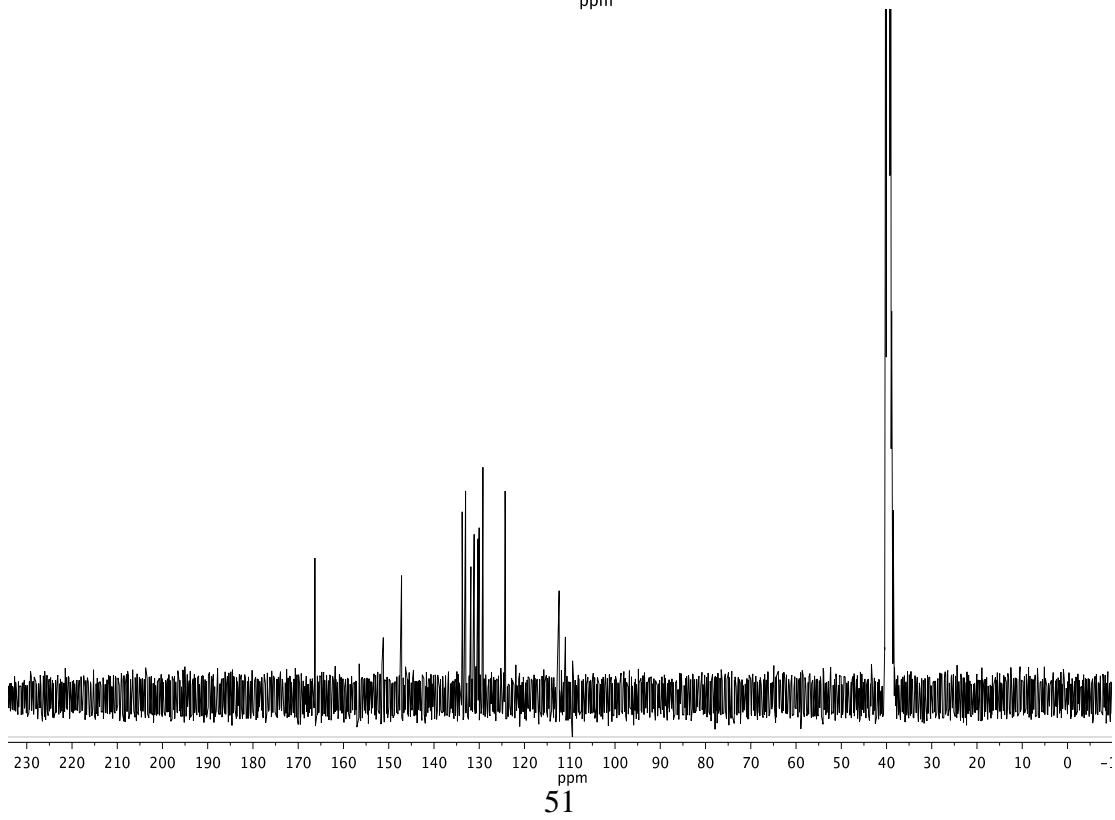
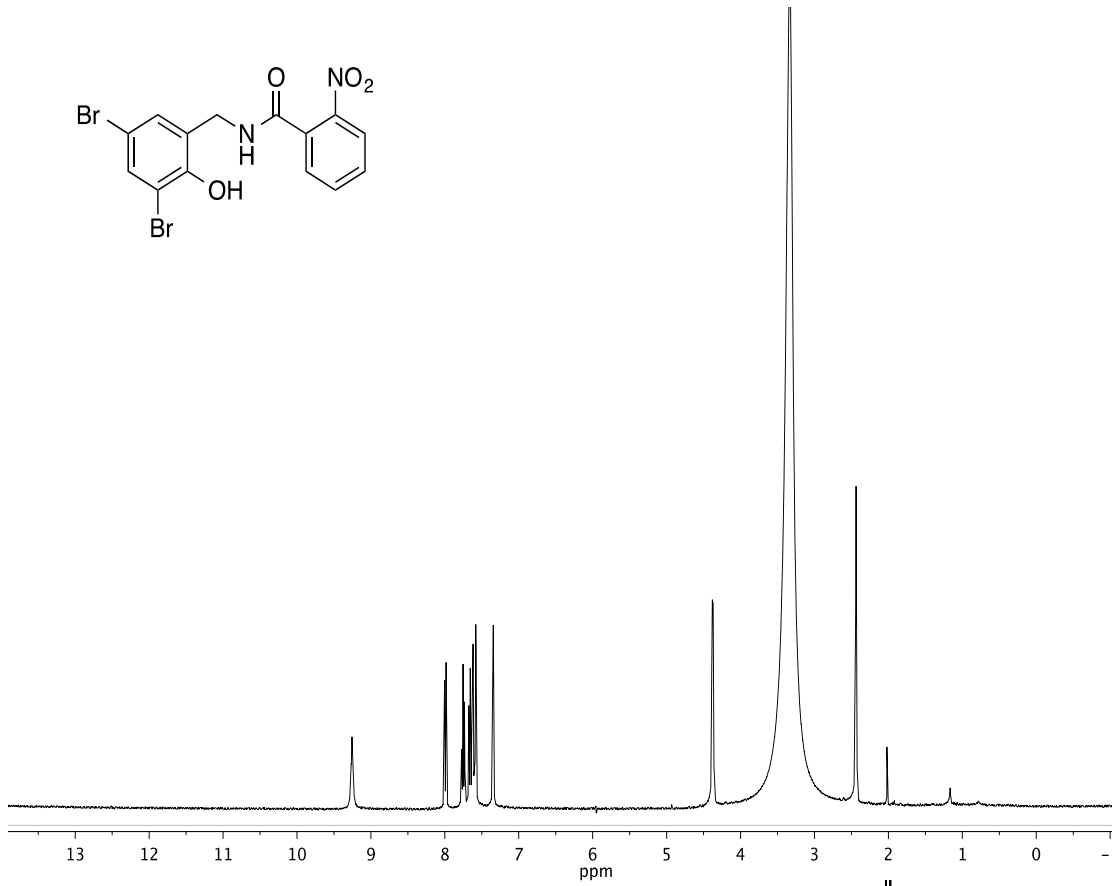
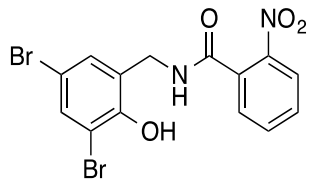
II-85, (2-(benzyloxy)-3,5-dibromophenyl)methanamine, SI3.



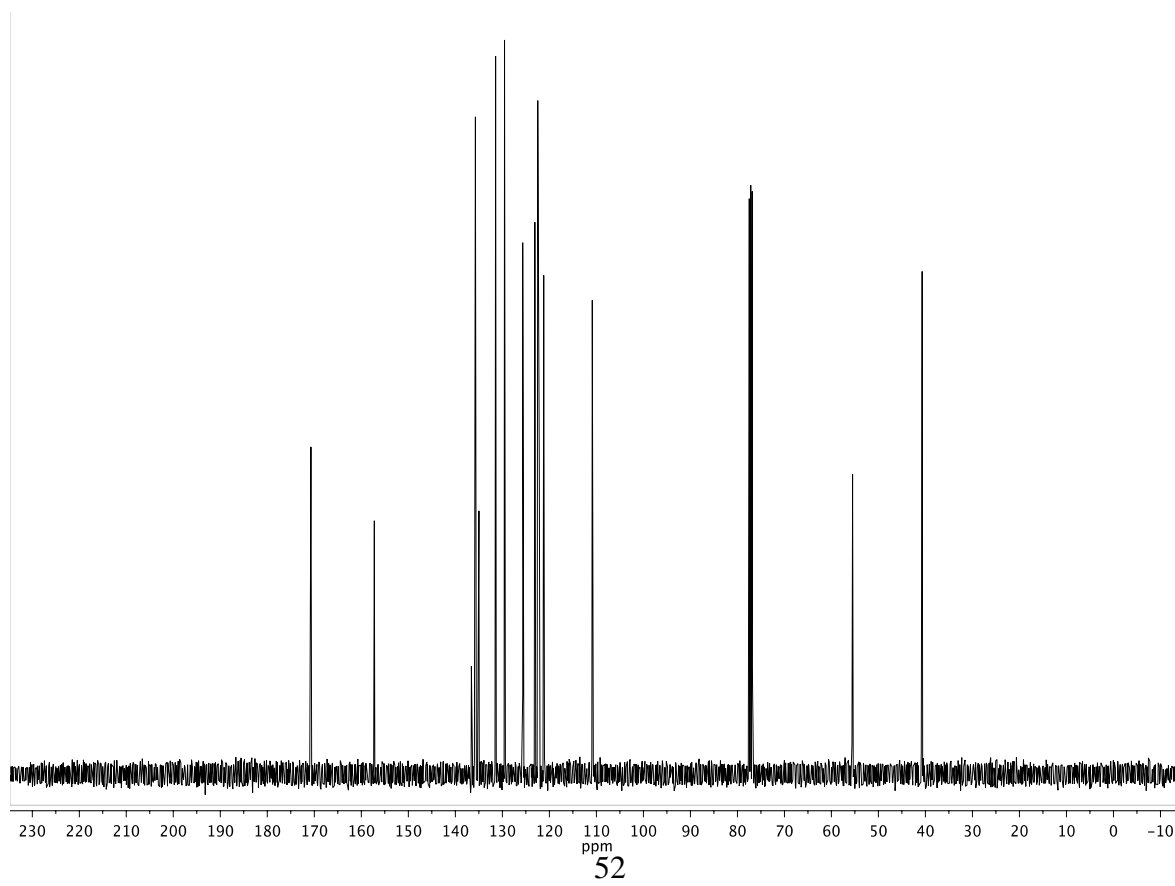
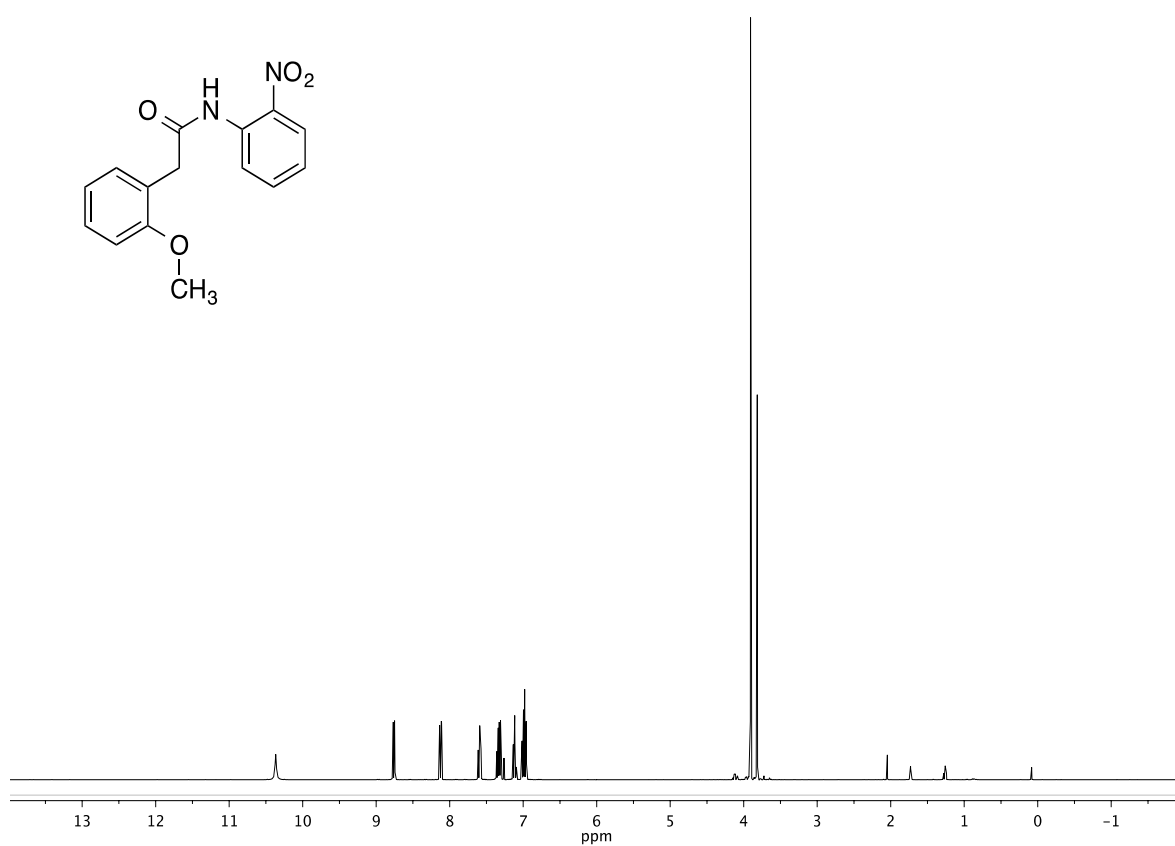
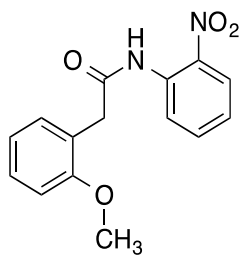
N-(2-(benzyloxy)-3,5-dibromobenzyl)-2-nitrobenzamide, SI4.

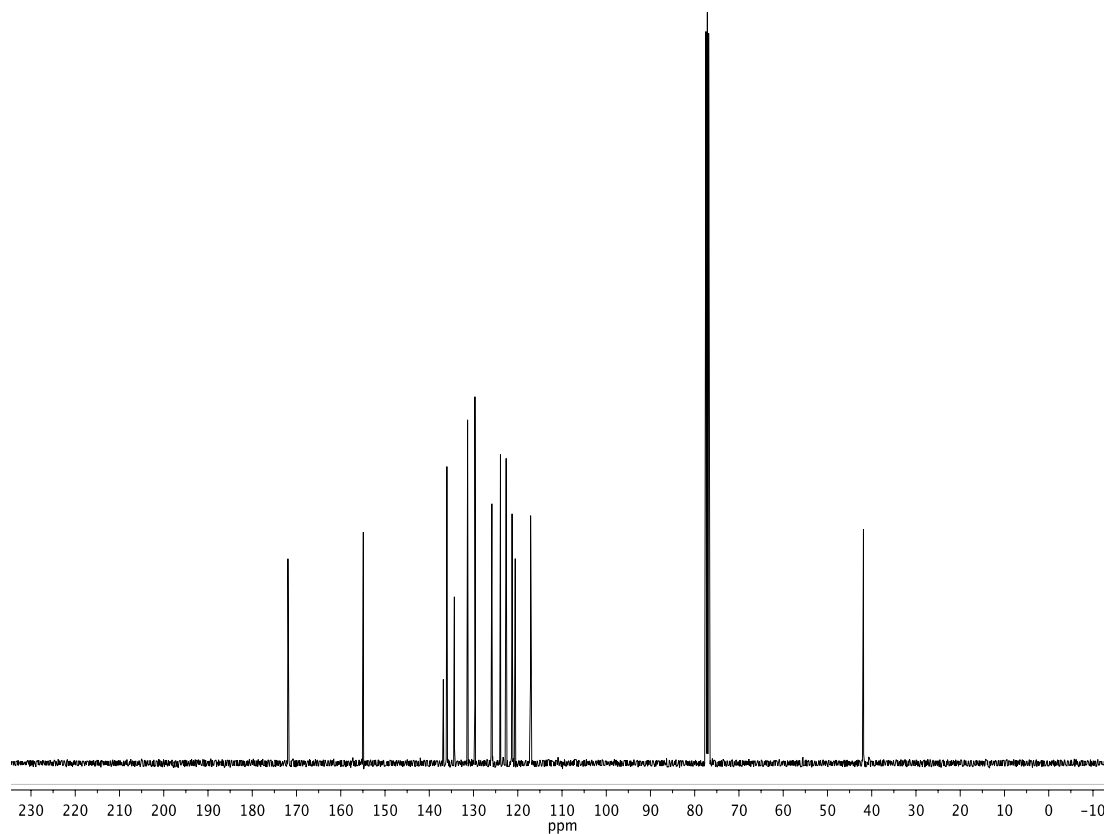
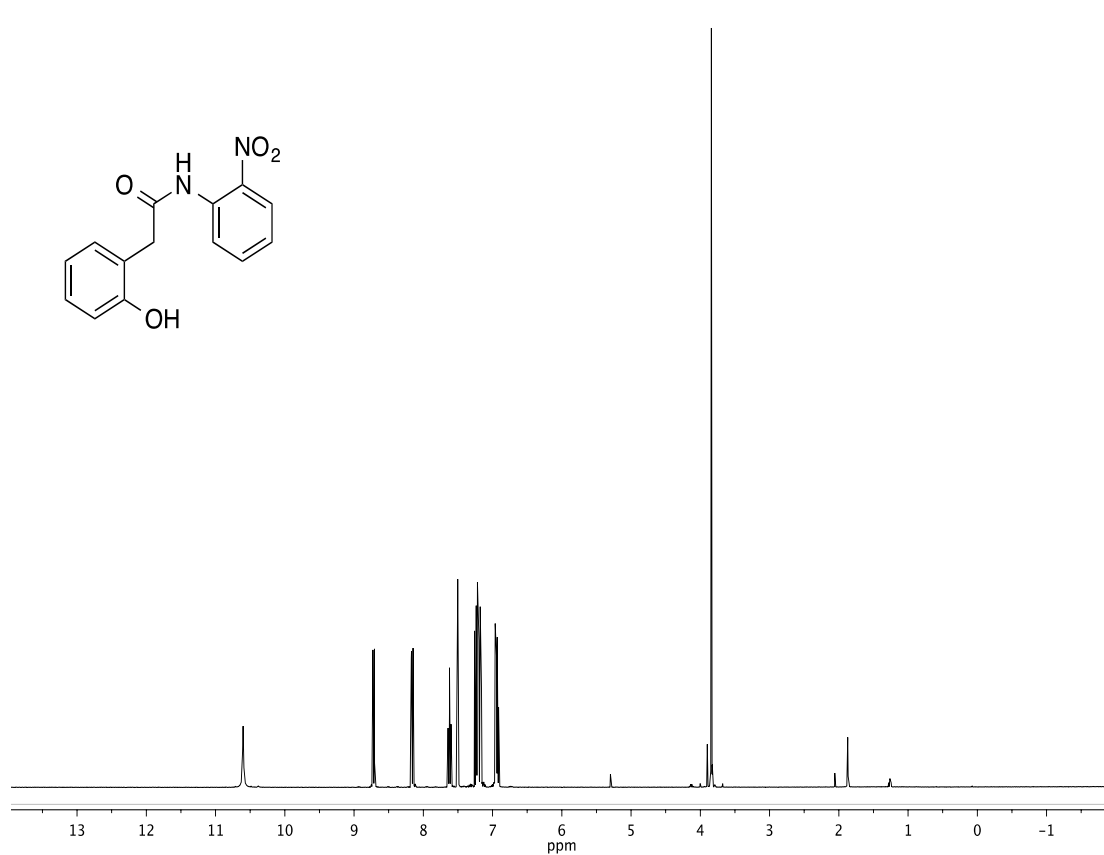
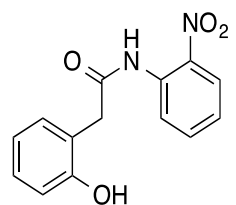


N-(3,5-dibromo-2-hydroxybenzyl)-2-nitrobenzamide, SI5.



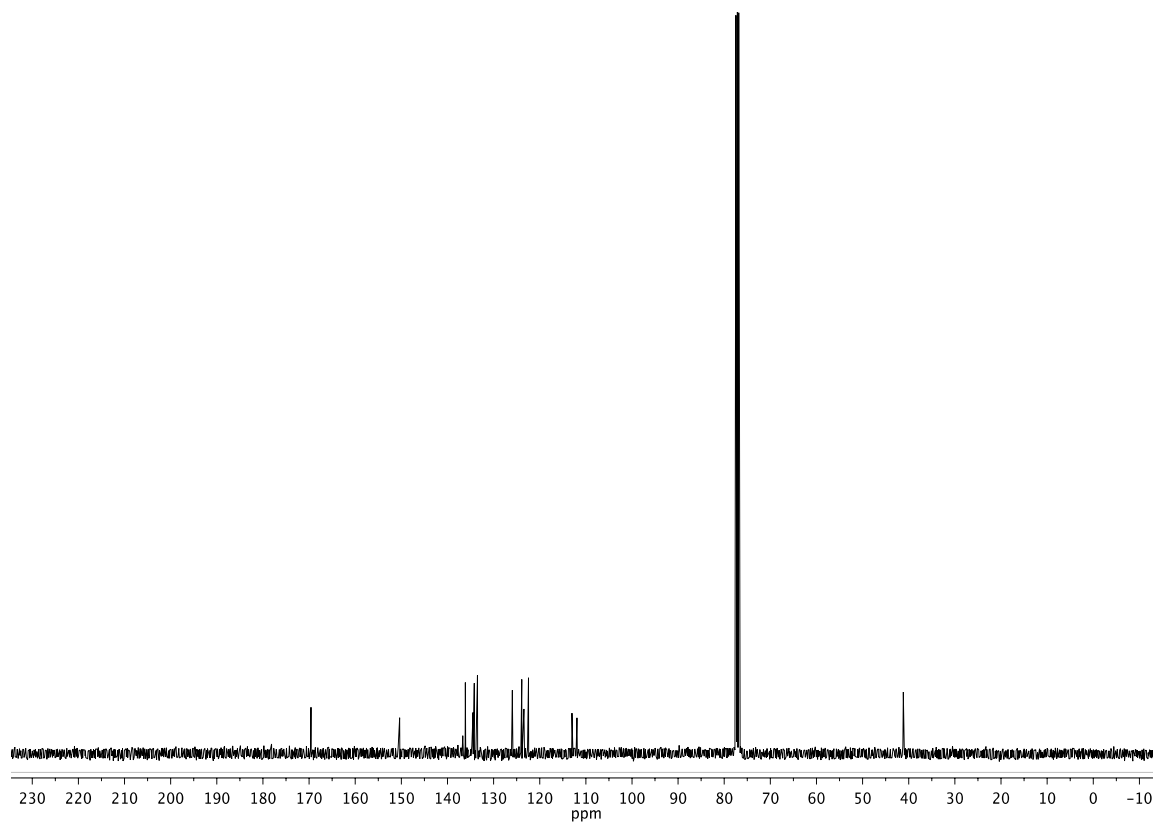
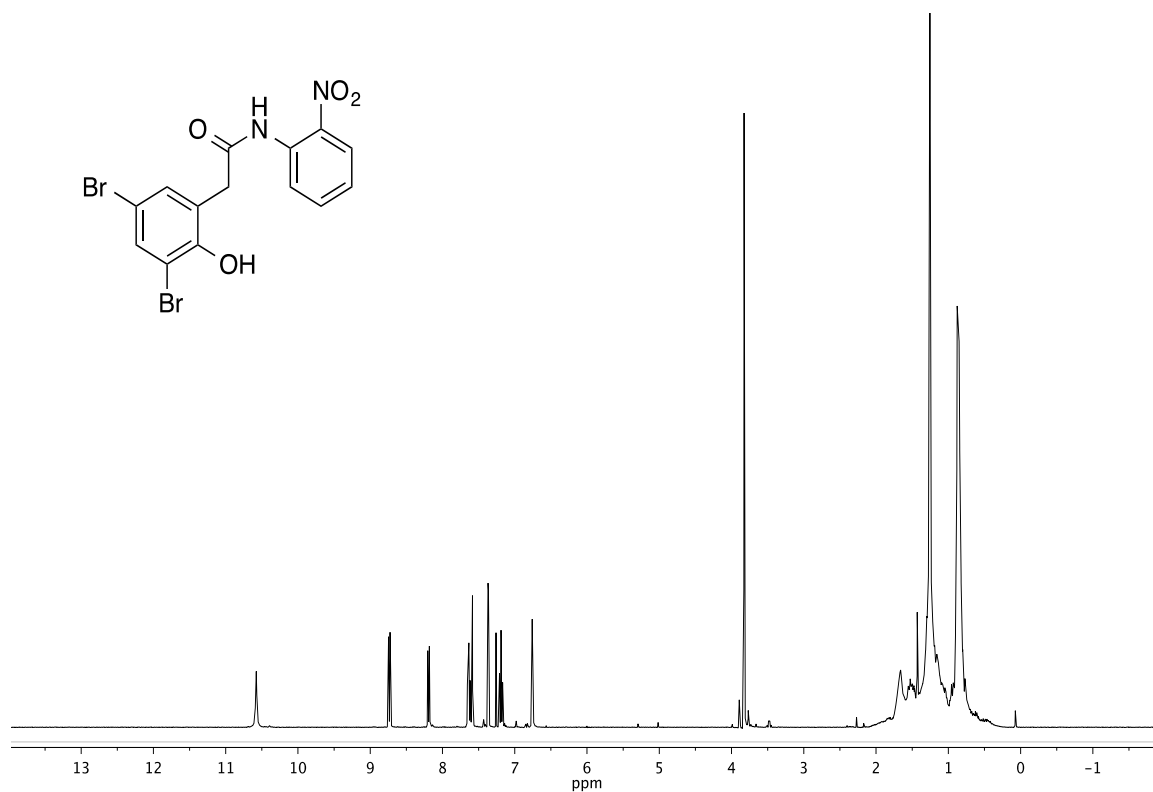
2-(2-methoxyphenyl)-*N*-(2-nitrophenyl)acetamide, SI6.



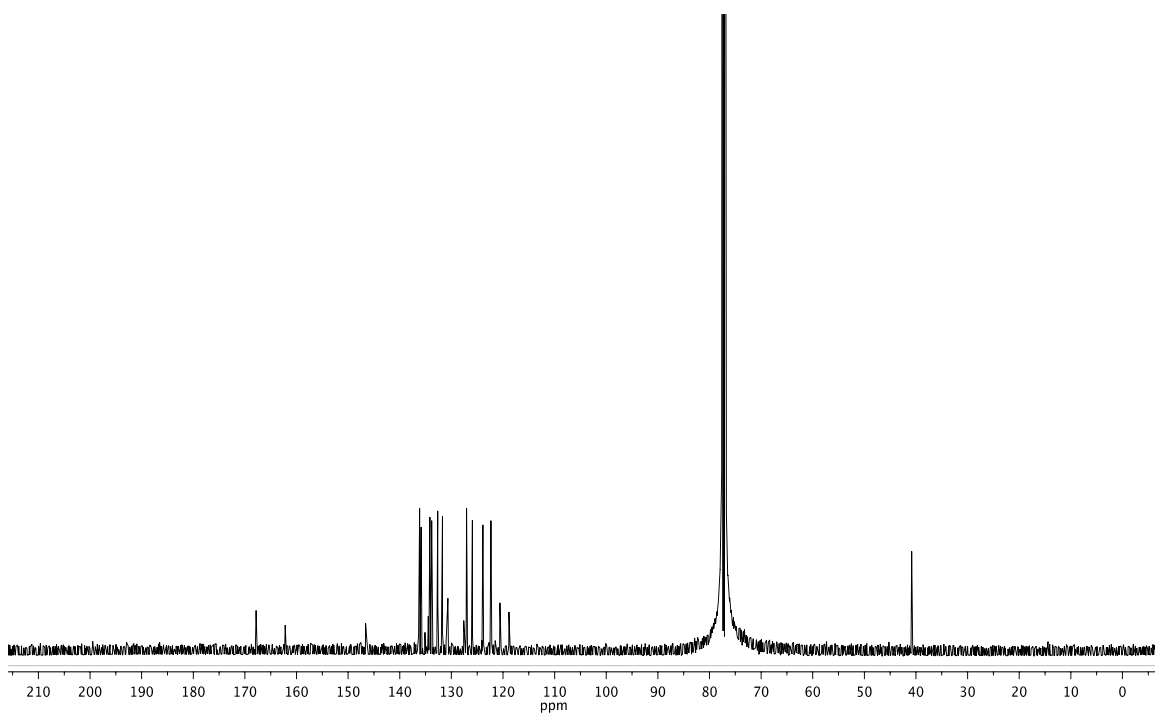
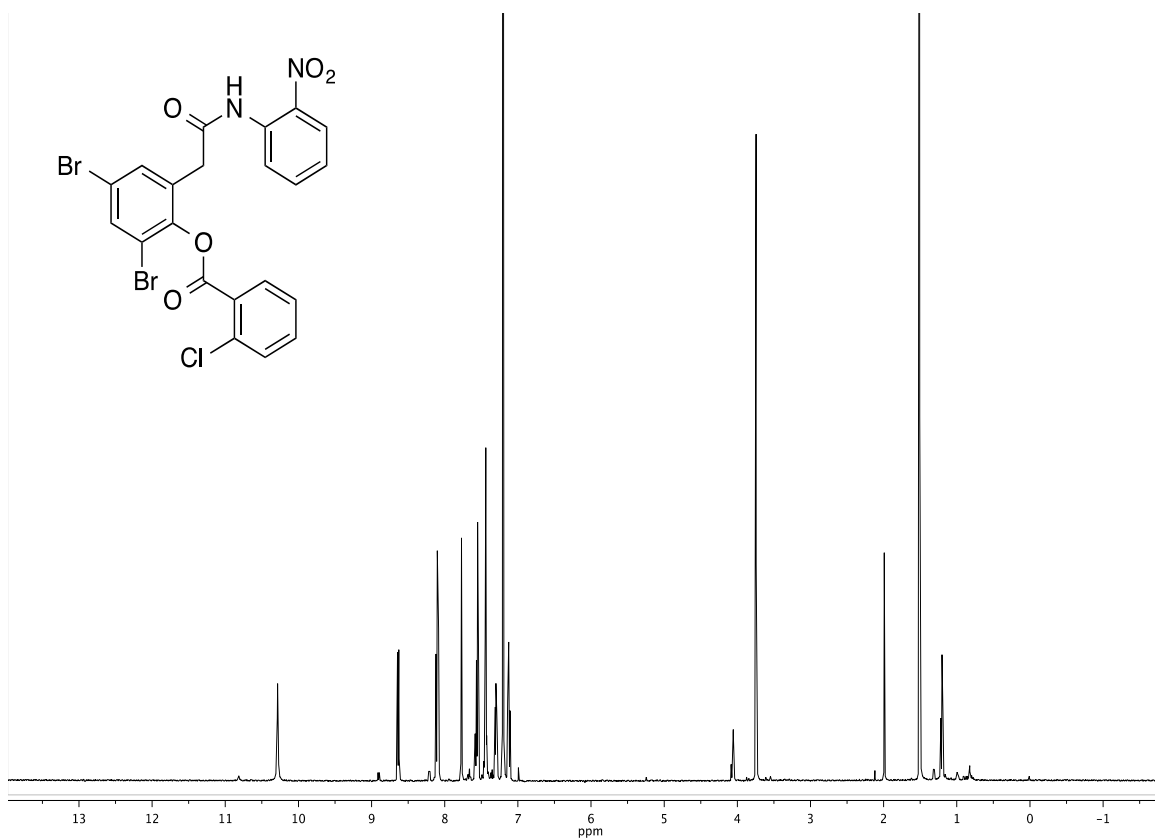


2-(2-hydroxyphenyl)-N-(2-nitrophenyl)acetamide, SI7.

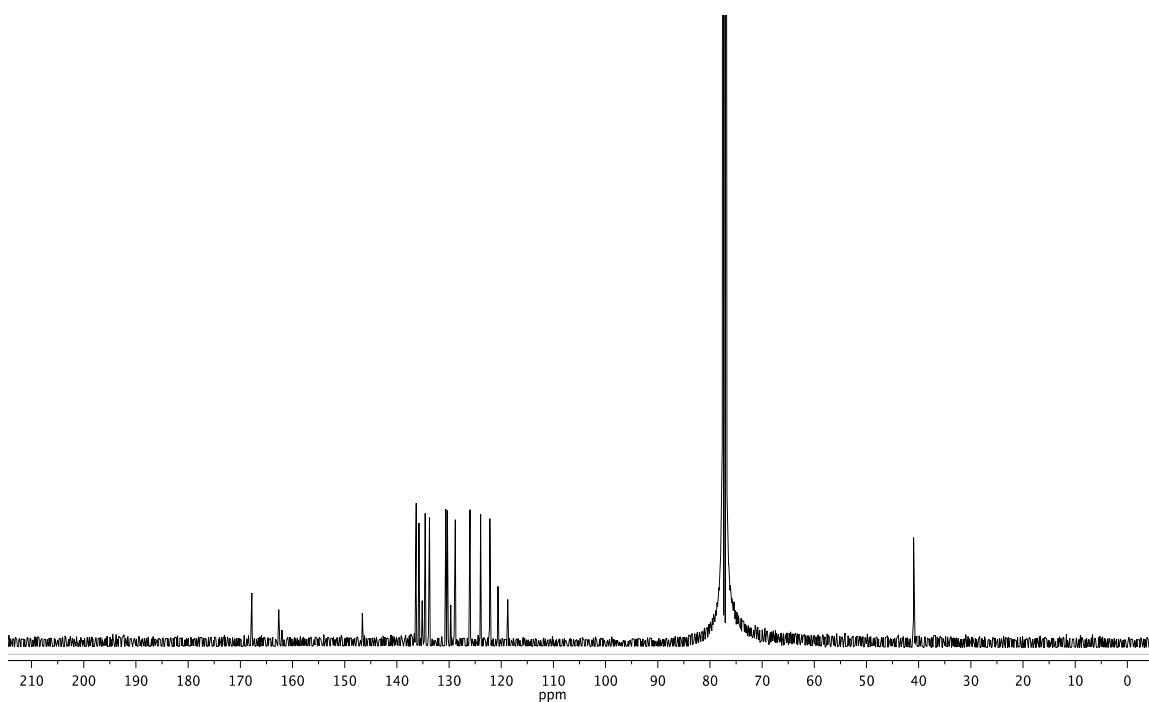
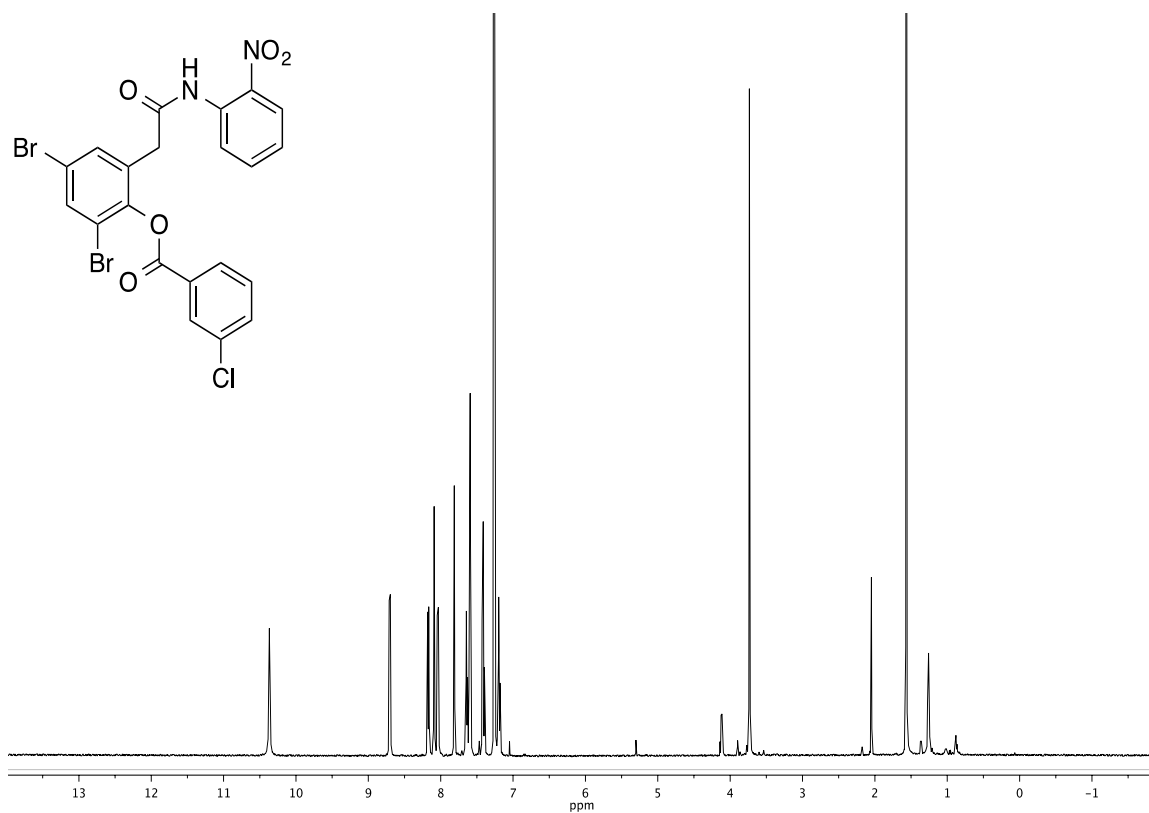
2-(3,5-dibromo-2-hydroxyphenyl)-*N*-(2-nitrophenyl)acetamide, SI8.



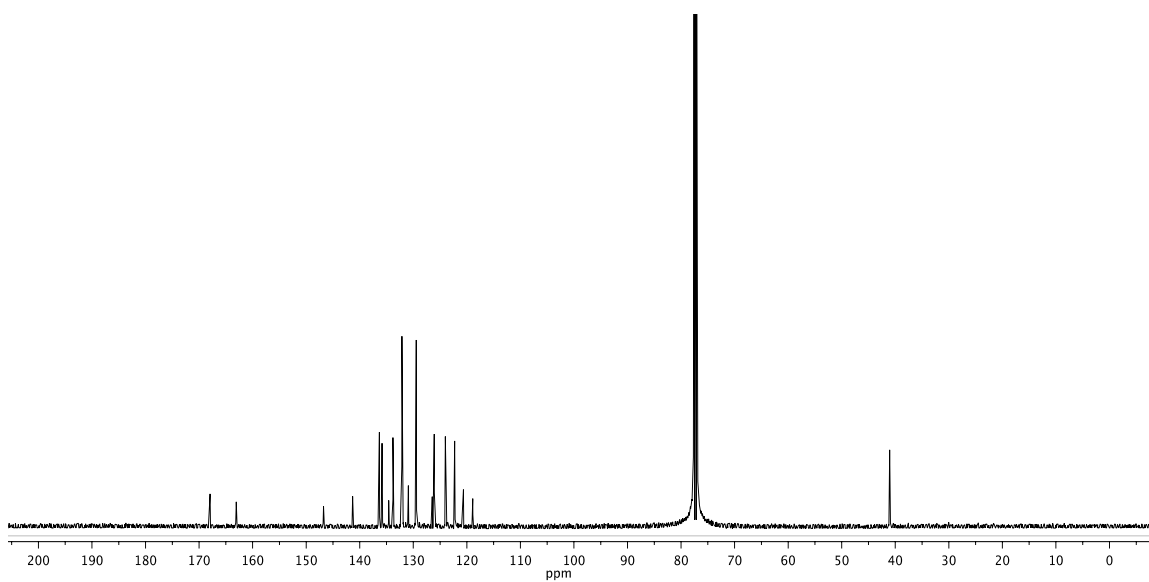
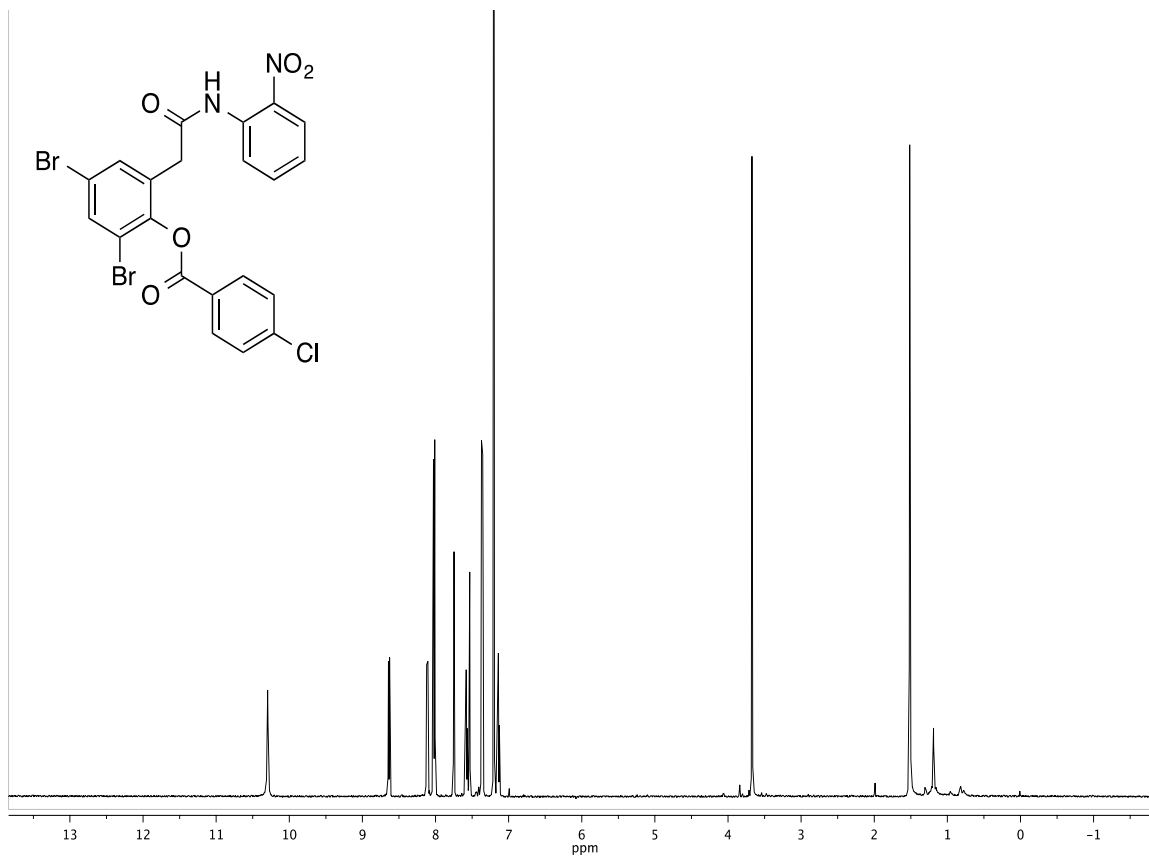
2,4-dibromo-6-(2-((2-nitrophenyl)amino)-2-oxoethyl)phenyl 2-chlorobenzoate, 3.



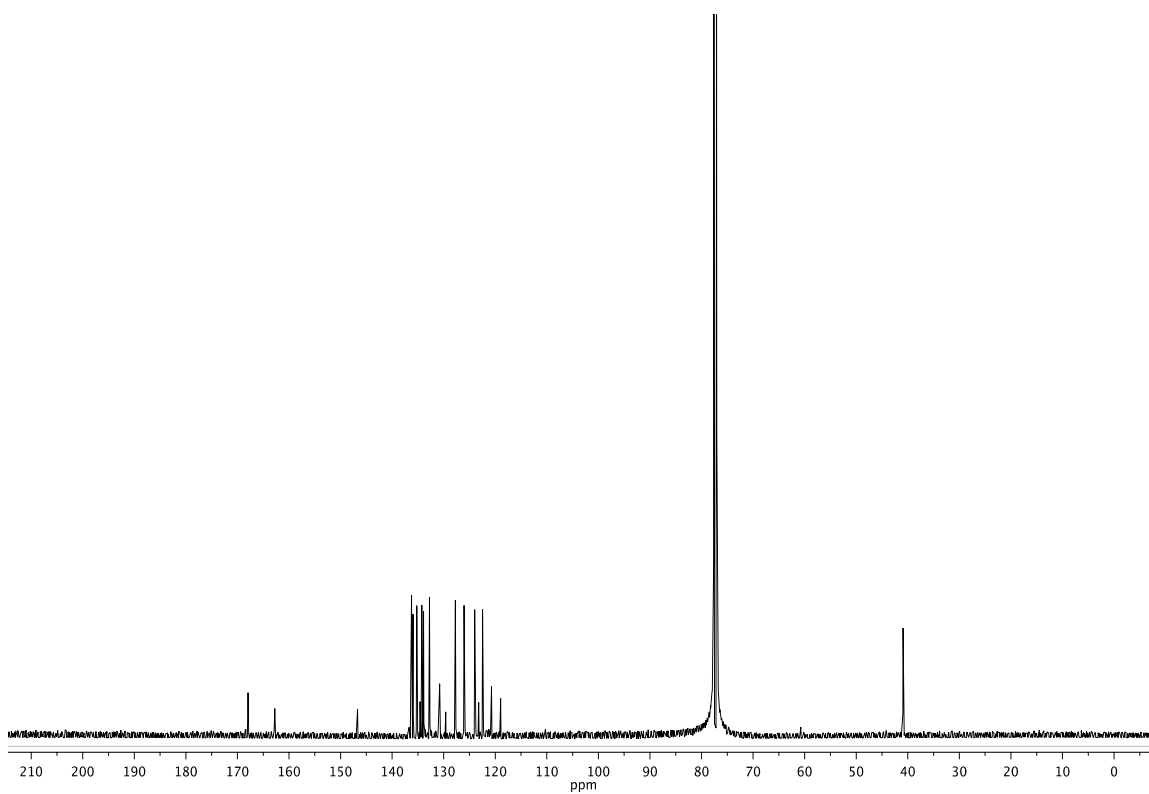
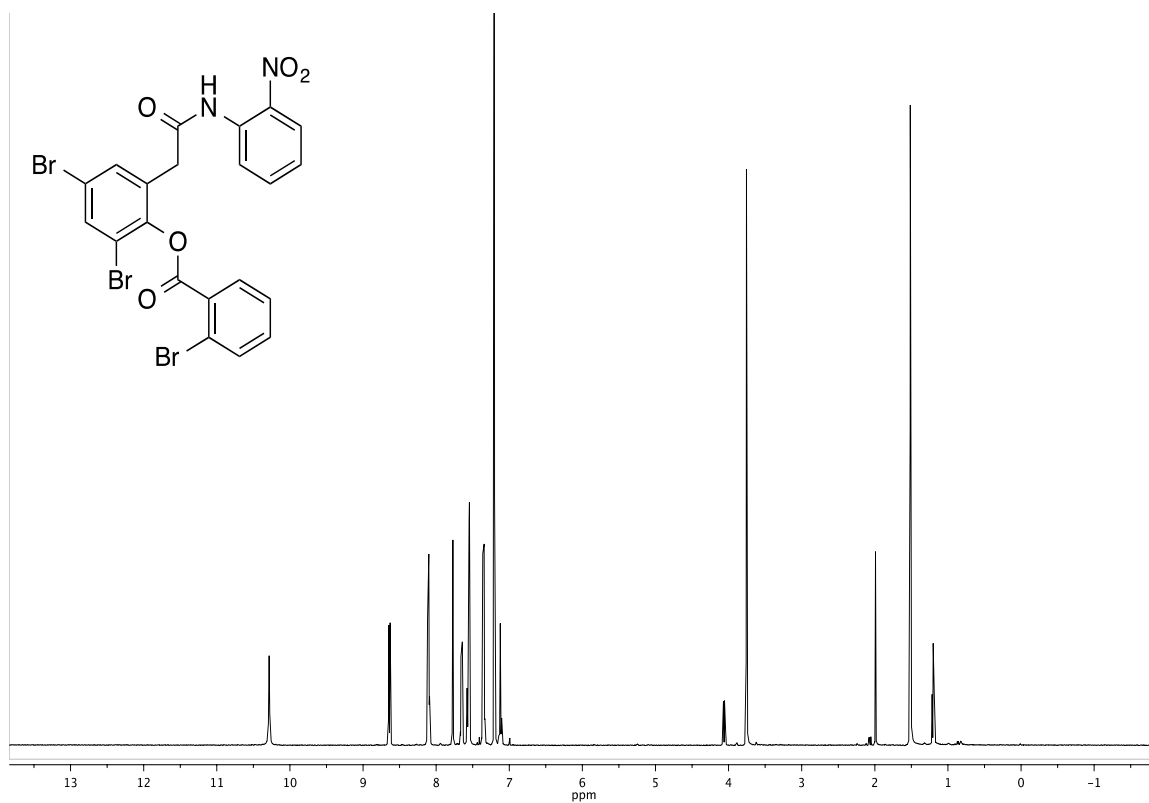
2,4-dibromo-6-(2-((2-nitrophenyl)amino)-2-oxoethyl)phenyl 3-chlorobenzoate, 13.



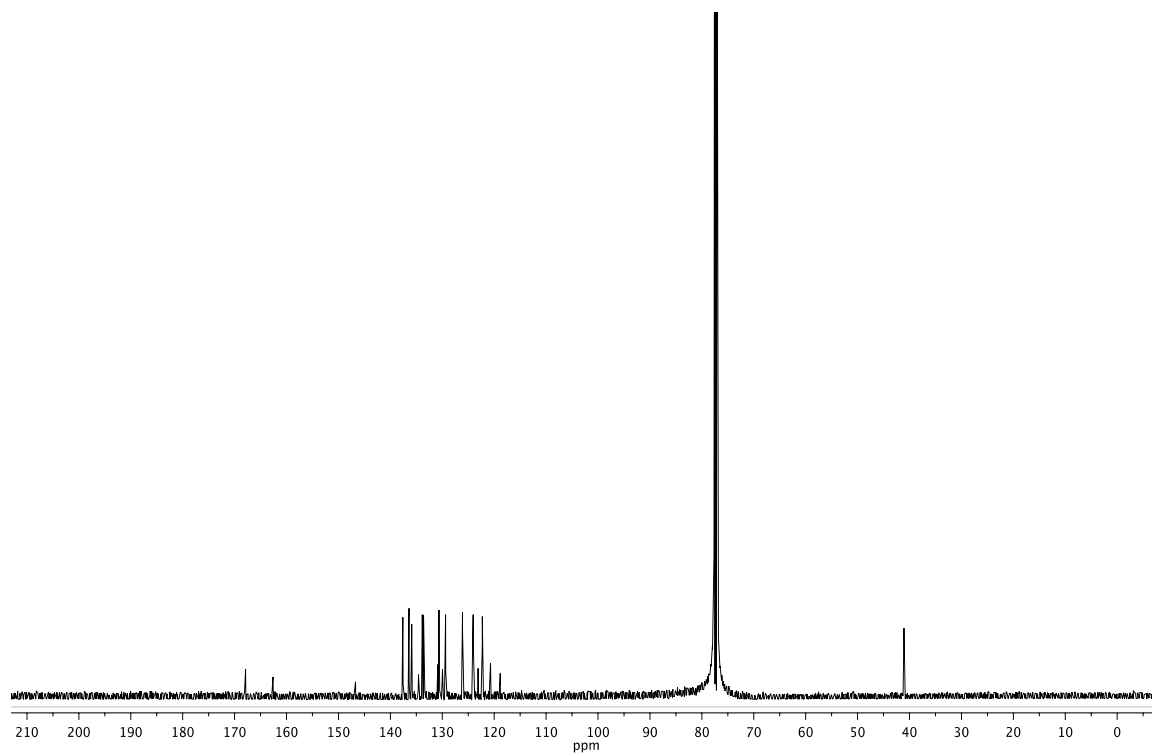
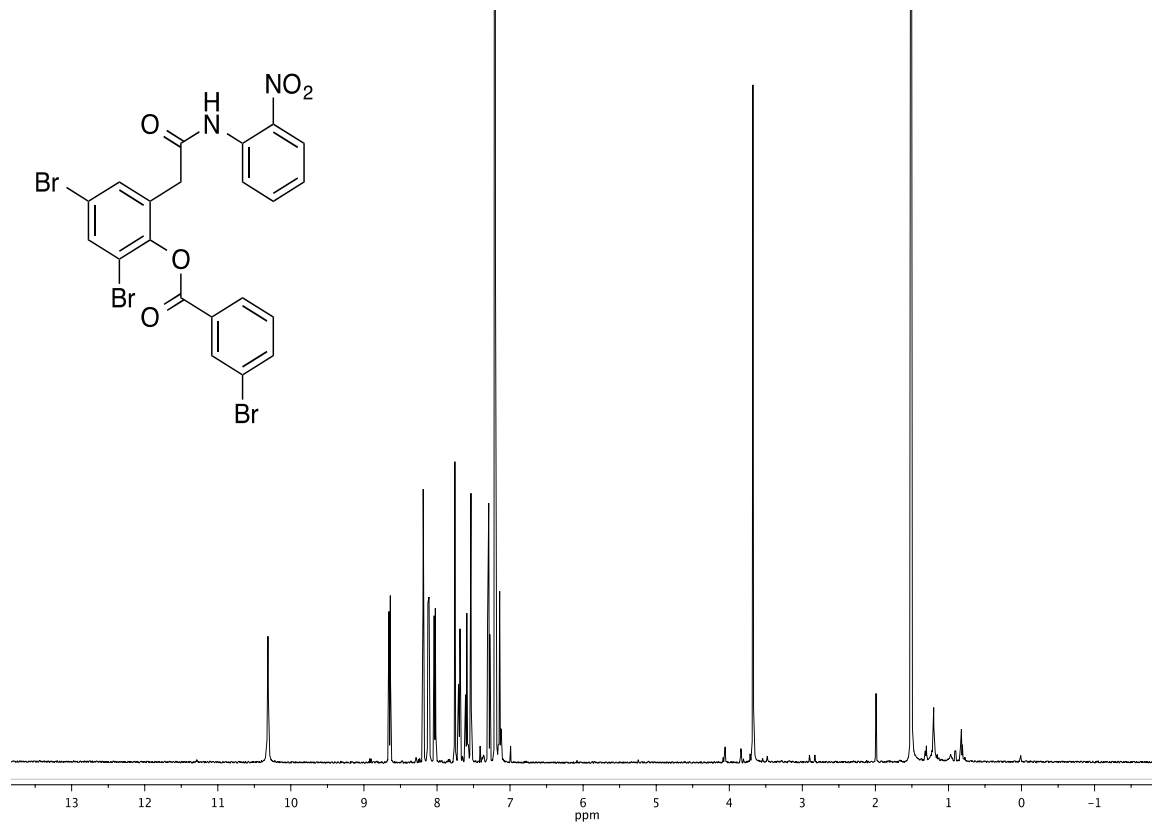
2,4-dibromo-6-(2-((2-nitrophenyl)amino)-2-oxoethyl)phenyl 4-chlorobenzoate, 14.



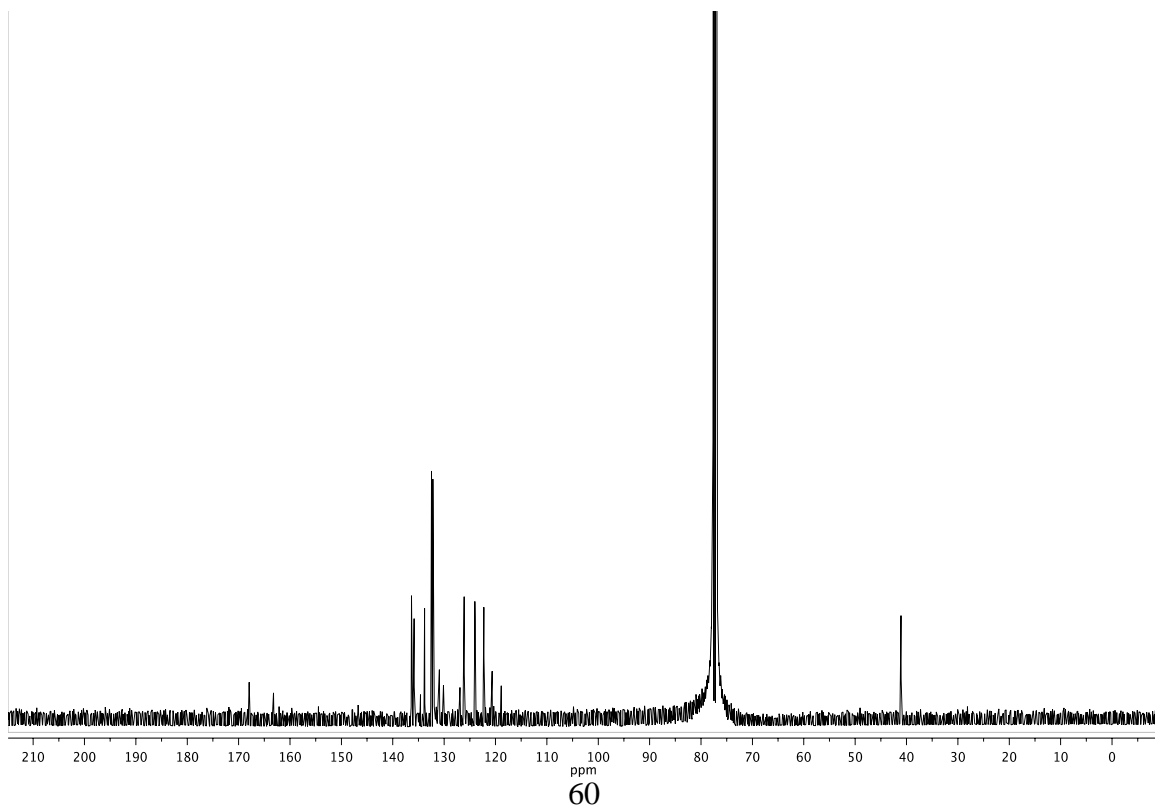
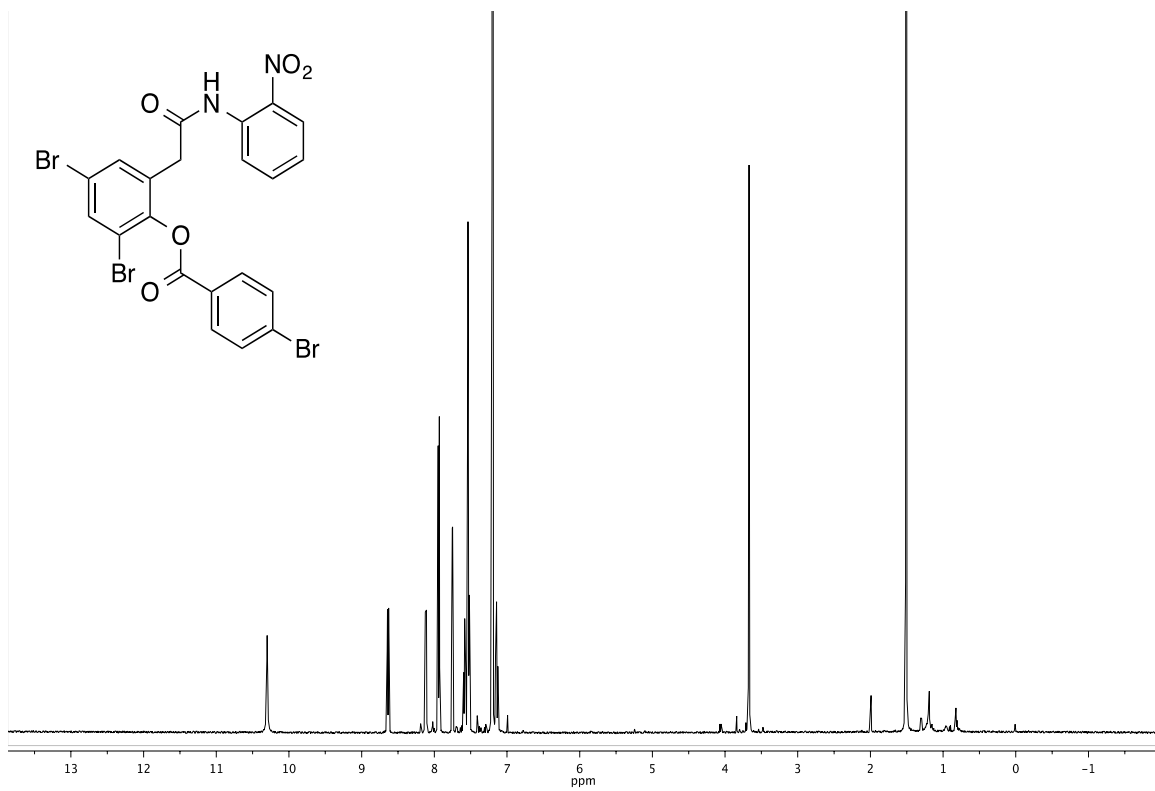
2,4-dibromo-6-(2-((2-nitrophenyl)amino)-2-oxoethyl)phenyl 2-bromobenzoate, 15.



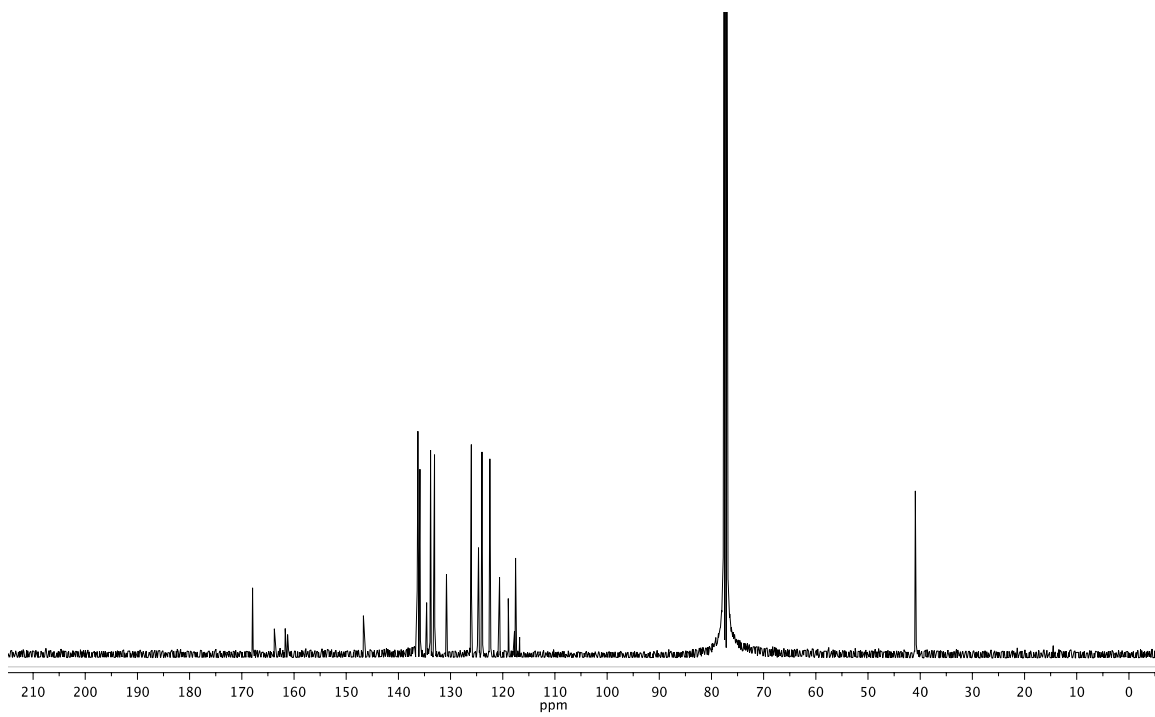
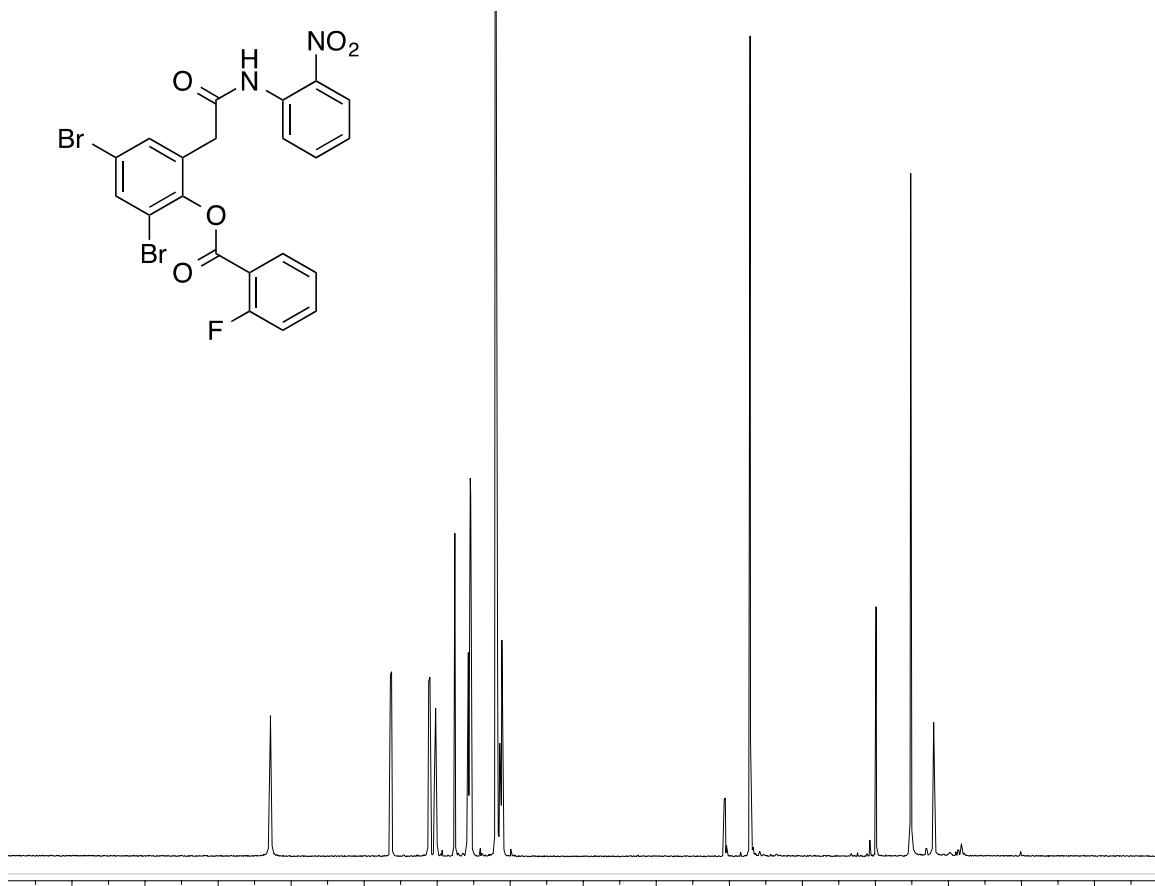
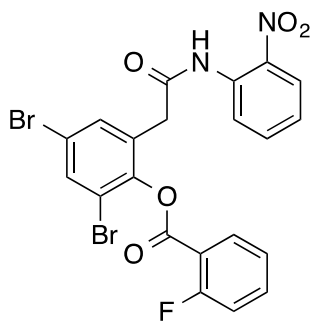
2,4-dibromo-6-(2-((2-nitrophenyl)amino)-2-oxoethyl)phenyl 3-bromobenzoate, 16.



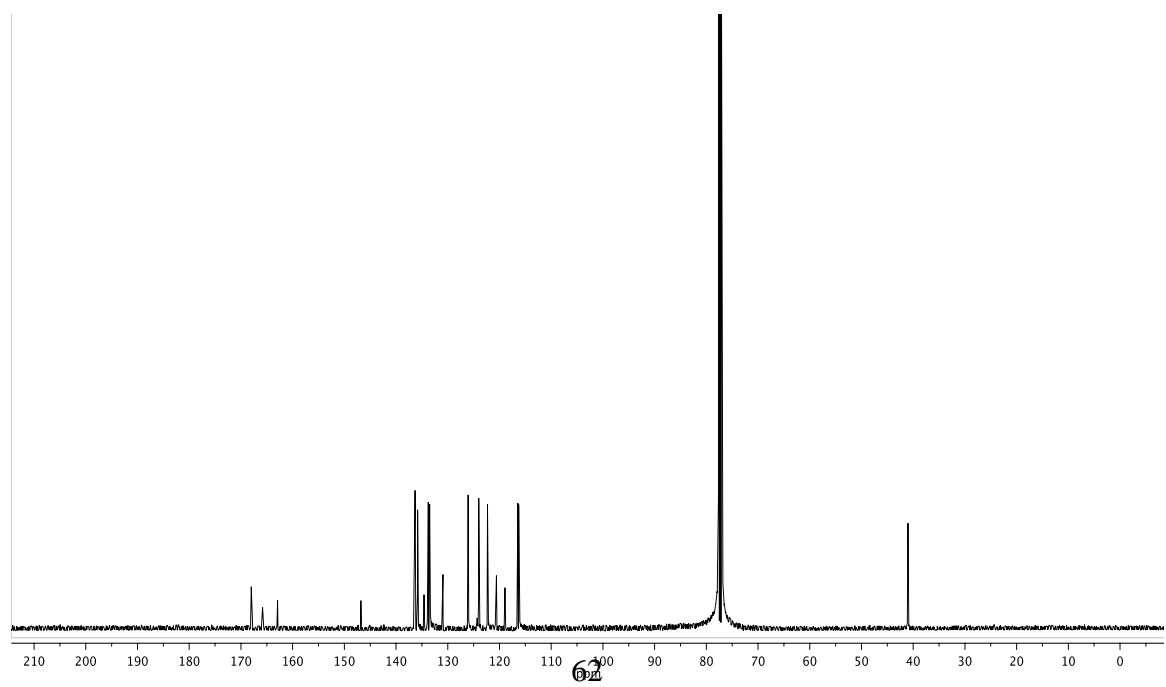
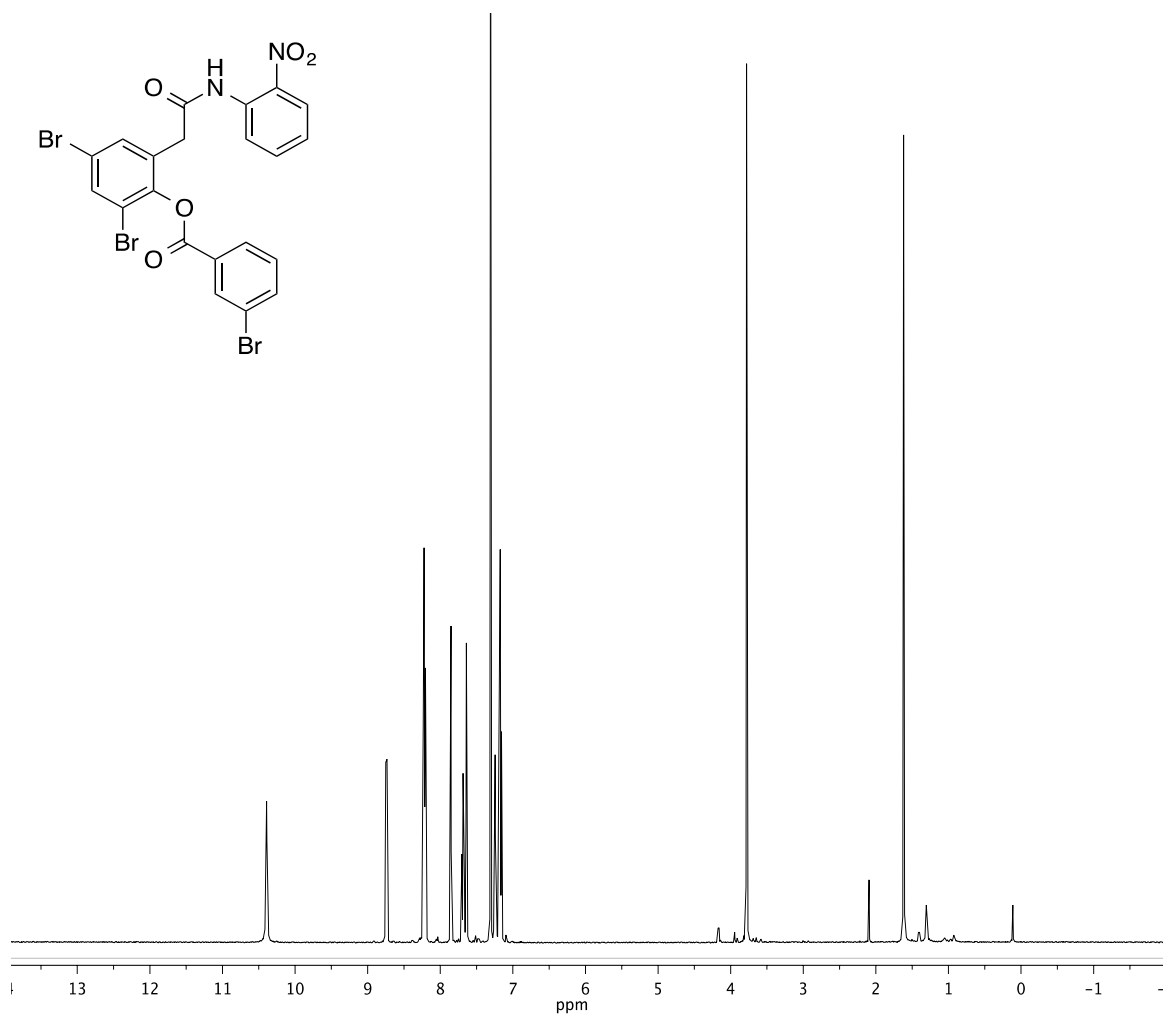
2,4-dibromo-6-(2-((2-nitrophenyl)amino)-2-oxoethyl)phenyl 4-bromobenzoate, 17.



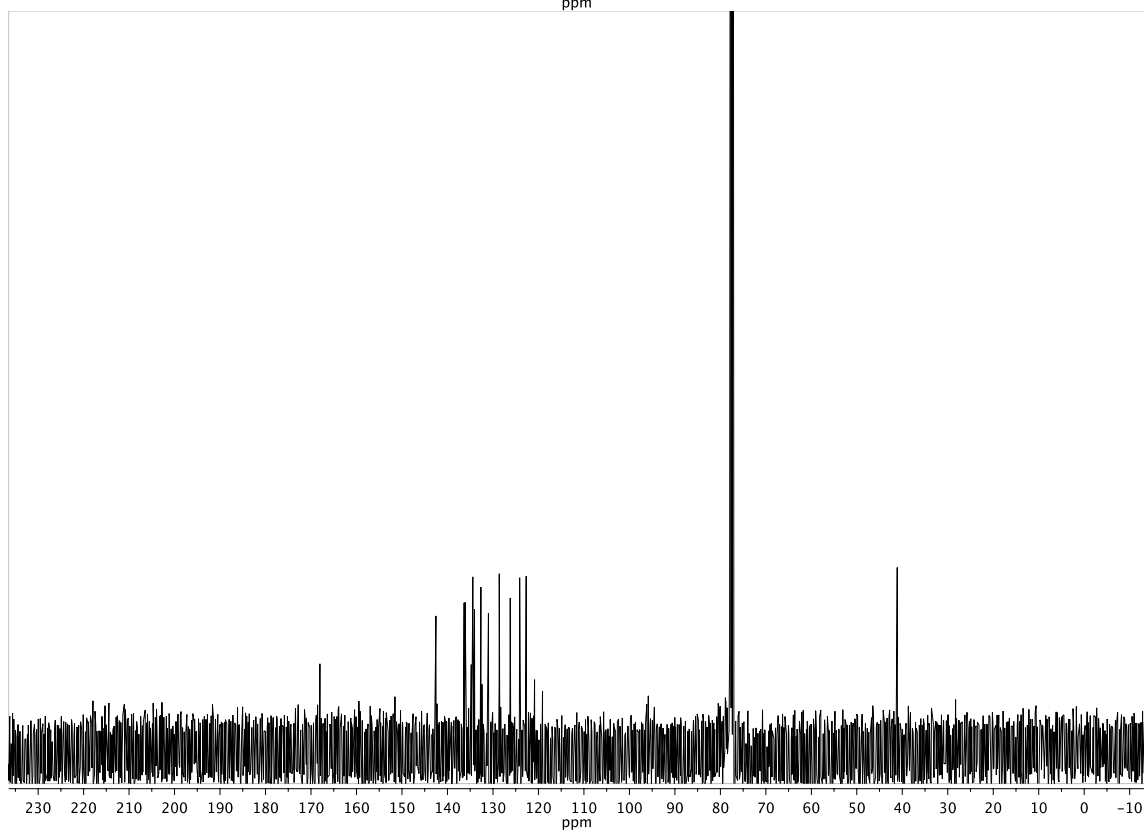
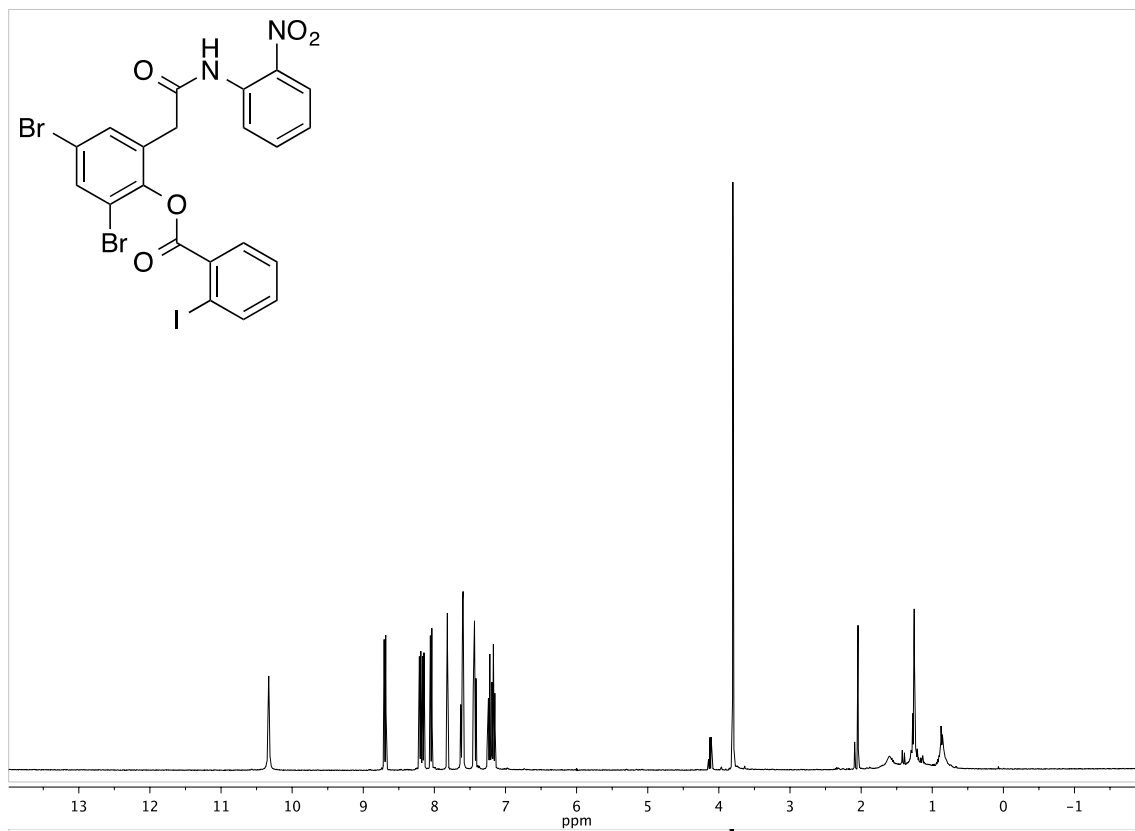
2,4-dibromo-6-(2-((2-nitrophenyl)amino)-2-oxoethyl)phenyl 2-fluorobenzoate, 18.



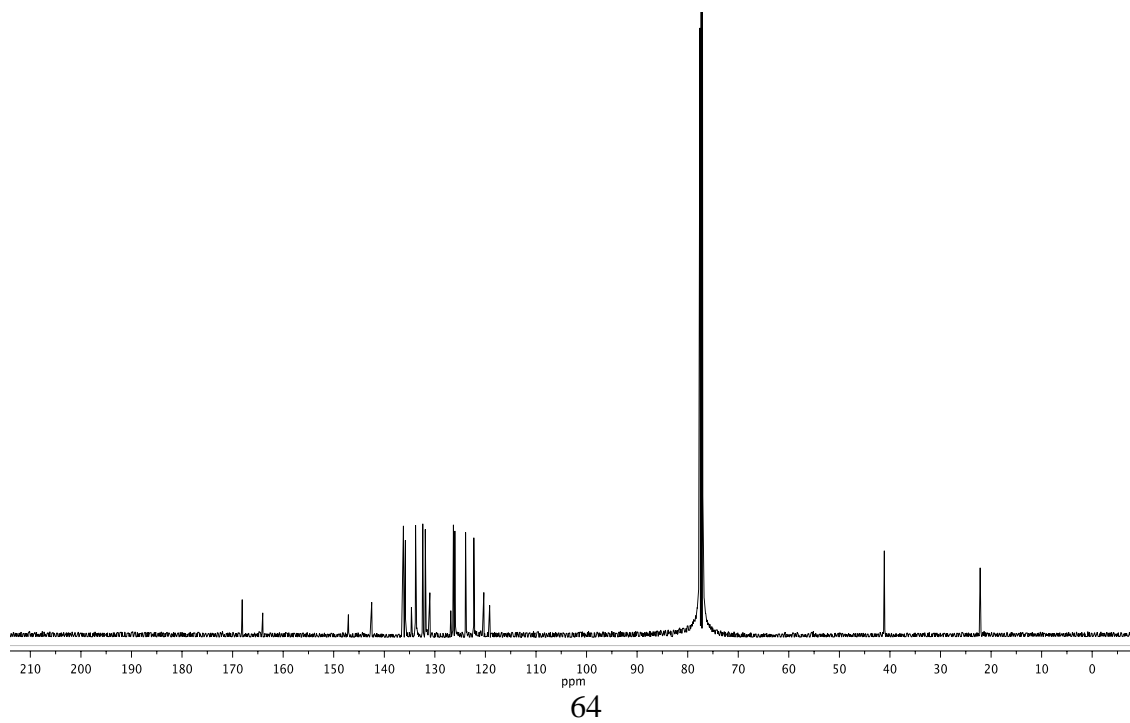
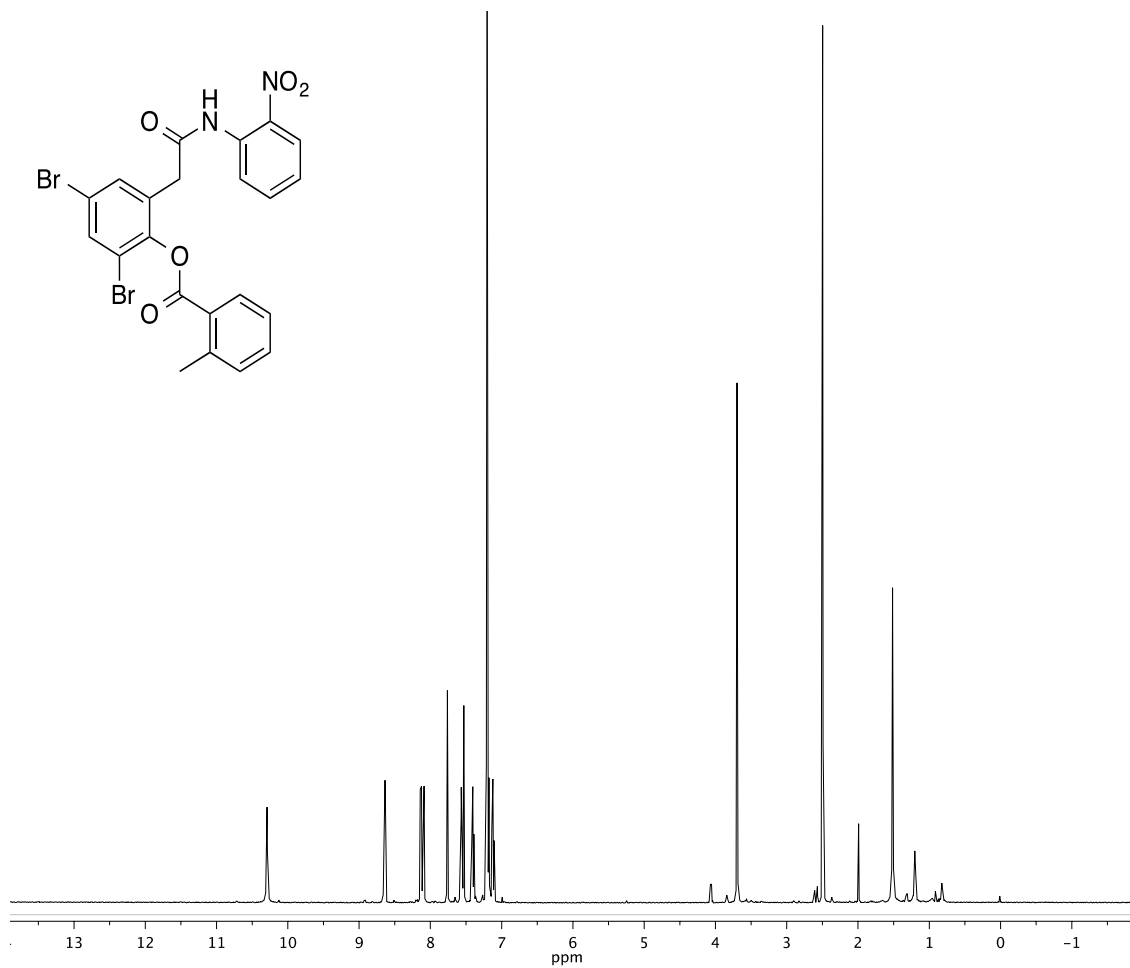
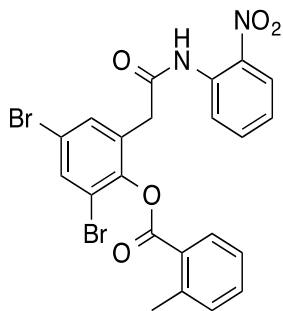
2,4-dibromo-6-(2-((2-nitrophenyl)amino)-2-oxoethyl)phenyl 4-fluorobenzoate, 19.



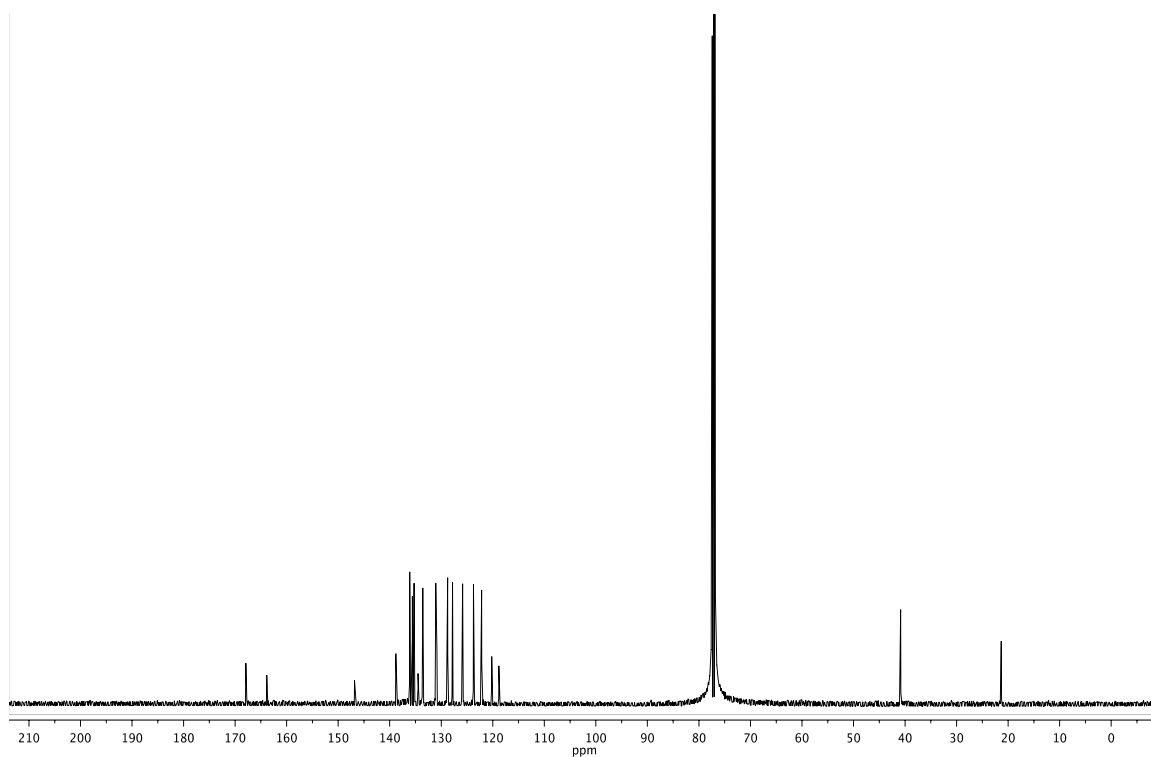
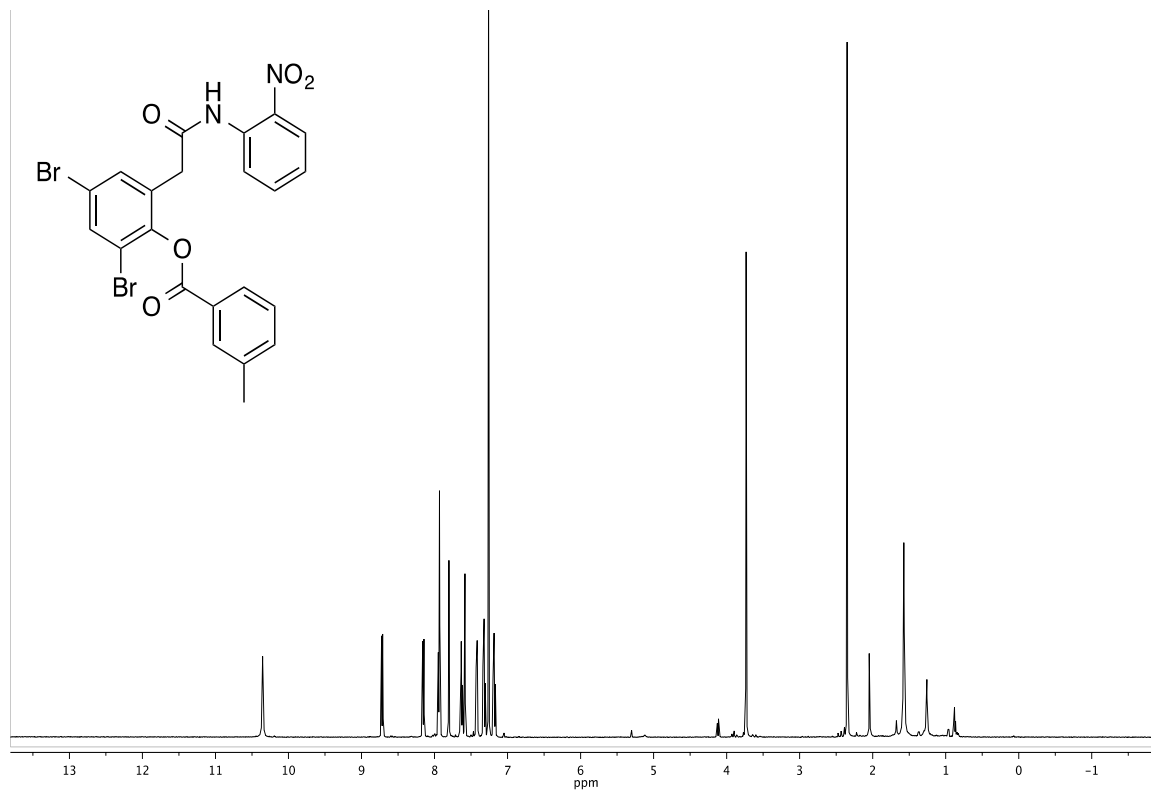
2,4-dibromo-6-(2-((2-nitrophenyl)amino)-2-oxoethyl)phenyl 2-iodobenzoate, 20.



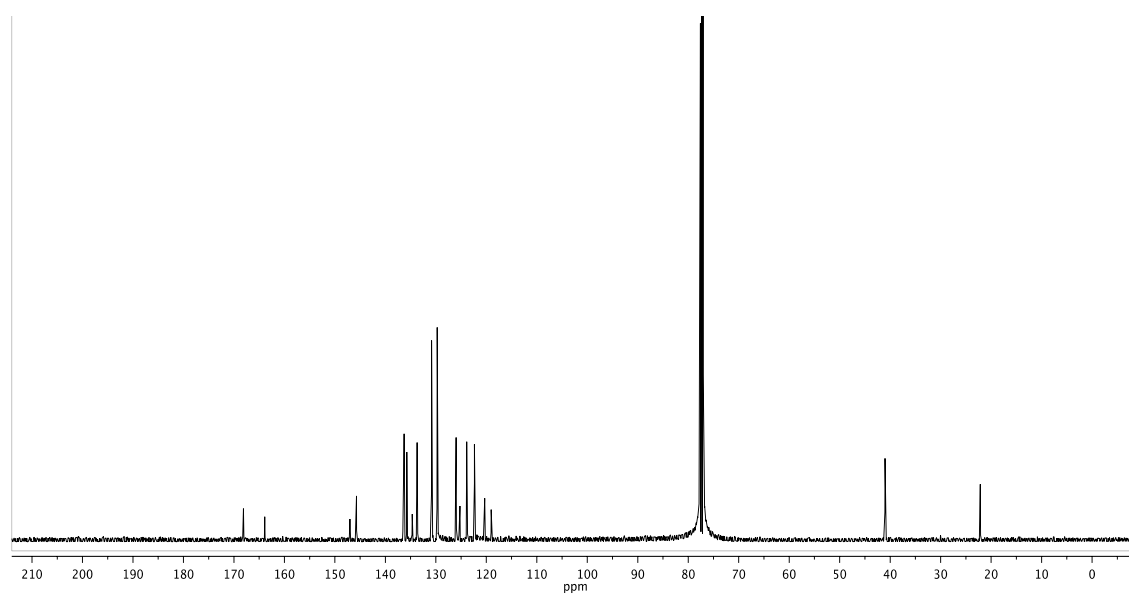
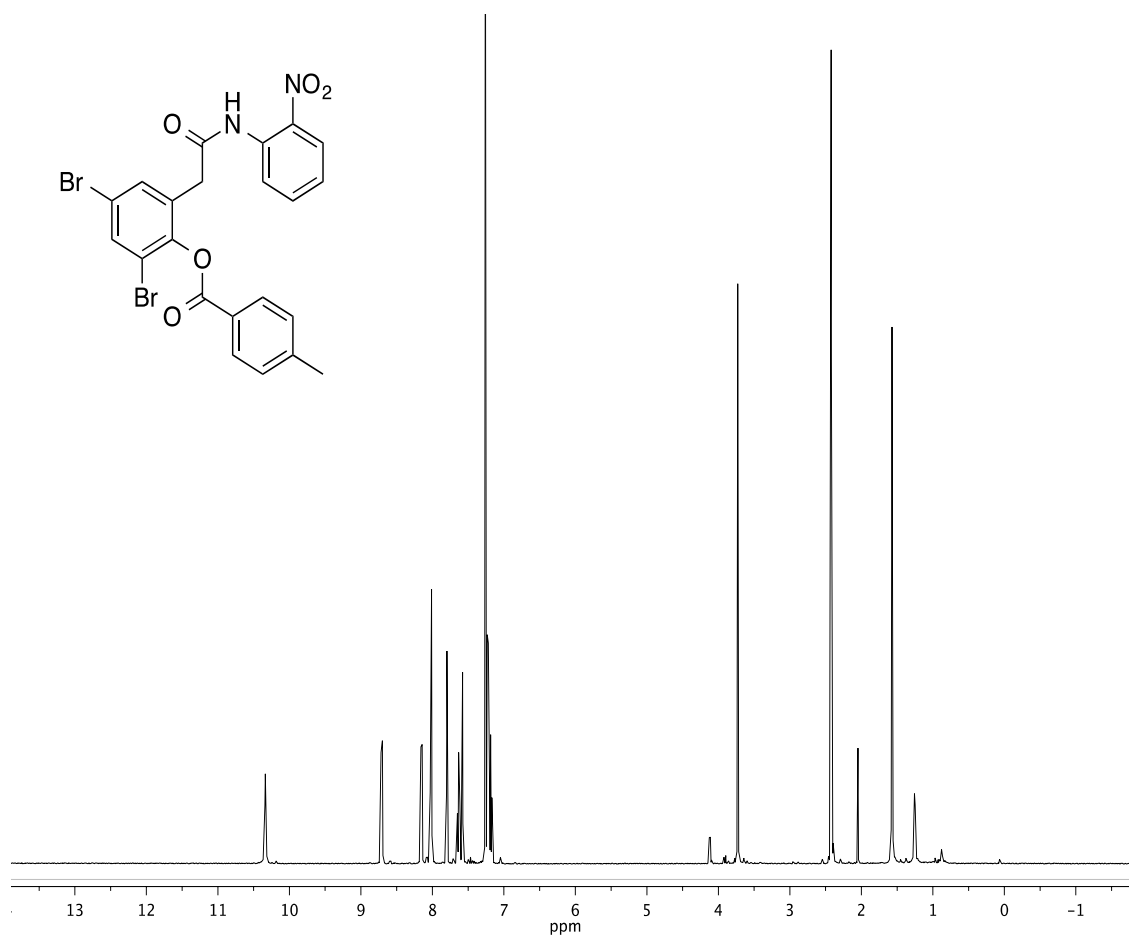
2,4-dibromo-6-(2-((2-nitrophenyl)amino)-2-oxoethyl)phenyl 2-methylbenzoate, 21.



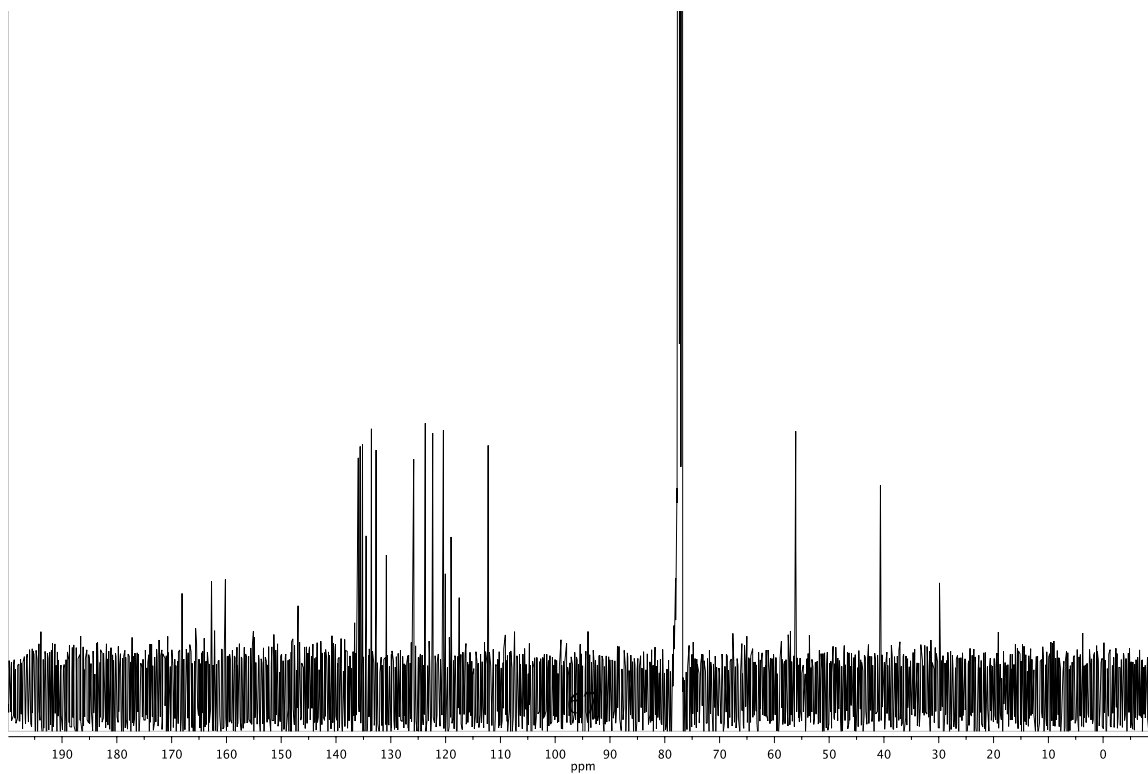
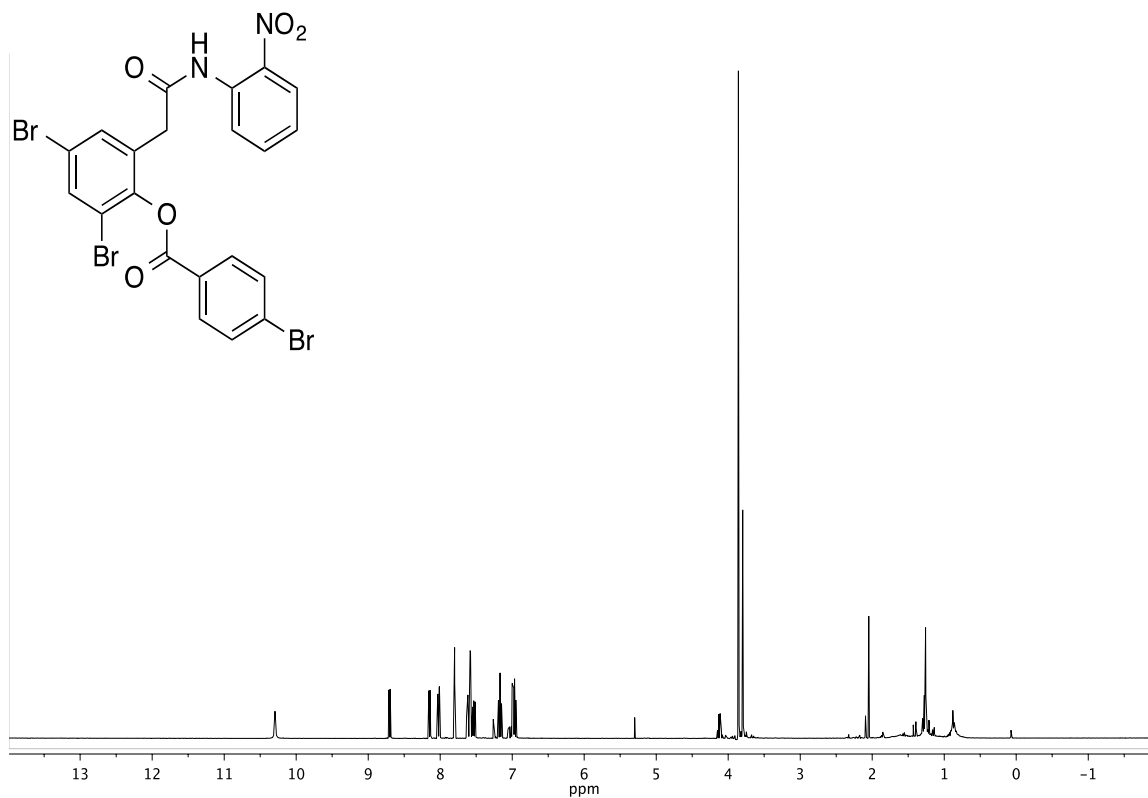
2,4-dibromo-6-(2-((2-nitrophenyl)amino)-2-oxoethyl)phenyl 3-methylbenzoate, 22.



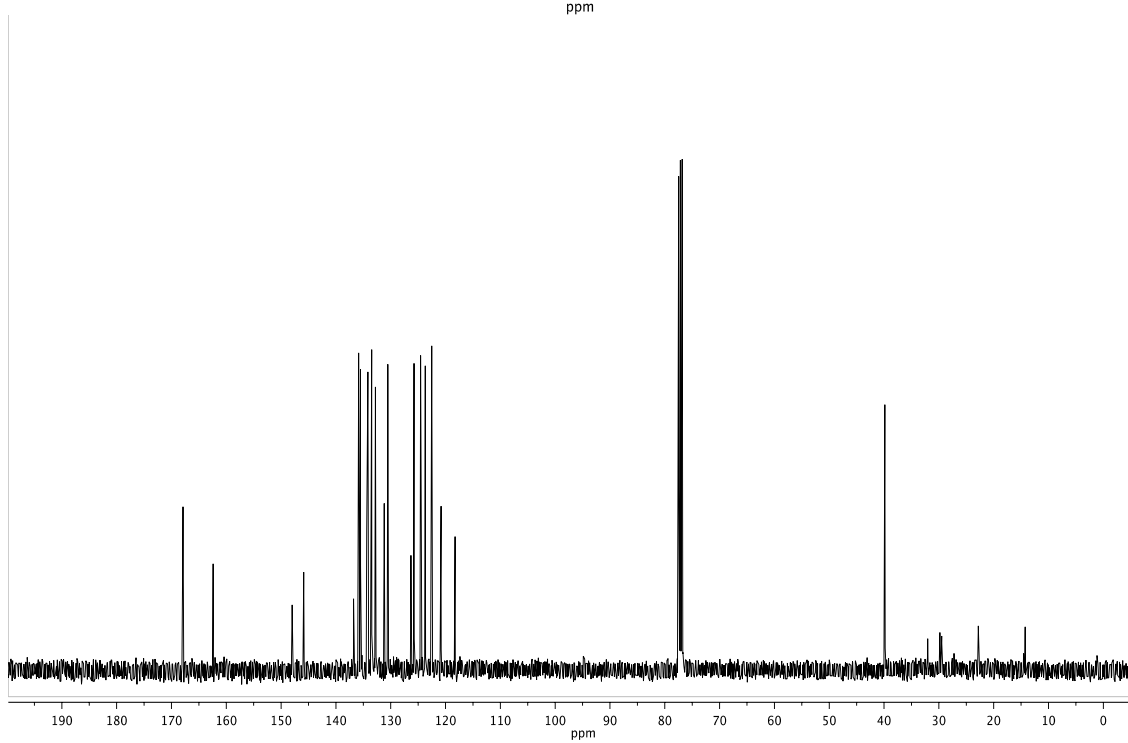
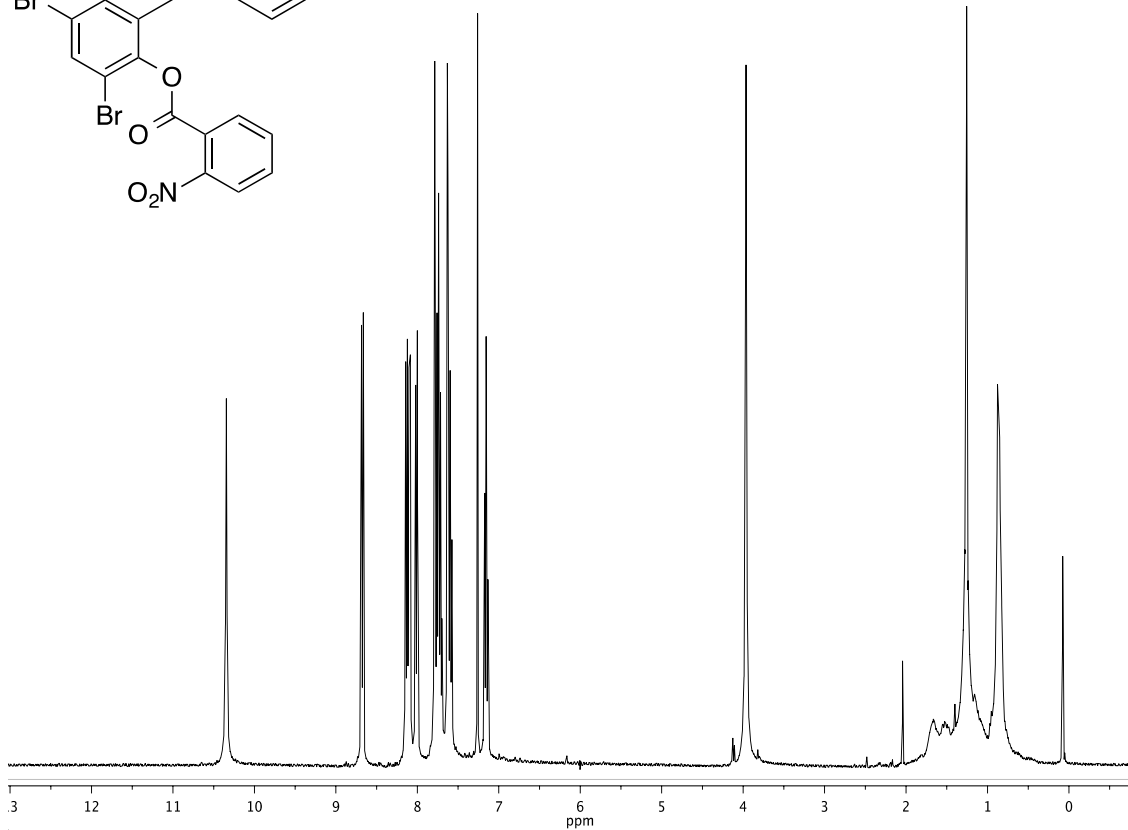
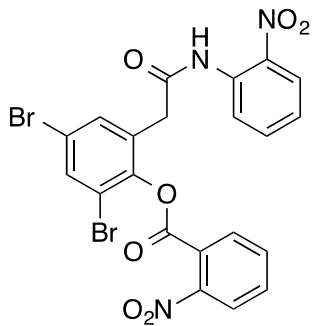
2,4-dibromo-6-(2-((2-nitrophenyl)amino)-2-oxoethyl)phenyl 4-methylbenzoate, 23.



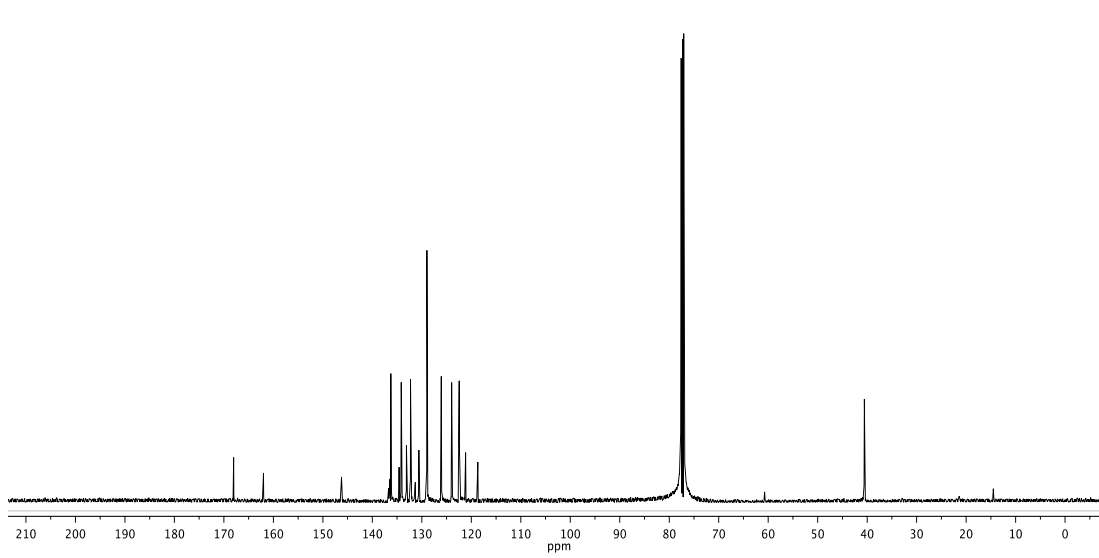
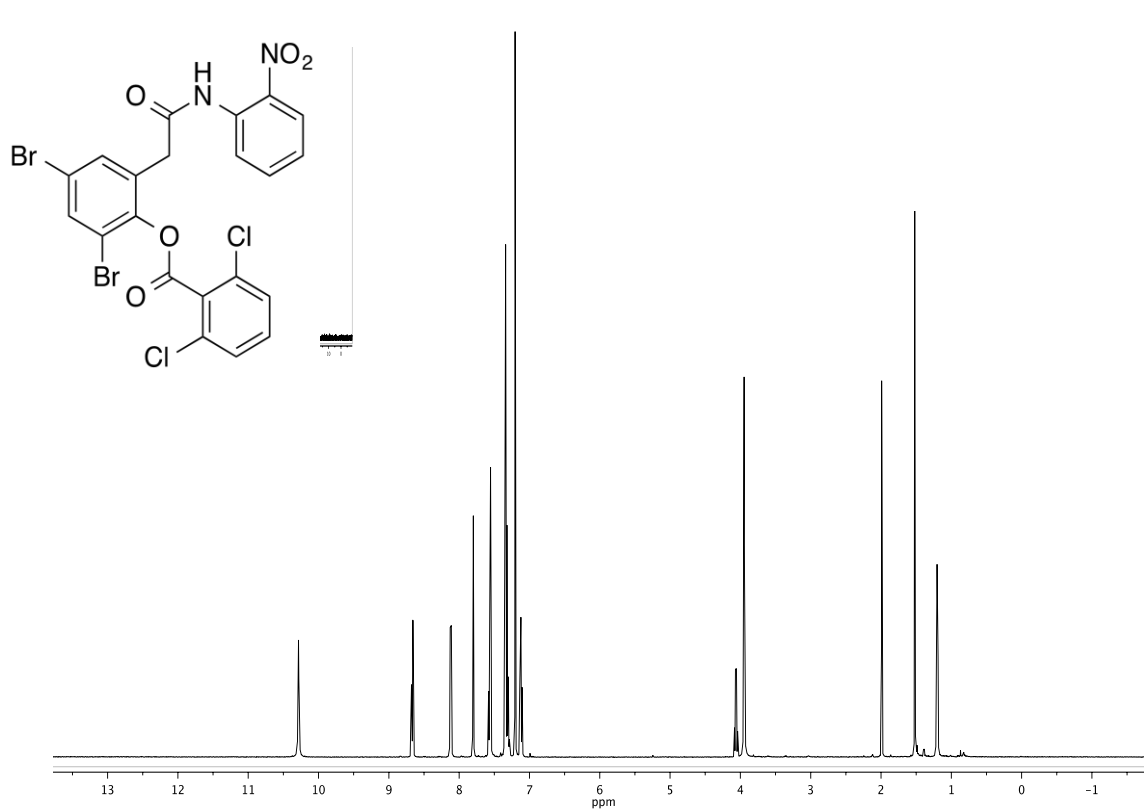
2,4-dibromo-6-(2-((2-nitrophenyl)amino)-2-oxoethyl)phenyl 2-methoxybenzoate, 24.



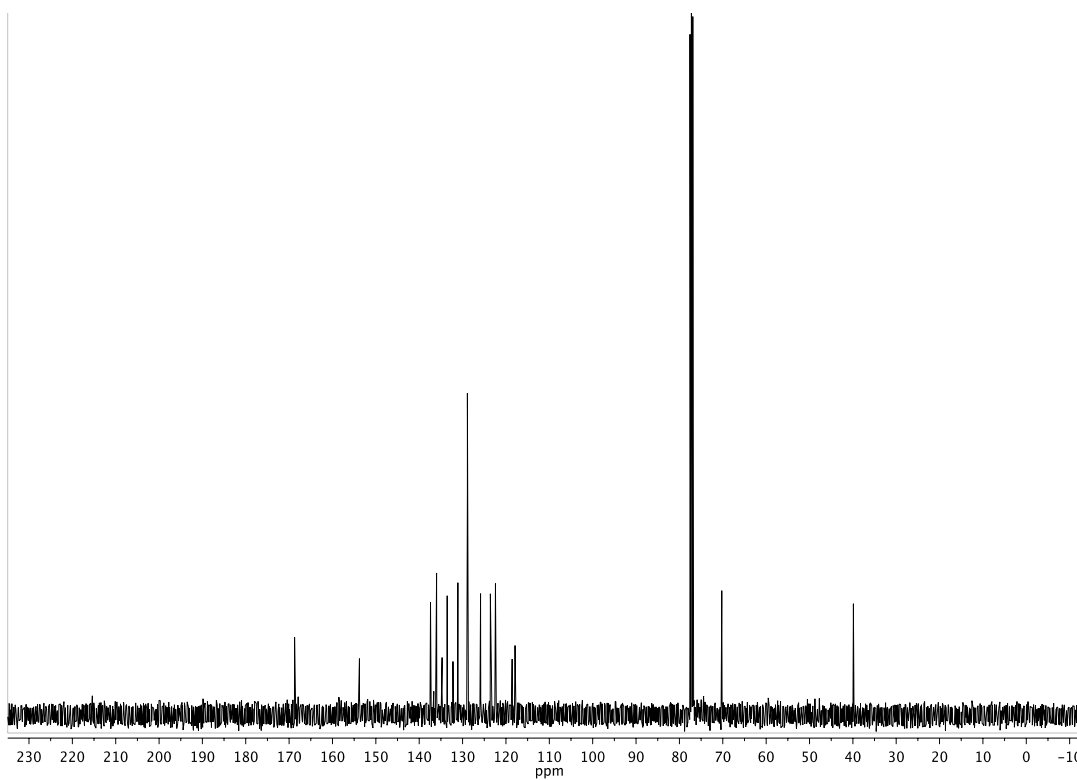
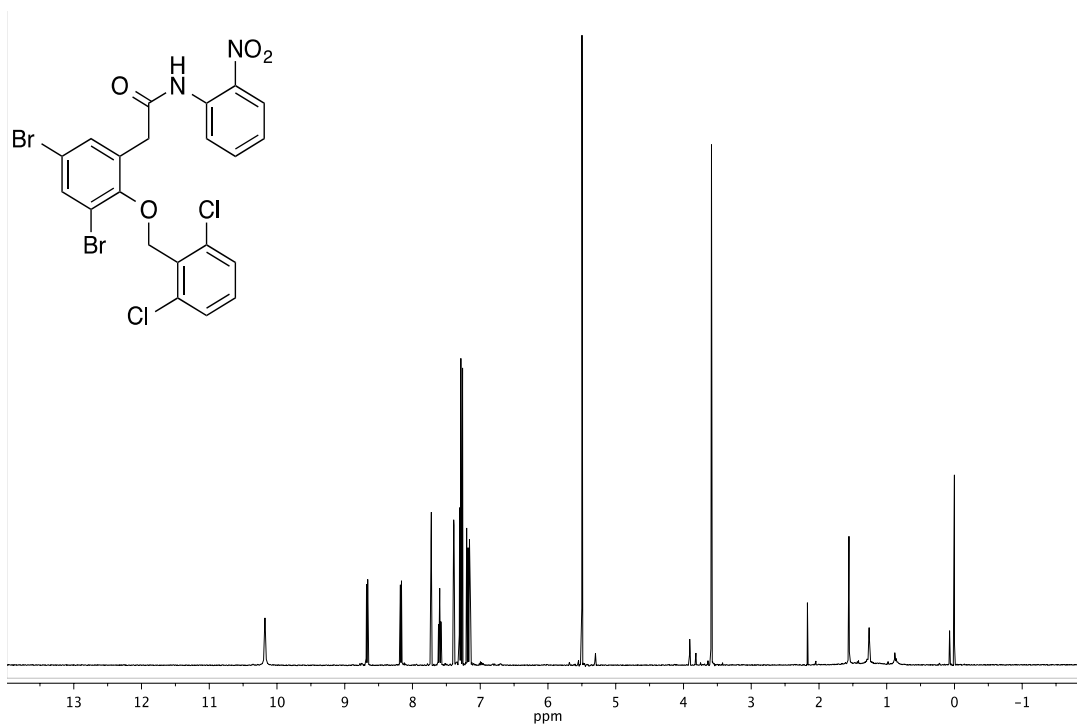
2,4-dibromo-6-(2-((2-nitrophenyl)amino)-2-oxoethyl)phenyl 2-nitrobenzoate, 25.



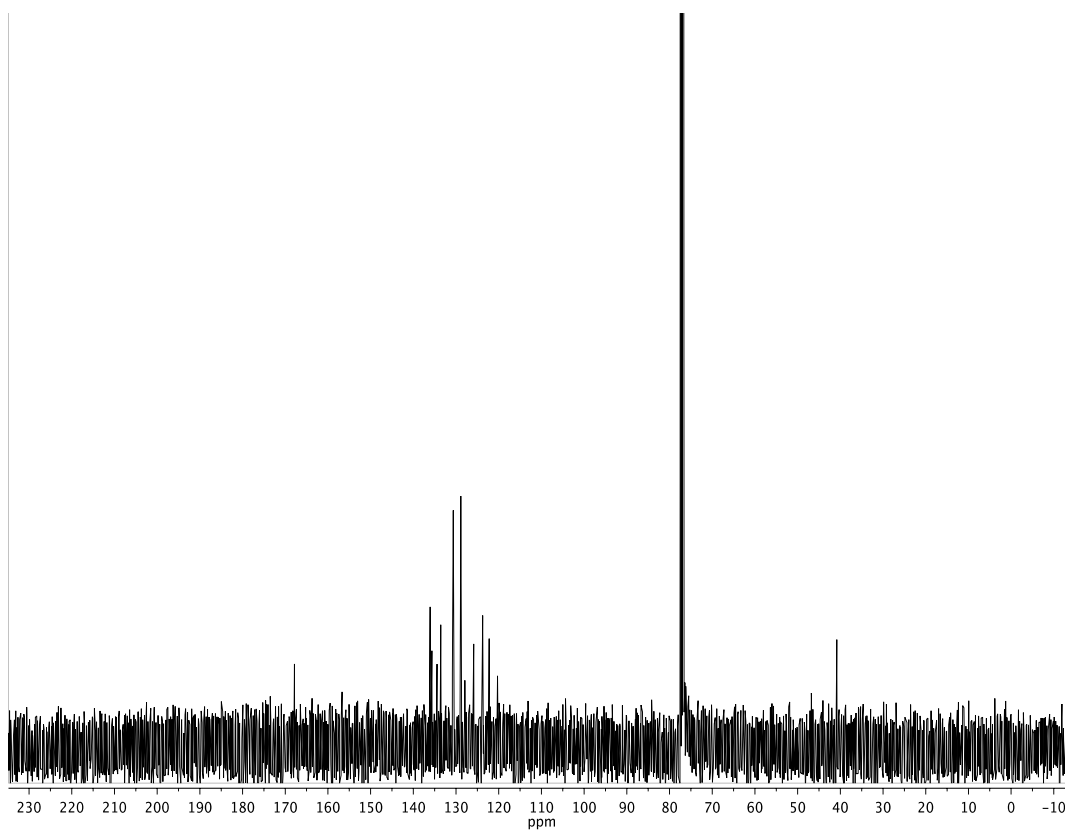
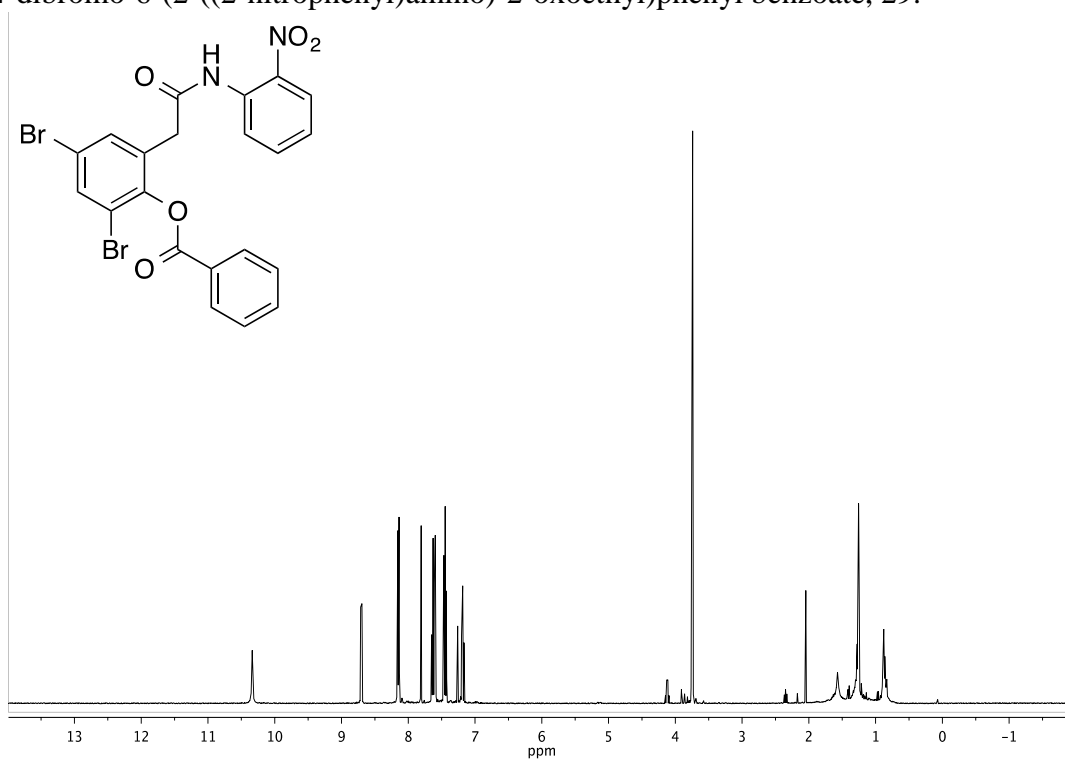
2,4-dibromo-6-(2-((2-nitrophenyl)amino)-2-oxoethyl)phenyl 2,6-dichlorobenzoate, 27.



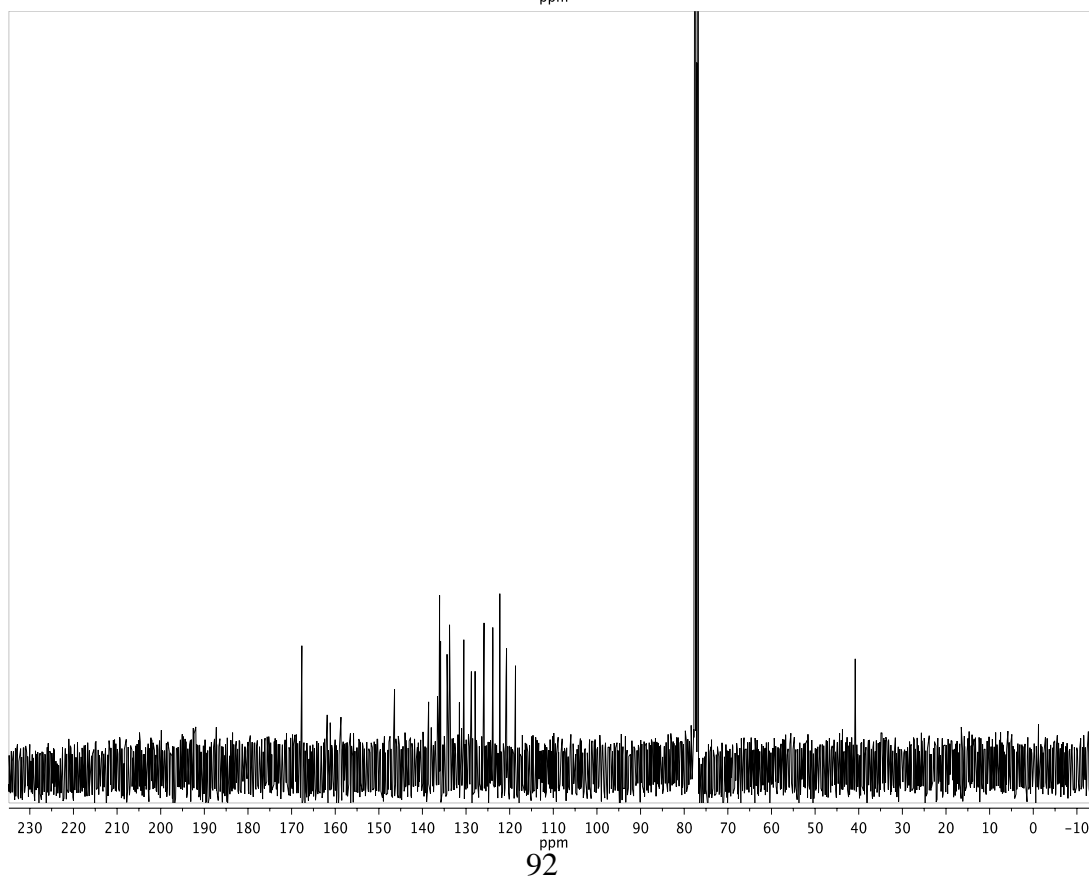
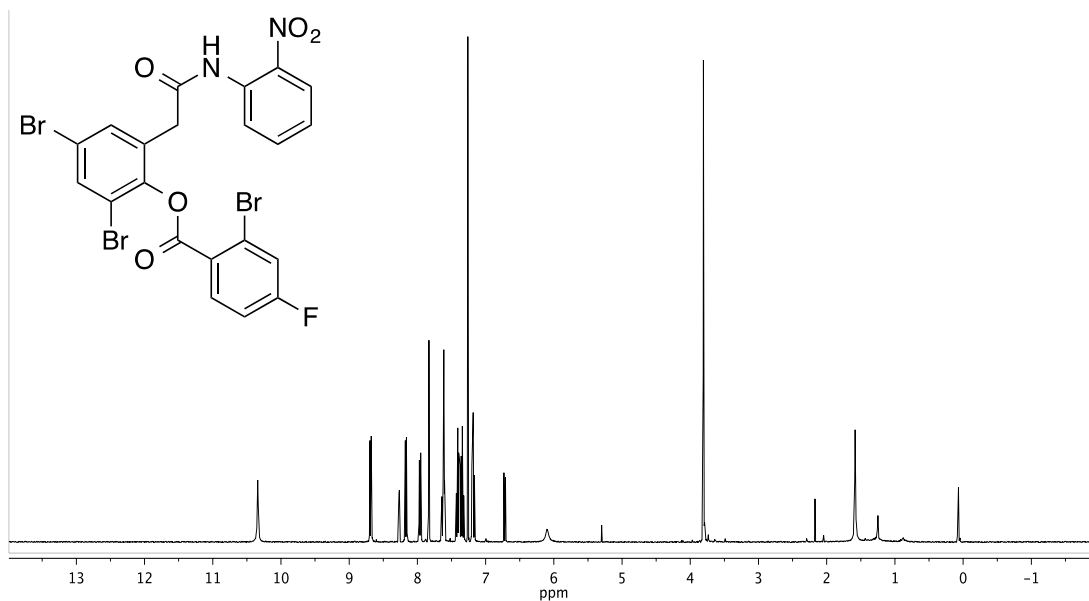
2-(3,5-dibromo-2-((2,6-dichlorobenzyl)oxy)phenyl)-*N*-(2-nitrophenyl)acetamide, 28.



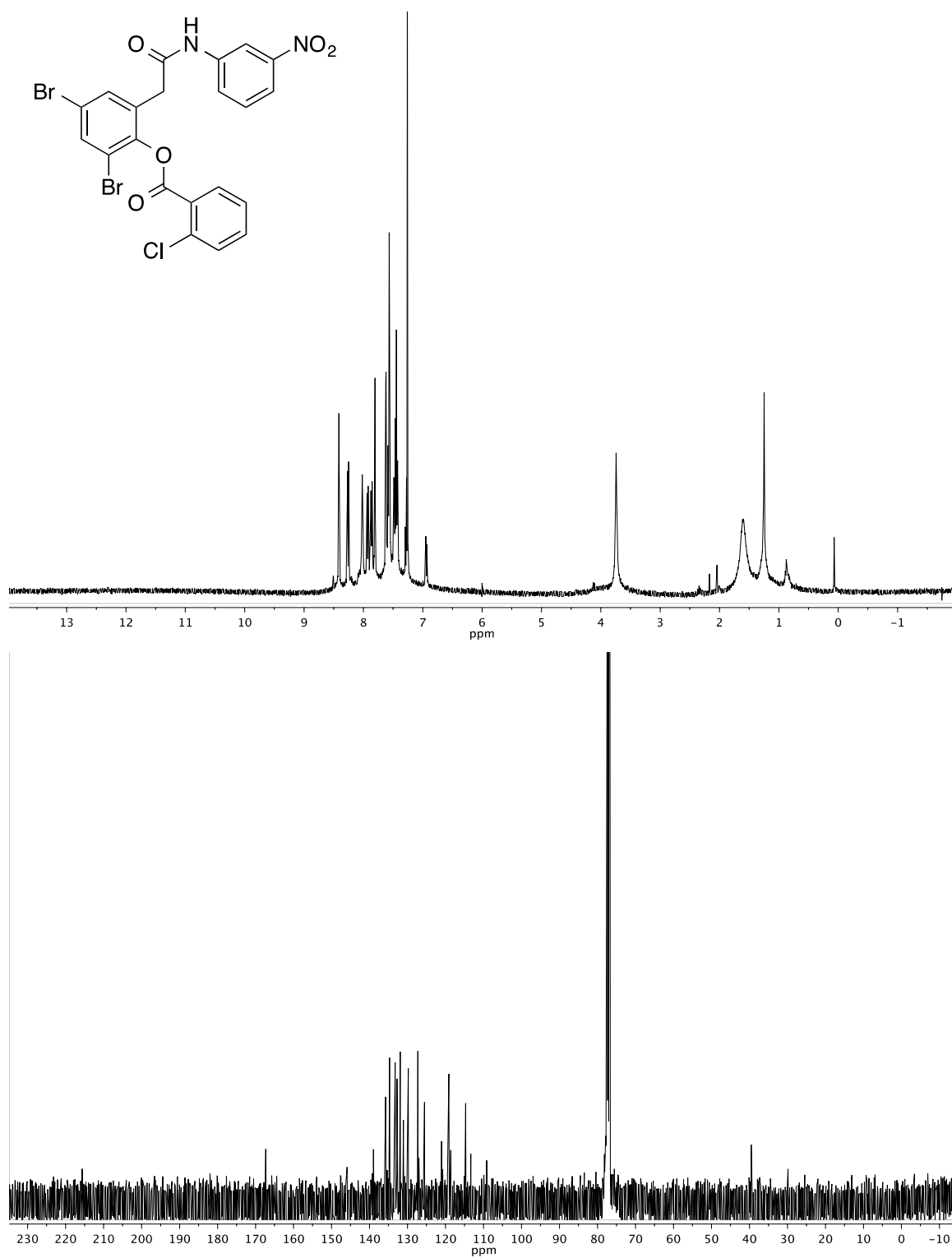
2,4-dibromo-6-(2-((2-nitrophenyl)amino)-2-oxoethyl)phenyl benzoate, 29.



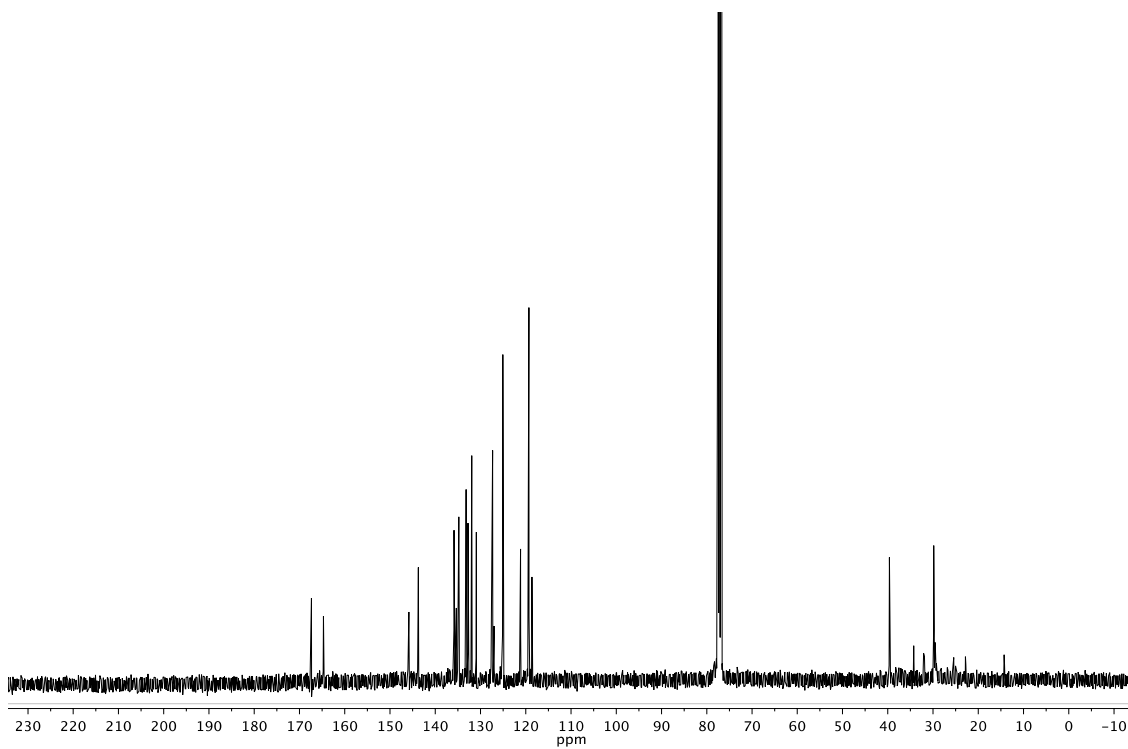
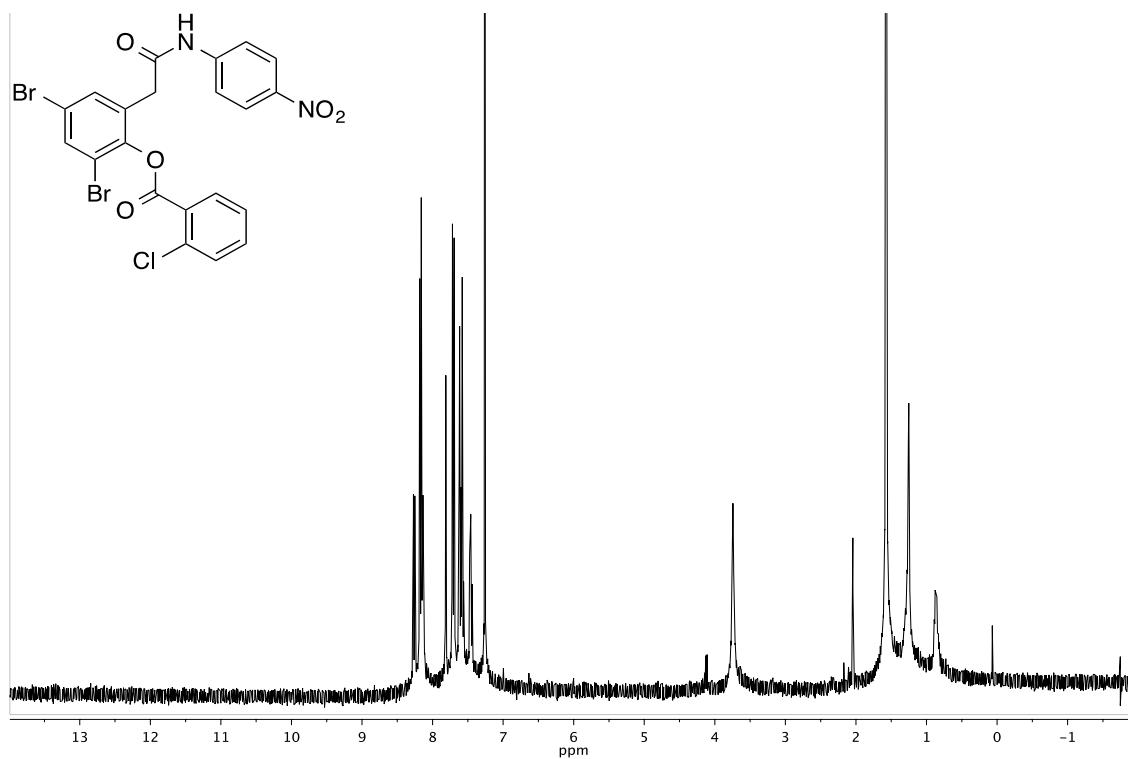
2,4-dibromo-6-(2-((2-nitrophenyl)amino)-2-oxoethyl)phenyl 2-bromo-4-fluorobenzoate,
26.



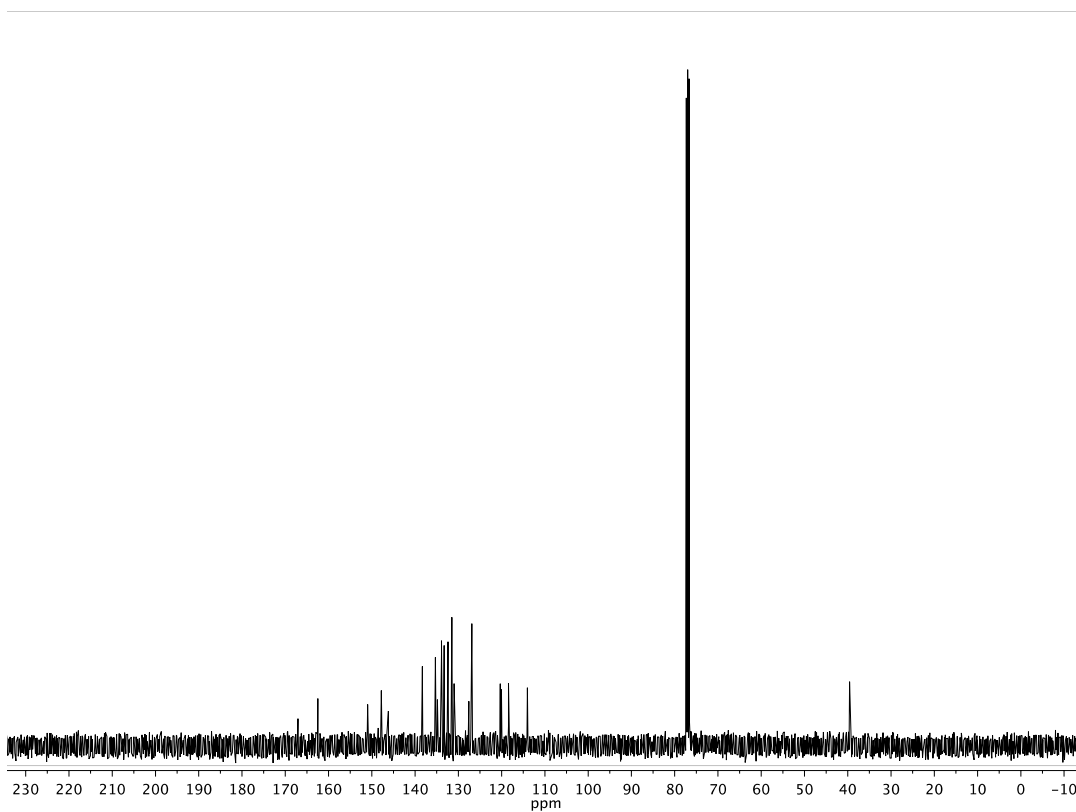
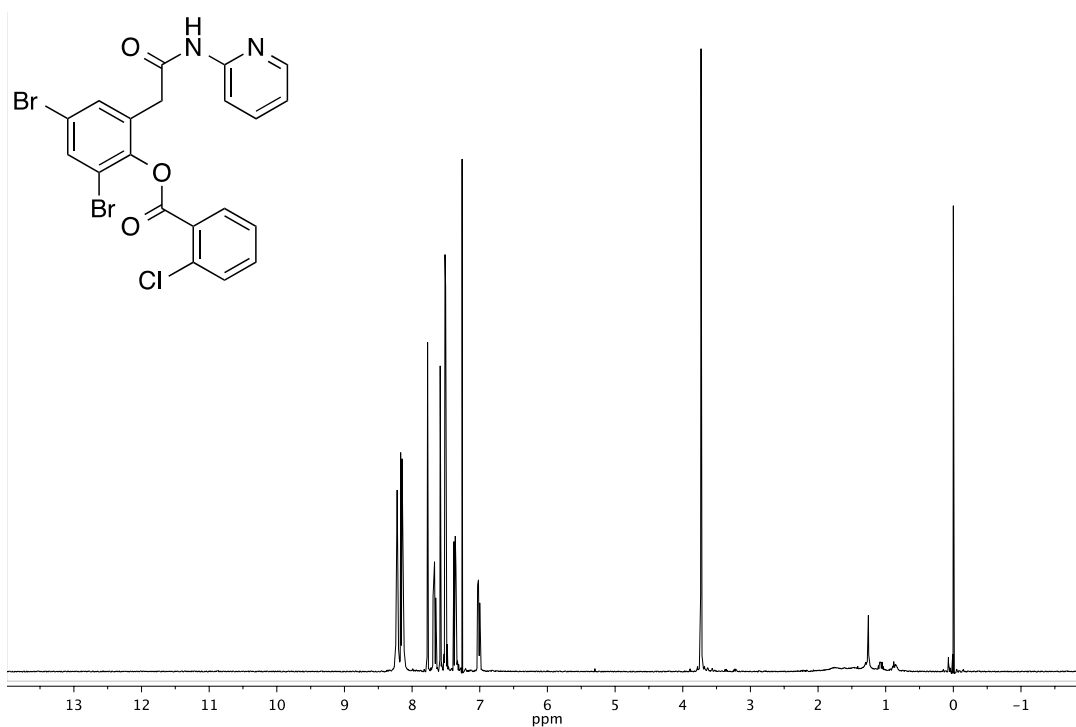
2,4-dibromo-6-(2-((3-nitrophenyl)amino)-2-oxoethyl)phenyl 2-chlorobenzoate, 30.



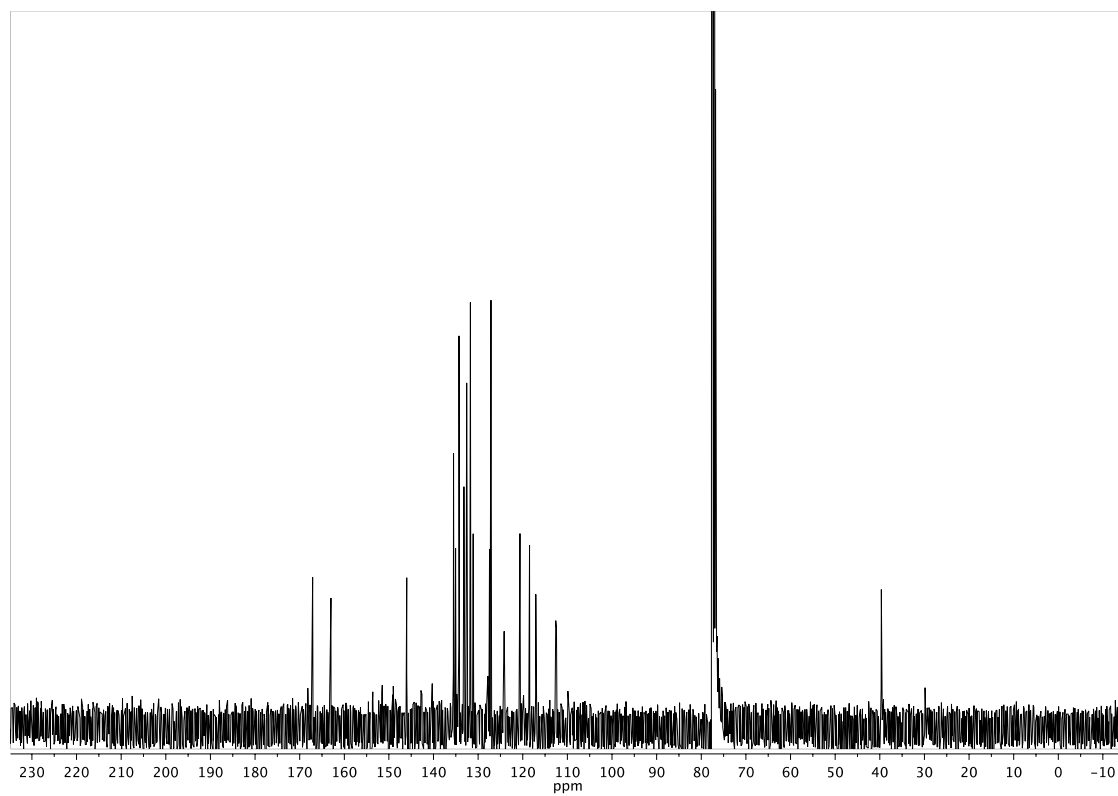
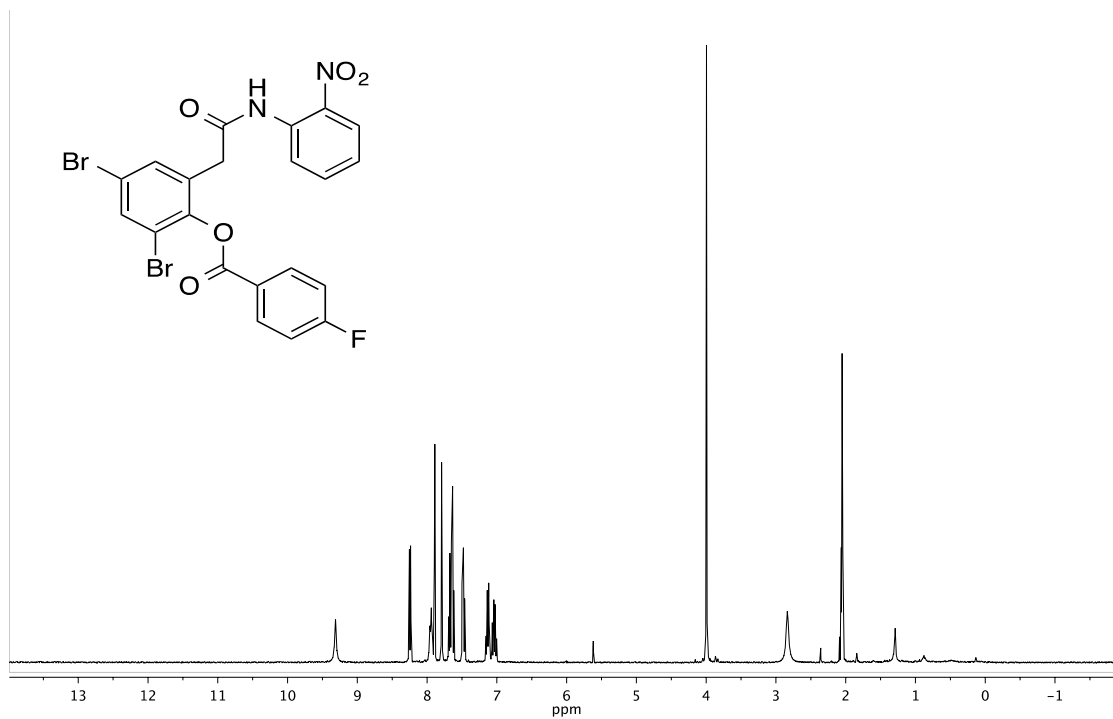
2,4-dibromo-6-(2-((4-nitrophenyl)amino)-2-oxoethyl)phenyl 2-chlorobenzoate, 31.



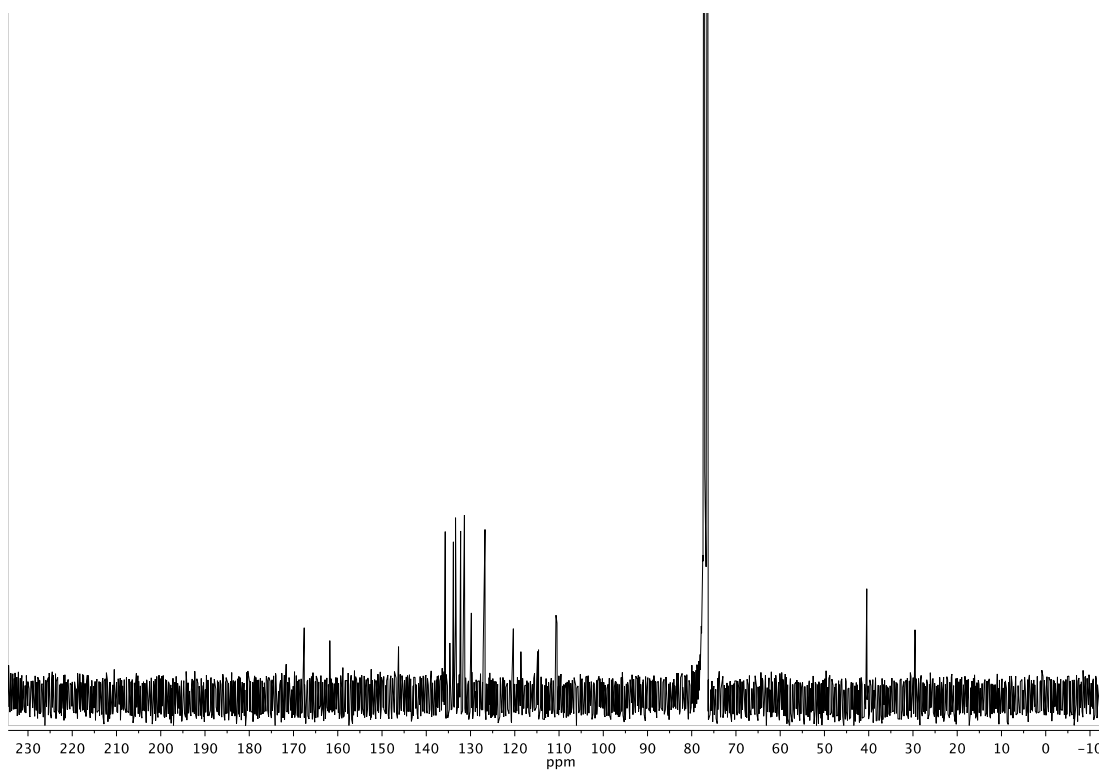
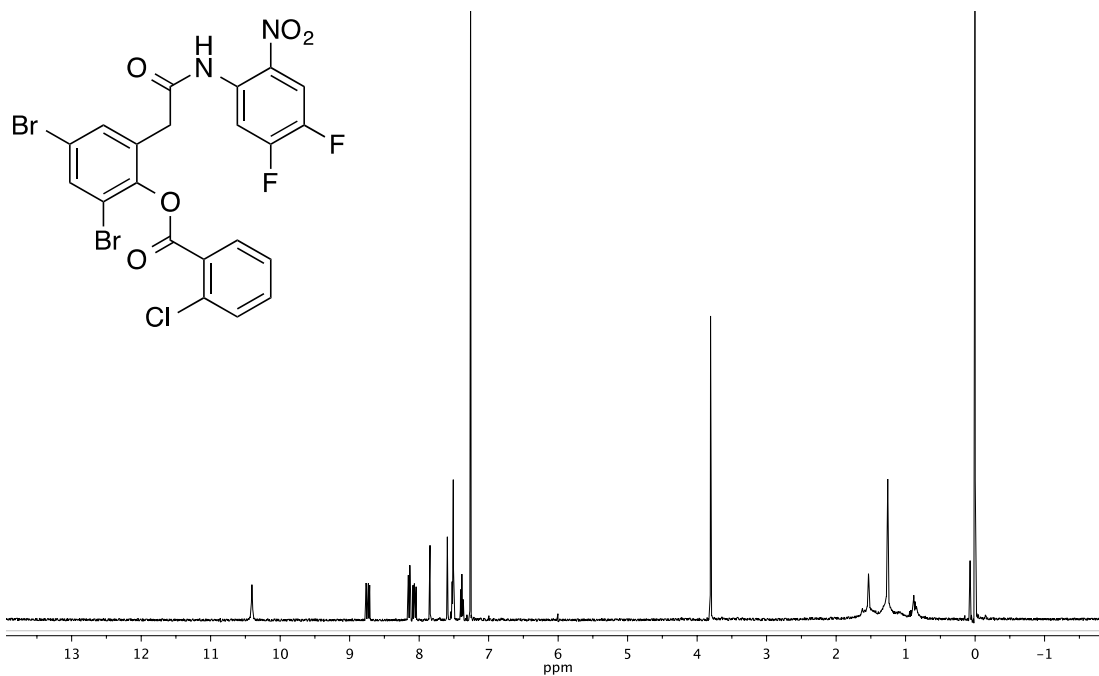
2,4-dibromo-6-(2-oxo-2-(pyridin-2-ylamino)ethyl)phenyl 2-chlorobenzoate, 32.



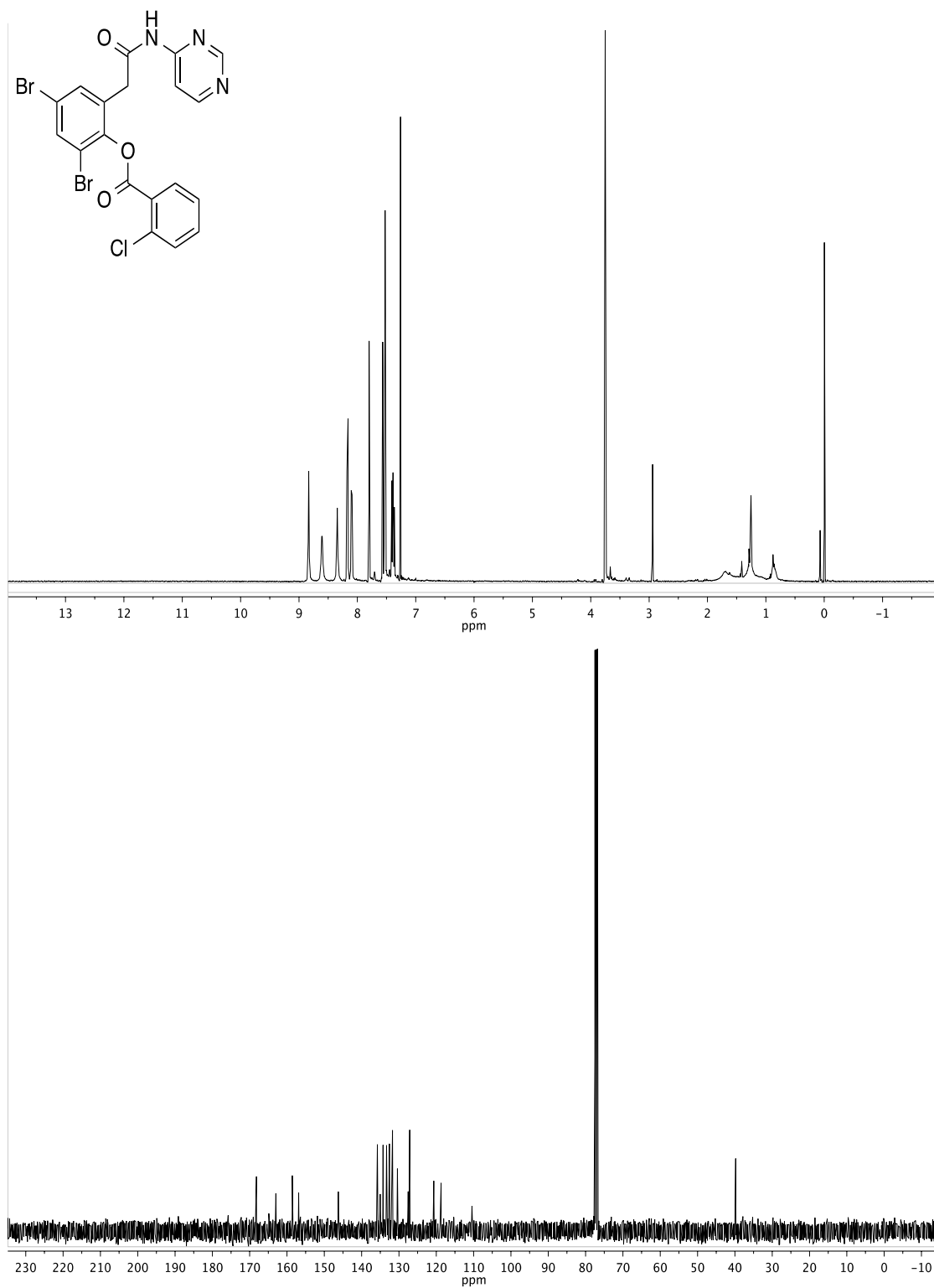
2,4-dibromo-6-(2-((2,3-difluorophenyl)amino)-2-oxoethyl)phenyl 2-chlorobenzoate, 33.



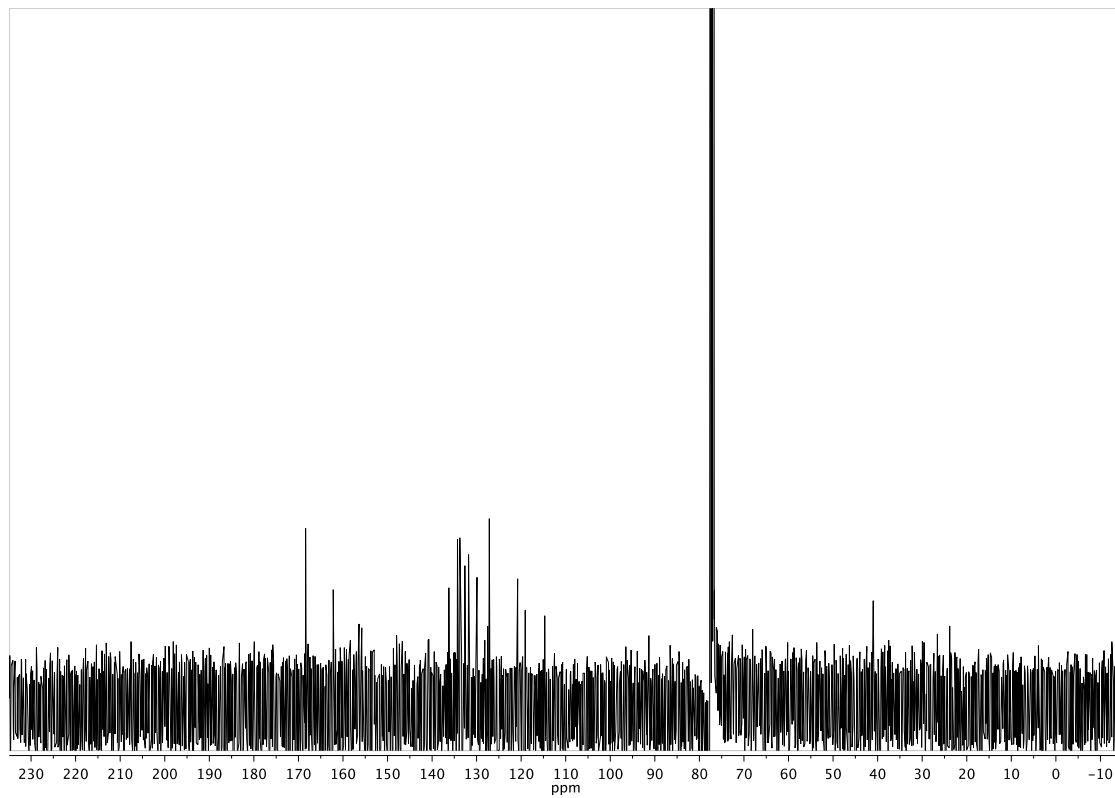
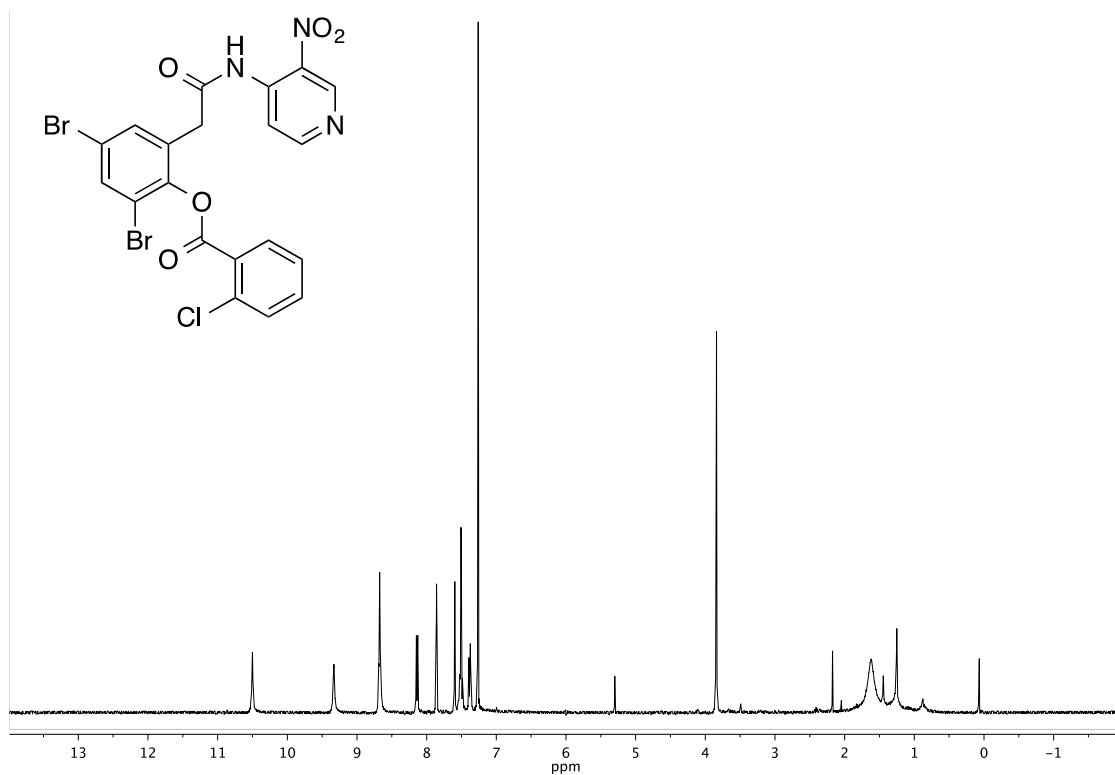
2,4-dibromo-6-(2-((4,5-difluoro-2-nitrophenyl)amino)-2-oxoethyl)phenyl 2-chlorobenzoate, 34.



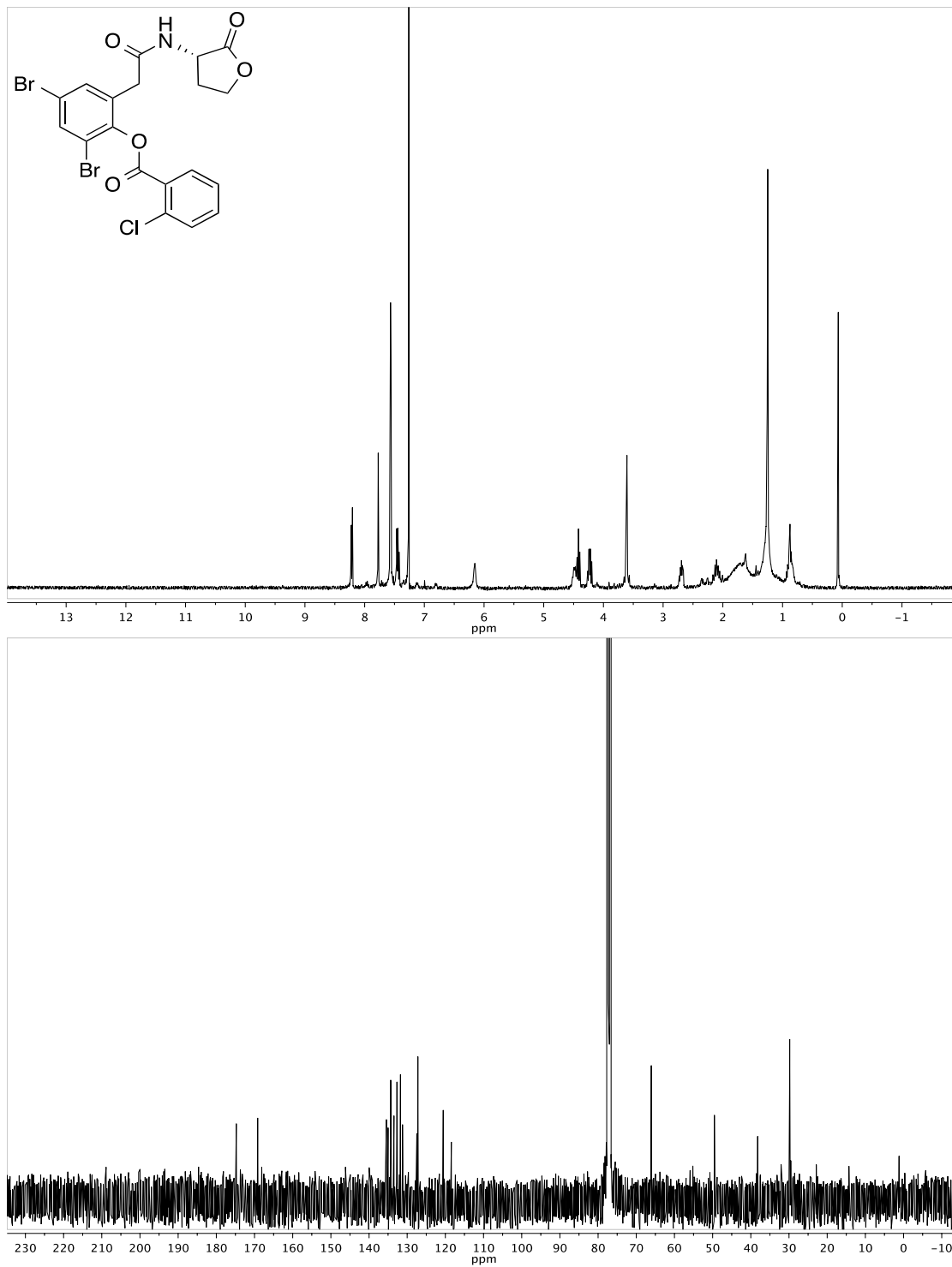
2,4-dibromo-6-(2-oxo-2-(pyrimidin-4-ylamino)ethyl)phenyl 2-chlorobenzoate, 35.



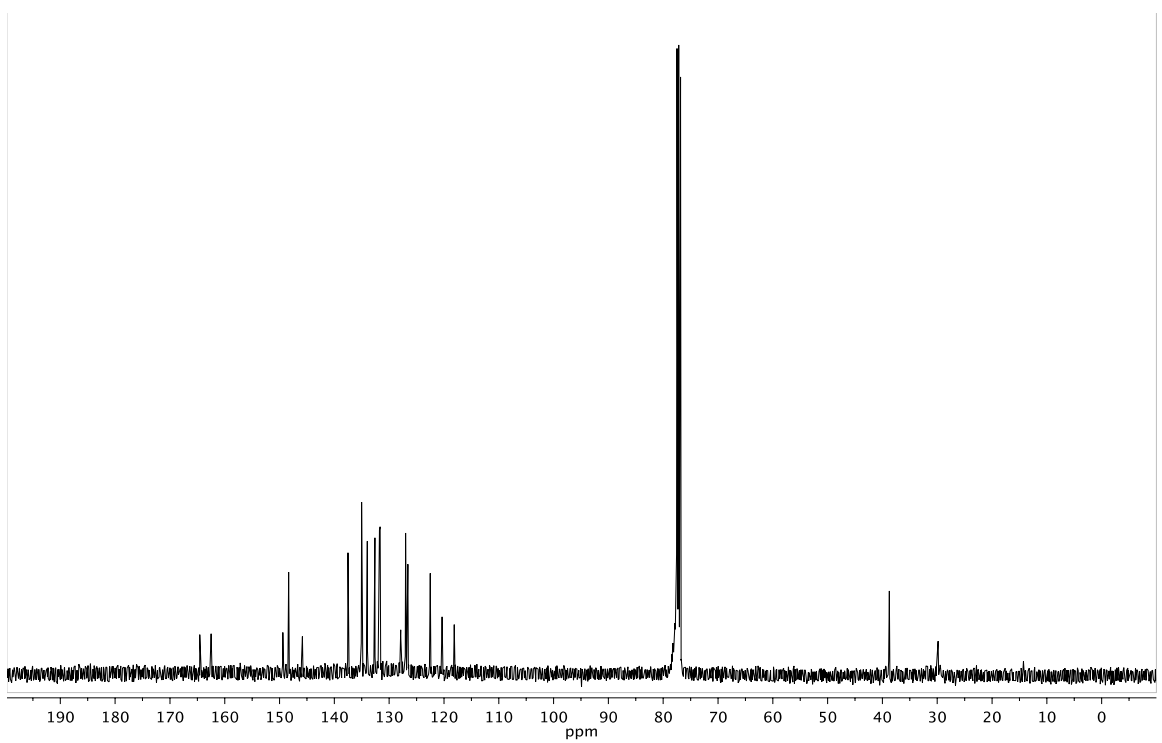
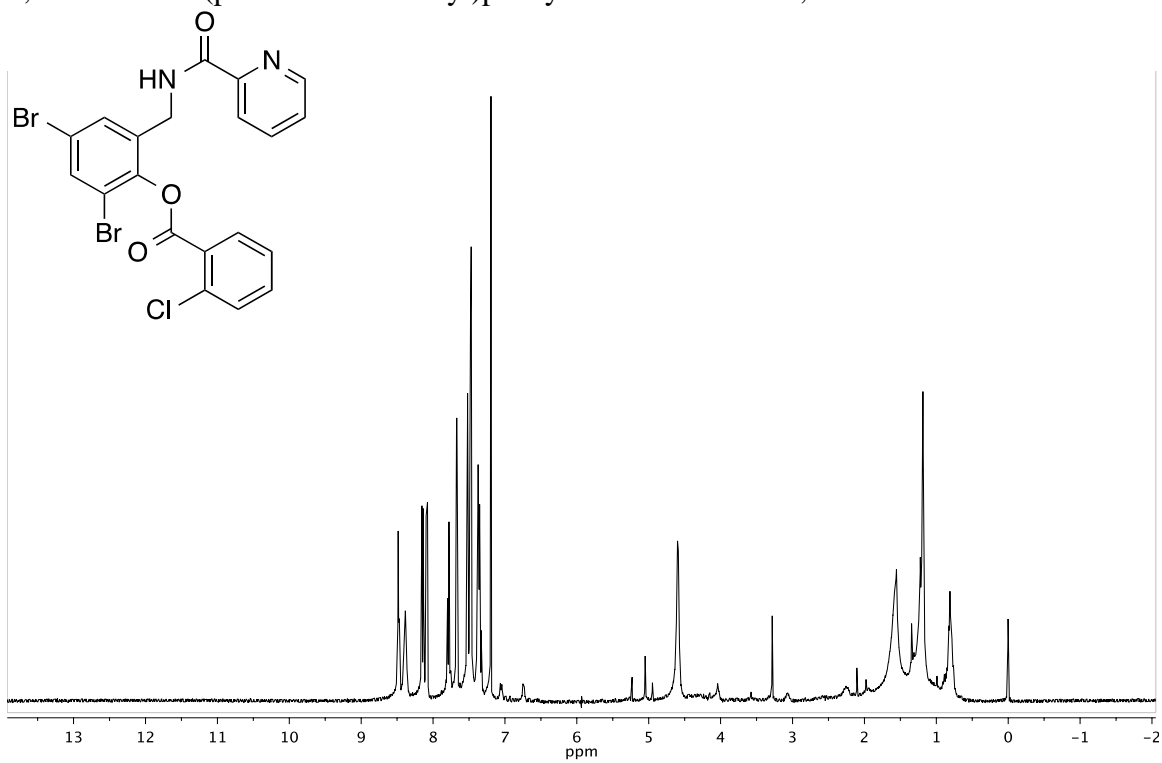
2,4-dibromo-6-(2-((3-nitropyridin-4-yl)amino)-2-oxoethyl)phenyl 2-chlorobenzoate, 36.



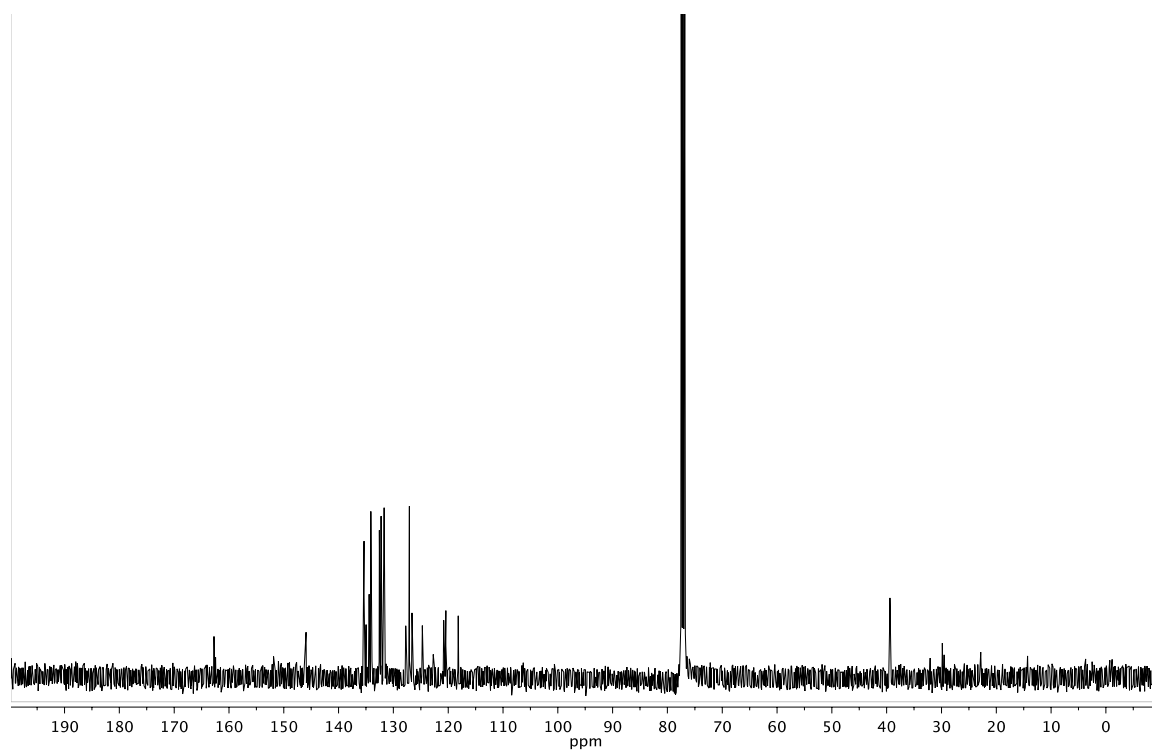
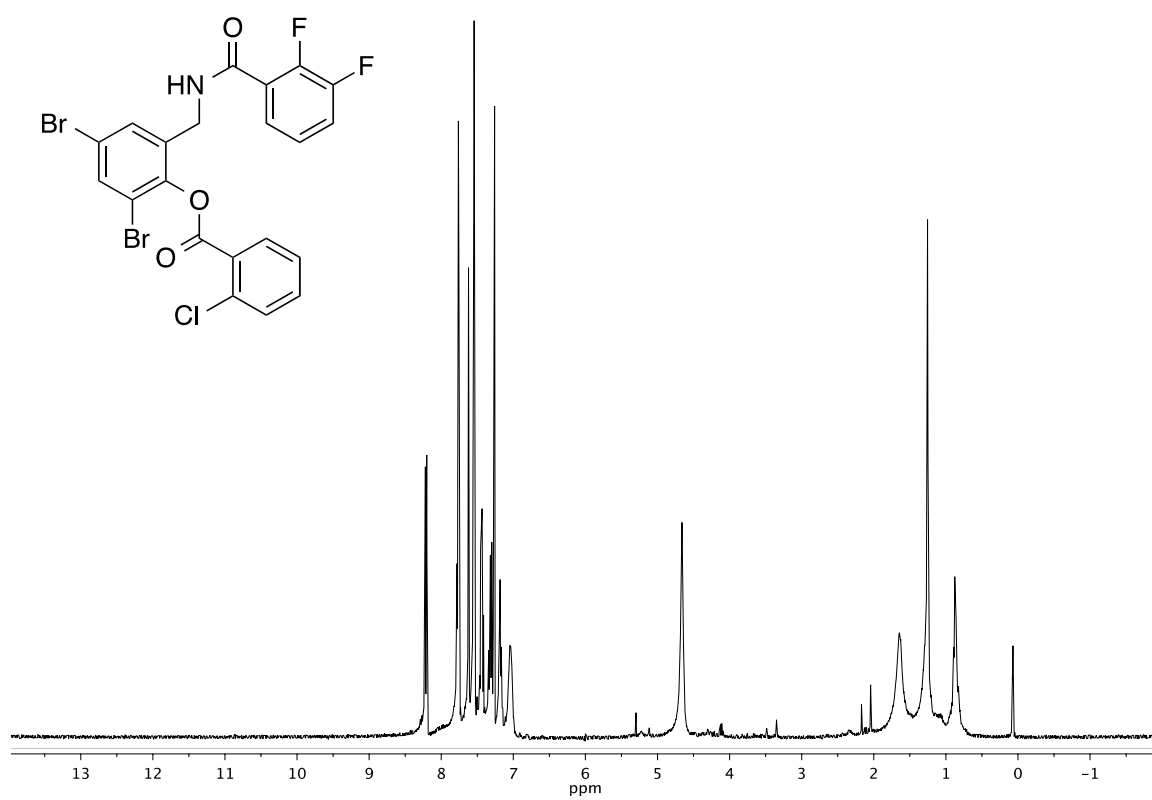
(S)-2,4-dibromo-6-(2-oxo-2-((2-oxotetrahydrofuran-3-yl)amino)ethyl)phenyl
chlorobenzoate, 37.



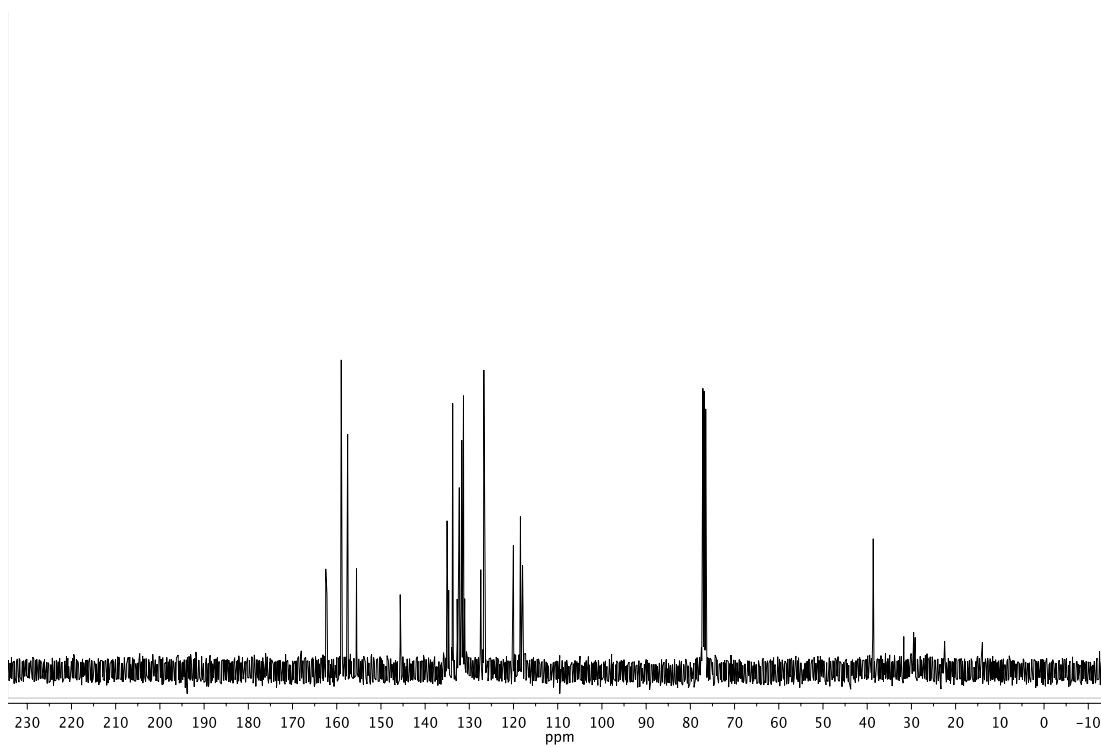
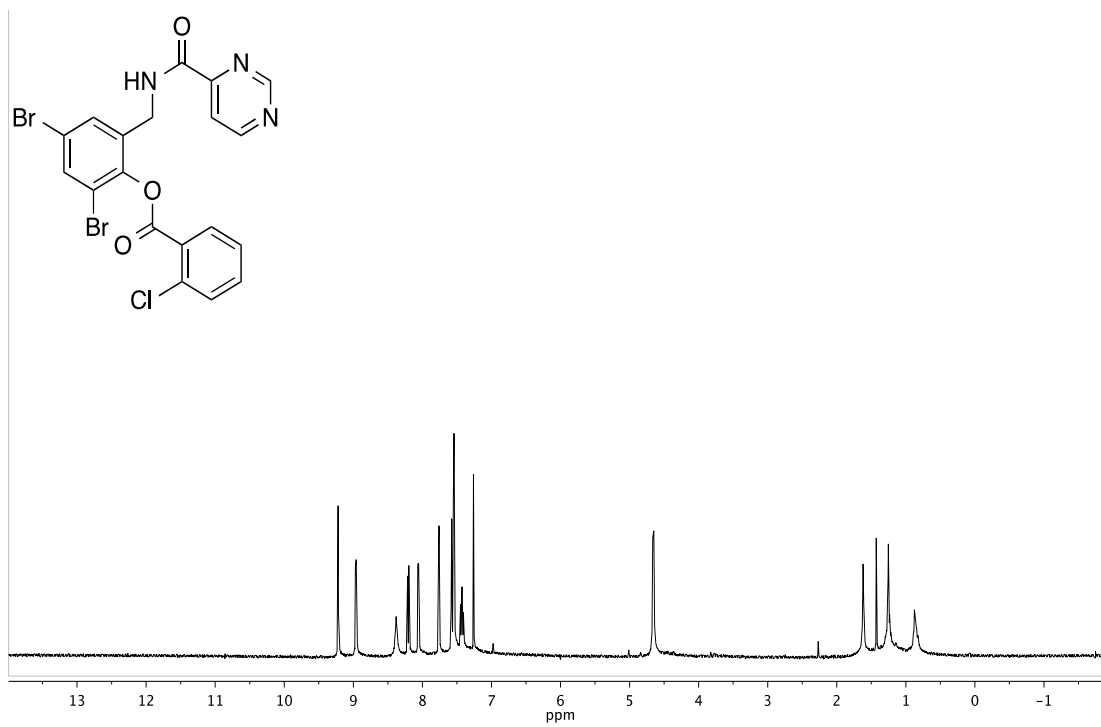
2,4-dibromo-6-(picolinamidomethyl)phenyl 2-chlorobenzoate, 38.



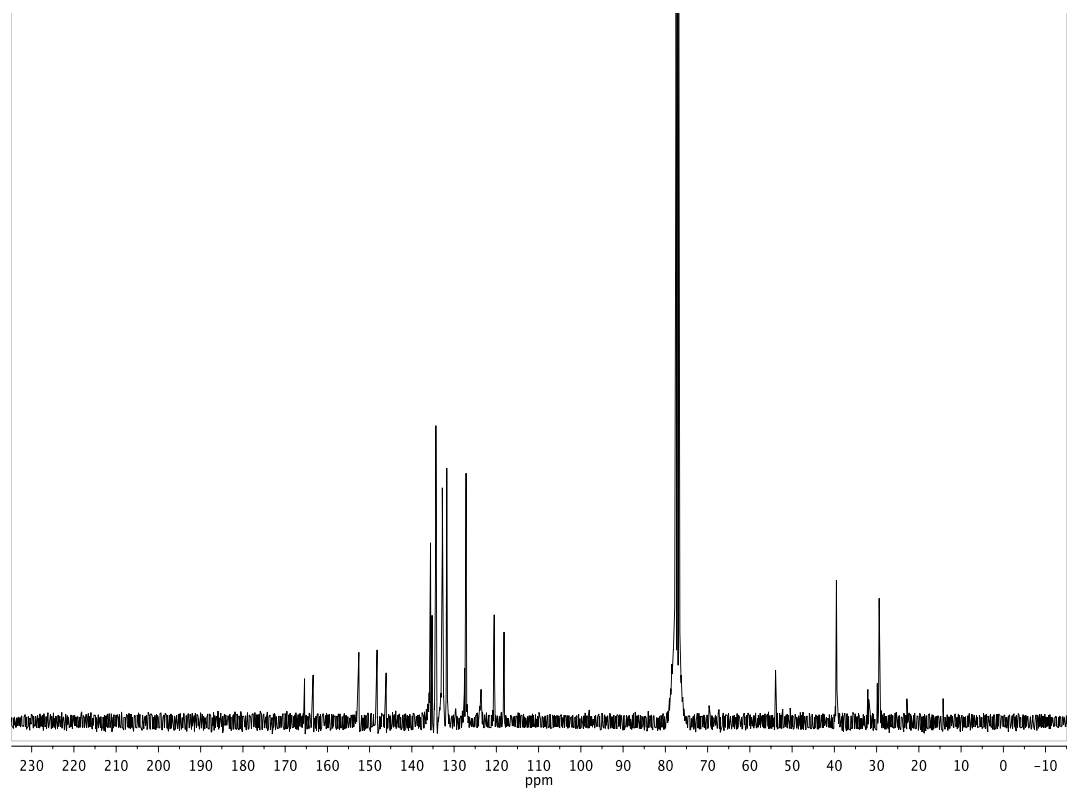
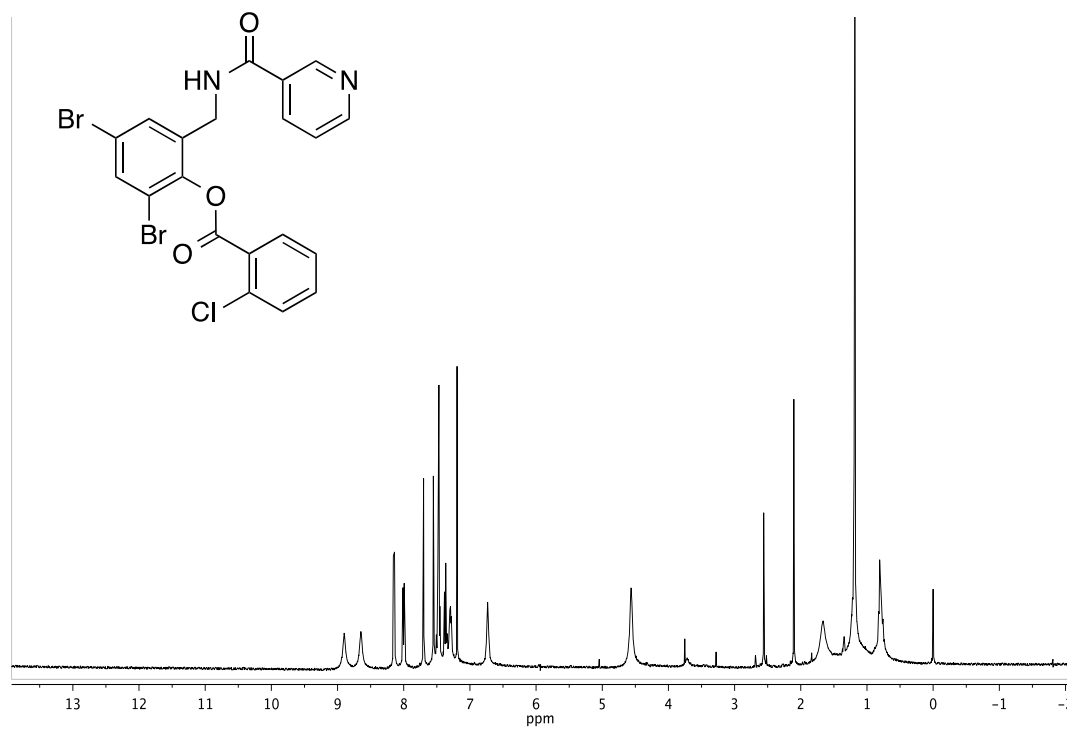
2,4-dibromo-6-((2,3-difluorobenzamido)methyl)phenyl 2-chlorobenzoate, 39.



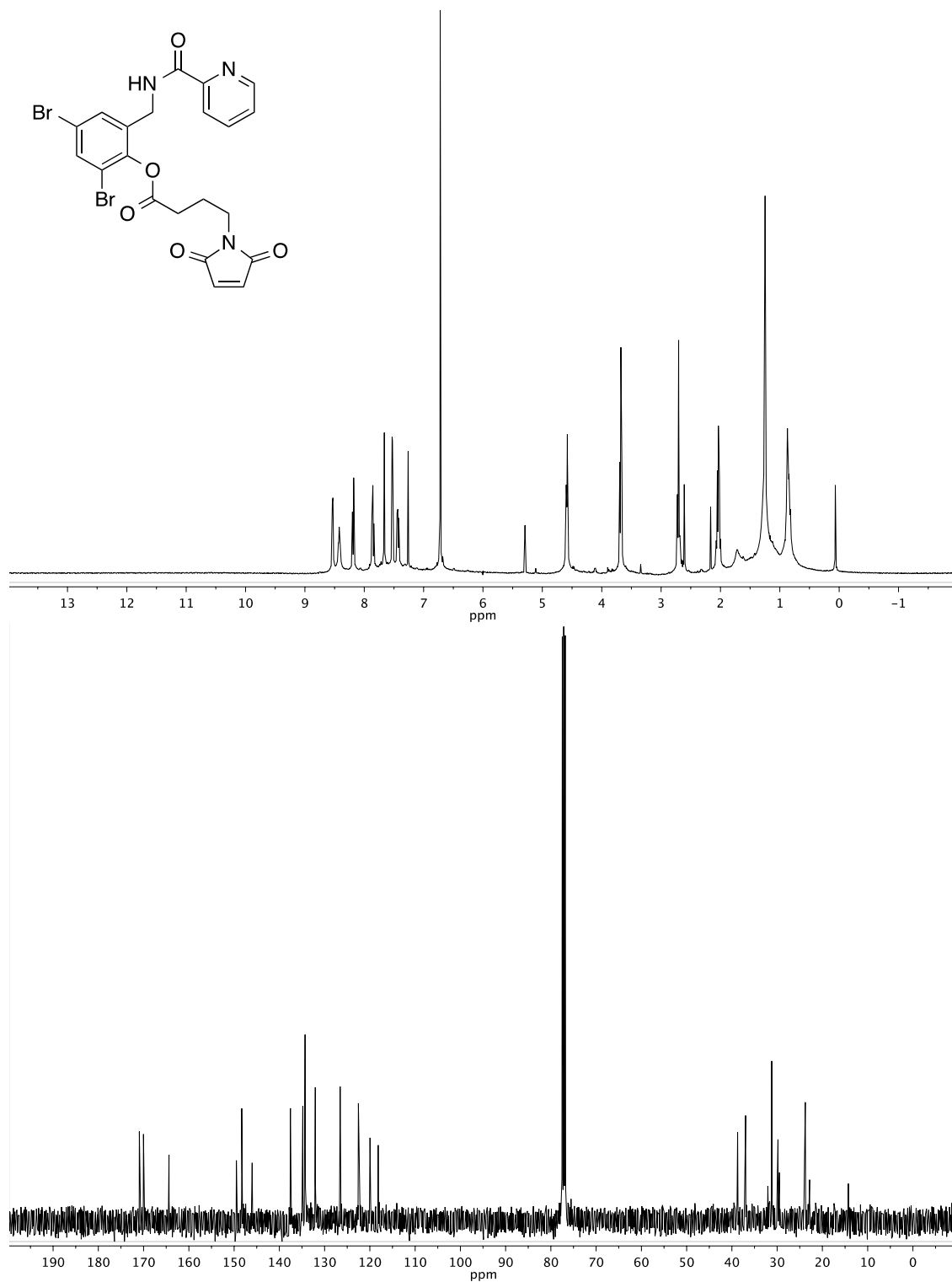
2,4-dibromo-6-((pyrimidine-4-carboxamido)methyl)phenyl 2-chlorobenzoate, 40.



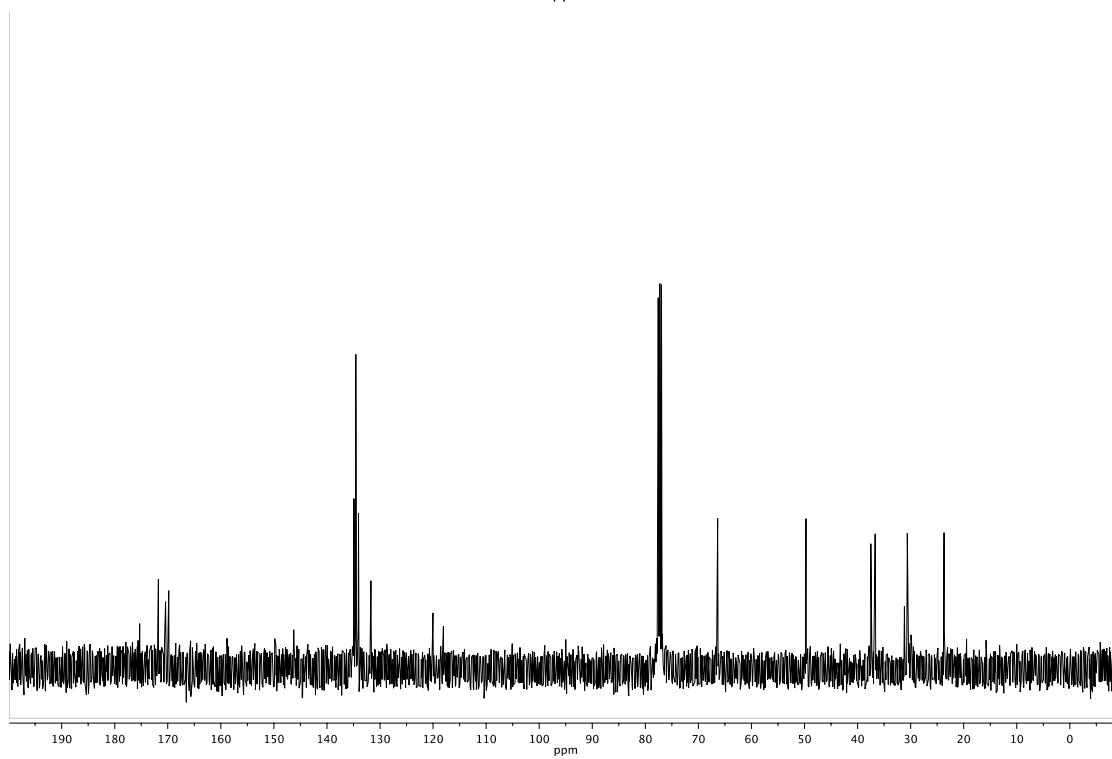
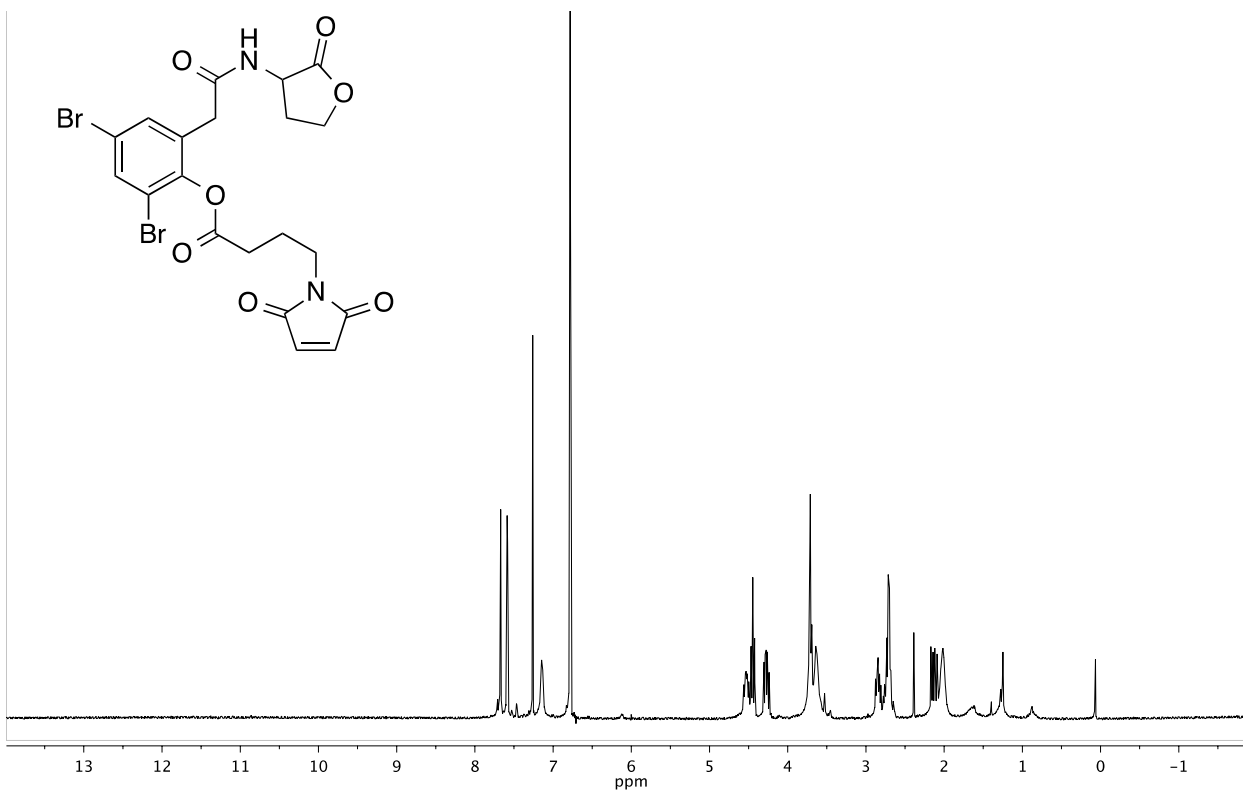
2,4-dibromo-6-(nicotinamidomethyl)phenyl 2-chlorobenzoate, 41.



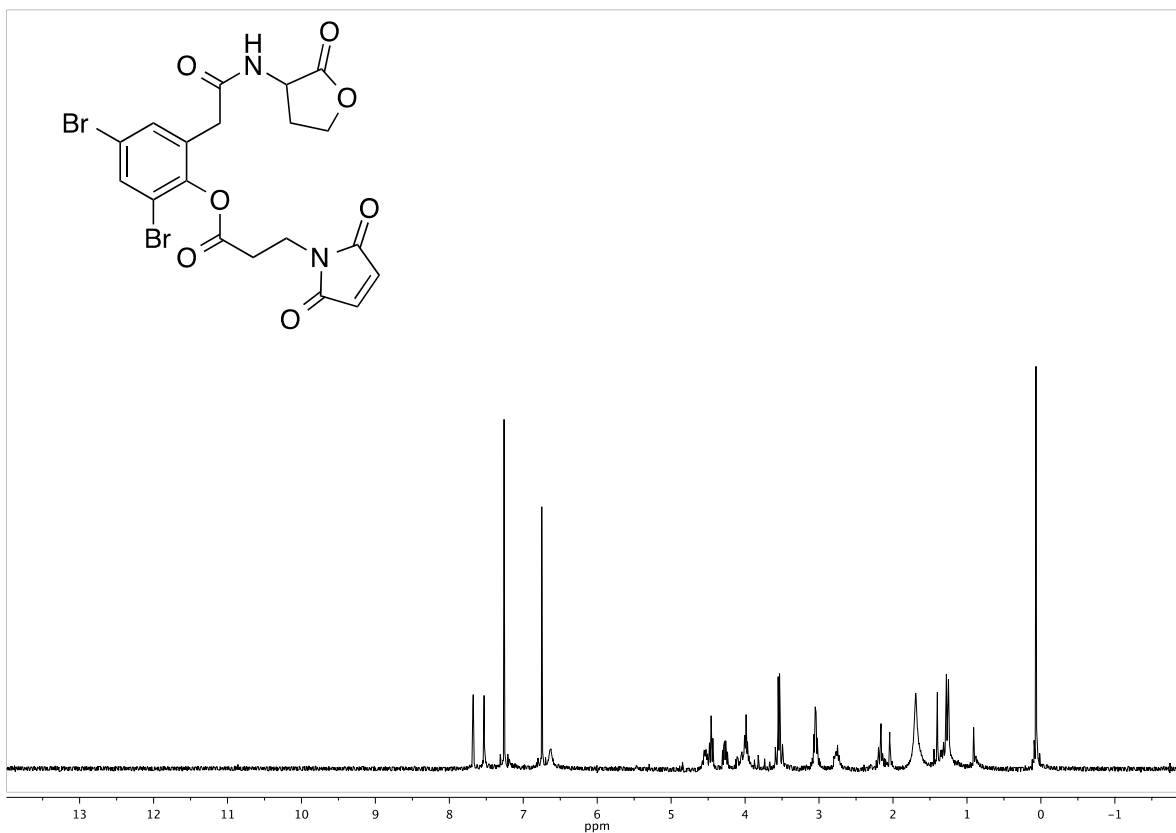
2,4-dibromo-6-(picolinamidomethyl)phenyl 4-(2,5-dioxo-2,5-dihydro-1H-pyrrol-1-yl)butanoate, 42.



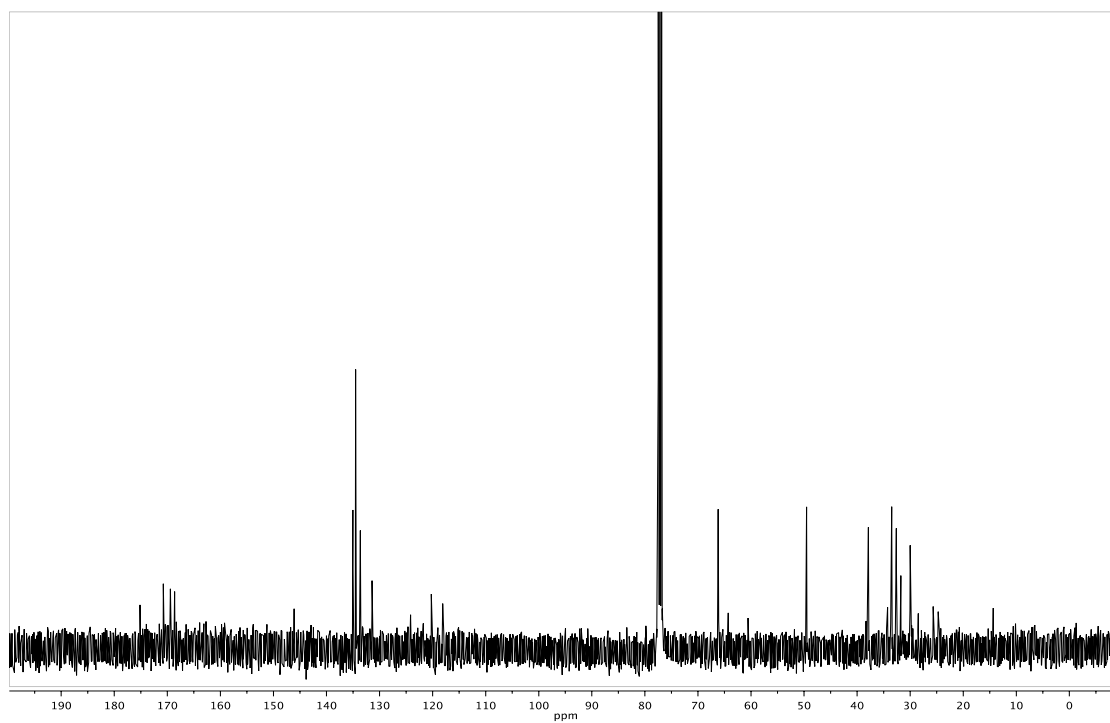
2,4-dibromo-6-(2-oxo-2-((2-oxotetrahydrofuran-3-yl)amino)ethyl)phenyl 4-(2,5-dioxo-2,5-dihydro-1H-pyrrol-1-yl)butanoate, 43.

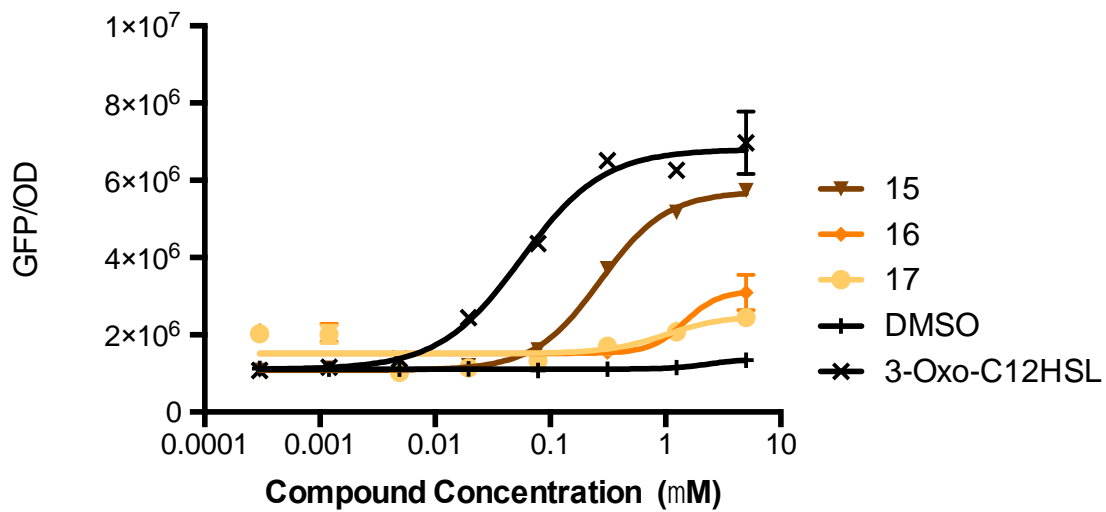
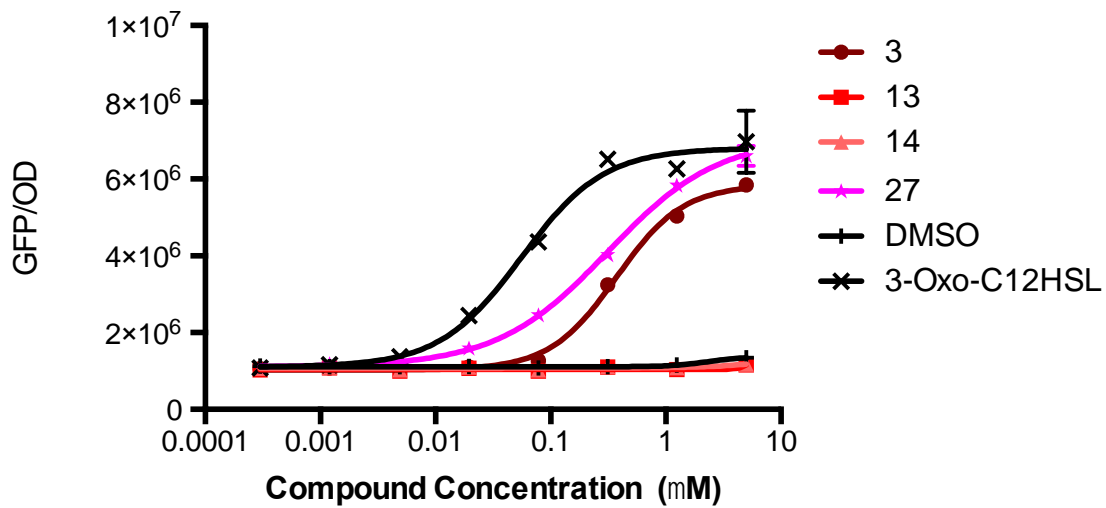


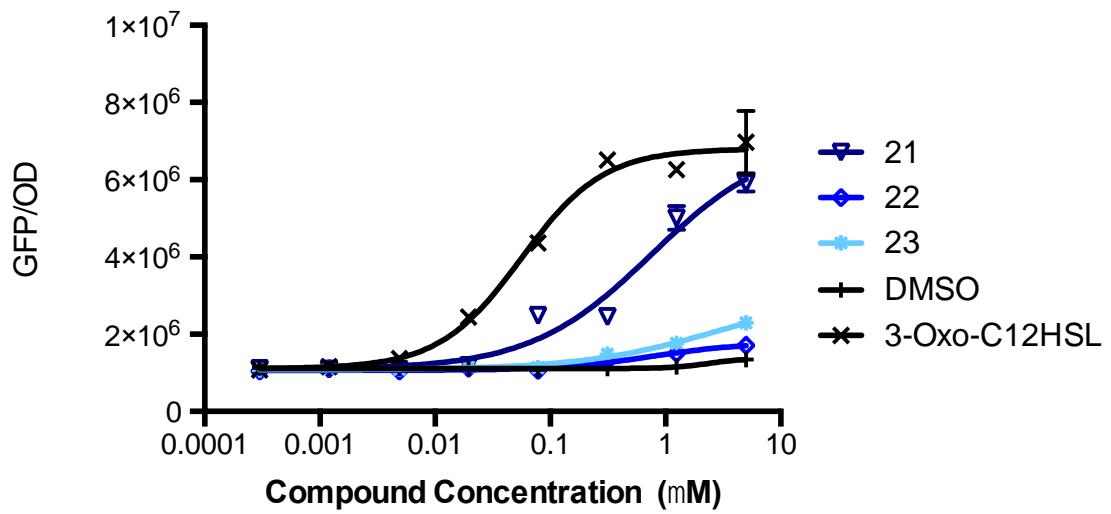
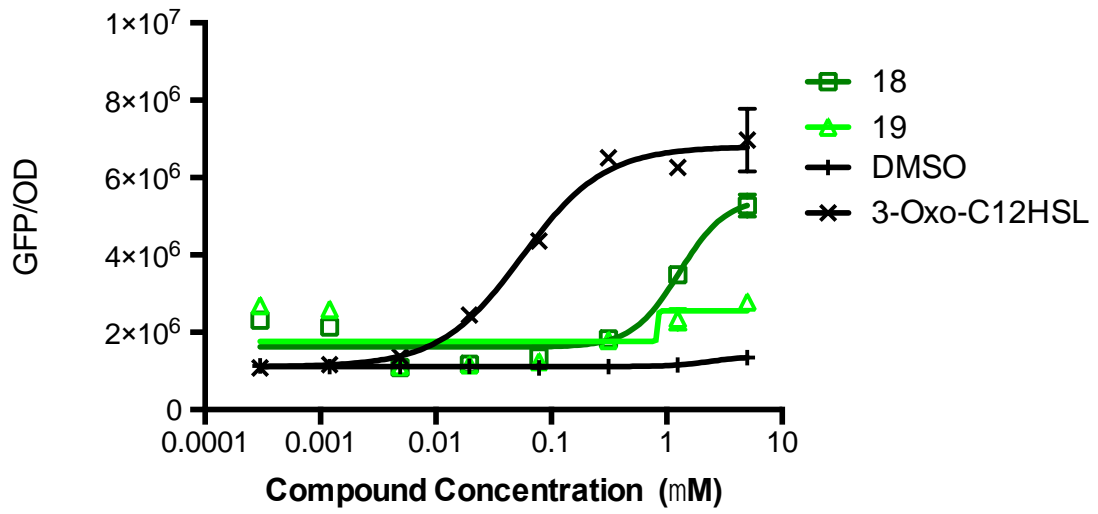
2,4-dibromo-6-(2-oxo-2-((2-oxotetrahydrofuran-3-yl)amino)ethyl)phenyl 3-(2,5-dioxo-

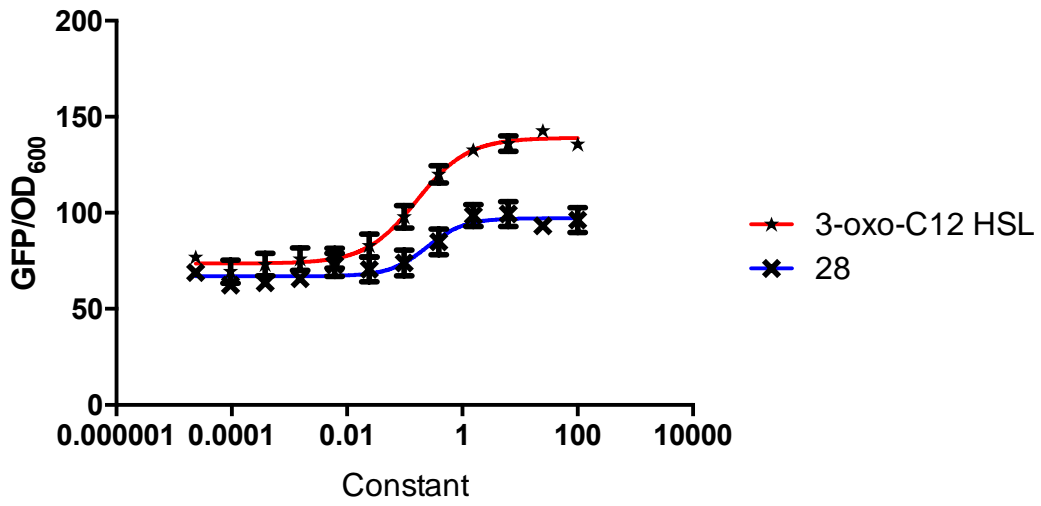
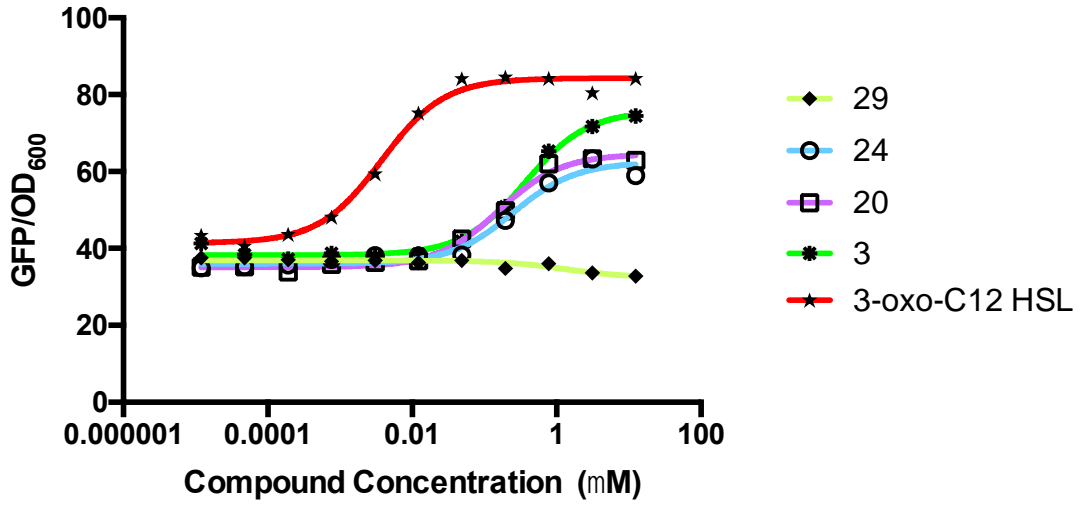


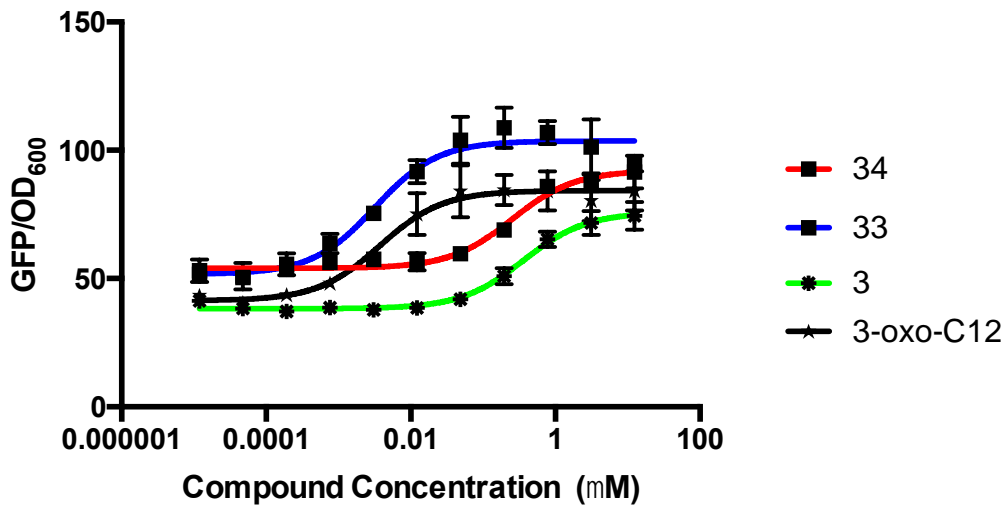
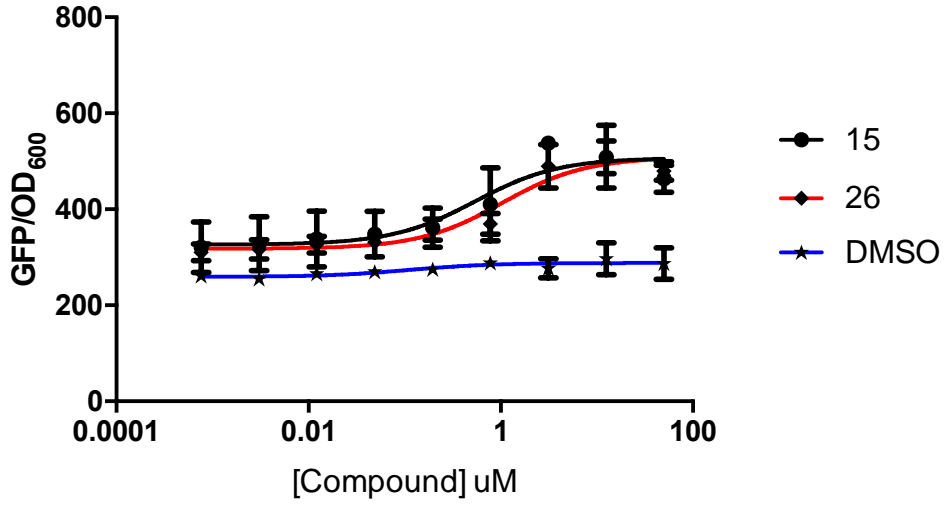
2,5-dihydro-1H-pyrrol-1-yl)propanoate, 44.

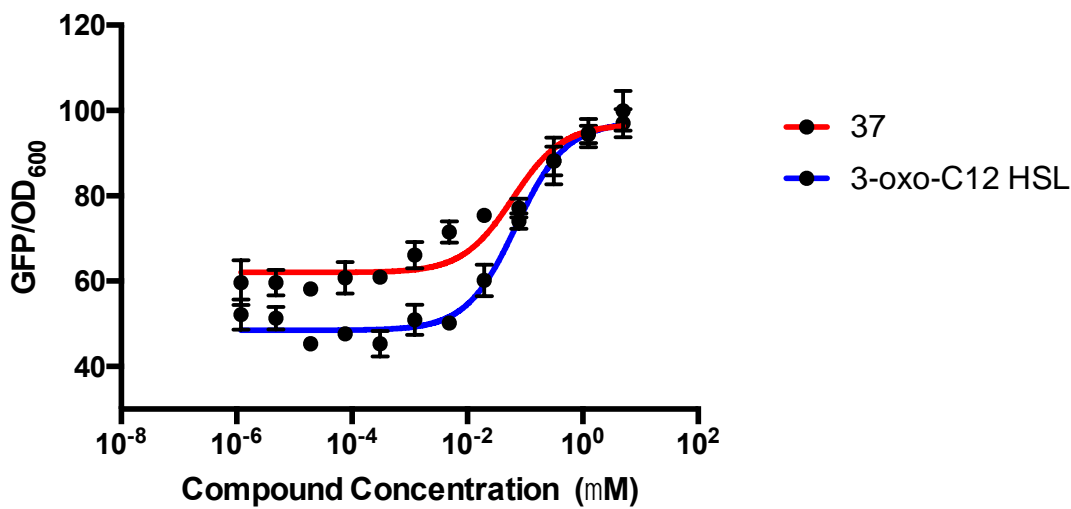
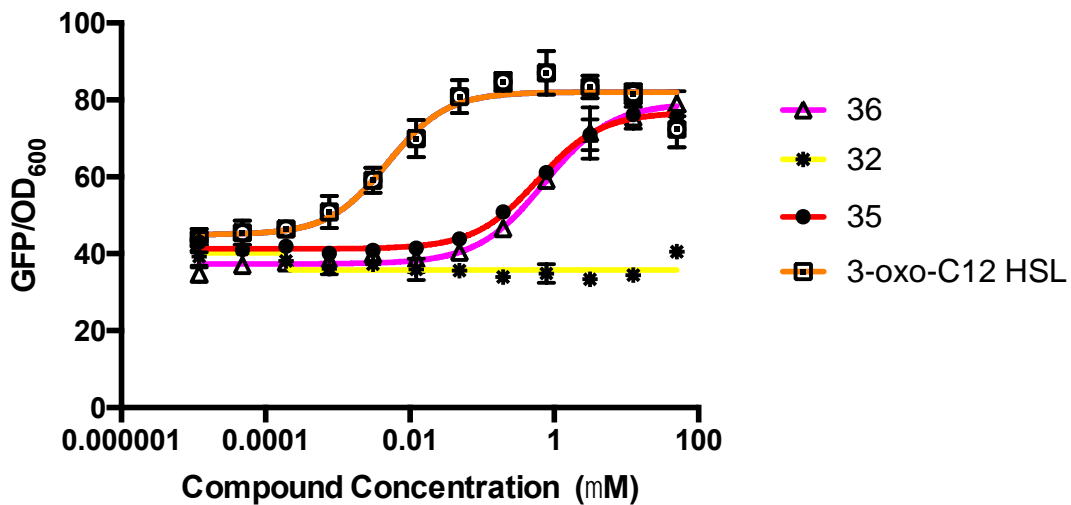


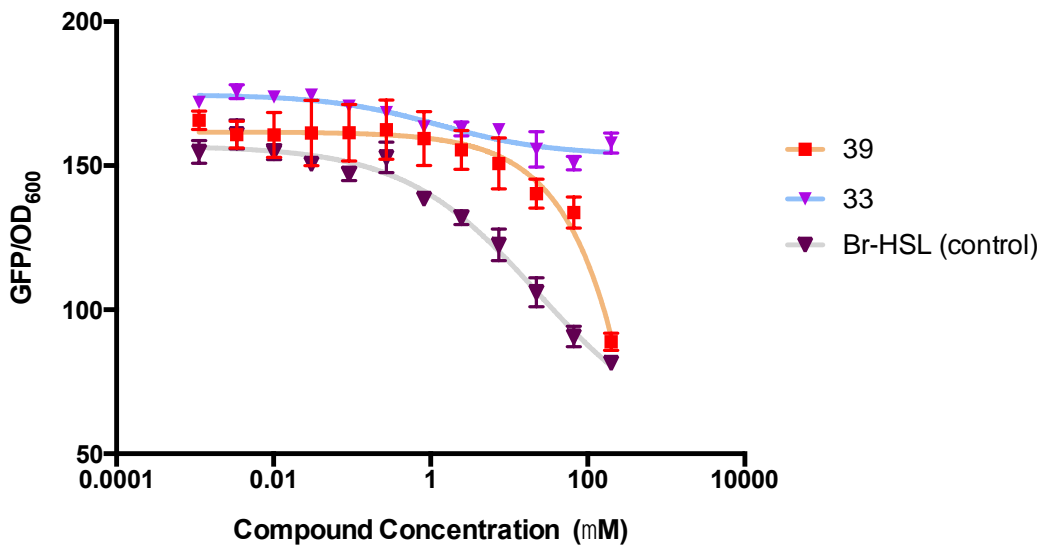
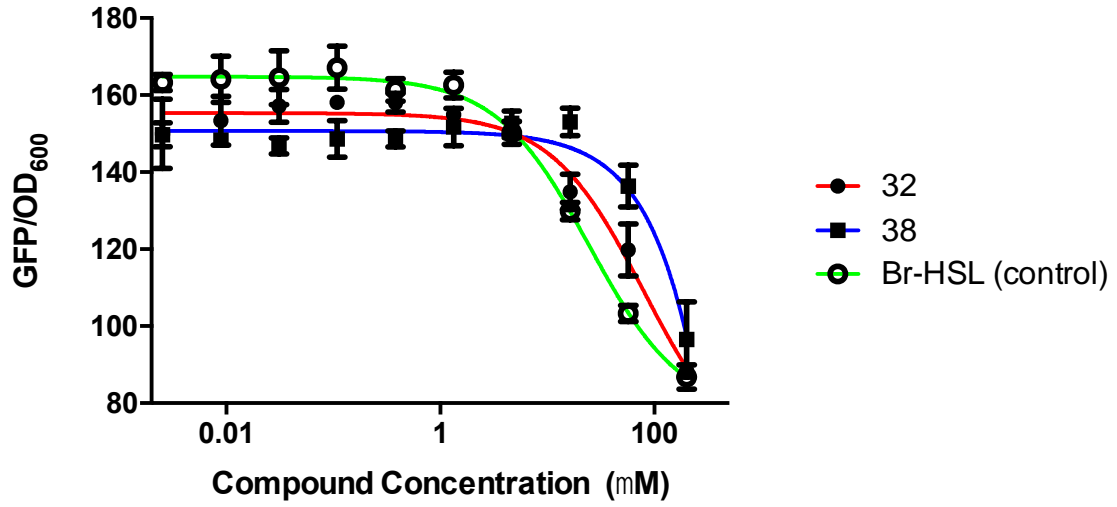


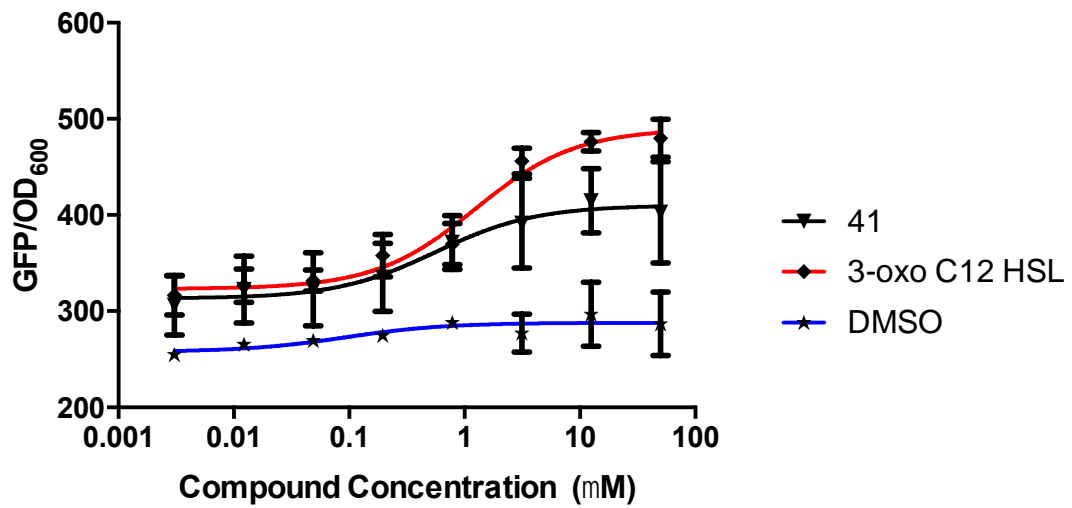
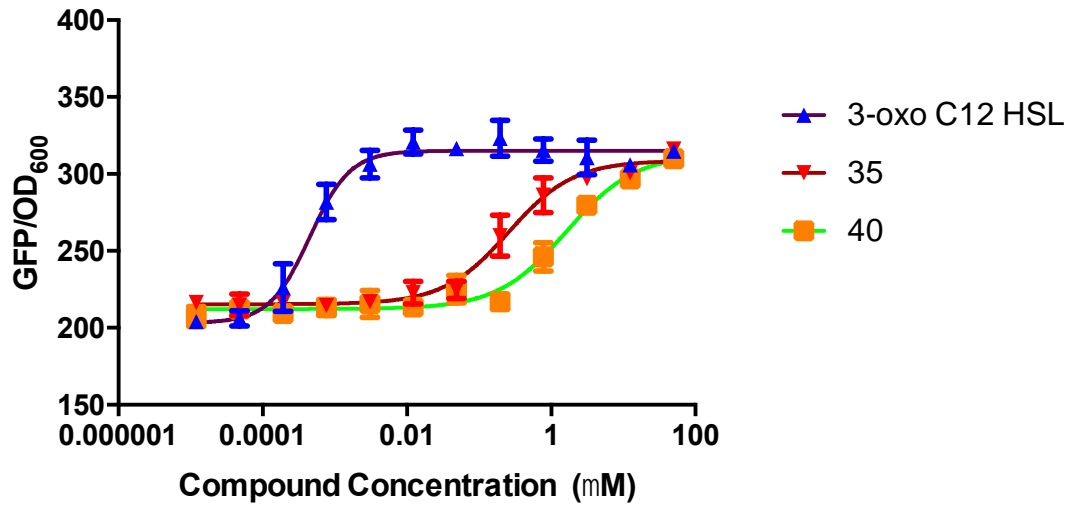


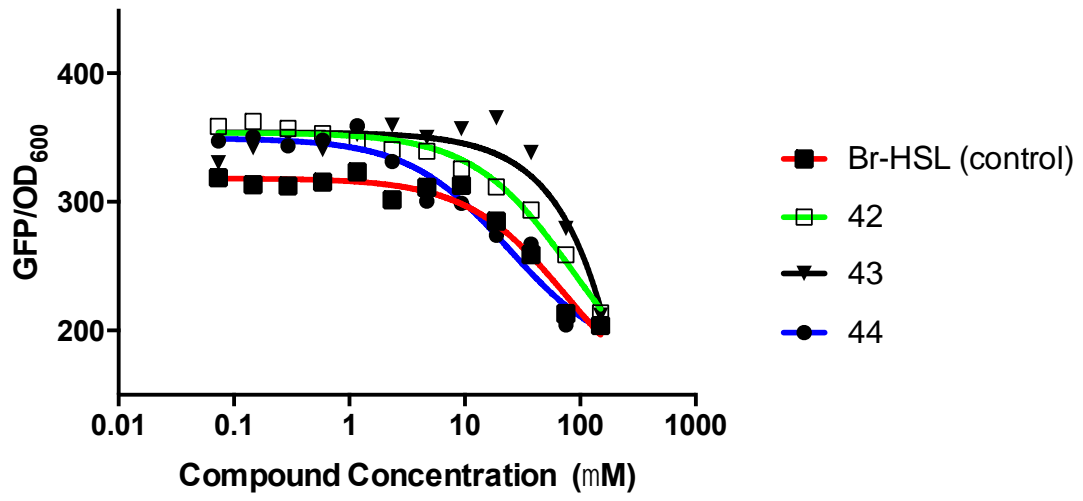












Chapter 2A

New Reaction Methodology

Introduction to New Reaction Development

Synthetic methodologies enabling the oxidative cleavage of carbon-carbon single bonds is an area of considerable recent interest. The development of methodologies to achieve this transformation would be anticipated to be of significant utility by expanding substrate scope for oxidative C-C functionalization reactions in academic and industrial applications. Due to the high activation energy for this transformation and the ubiquitous nature of C-C bonds strategies that achieve selective cleavages remain challenging. To overcome these challenges several methodologies have been developed employing strained scaffolds, chelation assisted reactions and adjacent keto functionality. Here we report a general strategy for the synthesis of carboxylic acid derivatives by oxidative cleavage of methyl ketones.

Aromatic carboxylic acid derivatives are prevalent structural motifs in drug molecules and materials. Synthetic access to these compounds is most commonly achieved by initial carboxylation of the corresponding arene, requiring strong oxidants (e.g. KMnO_4 , chromium-based oxidants) and harsh reaction conditions. Preparation of carboxylic acid derivatives requires a subsequent transformation of the carboxylic acid. Aromatic methyl ketones serve as an attractive alternative to aromatic carboxylic acids as they are readily available and can be efficiently prepared by acylation. Conversion of this alternative substrate requires the oxidative cleavage of a C-C single bond. The most widely employed methodology to achieve this transformation, the well-known haloform reaction allows ready access to the corresponding carboxylic acids however does not

allow for the direct assembly of other carboxylic acid derivatives. Hence, a reaction enabling direct conversion of aromatic methyl ketones to a diverse array of carboxylic acid derivatives would be desirable.

Inspired by the reliability of the well-established haloform reaction and based on early industrial studies on the reactivity of acetyl nitrite, we envisioned a process enabling the net oxidative C-C bond cleavage of aromatic methyl ketones. Analogous to the haloform reaction this process was anticipated to proceed via a series of sequential α -nitration reactions and subsequent nucleophilic displacement of an activated di- or tri-nitromethane. Contrasting the haloform reaction, in which the base (e.g. KOH) typically serves as nucleophile forming carboxylic acids we envisioned the ability to easily modulate the nature of the second nucleophile to allow direct access to a diverse array of carboxylic acid derivatives.

Reaction Optimization

Table 4

Optimization of the reaction changing stoichiometry and solvents, testing each reaction by percent conversion.

EQ HNO₃	EQ Ac₂O	Solvent (0.5 M)	Percent Conversion (by NMR)
1	1	AcOH	2%
2	1	AcOH	15%
3	3	AcOH	42%
6	3	AcOH	61%
6	3	THF	46%
6	3	DMSO	51%
6	3	ACN	83%
6	3	DMF	0%

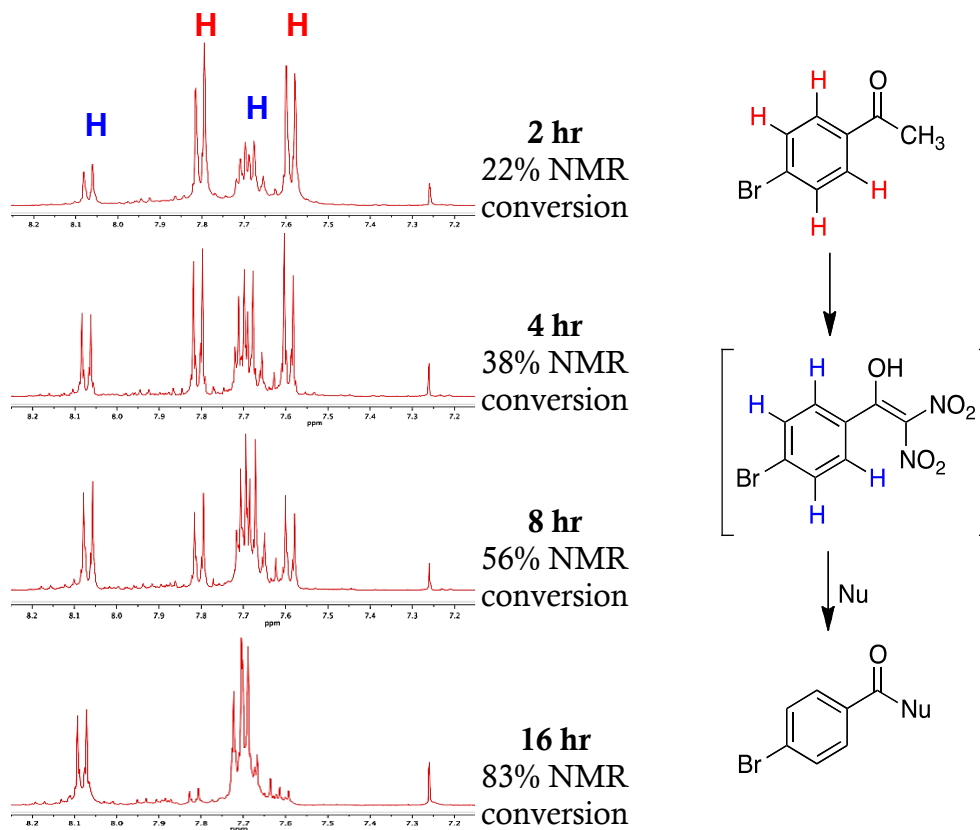


Figure 13. Percent conversion was calculated based on ¹H NMR, as starting material was converted to intermediate product.

The full optimization of the reaction can be seen in Table 4 and Figure 13 as the equivalents of each reactant is changed as well as the solvent being altered. As the time of the reaction was increased, we see the greatest percent conversion at 16 hours as the starting material transitions into intermediate, as determined by ¹H NMR. This intermediate was completely isolated and characterized. Once the reaction was ran past 16 hours, no increase in conversion was seen. The overall reaction was settled at 6 EQ of nitric acid, 3 EQ of acetic anhydride, and acetonitrile as solvent.

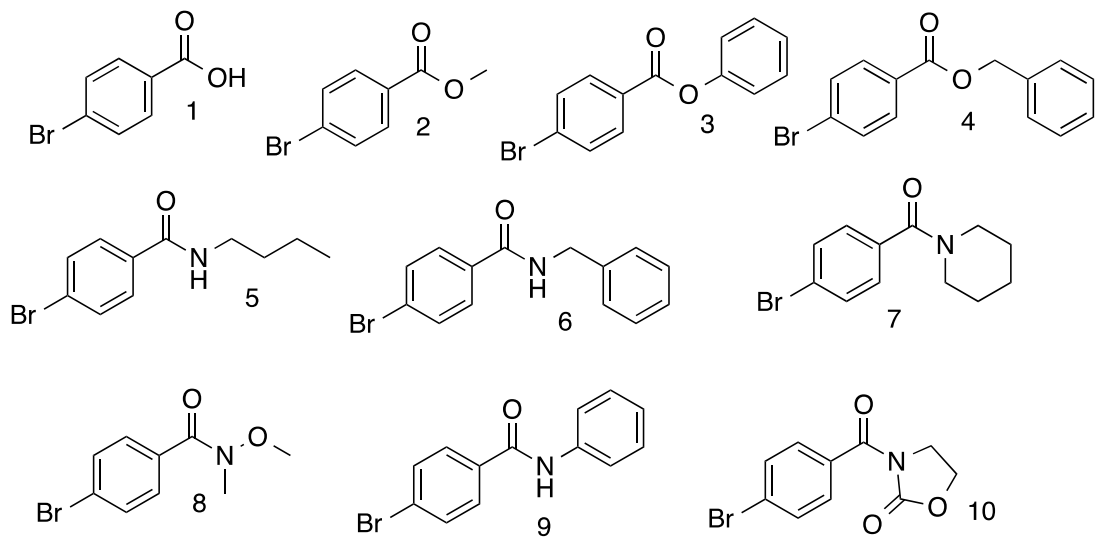
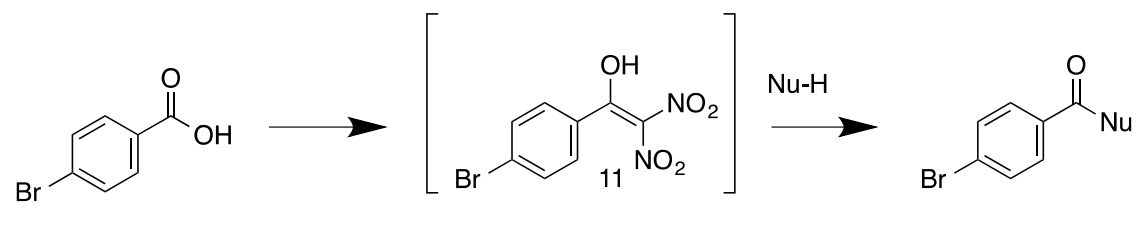


Figure 14. Scope of the Nucleophile.

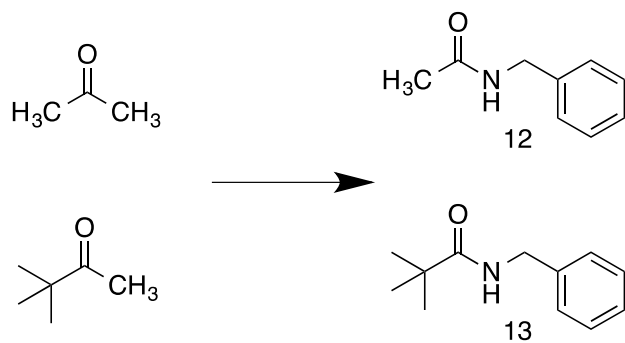


Figure 15. Scope of the Electrophile

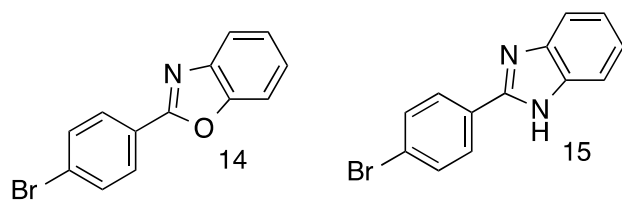


Figure 16. Heterocycle Synthesis

The overall scope of the various Nucleophiles can be seen in Figure 14 and Figure 16. The reaction worked very successfully with both Oxygen and Nitrogen based nucleophiles of various kinds. The reaction even has some success when using electron poor nucleophiles such as Molecules **8** and **10**, but at much lower yields compared to the rest of the field. Heterocycle synthesis was also possible under these reaction conditions to produce molecules **14** and **15**. The scope of the electrophile overall was less successful as seen in Figure 15. 4-bromoacetophenone was the most optimized electrophile, and attempting to vary this lead us to Molecules **12** and **13**.

Conclusion

Overall, a new reaction was developed mimicking the Haloform reaction. This reaction differs itself from that based on its scope and reaction conditions used to achieve a successful reaction. The Haloform reaction only found success with oxygen based nucleophiles, while this reaction works with nitrogen and oxygen based nucleophiles. The conditions of this reaction differ greatly as we use strong acid while the Haloform reaction used a strong base in order to substitute ketone.

Chapter 2B

Experimental Data for New Reaction Methodology

General Experimental Data

Unless otherwise noted, all reactions were performed in flame-dried glassware under an atmosphere of nitrogen or argon using dried reagents and solvents. All chemicals were purchased from commercial vendors and used without further purification. Anhydrous clean solvents were purchased from commercial vendors.

Flash chromatography was performed using standard grade silica gel 60 230-400 mesh from SORBENT Technologies or was performed using a Biotage Flash Purification system equipped with Biotage SNAP columns. All purifications were performed using gradients of mixtures of ethyl acetate and hexanes. Analytical thin-layer chromatography was carried out using Silica G TLC plates, 200 μm with UV₂₅₄ fluorescent indicator (SORBENT Technologies), and visualization was performed by staining and/or by absorbance of UV light.

NMR spectra were recorded using a Varian Mercury Plus spectrometer (400 MHz for ¹H-NMR; 100 MHz for ¹³C-NMR). Chemical shifts are reported in parts per million (ppm) and were calibrated according to residual protonated solvent. Mass spectroscopy data was collected using an Agilent 1100-Series LC/MSD Trap LC-MS or a Micromass Quattro micro with a Waters 2795 Separations Module LC-MS with acetonitrile containing 0.1% formic acid as the mobile phase in positive ionization mode. Purity was determined on a Agilent 1100 series equipped with a Phenomenex Kinetex 2.6 μm C18-UPLC column using a gradient of water to acetonitrile with 0.1% TFA.

Procedure A: This is a two-day reaction. On day one, the electrophile 4-bromoacetophenone(122.2mg, 1EQ), DriSolv acetonitrile(1.22mL, 0.5M), acetic anhydride(0.171mL, 3EQ), and nitric acid(0.171mL, 6EQ) were added on ice to a 20ml scintillation vial. This solution stirred overnight. On day two, N-ethyl-diisopropylamine(1.3mL, 12EQ) was added along with each reaction's respective nucleophile(0.5EQ) both on ice. This solution stirred overnight and the next day the reaction was complete.

Procedure B: This is a three-day reaction. The first and second day of this reaction is the same as procedure A. On day three, acetic acid(1.22mL) is added and the reaction is stirred overnight at 60°C.

¹H-NMR and ¹³C-NMR Spectra for all Final Compounds and Key Intermediates

4-bromobenzoic acid, 1.

Product was produced following Procedure A with KOH (0.5 EQ) as nucleophile and yielded 42.9 mg, 0.213 mmol, 69.6%. ¹H NMR (400 MHz, CD₃OD) δ 12.0(1H) 7.91 (d, 2H), 7.64 (d, 2H). ¹³C NMR (101 MHz, CD₃OD) δ 168.82, 132.79, 132.45, 131.12, 128.77. ESI-MS calculated for C₇H₆BrO₂, 202.027 [M+H], observed, 202.498; HPLC purity=90.8%.

Methyl 4-bromobenzoate, 2.

Product was produced following Procedure A with methanol (0.5EQ) as nucleophile and yielded 53.4 mg, 0.248 mmol, 81.0%. ¹H NMR (400 MHz, CDCl₃) δ 7.90 (d, 2H), 7.58 (d, 2H), 3.91 (s, 3H). ¹³C NMR (101 MHz, CDCl₃) δ 166.60, 131.94, 131.34, 129.25,

128.27, 52.54. ESI-MS calculated for $C_8H_8BrO_2$, 216.971 [M+H], observed, 216.414; HPLC purity=87.5%.

Phenyl 4-bromobenzoate, 3.

Product was produced following Procedure A with phenol (0.5EQ) as nucleophile and yielded 54.3 mg, 0.196 mmol, 64.0%. 1H NMR (400 MHz, $CDCl_3$) δ 8.07 (d, 2H), 7.66 (d, 2H), 7.44 (t, 2H), 7.29 (t, 1H), 7.21 (dd, 2H). ^{13}C NMR (101 MHz, $CDCl_3$) δ 164.72, 150.96, 132.18, 131.88, 129.77, 129.05, 128.70, 126.28, 121.83. ESI-MS calculated for $C_{13}H_{10}BrO_2$, 278.125 [M+H], observed, 278.414; HPLC purity=90.6%.

Benzyl 4-bromobenzoate, 4.

Product was produced following Procedure A with benzyl alcohol (0.5EQ) as nucleophile and yielded 49.8 mg, 0.171 mmol, 55.8%. 1H NMR (400 MHz, $CDCl_3$) δ 7.94 (d, 2H), 7.58 (d, 2H), 7.47 – 7.31 (m, 5H), 5.36 (s, 2H). ^{13}C NMR (101 MHz, $CDCl_3$) δ 165.84, 135.88, 132.64, 131.86, 131.36, 129.15, 128.78, 128.52, 128.39, 67.11. ESI-MS calculated for $C_{14}H_{12}BrO_2$, 292.152 [M+H], observed, 292.125; HPLC purity=96.4%.

4-bromo-N-butylbenzamide, 5.

Product was produced following Procedure A with 1-butyl amine (0.5EQ) as nucleophile and yielded 63.4 mg, 0.258 mmol, 80.8%. 1H NMR (400 MHz, $CDCl_3$) δ 7.62 (d, 2H), 7.55 (d, 2H), 6.15 (s, 1H), 3.44 (q, $J = 7.2, 5.6$ Hz, 2H), 1.66 – 1.52 (m, 2H), 1.47 – 1.33 (m, 2H), 0.95 (t, $J = 7.3$ Hz, 3H). ^{13}C NMR (101 MHz, $CDCl_3$) δ 166.73, 133.74, 131.89, 128.61, 126.10, 40.07, 31.80, 20.29, 13.92. ESI-MS calculated for $C_{11}H_{15}BrNO$, 257.151 [M+H], observed, 257.151; HPLC purity = 91.5%.

N-benzyl-4-bromobenzamide, 6.

Product was produced following Procedure A with benzyl amine (0.5EQ) as nucleophile and yielded 70.6 mg, 0.243 mmol, 79.4%. ¹H NMR (400 MHz, CDCl₃) δ 7.65 (d, 2H), 7.55 (d, 2H), 7.39 – 7.27 (m, 5H), 6.49 (s, 1H), 4.61 (d, *J* = 5.6 Hz, 2H). ¹³C NMR (101 MHz, CDCl₃) δ 166.52, 138.01, 133.28, 131.94, 128.96, 128.72, 128.06, 127.87, 126.37, 44.36. ESI-MS calculated from C₁₄H₁₃BrNO, 291.168 [M+H], observed, 291.388; HPLC purity=94.1%.

(4-bromophenyl)(piperidin-1-yl)methanone, 7.

Product was produced following Procedure A with piperidine (0.5EQ) as nucleophile and yielded 48.7 mg, 0.182 mmol, 59.3%. ¹H NMR (400 MHz, CDCl₃) δ 7.53 (d, 2H), 7.26 (d, 2H), 3.68 (s, 2H), 3.32 (s, 2H), 1.80 – 1.40 (m, 6H). ¹³C NMR (101 MHz, CDCl₃) δ 169.37, 135.40, 131.76, 128.70, 123.75, 48.89, 43.36, 26.55, 25.78, 24.65. ESI-MS calculated from C₁₂H₁₅BrNO, 269.162 [M+H], observed, 269.162; HPLC purity=90.1%.

4-bromo-N-methoxy-N-methylbenzamide, 8.

Product was produced following Procedure A with N,O dimethyl hydroxylamine HCl (0.5EQ) as nucleophile and yielded 58.1 mg, 0.238 mmol, 77.7%. ¹H NMR (400 MHz, CDCl₃) δ 7.58 (d, 2H), 7.54 (d, 2H), 3.53 (s, 3H), 3.35 (s, 3H). ¹³C NMR (101 MHz, CDCl₃) δ 168.85, 132.89, 131.37, 130.15, 125.28, 61.27, 33.64. ESI-MS calculated from C₉H₁₁BrNO₂, 245.096 [M+H], observed, 245.096; HPLC purity=95.7%.

4-bromo-N-phenylbenzamide, 9.

Product was produced following Procedure A with aniline (0.5EQ) as nucleophile and yielded 34.1 mg, 0.124 mmol, 40.3%. ¹H NMR (400 MHz, CDCl₃) δ 7.74 (d, *J* = 8.5 Hz, 3H), 7.62 (d, 4H), 7.38 (t, 2H), 7.17 (t, *J* = 7.5, 1.1 Hz, 1H). ¹³C NMR (101 MHz, CDCl₃) δ 164.86, 137.74, 133.92, 132.20, 129.31, 128.76, 126.76, 124.98, 120.38. ESI-MS calculated from C₁₃H₁₁BrNO, 277.141 [M+H], observed, 277.141; HPLC purity=80.2%.

3-(4-bromobenzoyl)oxazolidin-2-one, 10.

Product was produced following Procedure A with oxazolidinone (0.5EQ) as nucleophile and yielded 9.2 mg, 0.034 mmol, 11.1%. ¹H NMR (400 MHz, CDCl₃) δ 7.57 (d, 2H), 7.55 (d, 2H), 4.51 (t, 2H), 4.18 (t, 2H). ¹³C NMR (101 MHz, CDCl₃) δ 168.98, 153.28, 131.42, 131.36, 130.86, 127.55, 62.46, 43.82. ESI-MS calculated from C₁₀H₉BrNO₃, 271.090[M+H], observed, 271.090; HPLC purity=80.5%.

2-(4-bromophenyl)-1H-benzo[d]imidazole, 15.

Product was produced following Procedure B with ortho-phenylene diamine (0.5EQ) as nucleophile and yielded 42.0 mg, 0.154 mmol, 85.7%. ¹H NMR (400 MHz, CD₃OD) δ 8.00 (d, 2H), 7.72 (d, 2H), 7.65 – 7.58 (m, 2H), 7.31 – 7.25 (m, 2H). ¹³C NMR (101 MHz, CD₃OD) δ 152.24, 133.40, 130.13, 129.45, 125.53, 124.18. ESI-MS calculated from C₁₃H₁₀BrN₂, 274.141 [M+H], observed, 274.141; HPLC purity=93.8%.

N-benzylpivalamide, 13.

Product was produced following Procedure A with pN-benzyl-4-bromobenzamide (0.5EQ) as nucleophile, pinacolone (1EQ) as electrophile, and yielded 114.7 mg, 0.600 mmol, 58.4%. ¹H NMR (400 MHz, CDCl₃) δ 7.34 – 7.20 (m, 5H), 6.14 (s, 1H), 4.39 (d, *J*

= 5.7 Hz, 2H), 1.21 (s, 9H). ¹³C NMR (101 MHz, CDCl₃) δ 178.42, 138.68, 128.65, 127.54, 127.34, 43.49, 38.70, 27.61. ESI-MS calculated from C₁₂H₁₈NO, 192.282 [M+H], observed, 192.380.

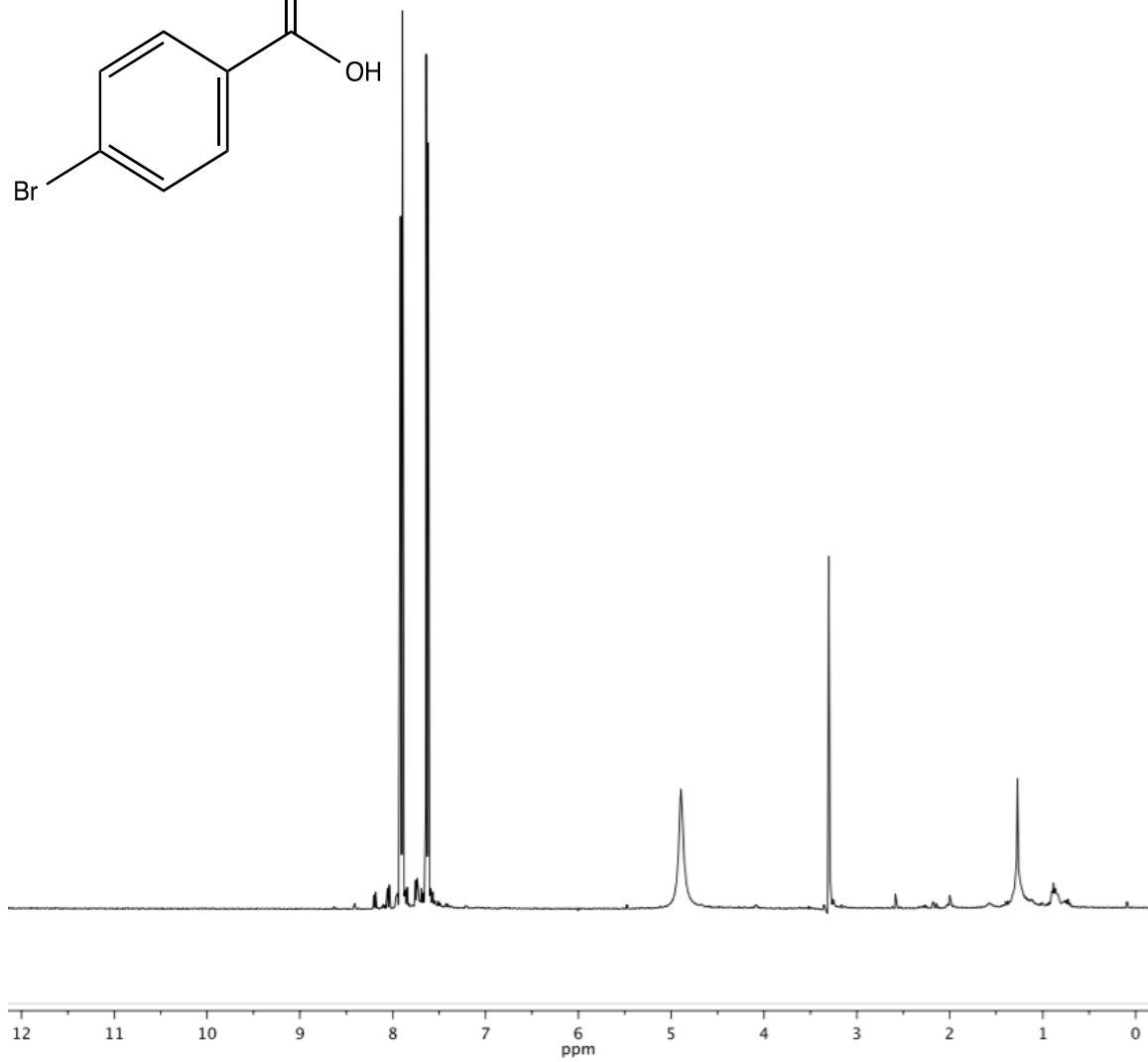
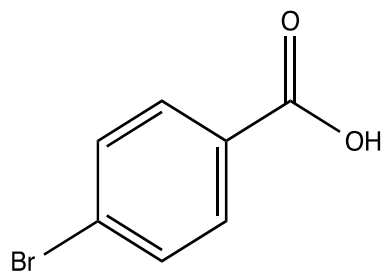
1-(4-bromophenyl)-2,2-dinitroethen-1-ol, 11.

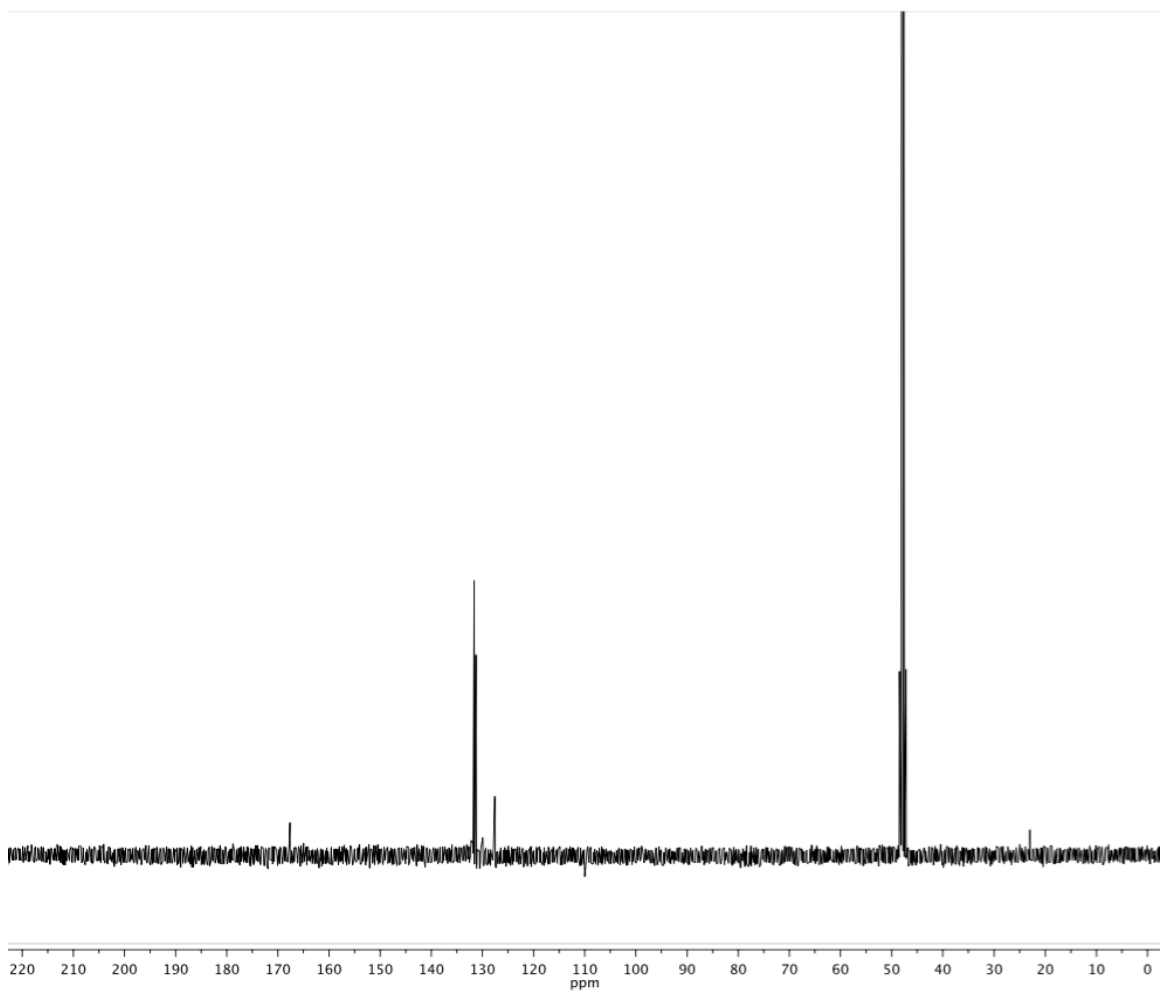
Isolated intermediate. ¹H NMR (400 MHz, CDCl₃) δ 8.00 (d, 2H), 7.72 (d, 2H). ¹³C NMR (101 MHz, CDCl₃) δ 181.79, 152.56, 133.48, 132.65, 131.82, 131.37.

2-(4-bromophenyl)benzo[d]oxazole, 14.

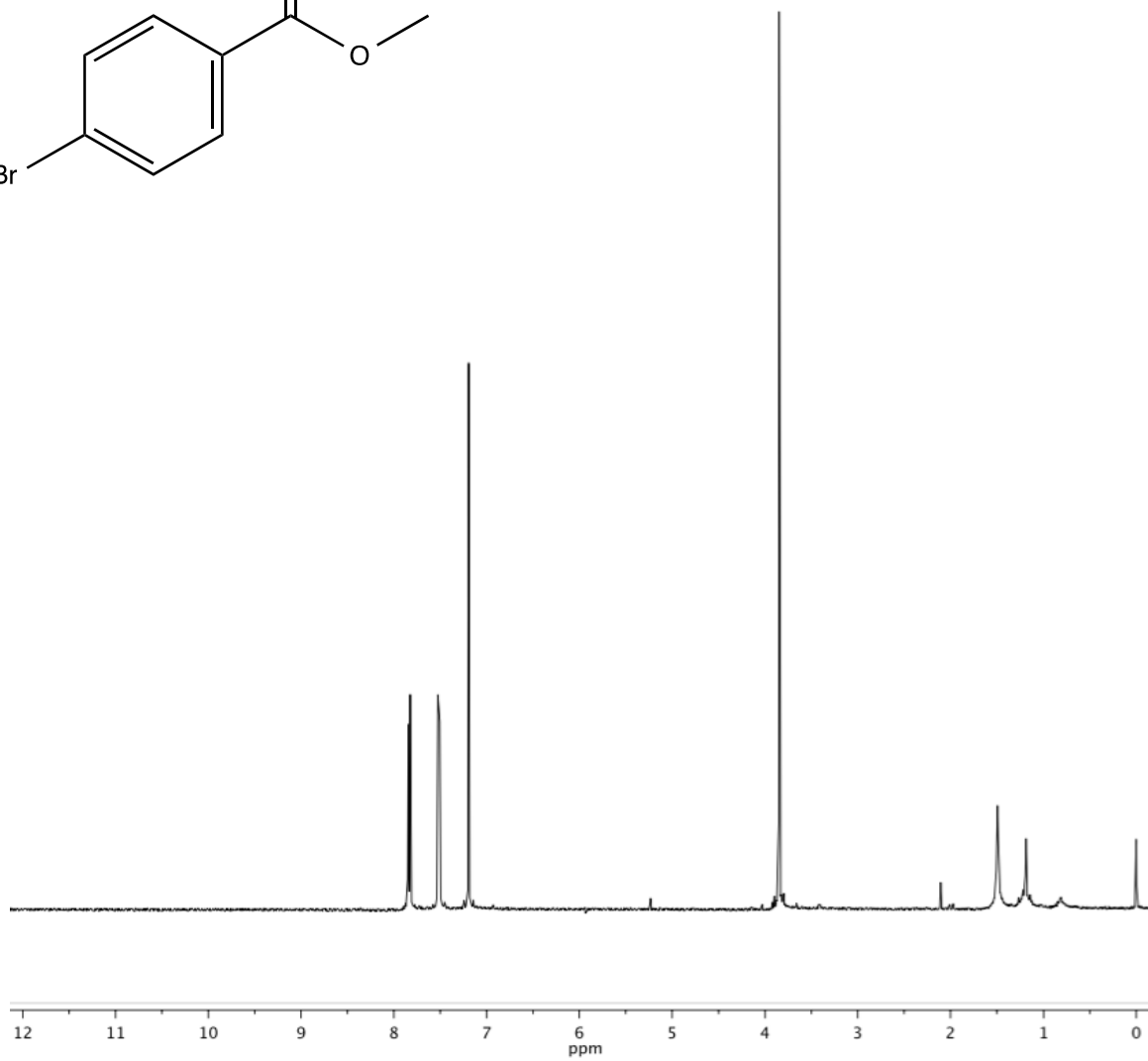
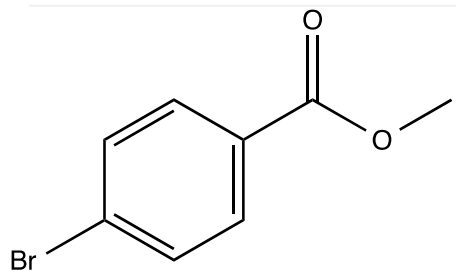
The product was produced following Procedure B with 2-amino phenol (0.5EQ) as the nucleophile and yielded 80.6 mg, 0.294 mmol, 95.8%. ¹H NMR (400 MHz, Chloroform-*d*) δ 7.78 (d, *J* = 8.6 Hz, 2H), 7.66 (d, *J* = 8.5 Hz, 2H), 7.25 (d, *J* = 8.9 Hz, 3H), 7.20 – 7.15 (m, 1H), 7.07 (dd, *J* = 8.1, 1.4 Hz, 1H), 6.94 (td, *J* = 7.9, 1.4 Hz, 1H). ¹³C NMR (101 MHz, cdcl₃) δ 165.99, 148.56, 132.23, 132.12, 132.08, 132.00, 128.85, 127.40, 127.36, 125.42, 122.28, 120.82, 119.71. ESI-MS calculated from C₁₃H₉BrNO, 275.125 [M+H], observed, 275.234; HPLC purity = 79.1%.

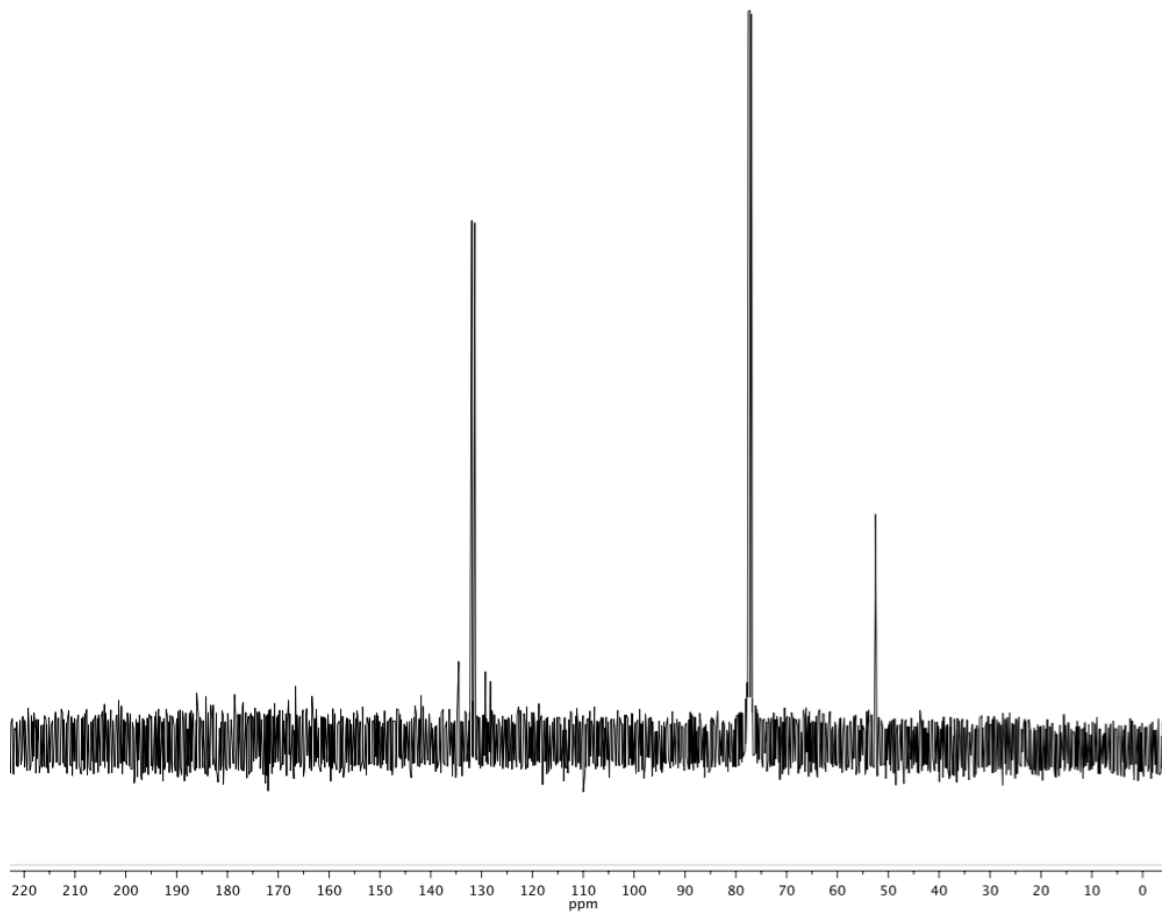
4-bromobenzoic acid, 1.



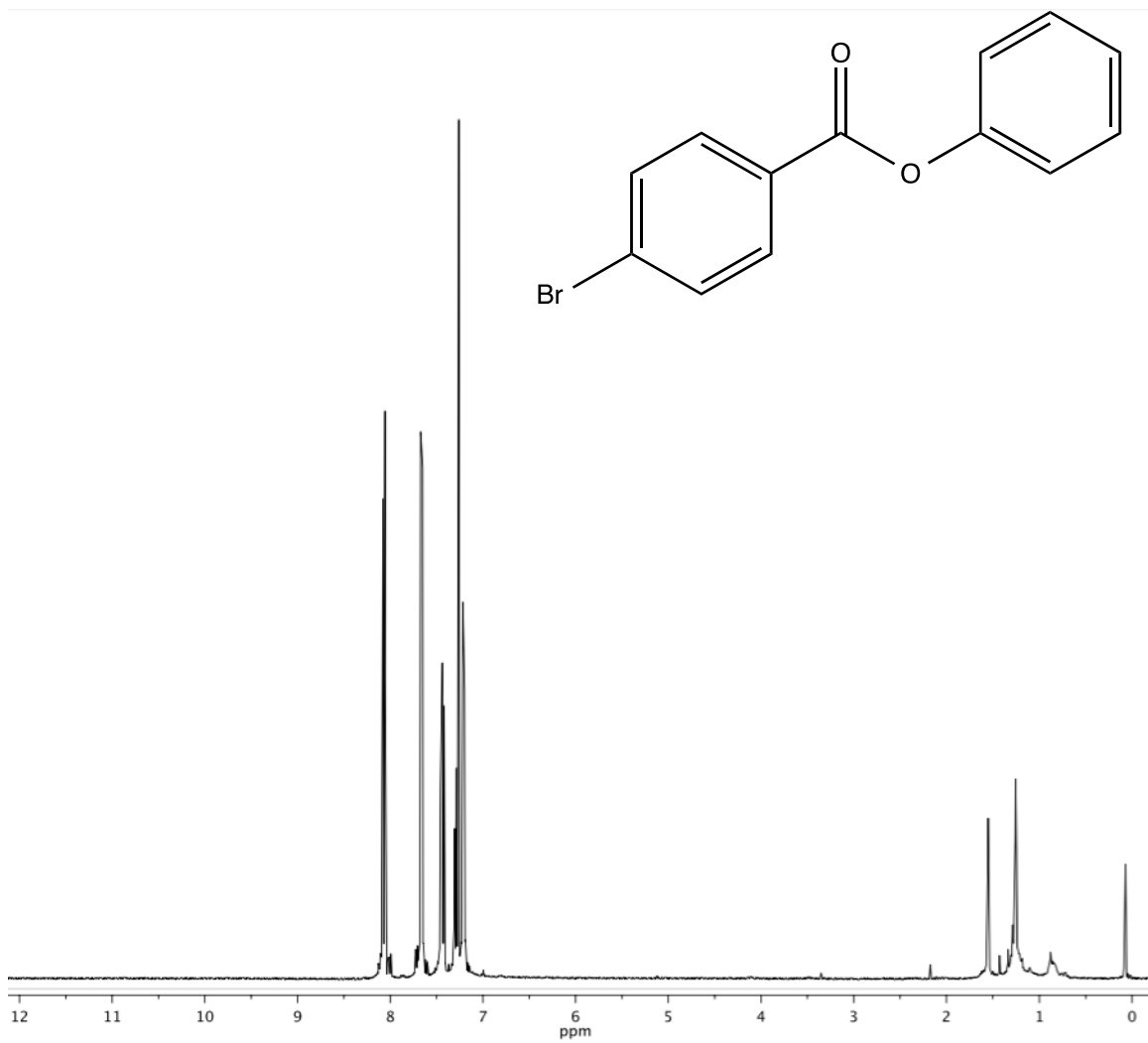


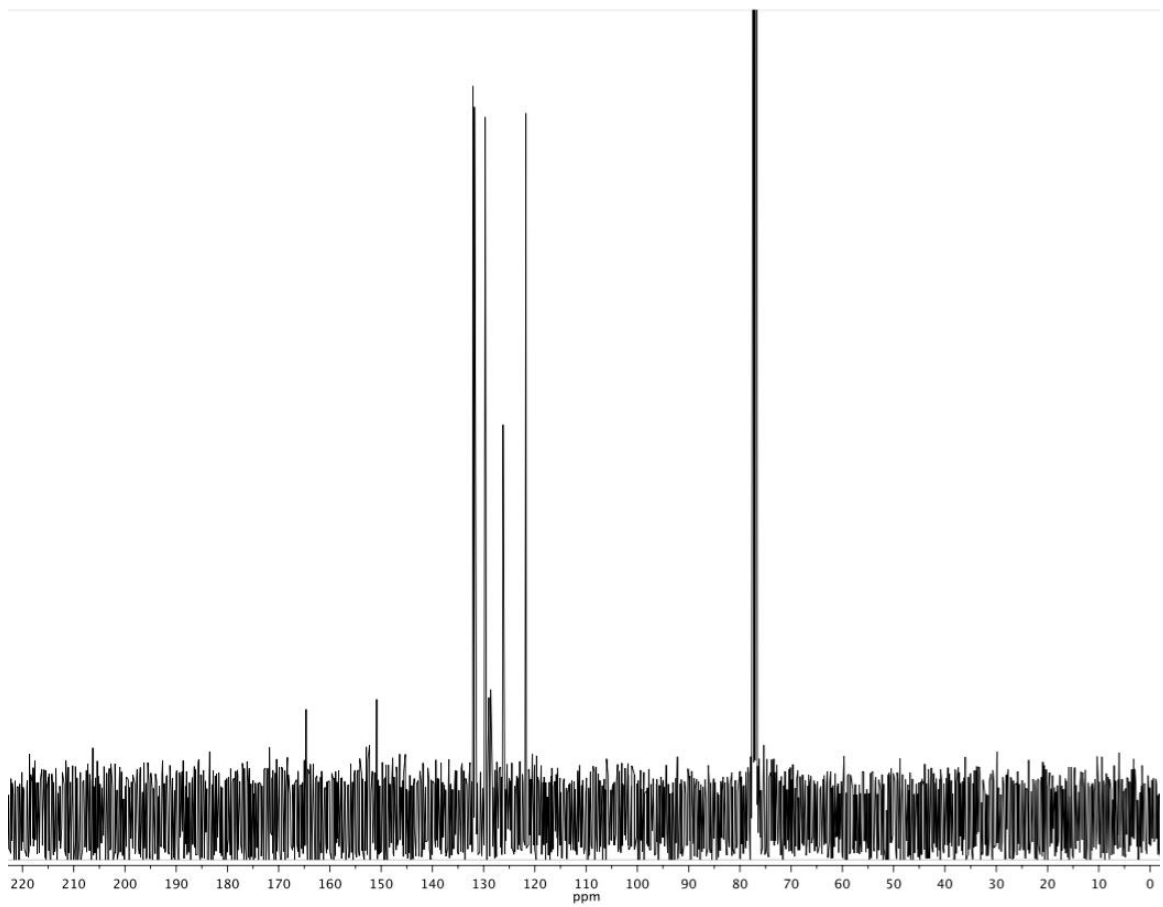
Methyl 4-bromobenzoate, 2.



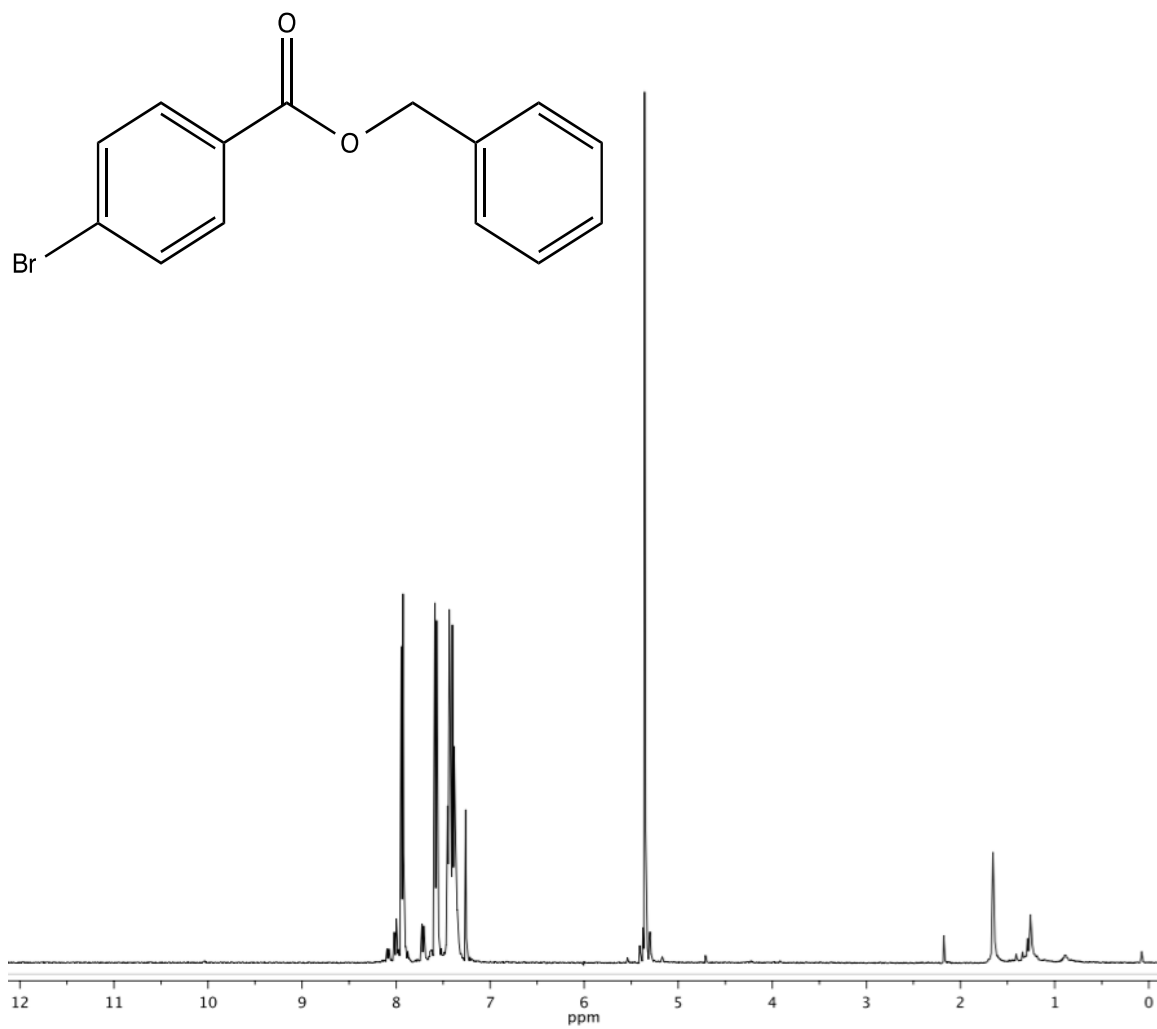


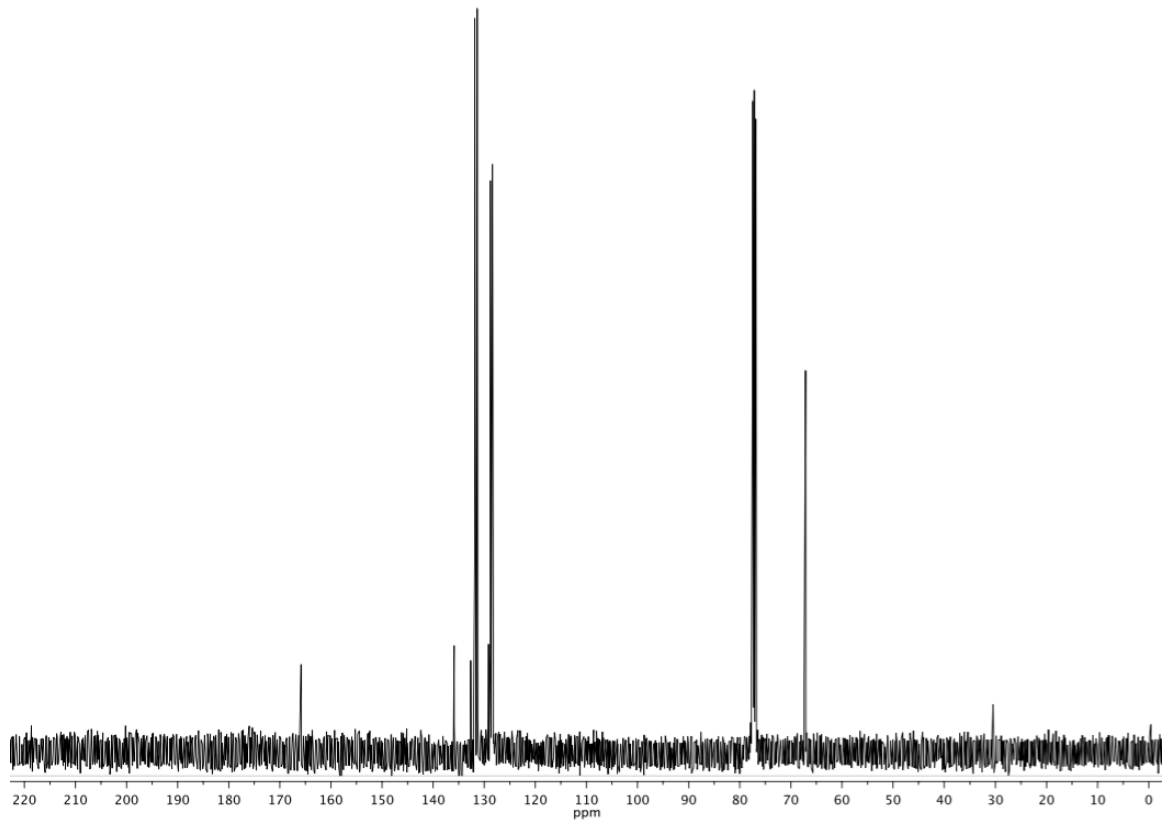
Phenyl 4-bromobenzoate, 3.



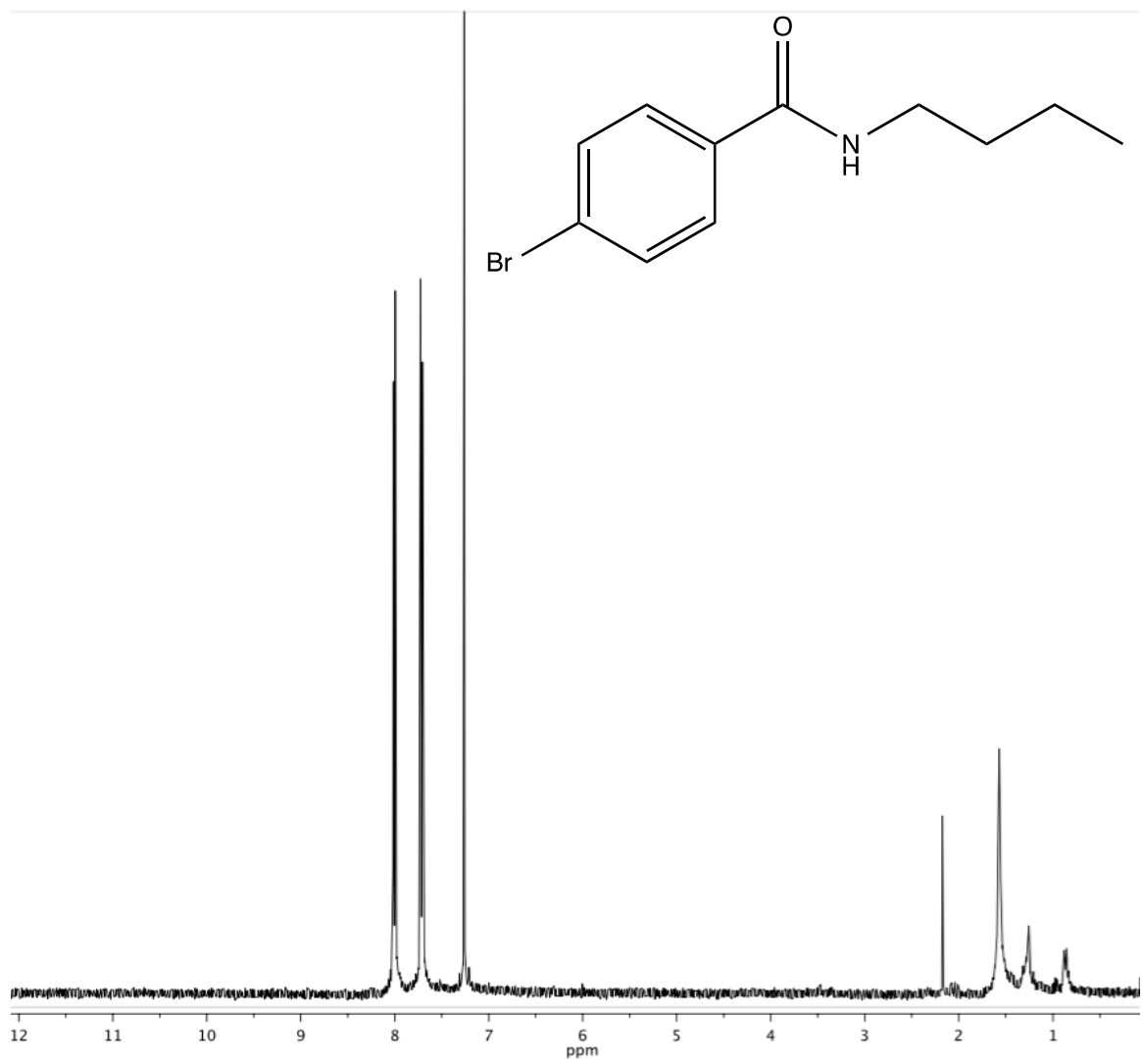


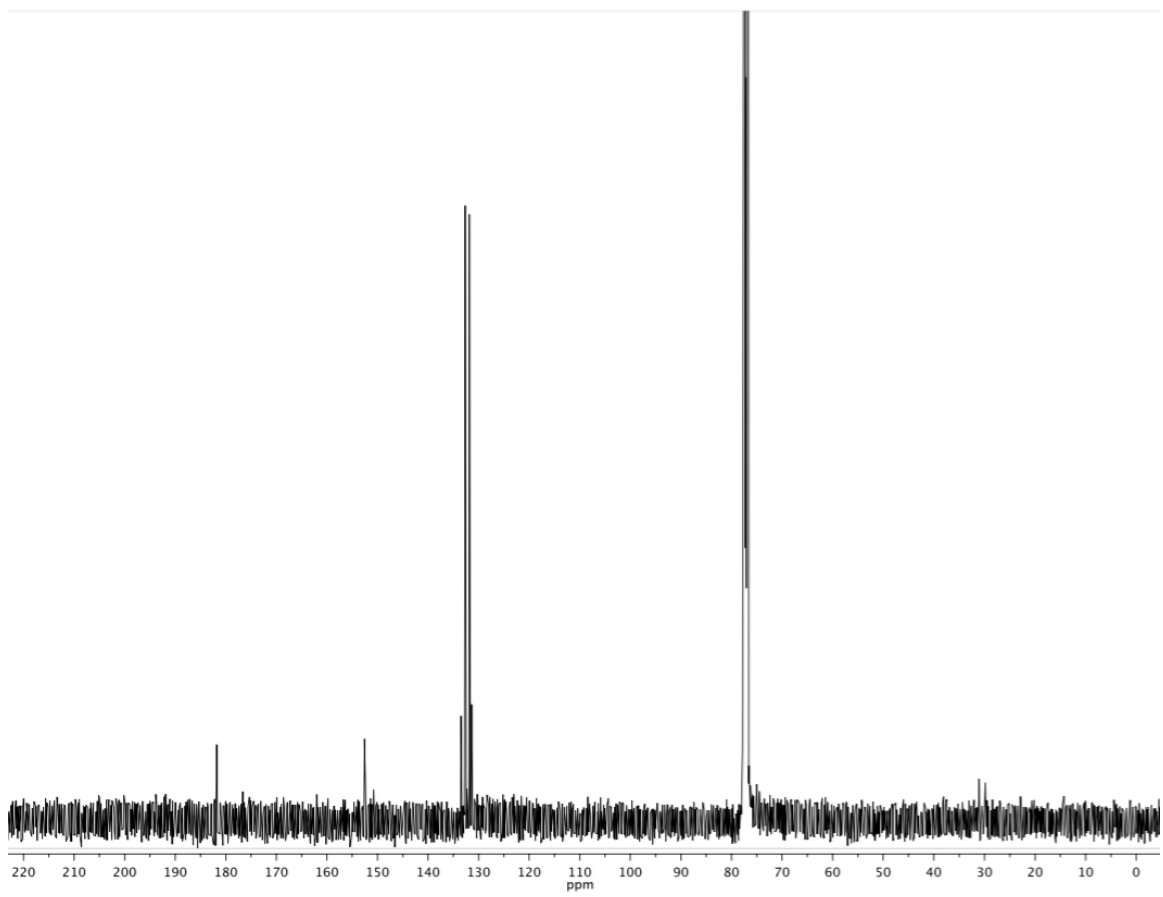
Benzyl 4-bromobenzoate, 4.



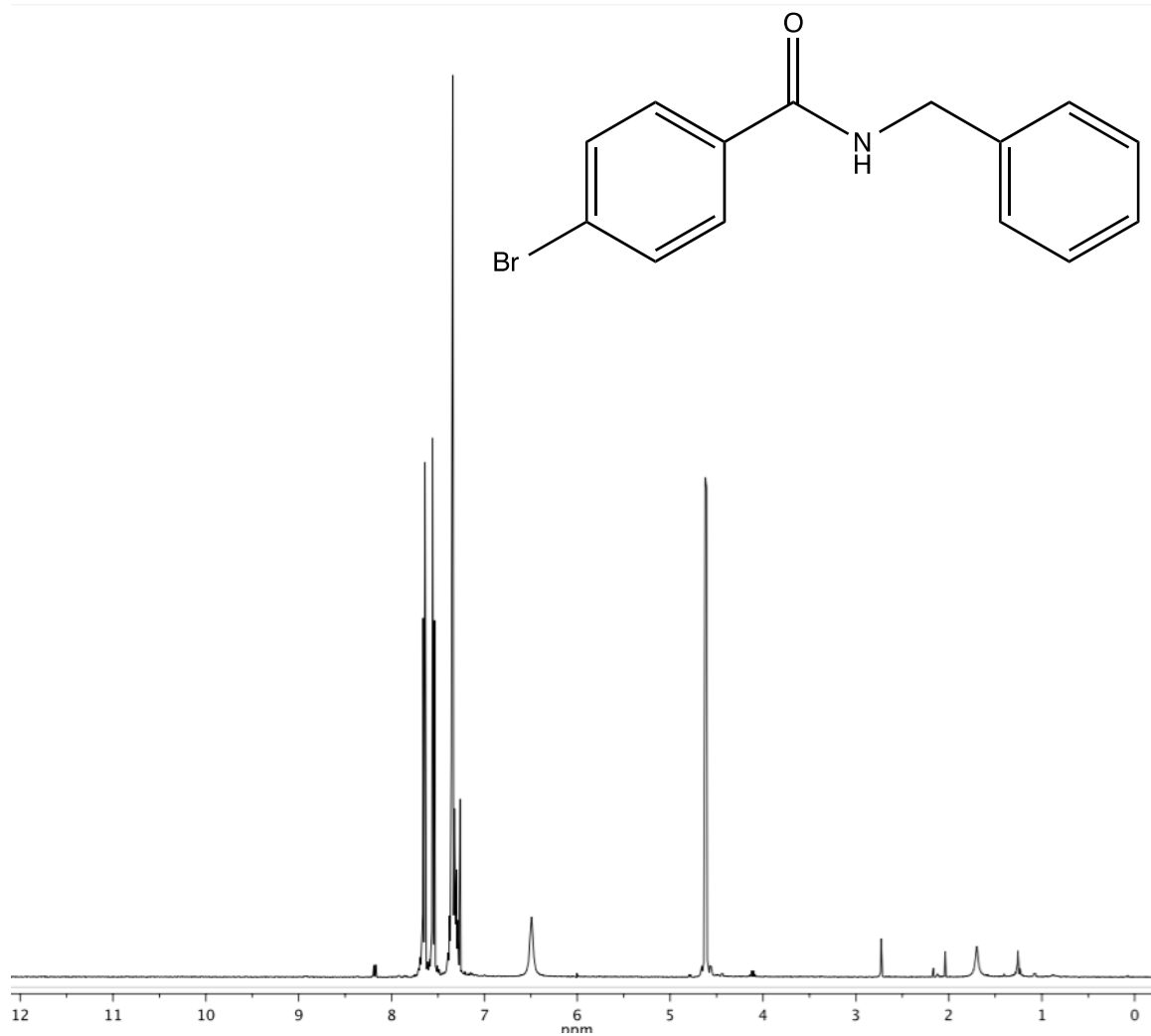


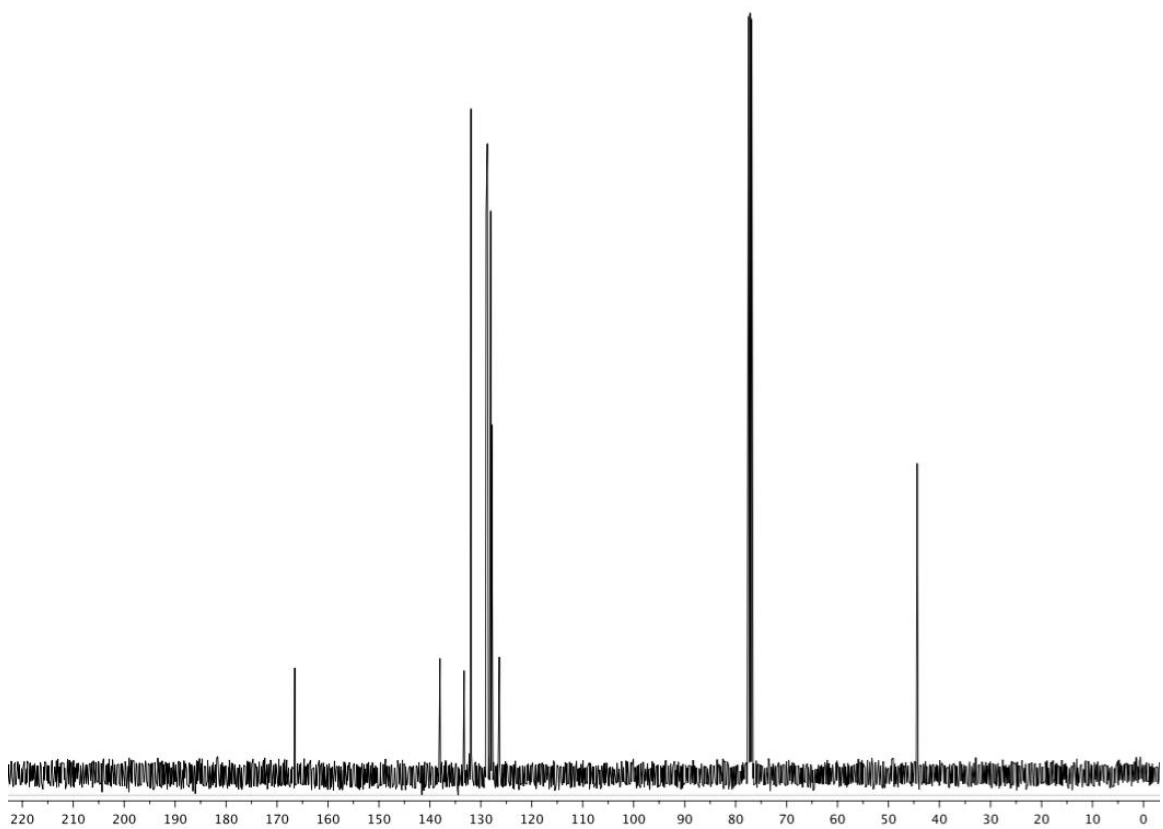
4-bromo-*N*-butylbenzamide, 5.



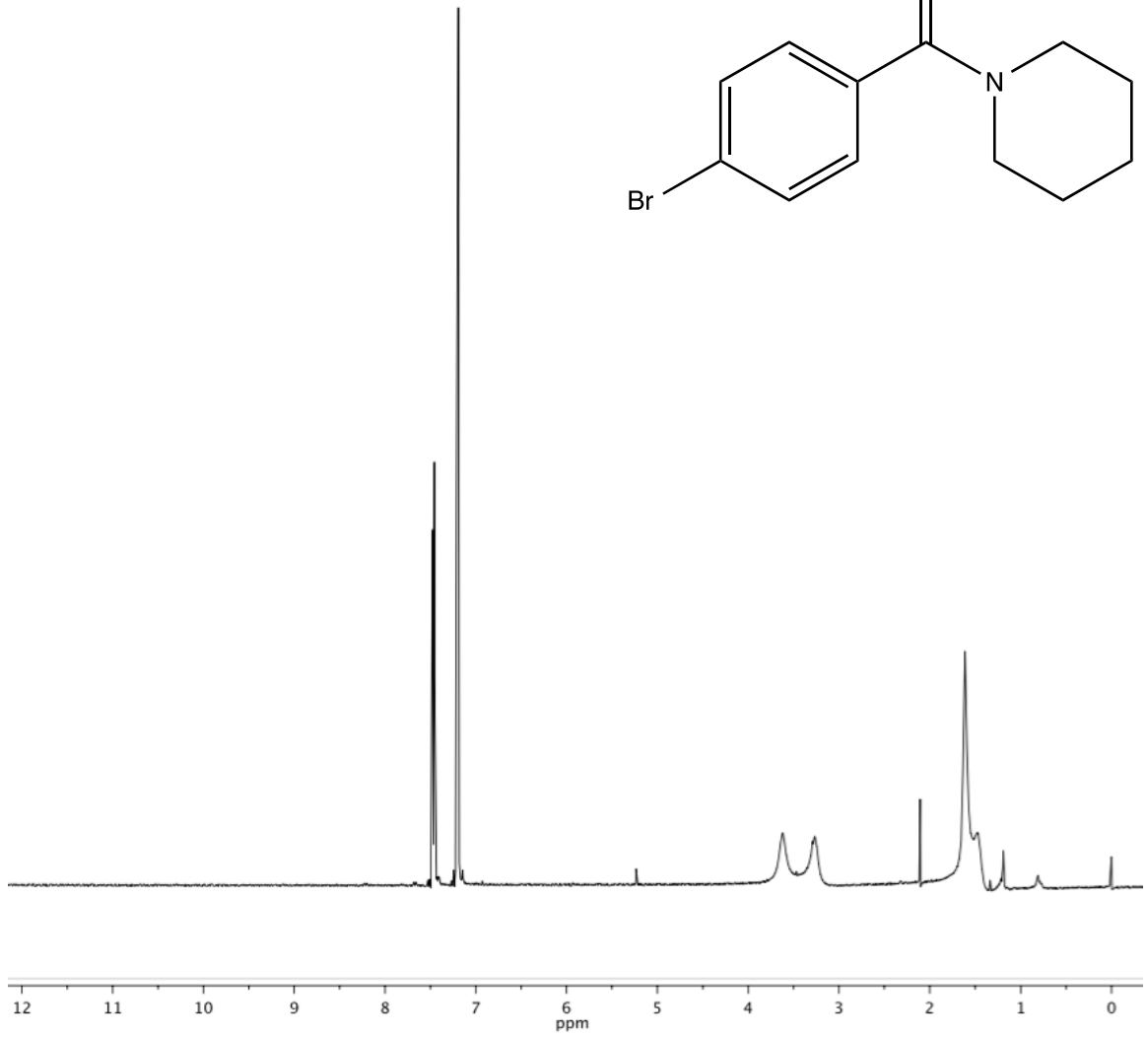
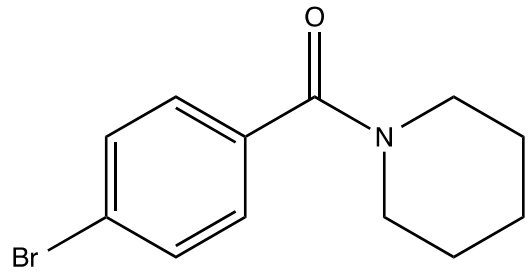


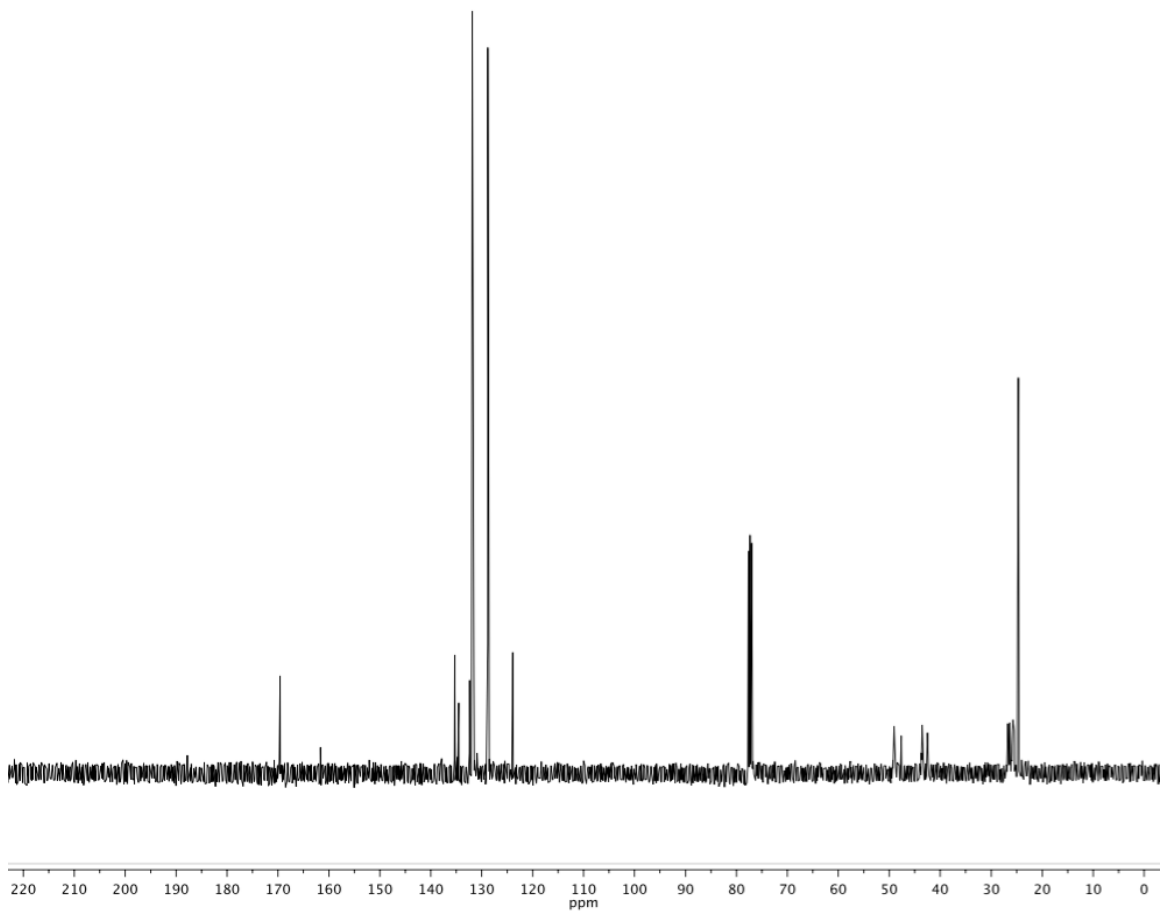
N-benzyl-4-bromobenzamide, 6.



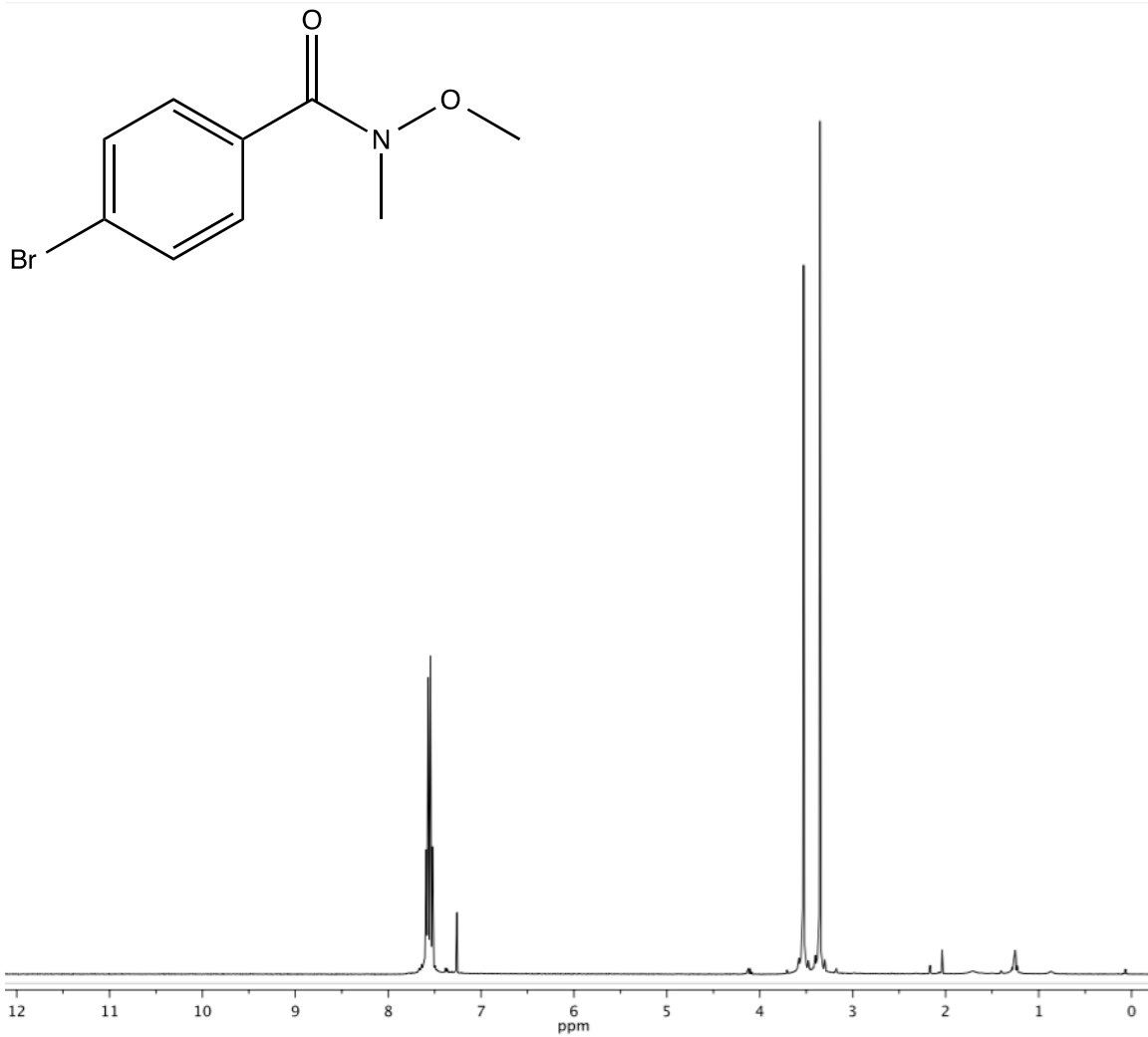


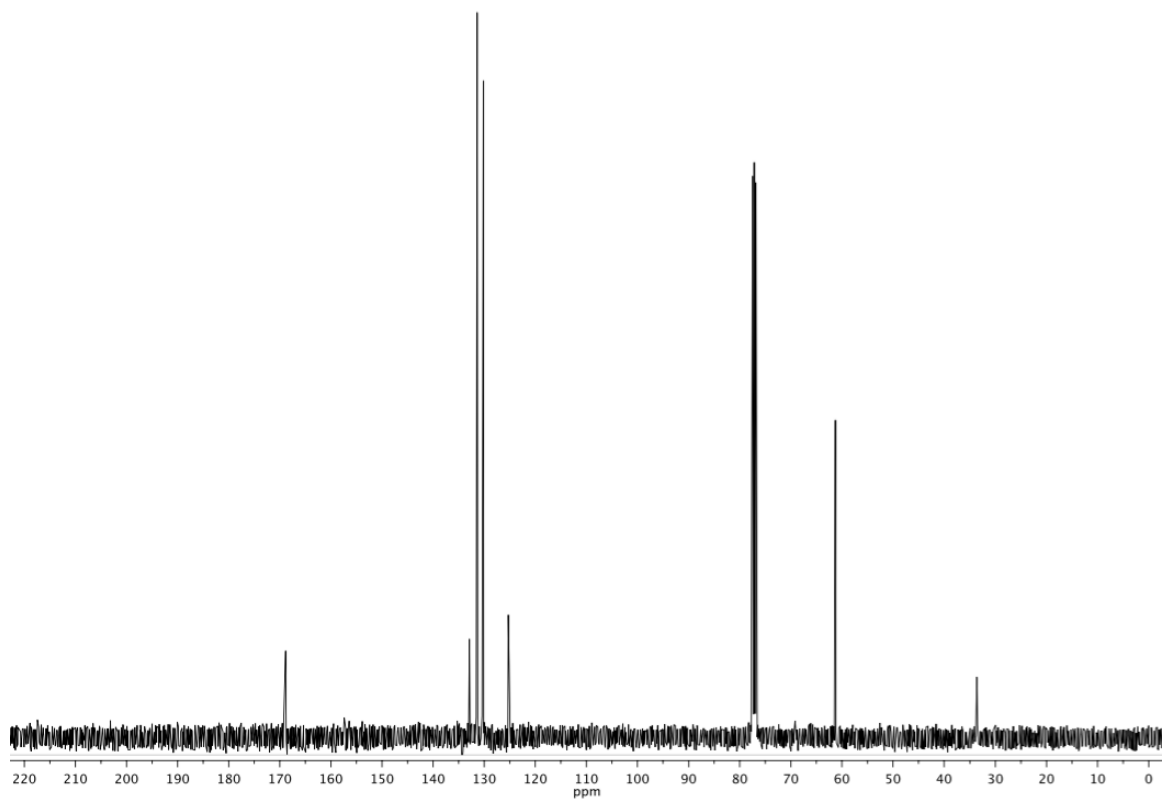
(4-bromophenyl)(piperidin-1-yl)methanone, 7.



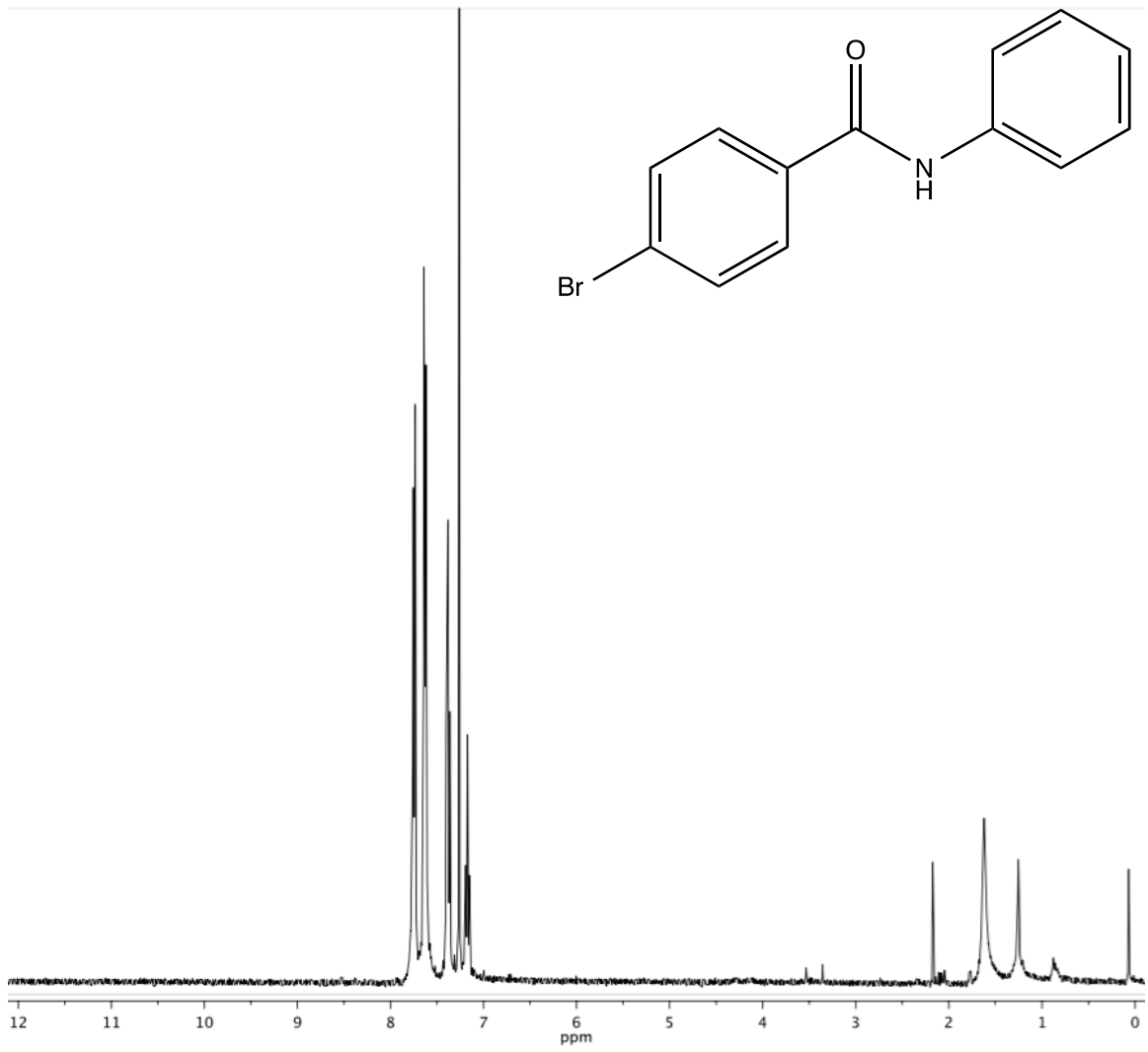


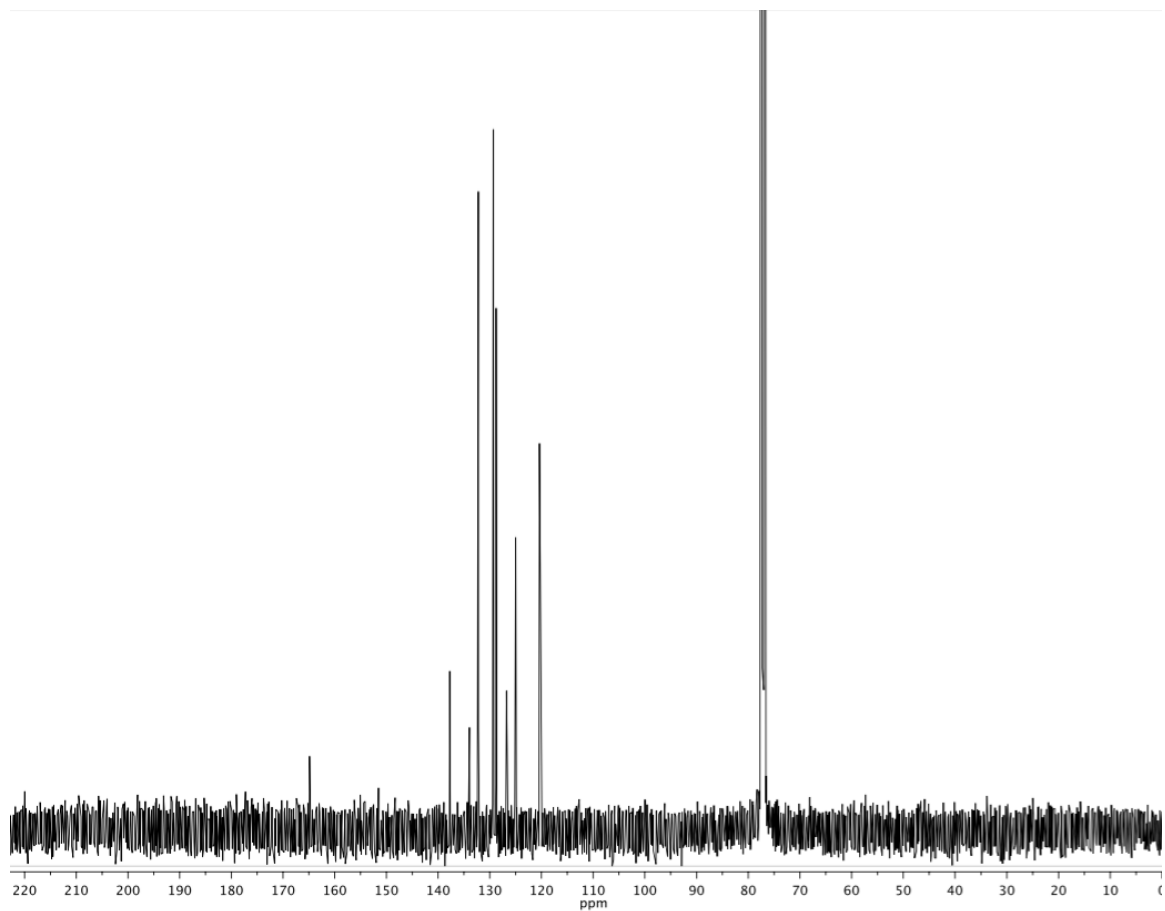
4-bromo-*N*-methoxy-*N*-methylbenzamide, 8.



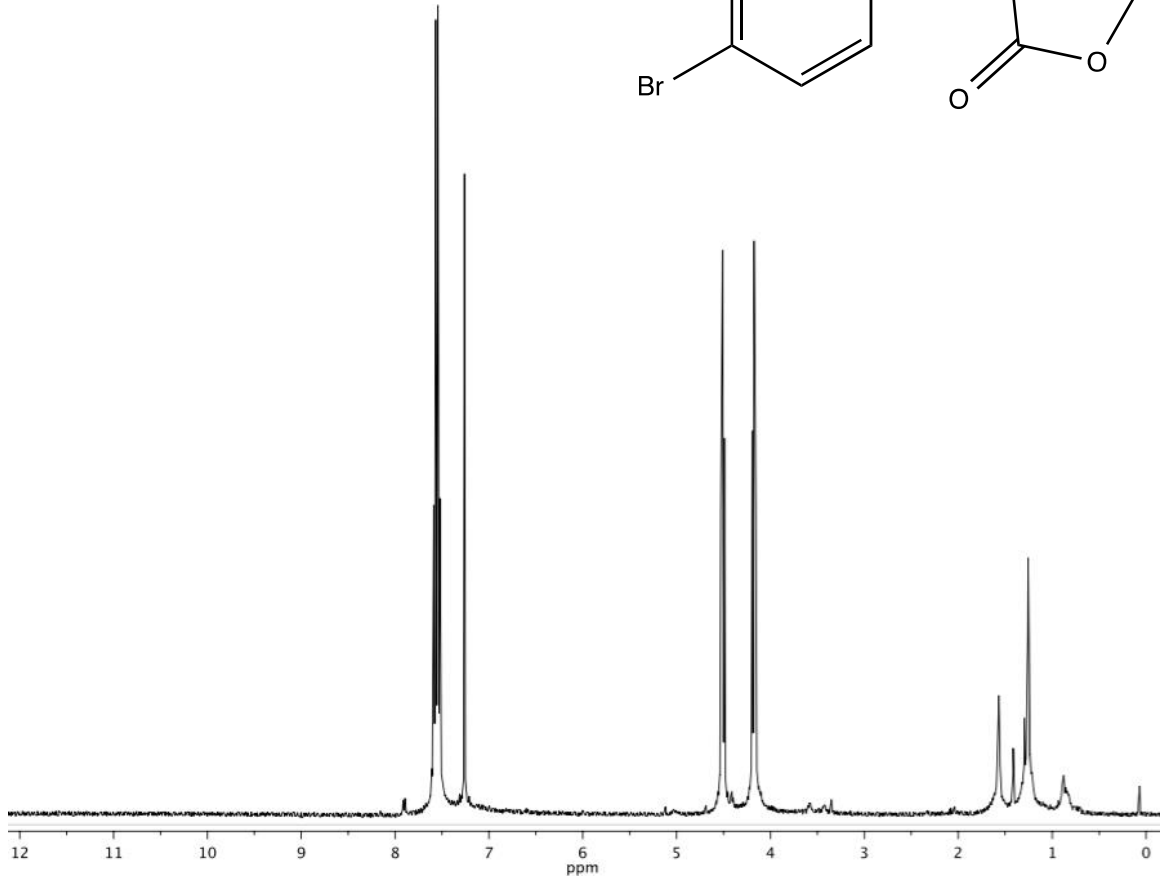
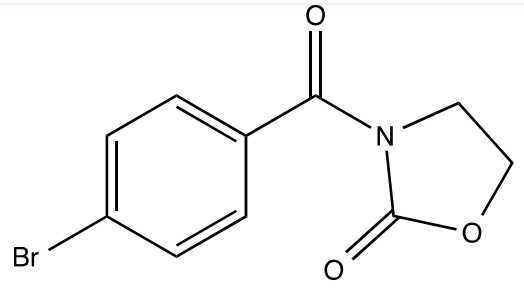


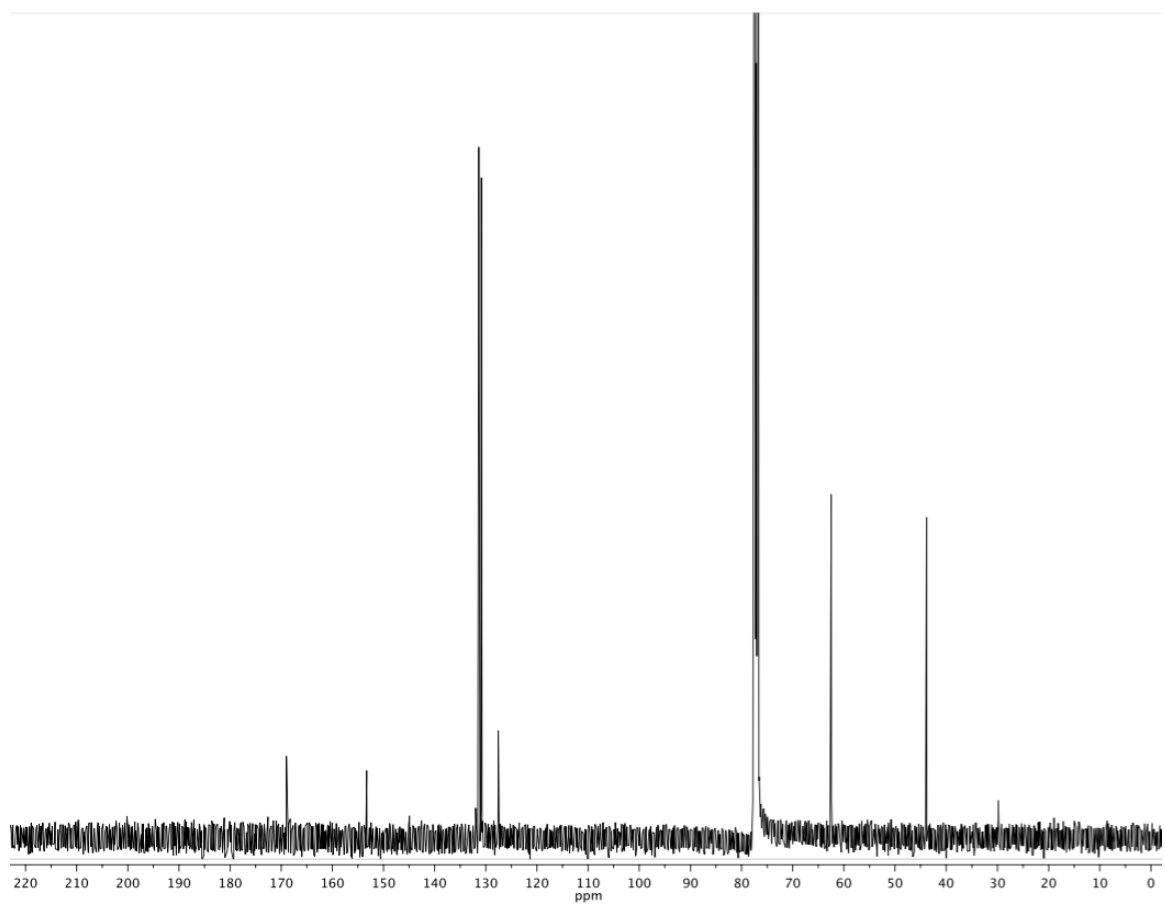
4-bromo-*N*-phenylbenzamide, 9.



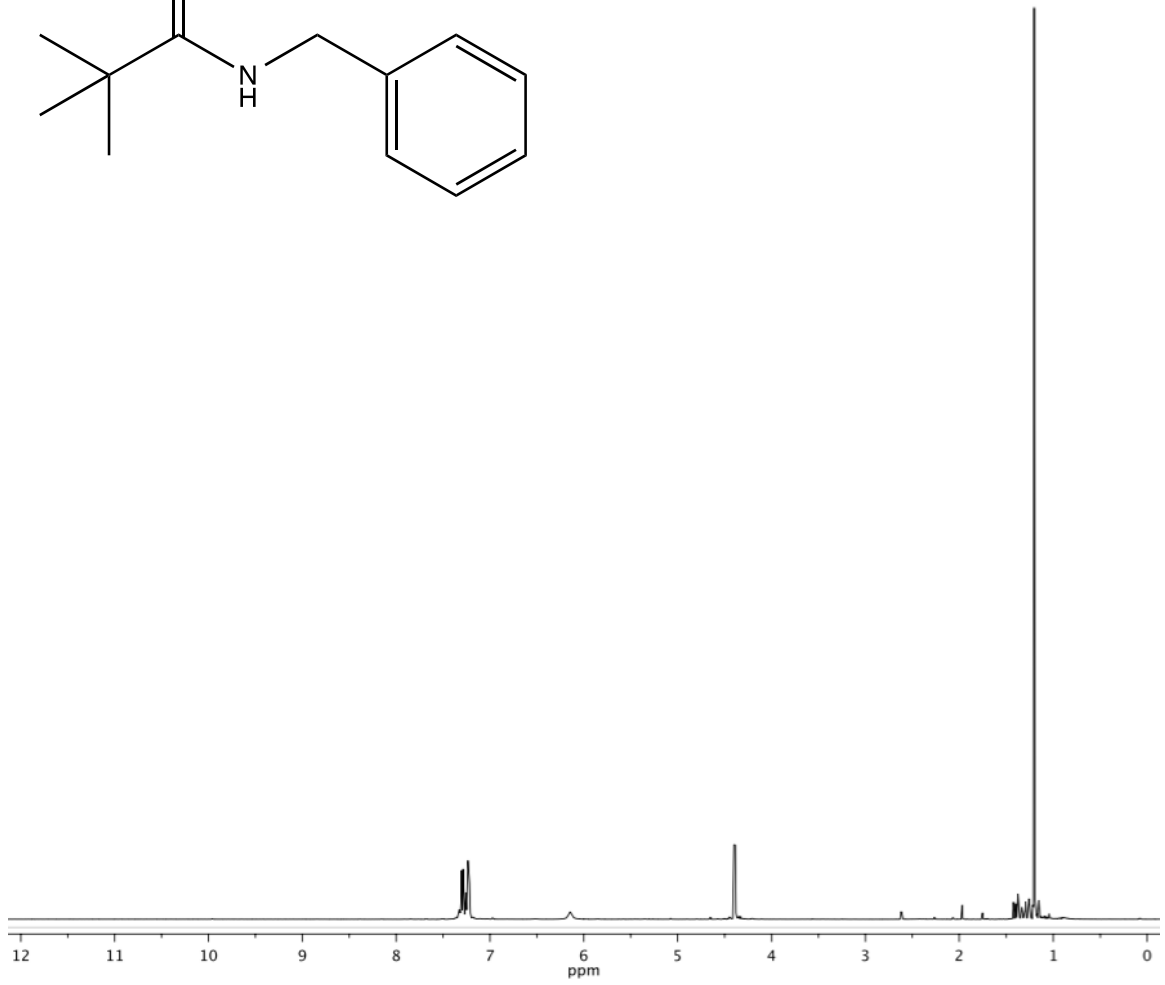
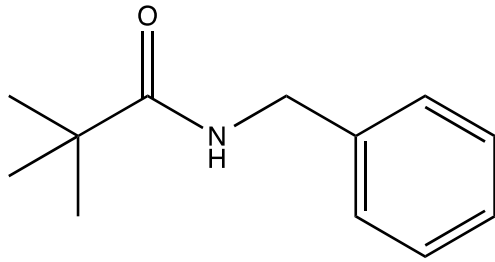


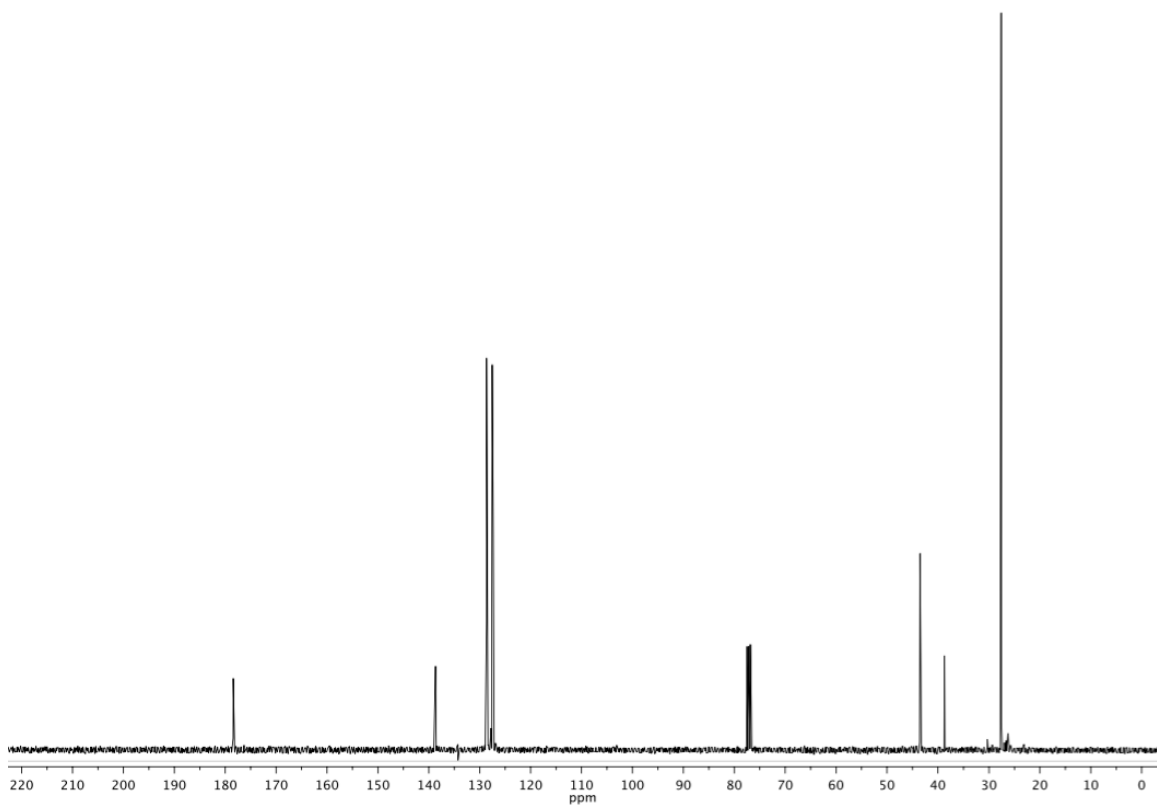
3-(4-bromobenzoyl)oxazolidin-2-one, 10.



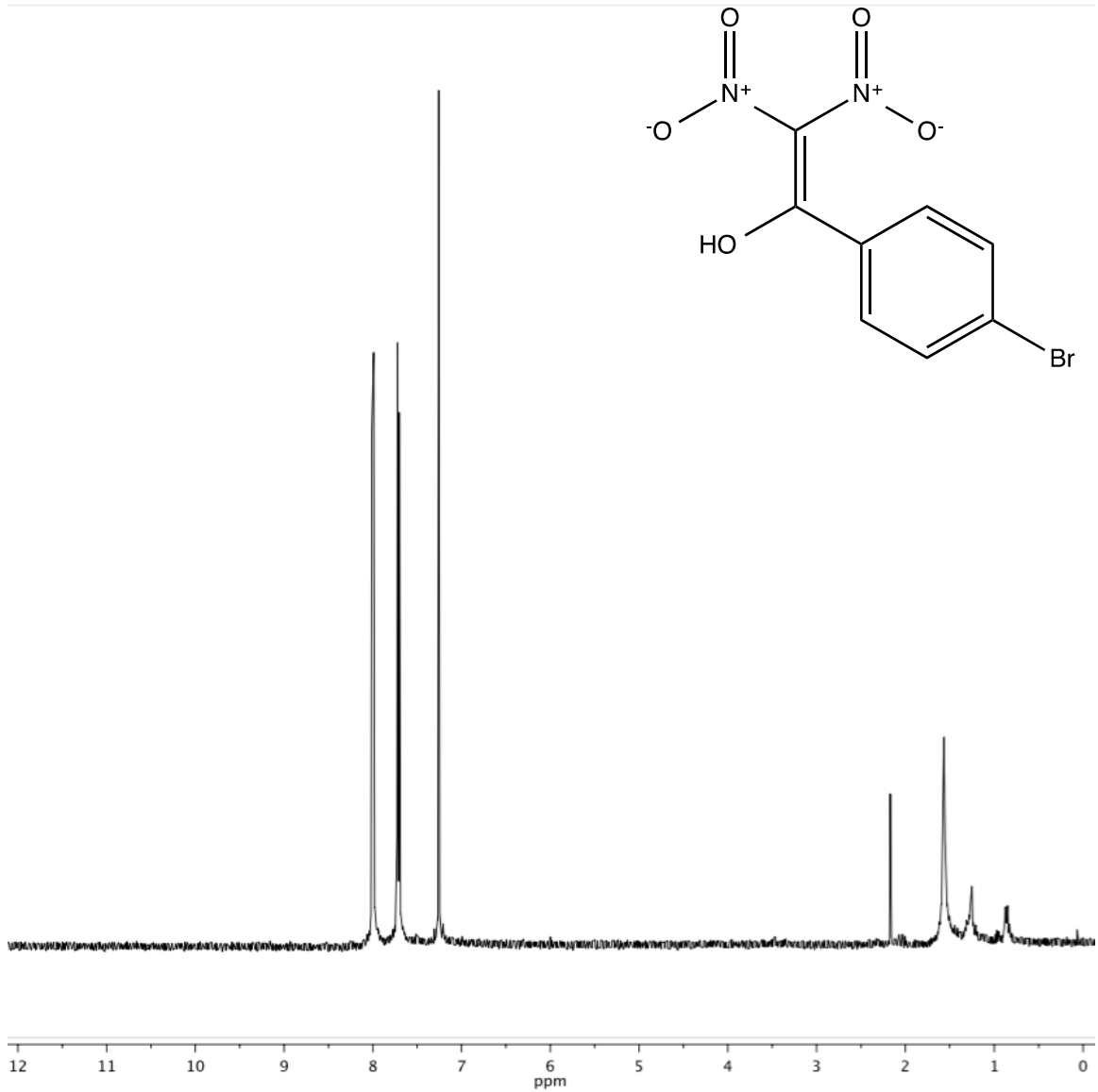


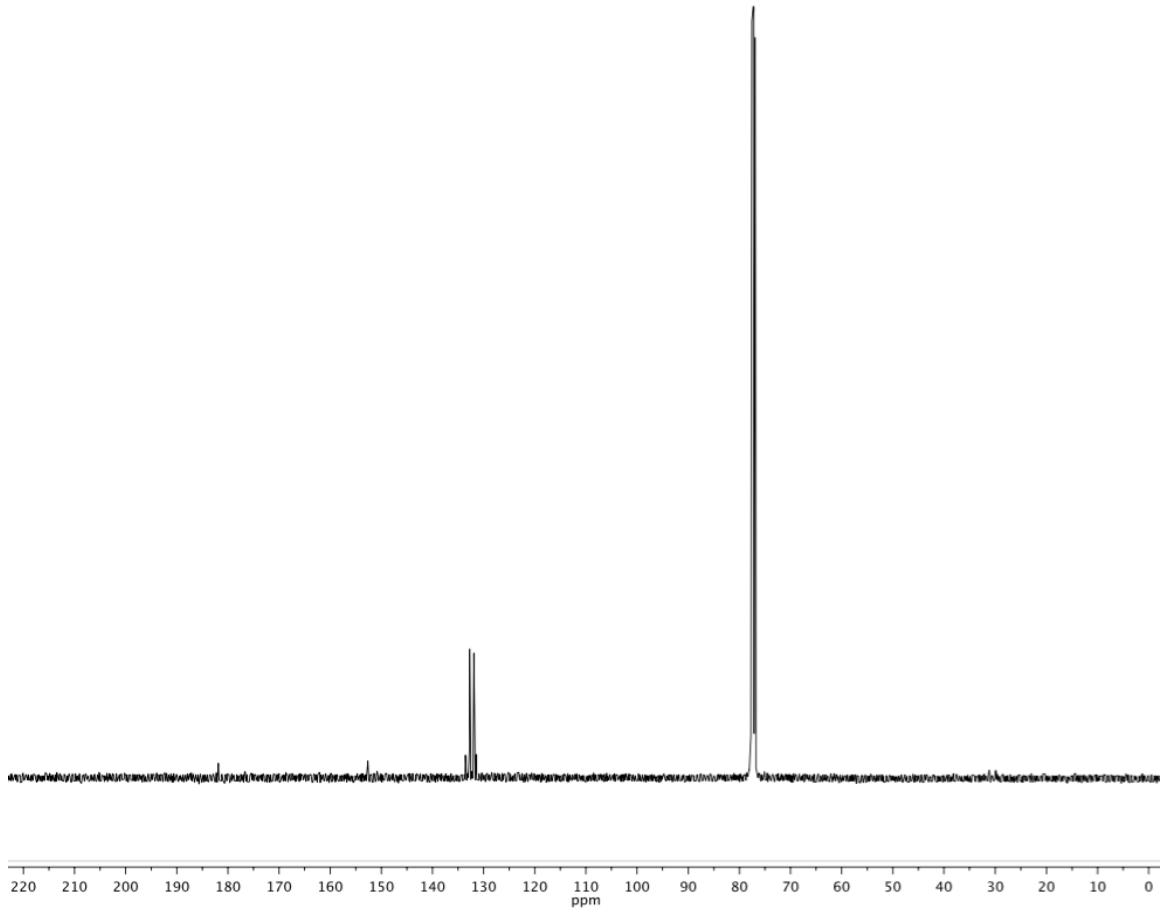
N-benzylpivalamide, 13.



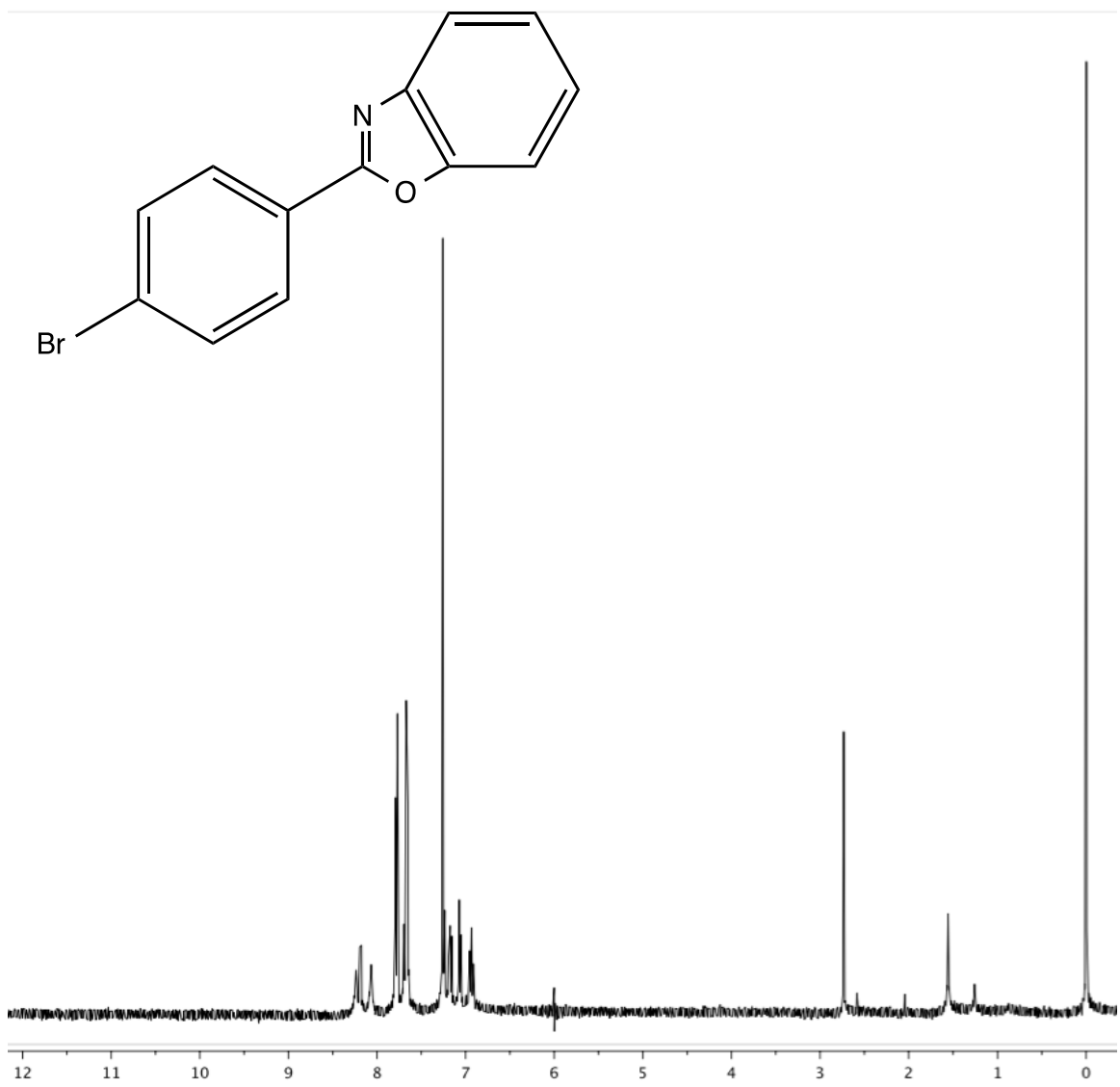


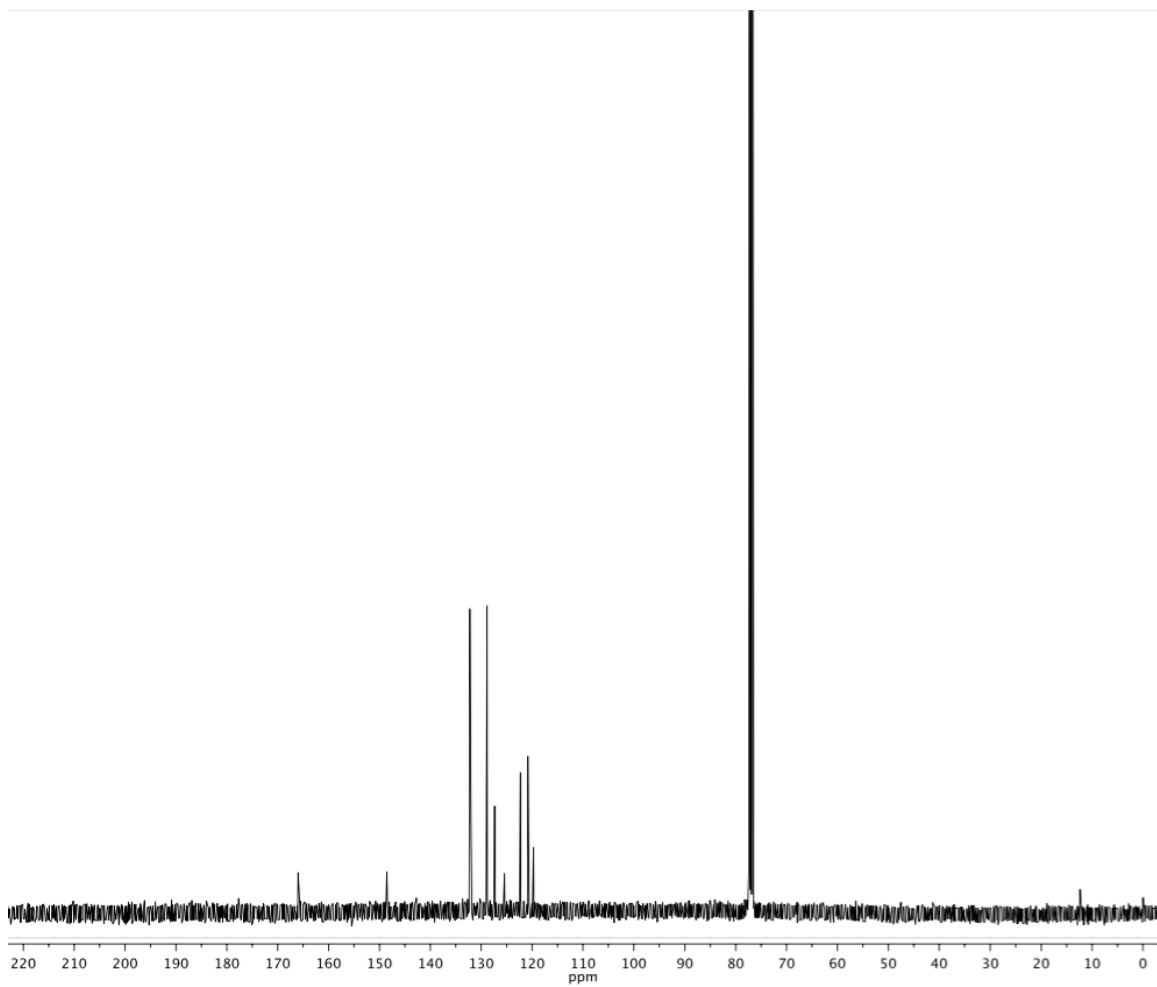
1-(4-bromophenyl)-2,2-dinitroethen-1-ol.





2-(4-bromophenyl)benzo[*d*]oxazole, 14.





Chapter 3A

Narrow Spectrum Antibiotic Development

Introduction

Narrow spectrum antibiotics show activity against a small scope of bacteria. We prepared a focused series of molecules and tested their antibiotic activity against both *Acinetobacter baumannii* and *Pseudomonas aeruginosa*. The relationship of activity against both bacteria is identical, except this series of molecules proves to be more potent against *Acinetobacter baumannii*. Based on our own work and previous publications we believe these molecules to be inhibitors of fatty acid synthesis, giving a possible indication to the mechanism of action, but we are currently working on further figuring out the overall mechanism of action. Interestingly, we also see some antifungal activity from our collaborations with Dr. Mark Hickman. Our goal is to simply alter the molecule in various ways and use information we receive from bioassays against either bacteria to further produce a structure activity relationship.

Reaction Mechanism

The synthesis of these molecules is achieved by reacting an aldehyde or ketone (shown as the black portion), a hydrazine (shown as the red portion), and potassium thiocyanate (shown as the blue portion) all in dilute HCl as solvent, allowing the reaction to be water tolerant. These reactions were performed overnight and the product was simply separated with vacuum filtration and then recrystallized in hot methanol to produce pure product. The reaction was a multicomponent coupling reaction and began

with the nucleophilic attack of phenyl hydrazine's outer most nitrogen upon the protonated ketone or aldehyde. This intermediate would then have nitrogen's lone pair come down and kick off water as a good leaving group, forming an imine intermediate. This imine intermediate proves to be a good electrophile for potassium thiocyanate to attack the carbonyl, which is followed by a cyclization that forms our 5 membered heterocycle product. This reaction mechanism with arrow pushing can be seen below in Figure 17.

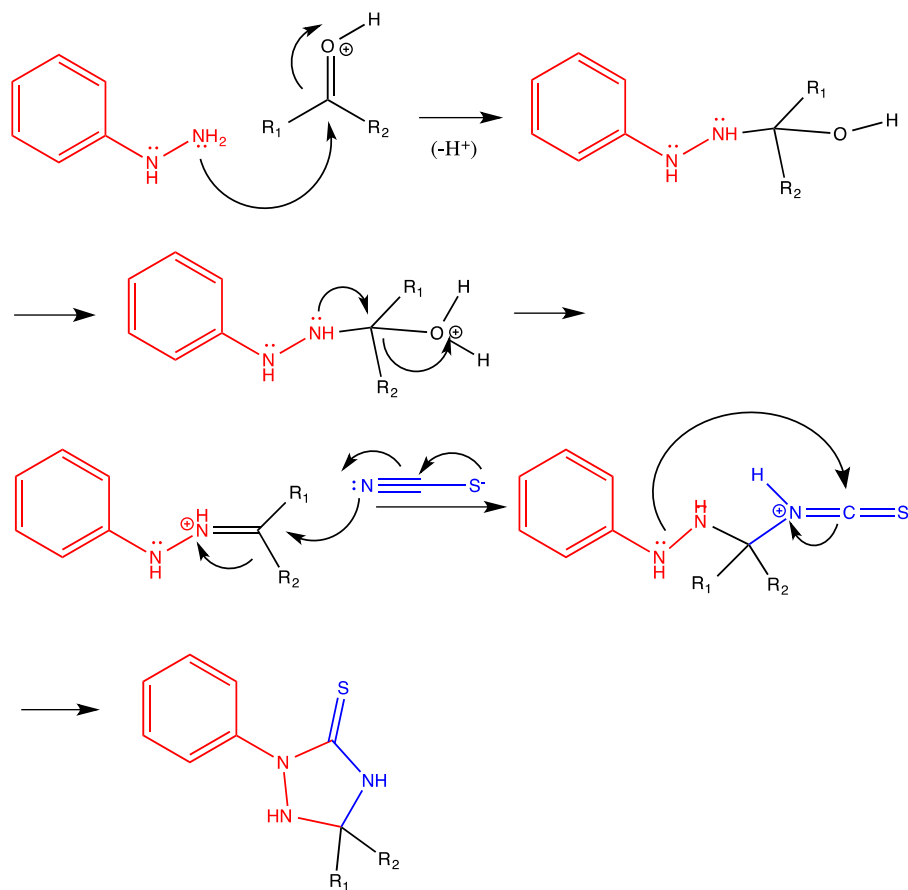


Figure 17. Arrow pushing mechanism of this multicomponent coupling reaction

Structure Activity Relationship

In order to develop an SAR for this reaction, we aimed to change one portion of this molecule at a time so we could truly see the effect each change had on the activity of the molecule. We begin by changing the ketone portion of the molecule, testing mostly for sterics but also add in some electronic changes. Overall we see the activity increase when the smaller substituents are present, such as the methyl/methyl groups or the methyl/ethyl group. The rest of these molecules have less activity than these two substituents, especially the larger methyl/hexyl groups. This scope can be seen below in Figure 18.

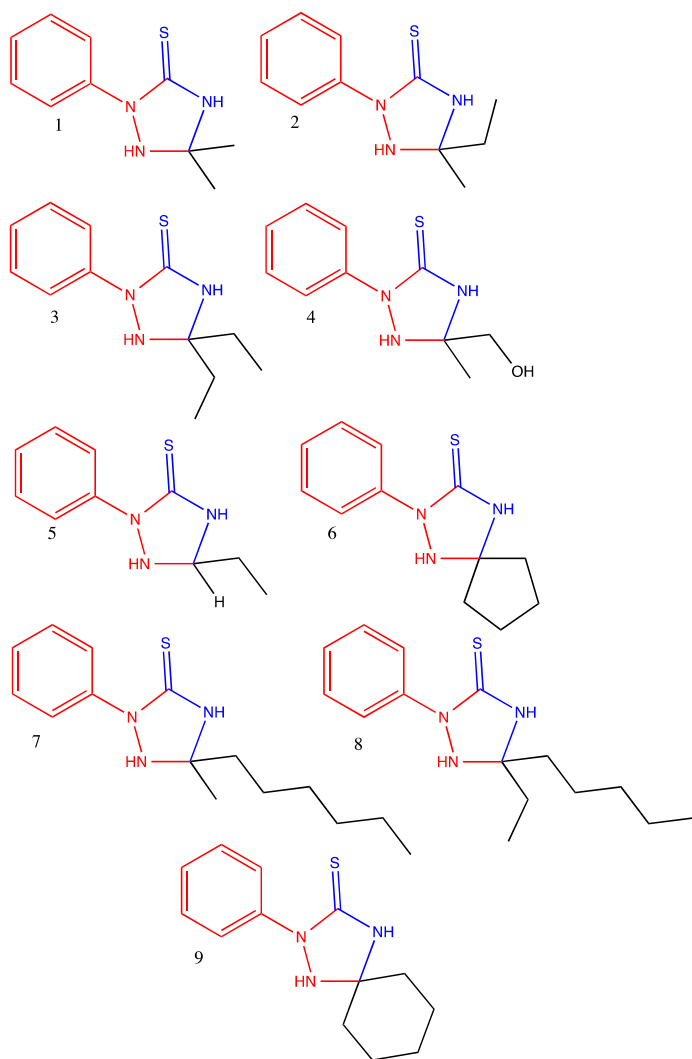


Figure 18. Scope of the ketone or aldehyde portion of the molecule.

Moving forward as we begin to test the various positions of the hydrazine ring for steric and electronic effects, we only make these products with the methyl/methyl and methyl/ethyl group. Our goal here is firstly test electronic effects. We accomplish this by moving chlorine which is slightly electron donating from para to meta to ortho. This shows to be most potent in the para position. From here we change the electronics by

testing para methoxy, greatly increasing the electron donating effect, and by testing para nitro, which introduces an electron withdrawing effect. We see an activity increase in the para methoxy substitute, which turns out to be our current lead compound. For the para nitro molecule, we see a huge decrease in activity. This shows a drastic difference in activity due to the changing of electronic effects at the para position of the hydrazine ring. We also pushed our SAR further by attempting a few other hydrazine substituents, such removing the aromaticity from the ring or substituting the ring with more than 1 molecule. This scope of the hydrazine can be seen below in Figure 19. Overall, we find para methoxy with the methyl/methyl ketone portion to be our current lead compound.

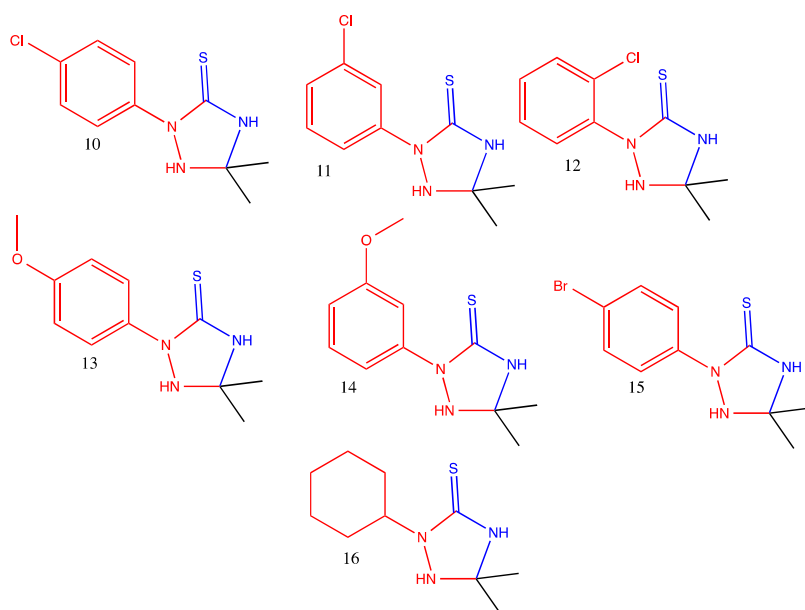


Figure 19. Scope of the hydrazine portion of the molecule, made with the methyl/methyl group.

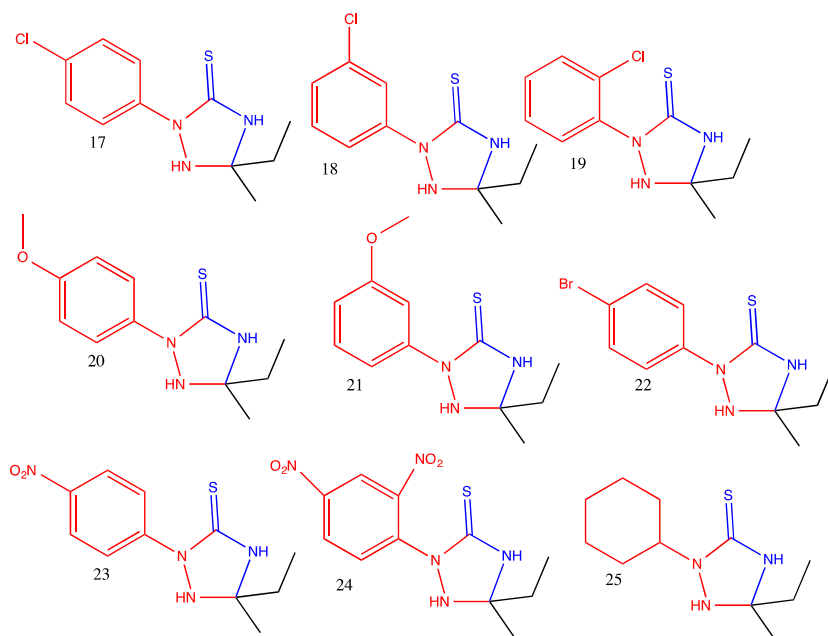


Figure 20. Scope of the hydrazine portion of the molecule, made with the methyl/ethyl group.

Biological Data Overview

For every molecule, we ran a growth based overnight bioassay on an incubating plate reader. This provided us with both kinetic and end point data to evaluate our molecules with and *use in optimization*. We began testing molecules against *Pseudomonas aeruginosa*, which provided a trend of where our SAR was heading. *Acinetobacter baumannii* proved to be 16 fold more potent comparatively, but showed the same trend. We quickly moved to testing these molecules solely against *Acinetobacter baumannii* while we changed just one portion of the molecule at a time to find the true effect for activity change.

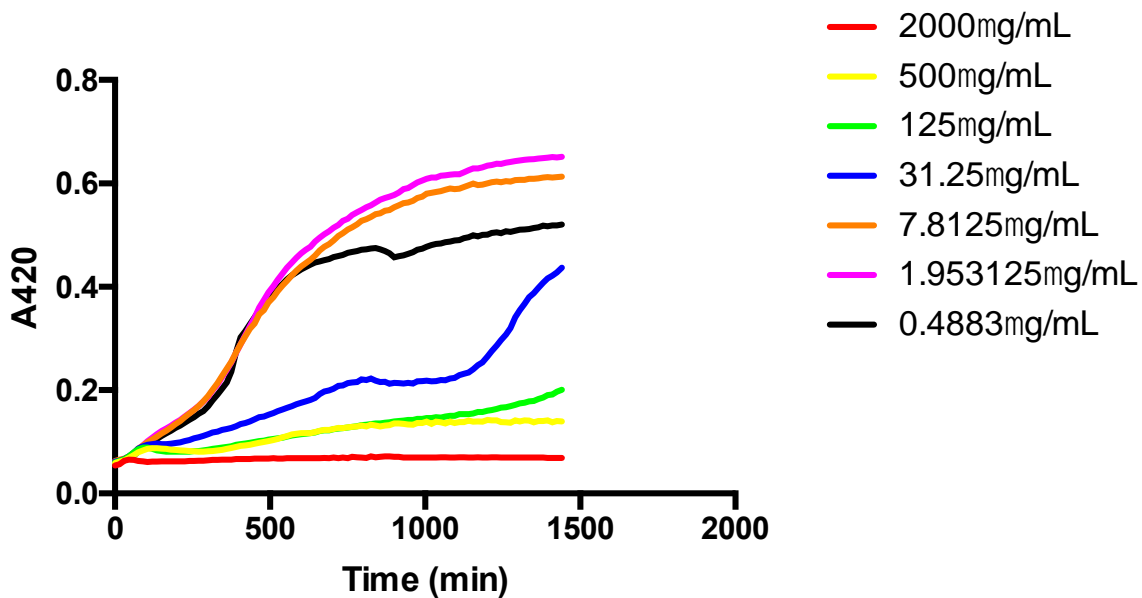


Figure 21. Bioassay data against *Acinetobacter baumannii* for Molecule 1.

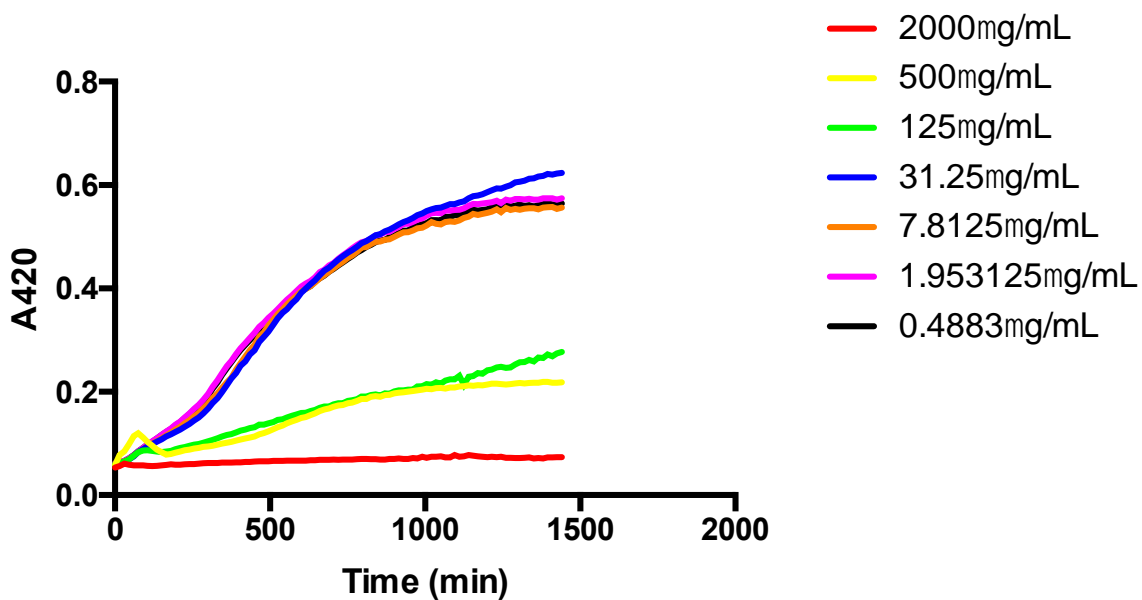


Figure 22. Bioassay data against *Acinetobacter baumannii* for Molecule 2.

The trend of the ketone portion of the molecule can be extrapolated from Figures 21 and 22 and seen further in the supporting information. As the sterics of this position are increased, the activity is decreased. Changing the electronics of this position did not seem to help the activity either. As we moved forward and began to change the phenylhydrazine portion of the molecule, we did so only using the methyl/methyl ketone and methyl/ethyl ketone but knew that our best activity would be the with the methyl/methyl group.

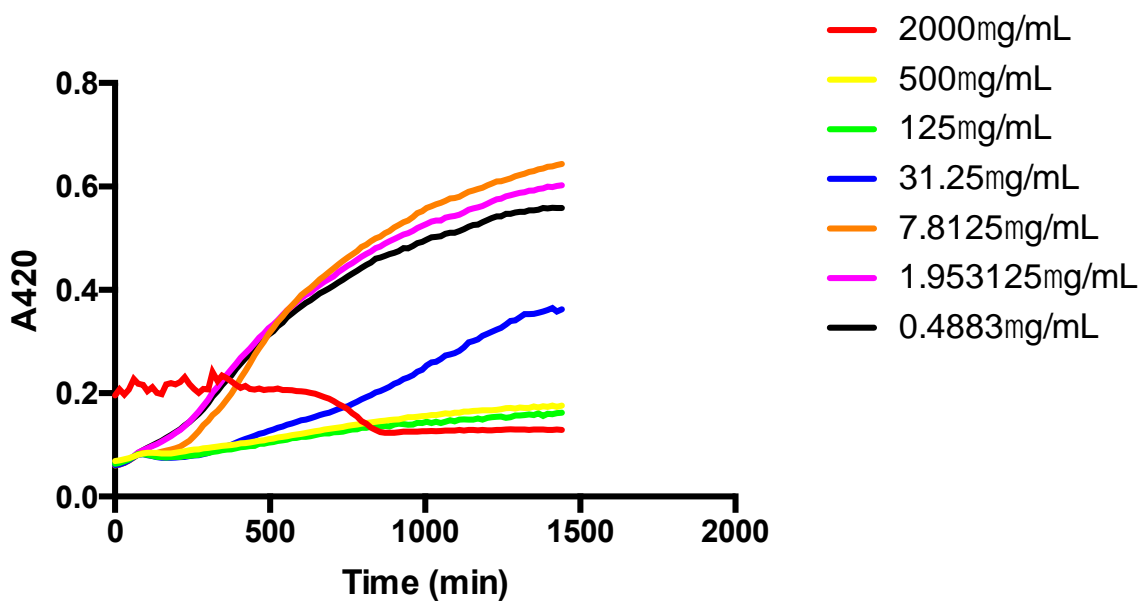


Figure 23. Bioassay data against *Acinetobacter baumannii* for Molecule 10.

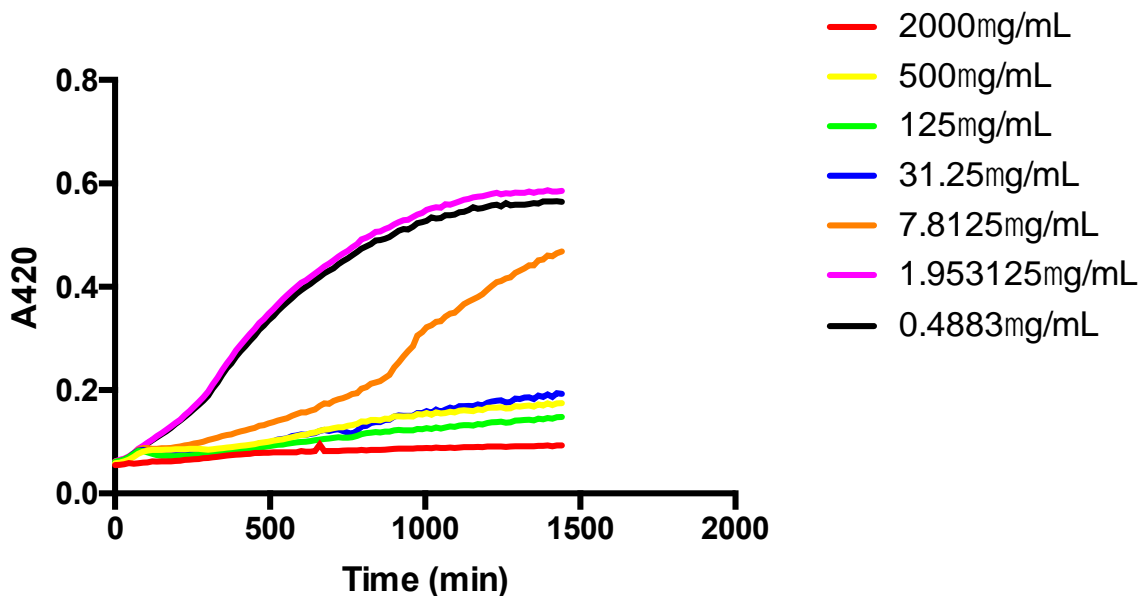


Figure 24. Bioassay data against *Acinetobacter baumannii* for Molecule 13.

As we began testing the electronics and sterics of the ring on this molecule we quickly found that the para position was the most ideal for activity. Placing chlorine at the para position (Molecule 10) provides a slight electron donating effect to the ring. Not only does this increase the rate of the reaction based upon our synthesis, but also increases the activity in comparison to having no substituent on the ring. Moving chlorine to the meta and ortho position kills any activity the compound had, so from here we decided to change the para position. We tested sterics by changing chlorine into bromine. This molecule had less activity but still some. We tested electronics by drastically changing the effect of this position. When switching the chlorine to an electron withdrawing nitro group, we saw the activity of the molecule vanish. However, changing chlorine to a more potent electron donating group such as a methoxy group (*Molecule*

13) actually increased the activity. Figure 24 shows where our current lead compound's MIC might lie.

Future Directions

In order to make a breakthrough with our SAR we are aiming to change the core structure of these molecules in order to increase stability. We believe these molecules to have short half-lives due to our observations of the biological activity decreasing over time at certain concentrations. If we can remove heteroatoms from the core 5-member ring or change the sulfur to an oxygen we can possibly increase the stability and allow these molecules to function for longer against bacteria. This has proved difficult and we are currently altering our reaction conditions in order to complete this goal.

Conclusions

A focused series of molecules were made and tested against two bacteria for an antibiotic effect in order to develop a structure activity relationship. Our current lead compound is Molecule 13 with a highly electron donating group in the para position of the phenyl hydrazine ring, with small sterics in the ketone position of the molecule. Pushing the SAR further would require more detailed changes to the core structure of these molecules, and this is our current focus.

Chapter 3B

Experimental Data for Narrow Spectrum Antibiotic Development

General Experimental

Unless otherwise noted, all reactions were performed in flame-dried glassware under an atmosphere of nitrogen or argon using dried reagents and solvents. All chemicals were purchased from commercial vendors and used without further purification. Anhydrous clean solvents were purchased from commercial vendors.

Flash chromatography was performed using standard grade silica gel 60 230-400 mesh from SORBENT Technologies or was performed using a Biotage Flash Purification system equipped with Biotage SNAP columns. All purifications were performed using gradients of mixtures of ethyl acetate and hexanes. Analytical thin-layer chromatography was carried out using Silica G TLC plates, 200 μm with UV₂₅₄ fluorescent indicator (SORBENT Technologies), and visualization was performed by staining and/or by absorbance of UV light.

NMR spectra were recorded using a Varian Mercury Plus spectrometer (400 MHz for ¹H-NMR; 100 MHz for ¹³C-NMR). Chemical shifts are reported in parts per million (ppm) and were calibrated according to residual protonated solvent. Mass spectroscopy data was collected using an Agilent 1100-Series LC/MSD Trap LC-MS or a Micromass Quattromicro with a Waters 2795 Separations Module LC-MS with acetonitrile containing 0.1% formic acid as the mobile phase in positive ionization mode. Purity was determined on a Agilent 1100 series equipped with a Phenomenex Kinetex 2.6 μm C18-UPLC column using a gradient of water to acetonitrile with 0.1% TFA.

¹H-NMR and ¹³C-NMR Spectra for all Final Compounds and Key Intermediates

2-phenyl-1,2,4-triazaspiro[4,5]decane-3-thione, 9, This is a two-day reaction. For day one, hydrochloric acid (3 mL, 1 M), potassium thiocyanate (0.291g, 3 mmol), and phenylhydrazine (0.324 g, 3 mmol) were added to a 20 mL scintillation vial. Then, cyclohexanone (0.311 mL, 3 mmol) was added dropwise to the vial. This solution was stirred for 16 hours at room temperature in dark conditions. For day two, the precipitate was vacuum filtrated and washed with water four times. Then the layer was recrystallized with methanol. ¹H NMR (400 MHz, DMSO-*d*₆) δ 9.20 (s, 1H), 7.95 (d, *J* = 8.6 Hz, 2H), 7.33 (t, *J* = 7.7 Hz, 2H), 7.11 (t, *J* = 7.4 Hz, 1H), 6.73 (s, 1H), 1.34 (s, 6H). ¹³C-NMR (120MHz, DMSO-*d*₆) δ 176.17, 140.42, 127.94, 124.11, 121.47, 75.95, 34.44, 24.73, 22.17.

5,5-dimethyl-2-phenyl-1,2,4-triazolidine-3-thione, 1, This is a two-day reaction. For day one, hydrochloric acid (3 mL, 1 M), potassium thiocyanate (0.291g, 3 mmol), and phenylhydrazine (0.324 g, 3 mmol) were added to a 20 mL scintillation vial. Then, acetone (0.222 mL, 3 mmol) was added dropwise to the vial. This solution was stirred for 16 hours at room temperature in dark conditions. For day two, the precipitate was vacuum filtrated and washed with water four times. Then the layer was recrystallized with methanol. ¹H NMR (400 MHz, DMSO-*d*₆) δ 9.20 (s, 1H), 7.95 (d, *J* = 8.6 Hz, 2H), 7.33 (t, *J* = 7.7 Hz, 2H), 7.11 (t, *J* = 7.4 Hz, 1H), 6.73 (s, 1H), 1.34 (s, 6H). ¹³C-NMR (120MHz, DMSO-*d*₆) δ 176.32, 140.17, 127.87, 124.05, 121.29, 74.07, 24.96.

5-ethyl-5-pentyl-2-phenyl-1,2,4-triazolidine-3-thione, 8, This is a two-day reaction. For day one, hydrochloric acid (3 mL, 1 M), potassium thiocyanate (0.291g, 3 mmol), and phenylhydrazine (0.324 g, 3 mmol) were added to a 20 mL scintillation vial. Then, 3-

octanone (0.469 mL, 3 mmol) was added dropwise to the vial. This solution was stirred for 16 hours at room temperature in dark conditions. For day two, the precipitate was vacuum filtrated and washed with water four times. Then the layer was recrystallized with methanol. ^1H NMR (400 MHz, $\text{DMSO-}d_6$) δ 9.20 (s, 1H), 7.95 (d, $J = 8.6$ Hz, 2H), 7.33 (t, $J = 7.7$ Hz, 2H), 7.11 (t, $J = 7.4$ Hz, 1H), 6.73 (s, 1H), 1.34 (s, 6H). ^{13}C -NMR (120MHz, $\text{DMSO-}d_6$) δ 175.93, 140.28, 128.08, 124.26, 121.49, 79.00, 48.88, 36.56, 31.75, 29.79, 22.25, 14.08, 7.92.

5-hexyl-5-methyl-2-phenyl-1,2,4-triazolidine-3-thione, **7**, This is a two-day reaction. For day one, hydrochloric acid (3 mL, 1 M), potassium thiocyanate (0.291g, 3 mmol), and phenylhydrazine (0.324 g, 3 mmol) were added to a 20 mL scintillation vial. Then, 2-octanone (0.469 mL, 3 mmol) was added dropwise to the vial. This solution was stirred for 16 hours at room temperature in dark conditions. For day two, the precipitate was vacuum filtrated and washed with water four times. Then, the layer was recrystallized with methanol. ^1H NMR (400 MHz, $\text{DMSO-}d_6$) δ 9.20 (s, 1H), 7.95 (d, $J = 8.6$ Hz, 2H), 7.33 (t, $J = 7.7$ Hz, 2H), 7.11 (t, $J = 7.4$ Hz, 1H), 6.73 (s, 1H), 1.34 (s, 6H). ^{13}C -NMR (120MHz, $\text{DMSO-}d_6$) δ 175.96, 140.17, 127.82, 123.90, 121.14, 76.19, 31.18, 28.96, 23.21, 23.01, 22.01, 13.93.

5-ethyl-5-methyl-2-phenyl-1,2,4-triazolidine-3-thione, **2**, This is a two-day reaction. For day one, hydrochloric acid (3 mL, 1 M), potassium thiocyanate (0.291g, 3 mmol), and phenylhydrazine (0.324 g, 3 mmol) were added to a 20 mL scintillation vial. Then, 2-butanone (0.269 mL, 3 mmol) was added dropwise to the vial. This solution was stirred for 16 hours at room temperature in dark conditions. For day two, the precipitate was vacuum filtrated and washed with water four times. Then the layer was recrystallized

with methanol. ^1H NMR (400 MHz, $\text{DMSO-}d_6$) δ 9.20 (s, 1H), 7.95 (d, $J = 8.6$ Hz, 2H), 7.33 (t, $J = 7.7$ Hz, 2H), 7.11 (t, $J = 7.4$ Hz, 1H), 6.73 (s, 1H), 1.34 (s, 6H). ^{13}C -NMR (120MHz, $\text{DMSO-}d_6$) δ 175.99, 140.16, 127.91, 124.01, 121.23, 76.55, 31.76, 22.53, 7.99.

5,5-diethyl-2-phenyl-1,2,4-triazolidine-3-thione, **3**, This is a two-day reaction. For day one, hydrochloric acid (3 mL, 1 M), potassium thiocyanate (0.291g, 3 mmol), and phenylhydrazine (0.324 g, 3 mmol) were added to a 20 mL scintillation vial. Then, 3-pentanone (0.312 mL, 3 mmol) was added dropwise to the vial. This solution was stirred for 16 hours at room temperature in dark conditions. For day two, the precipitate was vacuum filtrated and washed with water four times. Then the layer was recrystallized with methanol. ^1H NMR (400 MHz, $\text{DMSO-}d_6$) δ 9.20 (s, 1H), 7.95 (d, $J = 8.6$ Hz, 2H), 7.33 (t, $J = 7.7$ Hz, 2H), 7.11 (t, $J = 7.4$ Hz, 1H), 6.73 (s, 1H), 1.34 (s, 6H). ^{13}C -NMR (120MHz, $\text{DMSO-}d_6$) δ 175.72, 140.11, 127.84, 123.88, 121.14, 78.98, 29.09, 7.66.

5-ethyl-2-phenyl-1,2,4-triazolidine-3-thione, **5**, This is a two-day reaction. For day one, hydrochloric acid (3 mL, 1 M), potassium thiocyanate (0.291g, 3 mmol), and phenylhydrazine (0.324 g, 3 mmol) were added to a 20 mL scintillation vial. Then, propionaldehyde (0.215 mL, 3 mmol) was added dropwise to the vial. This solution was stirred for 16 hours at room temperature in dark conditions. For day two, the precipitate was vacuum filtrated and washed with water four times. Then the layer was recrystallized with methanol. ^1H NMR (400 MHz, $\text{DMSO-}d_6$) δ 9.20 (s, 1H), 7.95 (d, $J = 8.6$ Hz, 2H), 7.33 (t, $J = 7.7$ Hz, 2H), 7.11 (t, $J = 7.4$ Hz, 1H), 6.73 (s, 1H), 1.34 (s, 6H). ^{13}C -NMR (120MHz, $\text{DMSO-}d_6$) δ 177.49, 151.53, 129.00, 122.56, 115.81, 83.45, 28.81, 7.95.

2-phenyl-1,2,4-triazaspiro[4,4]nonane-3-thione, **6**, This is a two-day reaction. For day one, hydrochloric acid (3 mL, 1 M), potassium thiocyanate (0.291g, 3 mmol), and phenylhydrazine (0.324 g, 3 mmol) were added to a 20 mL scintillation vial. Then, cyclopentanone (0.266 mL, 3 mmol) was added dropwise to the vial. This solution was stirred for 16 hours at room temperature in dark conditions. For day two, the precipitate was vacuum filtrated and washed with water four times. Then the layer was recrystallized with methanol. ¹H NMR (400 MHz, DMSO-*d*₆) δ 9.20 (s, 1H), 7.95 (d, *J* = 8.6 Hz, 2H), 7.33 (t, *J* = 7.7 Hz, 2H), 7.11 (t, *J* = 7.4 Hz, 1H), 6.73 (s, 1H), 1.34 (s, 6H). ¹³C-NMR (120MHz, DMSO-*d*₆) δ 176.35, 140.04, 127.90, 124.08, 121.31, 83.87, 35.80, 22.92.

5-(hydroxymethyl)-5-methyl-2-phenyl-1,2,4-triazolidine-3-thione, **4**, This is a two-day reaction. For day one, hydrochloric acid (3 mL, 1 M), potassium thiocyanate (0.291g, 3 mmol), and phenylhydrazine (0.296 g, 3 mmol) were added to a 20 mL scintillation vial. Then, hydroxyacetone (0.206 mL, 3 mmol) was added dropwise to the vial. This solution was stirred for 16 hours at room temperature in dark conditions. For day two, the precipitate was vacuum filtrated and washed with water four times. Then the layer was recrystallized with methanol. ¹H NMR (400 MHz, DMSO-*d*₆) δ 9.20 (s, 1H), 7.95 (d, *J* = 8.6 Hz, 2H), 7.33 (t, *J* = 7.7 Hz, 2H), 7.11 (t, *J* = 7.4 Hz, 1H), 6.73 (s, 1H), 1.34 (s, 6H). ¹³C-NMR (120MHz, DMSO-*d*₆) δ 176.27, 140.19, 127.88, 124.16, 121.58, 64.47, 20.30.

2-(4-chlorophenyl)-5,5-dimethyl-1,2,4-triazolidine-3-thione, **10**, This is a two-day reaction. For day one, hydrochloric acid (3 mL, 1 M), potassium thiocyanate (0.291g, 3 mmol), and 4-chlorophenylhydrazine (0.537 g, 3 mmol) were added to a 20 mL scintillation vial. Then, acetone (0.222 mL, 3 mmol) was added to the vial. This solution was stirred for 16 hours at room temperature in dark conditions. For day two, the

precipitate was vacuum filtrated and washed with water four times. Then the layer was recrystallized with methanol. ^1H NMR (400 MHz, $\text{DMSO-}d_6$) δ 9.20 (s, 1H), 7.95 (d, J = 8.6 Hz, 2H), 7.33 (t, J = 7.7 Hz, 2H), 7.11 (t, J = 7.4 Hz, 1H), 6.73 (s, 1H), 1.34 (s, 6H). ^{13}C -NMR (120MHz, $\text{DMSO-}d_6$) δ 176.29, 139.13, 127.80, 127.71, 122.45, 74.19, 24.96.

2-(4-bromophenyl)-5,5-dimethyl-1,2,4-triazolidine-3-thione, **15**, This is a two-day reaction. For day one, hydrochloric acid (3 mL, 1 M), potassium thiocyanate (0.291g, 3 mmol), and 4-bromophenylhydrazine (0.671 g, 3 mmol) were added to a 20 mL scintillation vial. Then, acetone (0.222 mL, 3 mmol) was added to the vial. This solution was stirred for 16 hours at room temperature in dark conditions. For day two, the precipitate was vacuum filtrated and washed with water four times. Then the layer was recrystallized with methanol. ^1H NMR (400 MHz, $\text{DMSO-}d_6$) δ 9.20 (s, 1H), 7.95 (d, J = 8.6 Hz, 2H), 7.33 (t, J = 7.7 Hz, 2H), 7.11 (t, J = 7.4 Hz, 1H), 6.73 (s, 1H), 1.34 (s, 6H). ^{13}C -NMR (120MHz, $\text{DMSO-}d_6$) δ 176.25, 139.57, 130.70, 122.74, 115.81, 74.17, 24.94.

2-(2-chlorophenyl)-5,5-dimethyl-1,2,4-triazolidine-3-thione, **12**, This is a two-day reaction. For day one, hydrochloric acid (3 mL, 1 M), potassium thiocyanate (0.291g, 3 mmol), and 2-chlorophenylhydrazine (0.537 g, 3 mmol) were added to a 20 mL scintillation vial. Then, acetone (0.222 mL, 3 mmol) was added to the vial. This solution was stirred for 16 hours at room temperature in dark conditions. For day two, the precipitate was vacuum filtrated and washed with water four times. Then the layer was recrystallized with methanol. ^1H NMR (400 MHz, $\text{DMSO-}d_6$) δ 9.20 (s, 1H), 7.95 (d, J = 8.6 Hz, 2H), 7.33 (t, J = 7.7 Hz, 2H), 7.11 (t, J = 7.4 Hz, 1H), 6.73 (s, 1H), 1.34 (s, 6H). ^{13}C -NMR (120MHz, $\text{DMSO-}d_6$) δ 178.50, 132.57, 130.89, 129.86, 129.51, 127.42, 109.54, 75.67, 25.05.

2-(4-methoxyphenyl)-5,5-dimethyl-1,2,4-triazoline-3-thione, **13**, This is a two-day reaction. For day one, hydrochloric acid (3 mL, 1 M), potassium thiocyanate (0.291g, 3 mmol), and 4-methoxyphenylhydrazine (0.524 g, 3 mmol) were added to a 20 mL scintillation vial. Then, acetone (0.222 mL, 3 mmol) was added to the vial. This solution was stirred for 16 hours at room temperature in dark conditions. For day two, the precipitate was vacuum filtrated and washed with water four times. Then the layer was recrystallized with methanol. ¹H NMR (400 MHz, DMSO-*d*₆) δ 9.20 (s, 1H), 7.95 (d, *J* = 8.6 Hz, 2H), 7.33 (t, *J* = 7.7 Hz, 2H), 7.11 (t, *J* = 7.4 Hz, 1H), 6.73 (s, 1H), 1.34 (s, 6H). ¹³C-NMR (120MHz, DMSO-*d*₆) δ 176.31, 156.24, 133.15, 123.90, 113.10, 74.07, 55.27, 24.98.

2-(4-cyclohexylphenyl)-5,5-dimethyl-1,2,4-triazolidine-3-thione, **16**, This is a two-day reaction. For day one, hydrochloric acid (3 mL, 1 M), potassium thiocyanate (0.291g, 3 mmol), and cyclohexylhydrazine (0.452 g, 3 mmol) were added to a 20 mL scintillation vial. Then, acetone (0.222 mL, 3 mmol) was added to the vial. This solution was stirred for 16 hours at room temperature in dark conditions. For day two, the precipitate was vacuum filtrated and washed with water four times. Then the layer was recrystallized with methanol. ¹H NMR (400 MHz, DMSO-*d*₆) δ 9.20 (s, 1H), 7.95 (d, *J* = 8.6 Hz, 2H), 7.33 (t, *J* = 7.7 Hz, 2H), 7.11 (t, *J* = 7.4 Hz, 1H), 6.73 (s, 1H), 1.34 (s, 6H). ¹³C-NMR (120MHz, DMSO-*d*₆) δ 176.73, 74.67, 54.02, 29.49, 25.01.

2-(4-chlorophenyl)-5-ethyl-5-methyl-1,2,4-triazolidine-3-thione, **17**, This is a two-day reaction. For day one, hydrochloric acid (3 mL, 1 M), potassium thiocyanate (0.291g, 3 mmol), and 4-chlorophenylhydrazine (0.537 g, 3 mmol) were added to a 20 mL scintillation vial. Then, 2-butanone (0.269 mL, 3 mmol) was added to the vial. This

solution was stirred for 16 hours at room temperature in dark conditions. For day two, the precipitate was vacuum filtrated and washed with water four times. Then the layer was recrystallized with methanol. ^1H NMR (400 MHz, $\text{DMSO-}d_6$) δ 9.20 (s, 1H), 7.95 (d, J = 8.6 Hz, 2H), 7.33 (t, J = 7.7 Hz, 2H), 7.11 (t, J = 7.4 Hz, 1H), 6.73 (s, 1H), 1.34 (s, 6H). ^{13}C -NMR (120MHz, $\text{DMSO-}d_6$) δ 175.96, 139.11, 127.80, 127.59, 122.32, 76.63, 31.75, 22.49, 7.94.

2-(4-bromophenyl)-5-ethyl-5-methyl-1,2,4-triazolidine-3-thione, **22**, This is a two-day reaction. For day one, hydrochloric acid (3 mL, 1 M), potassium thiocyanate (0.291g, 3 mmol), and 4-bromophenylhydrazine (0.671 g, 3 mmol) were added to a 20 mL scintillation vial. Then, 2-butanone (0.269 mL, 3 mmol) was added to the vial. This solution was stirred for 16 hours at room temperature in dark conditions. For day two, the precipitate was vacuum filtrated and washed with water four times. Then the layer was recrystallized with methanol. ^1H NMR (400 MHz, $\text{DMSO-}d_6$) δ 9.20 (s, 1H), 7.95 (d, J = 8.6 Hz, 2H), 7.33 (t, J = 7.7 Hz, 2H), 7.11 (t, J = 7.4 Hz, 1H), 6.73 (s, 1H), 1.34 (s, 6H). ^{13}C -NMR (120MHz, $\text{DMSO-}d_6$) δ 175.93, 139.54, 130.69, 122.61, 115.68, 76.62, 31.75, 22.48, 7.93.

2-(2-chlorophenyl)-5-ethyl-5-methyl-1,2,4-triazolidine-3-thione, **19**, This is a two-day reaction. For day one, hydrochloric acid (3 mL, 1 M), potassium thiocyanate (0.291g, 3 mmol), and 2-chlorophenylhydrazine (0.537 g, 3 mmol) were added to a 20 mL scintillation vial. Then, 2-butanone (0.269 mL, 3 mmol) was added to the vial. This solution was stirred for 16 hours at room temperature in dark conditions. For day two, the precipitate was vacuum filtrated and washed with water four times. Then the layer was recrystallized with methanol. ^1H NMR (400 MHz, $\text{DMSO-}d_6$) δ 9.20 (s, 1H), 7.95 (d, J =

8.6 Hz, 2H), 7.33 (t, $J = 7.7$ Hz, 2H), 7.11 (t, $J = 7.4$ Hz, 1H), 6.73 (s, 1H), 1.34 (s, 6H).
 ^{13}C -NMR (120MHz, DMSO- d_6) δ 153.39, 152.31, 138.09, 126.30, 124.38, 111.62, 77.20, 31.95, 16.27, 11.15.

5-ethyl-2-(4-methoxyphenyl)-5-methyl-1,2,4-triazolidine-3-thione, **20**, This is a two-day reaction. For day one, hydrochloric acid (3 mL, 1 M), potassium thiocyanate (0.291g, 3 mmol), and 4-methoxyphenylhydrazine (0.524 g, 3 mmol) were added to a 20 mL scintillation vial. Then, 2-butanone (0.269 mL, 3 mmol) was added to the vial. This solution was stirred for 16 hours at room temperature in dark conditions. For day two, the precipitate was vacuum filtrated and washed with water four times. Then the layer was recrystallized with methanol. ^1H NMR (400 MHz, DMSO- d_6) δ 9.20 (s, 1H), 7.95 (d, $J = 8.6$ Hz, 2H), 7.33 (t, $J = 7.7$ Hz, 2H), 7.11 (t, $J = 7.4$ Hz, 1H), 6.73 (s, 1H), 1.34 (s, 6H).
 ^{13}C -NMR (120MHz, DMSO- d_6) δ 175.89, 156.15, 133.14, 123.72, 113.08, 76.50, 55.26, 31.68, 22.52, 7.96.

5-ethyl-5-methyl-2-(4-nitrophenyl)-1,2,4-triazolidine-3-thione, **23**, This is a two-day reaction. For day one, hydrochloric acid (3 mL, 1 M), potassium thiocyanate (0.291g, 3 mmol), and 4-nitrophenylhydrazine (0.569 g, 3 mmol) were added to a 20 mL scintillation vial. Then, 2-butanone (0.269 mL, 3 mmol) was added to the vial. This solution was stirred for 16 hours at room temperature in dark conditions. For day two, the precipitate was vacuum filtrated and washed with water four times. Then the layer was recrystallized with methanol. ^1H NMR (400 MHz, DMSO- d_6) δ 9.20 (s, 1H), 7.95 (d, $J = 8.6$ Hz, 2H), 7.33 (t, $J = 7.7$ Hz, 2H), 7.11 (t, $J = 7.4$ Hz, 1H), 6.73 (s, 1H), 1.34 (s, 6H).
 ^{13}C -NMR (120MHz, DMSO- d_6) δ ^{13}C NMR (101 MHz, DMSO- d_6) δ 176.19, 152.96, 151.88, 125.87, 111.19, 76.77, 31.52, 15.84, 10.72.

2-(2,4-dinitrophenyl)-5-ethyl-5-methyl-1,2,4-triazolidine-3-thione, **24**, This is a two-day reaction. For day one, hydrochloric acid (3 mL, 1 M), potassium thiocyanate (0.291 g, 3 mmol), and 2,4-dinitrophenylhydrazine (0.594 g, 3 mmol) were added to a 20 mL scintillation vial. Then, 2-butanone (0.269 mL, 3 mmol) was added to the vial. This solution was stirred for 16 hours at room temperature in dark conditions. For day two, the precipitate was vacuum filtrated and washed with water four times. Then the layer was recrystallized with methanol. ¹H NMR (400 MHz, DMSO-*d*₆) δ 9.20 (s, 1H), 7.95 (d, *J* = 8.6 Hz, 2H), 7.33 (t, *J* = 7.7 Hz, 2H), 7.11 (t, *J* = 7.4 Hz, 1H), 6.73 (s, 1H), 1.34 (s, 6H). ¹³C-NMR (120MHz, DMSO-*d*₆) δ 161.21, 145.06, 136.93, 130.40, 123.35, 116.27, 109.83, 48.87, 31.90, 16.06, 10.61.

2-(4-cyclohexylphenyl)-5-ethyl-5-methyl-1,2,4-triazolidine-3-thione, **25**, This is a two-day reaction. For day one, hydrochloric acid (3 mL, 1 M), potassium thiocyanate (0.291 g, 3 mmol), and cyclohexylhydrazine (0.452 g, 3 mmol) were added to a 20 mL scintillation vial. Then, 2-butanone (0.269 mL, 3 mmol) was added to the vial. This solution was stirred for 16 hours at room temperature in dark conditions. For day two, the precipitate was vacuum filtrated and washed with water four times. Then the layer was recrystallized with methanol. ¹H NMR (400 MHz, DMSO-*d*₆) δ 9.20 (s, 1H), 7.95 (d, *J* = 8.6 Hz, 2H), 7.33 (t, *J* = 7.7 Hz, 2H), 7.11 (t, *J* = 7.4 Hz, 1H), 6.73 (s, 1H), 1.34 (s, 6H). ¹³C-NMR (120MHz, DMSO-*d*₆) δ 176.40, 77.32, 54.34, 31.25, 29.61, 25.15, 22.33, 8.20.

2-(3-chlorophenyl)-5,5-dimethyl-1,2,4-triazolidine-3-thione, **11**, This is a two-day reaction. For day one, hydrochloric acid (3 mL, 1 M), potassium thiocyanate (0.291 g, 3 mmol), and 3-chlorophenylhydrazine (0.537 g, 3 mmol) were added to a 20 mL scintillation vial. Then, acetone (0.222 mL, 3 mmol) was added to the vial. This solution

was stirred for 16 hours at room temperature in dark conditions. For day two, the precipitate was vacuum filtrated and washed with water four times. Then the layer was recrystallized with methanol. ^1H NMR (400 MHz, $\text{DMSO-}d_6$) δ 8.17 (s, 1H), 7.98 (d, $J = 8.3$ Hz, 1H), 7.36 (t, $J = 8.1$ Hz, 1H), 7.15 (d, $J = 7.9$ Hz, 1H), 1.34 (s, 6H). ^{13}C NMR (101 MHz, $\text{DMSO-}d_6$) δ 176.27, 141.56, 132.19, 129.60, 123.30, 119.82, 118.81, 74.14, 24.89.

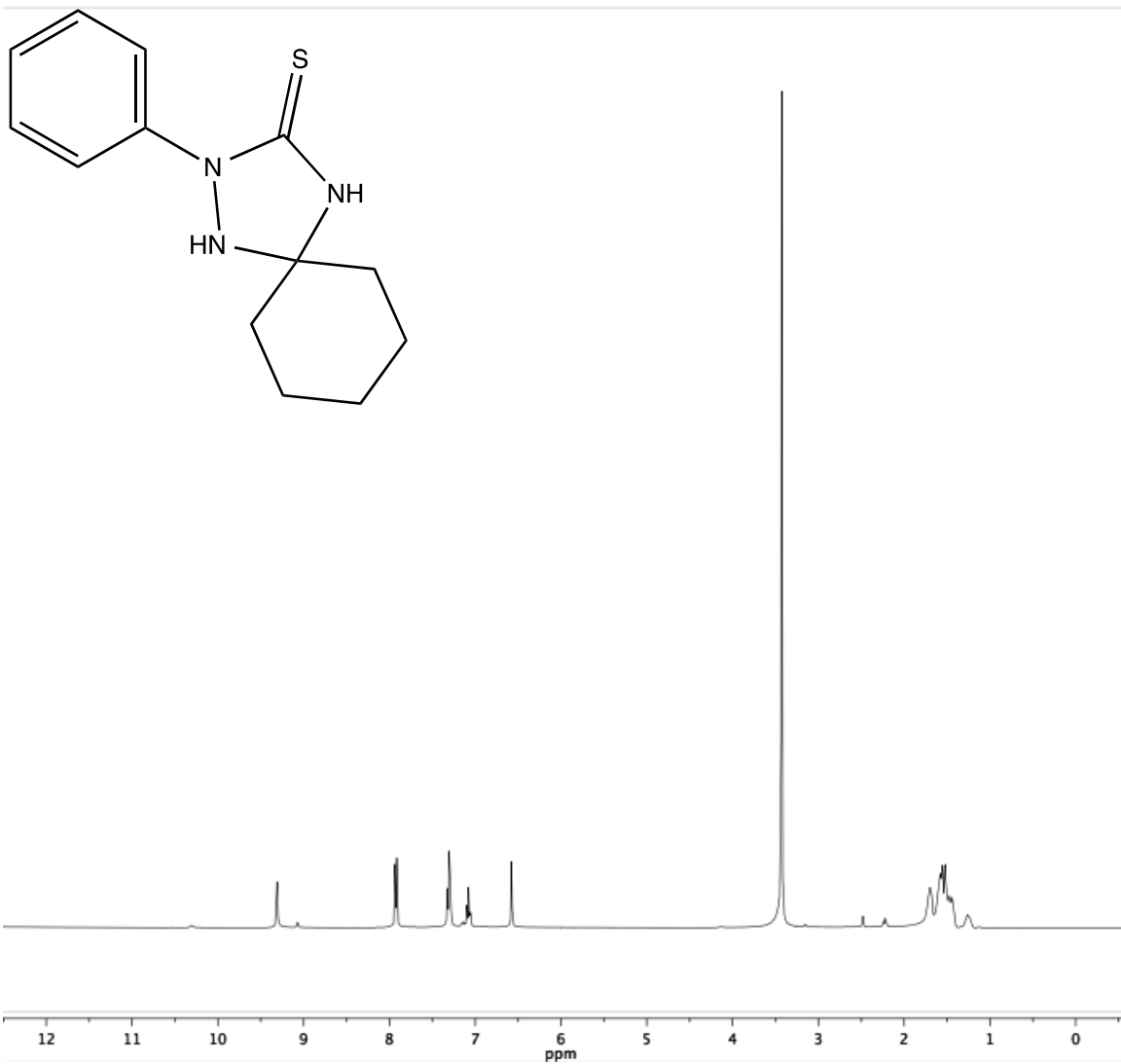
2-(3-chlorophenyl)-5-ethyl-5-methyl-1,2,4-triazolidine-3-thione, **18**, This is a two-day reaction. For day one, hydrochloric acid (3 mL, 1 M), potassium thiocyanate (0.291g, 3 mmol), and 3-chlorophenylhydrazie (0.537 g, 3 mmol) were added to a 20 mL scintillation vial. Then, 2-butanone (0.269 mL, 3 mmol) was added to the vial. This solution was stirred for 16 hours at room temperature in dark conditions. For day two, the precipitate was vacuum filtrated and washed with water four times. Then the layer was recrystallized with methanol. ^1H NMR (400 MHz, $\text{DMSO-}d_6$) δ 8.22 – 8.16 (m, 1H), 8.04 – 7.97 (m, 1H), 7.39 – 7.31 (m, 1H), 7.18 – 7.09 (m, 1H), 1.58 (d, $J = 7.4$ Hz, 2H), 1.33 (s, 3H), 0.88 (t, $J = 7.3$ Hz, 3H). ^{13}C NMR (101 MHz, $\text{DMSO-}d_6$) δ 175.97, 141.52, 132.19, 129.59, 123.18, 119.68, 118.69, 76.59, 31.68, 22.44, 7.88.

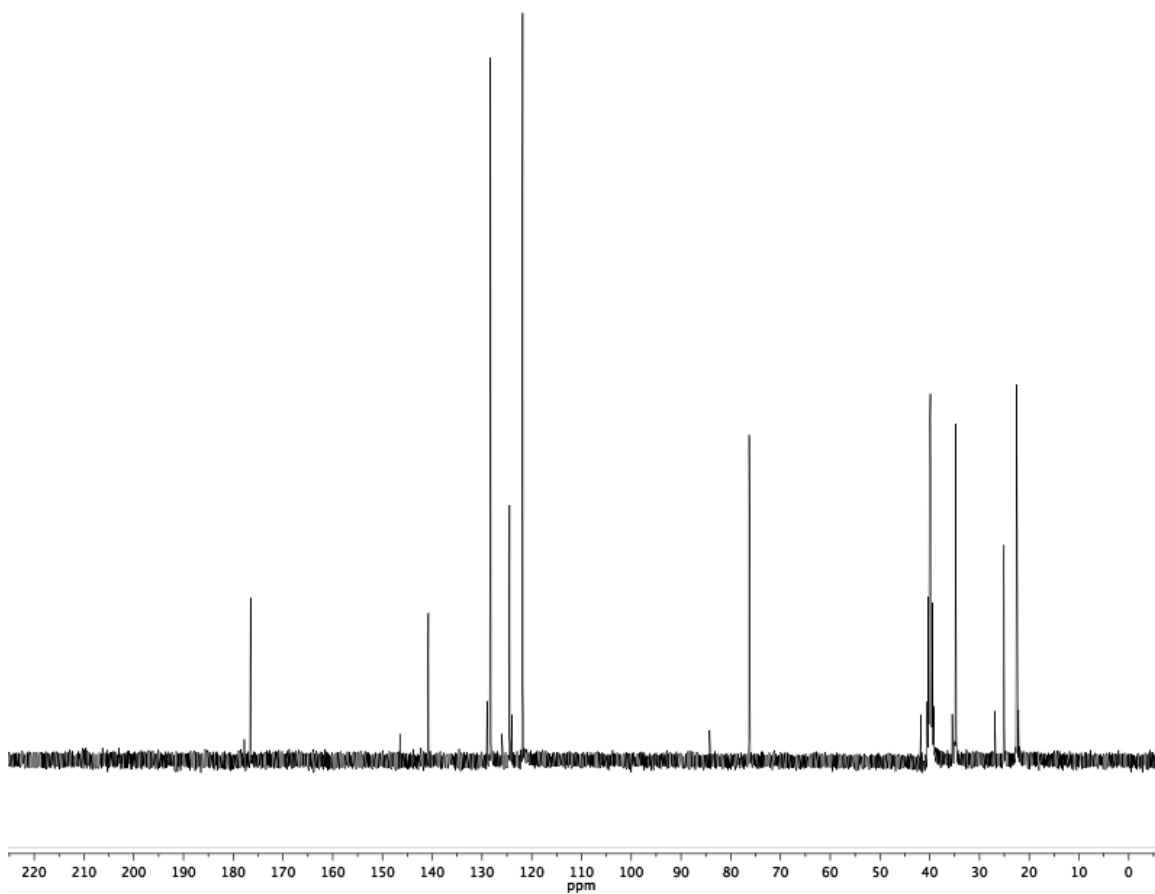
2-(3-methoxyphenyl)-5,5-dimethyl-1,2,4-triazolidine-3-thione, **14**, This is a two-day reaction. For day one, hydrochloric acid (3 mL, 1 M), potassium thiocyanate (0.291g, 3 mmol), and 3-methoxyphenylhydrazine (0.524 g, 3 mmol) were added to a 20 mL scintillation vial. Then, acetone (0.222 mL, 3 mmol) was added to the vial. This solution was stirred for 16 hours at room temperature in dark conditions. For day two, the precipitate was vacuum filtrated and washed with water four times. Then the layer was recrystallized with methanol. ^1H NMR (400 MHz, $\text{DMSO-}d_6$) δ 7.51 (d, $J = 8.1$ Hz, 1H),

7.23 (t, $J = 8.2$ Hz, 1H), 6.69 (d, $J = 13.3$ Hz, 2H), 3.74 (s, 3H), 1.33 (s, 6H). ^{13}C NMR (101 MHz, $\text{DMSO-}d_6$) δ 176.26, 158.75, 141.32, 128.67, 113.25, 109.38, 106.91, 73.97, 55.12, 24.92.

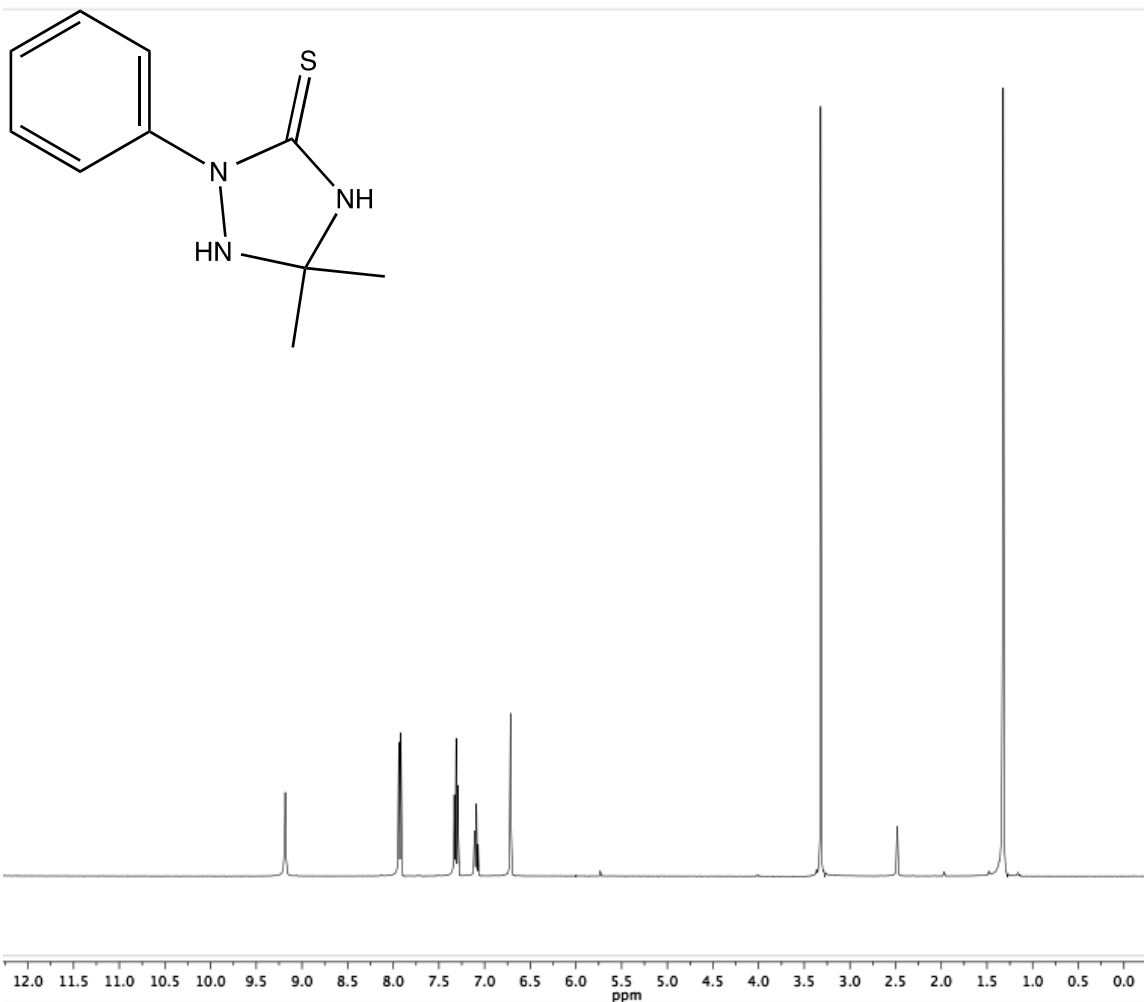
5-ethyl-2-(3-methoxyphenyl)-5-methyl-1,2,4-triazolidine-3-thione, **21**, This is a two-day reaction. For day one, hydrochloric acid (3 mL, 1 M), potassium thiocyanate (0.291 g, 3 mmol), and 3-methoxyphenylhydrazine (0.524 g, 3 mmol) were added to a 20 mL scintillation vial. Then, 2-butanone (0.269 mL, 3 mmol) was added to the vial. This solution was stirred for 16 hours at room temperature in dark conditions. For day two, the precipitate was vacuum filtrated and washed with water four times. Then the layer was recrystallized with methanol. ^1H NMR (400 MHz, $\text{DMSO-}d_6$) δ 7.74 (s, 1H), 7.53 (d, $J = 8.1$ Hz, 1H), 7.22 (t, $J = 8.1$ Hz, 1H), 6.68 (d, $J = 8.2$ Hz, 1H), 3.73 (s, 3H), 1.57 (d, $J = 7.4$ Hz, 2H), 1.32 (s, 3H), 0.89 (t, $J = 7.2$ Hz, 3H). ^{13}C NMR (101 MHz, $\text{DMSO-}d_6$) δ 175.93, 158.74, 141.29, 128.67, 113.13, 109.22, 106.84, 76.41, 31.69, 55.10, 22.43, 7.91.

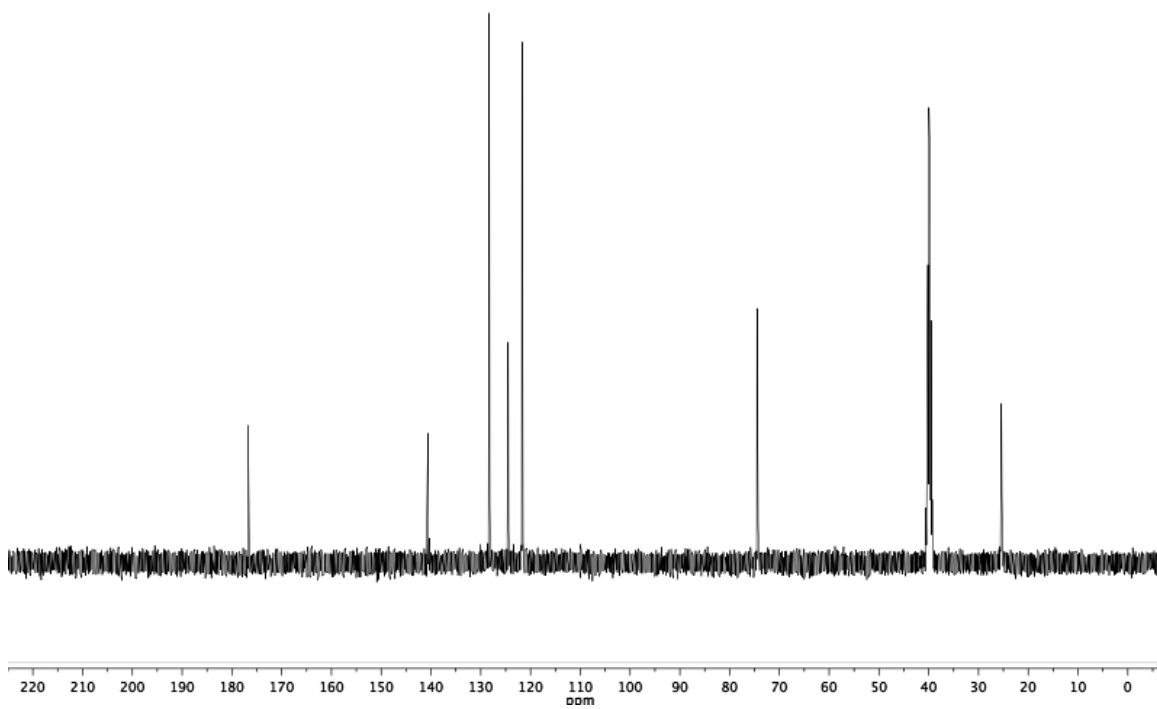
2-phenyl-1,2,4-triazaspiro[4,5]decane-3-thione, **9**.



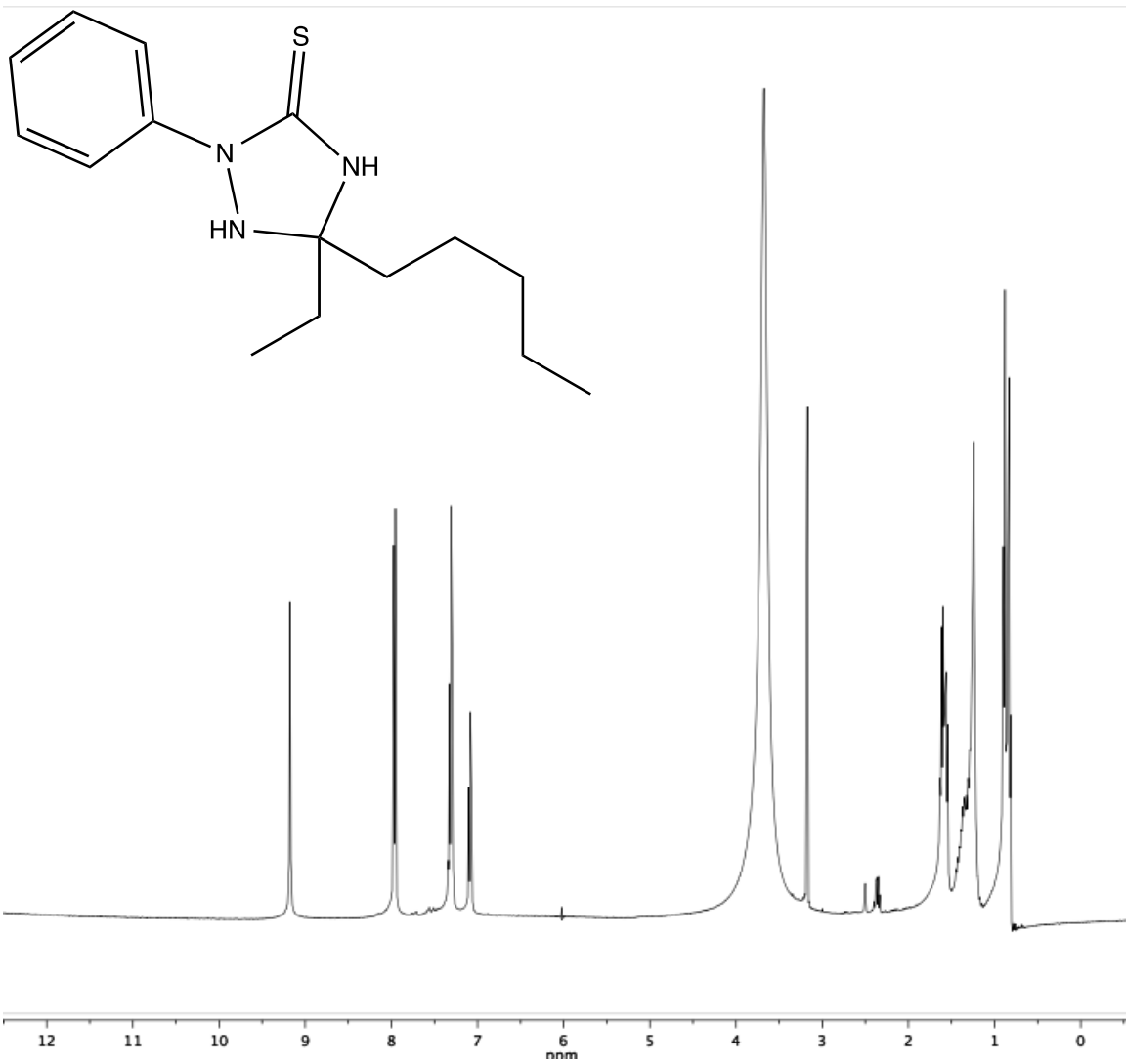


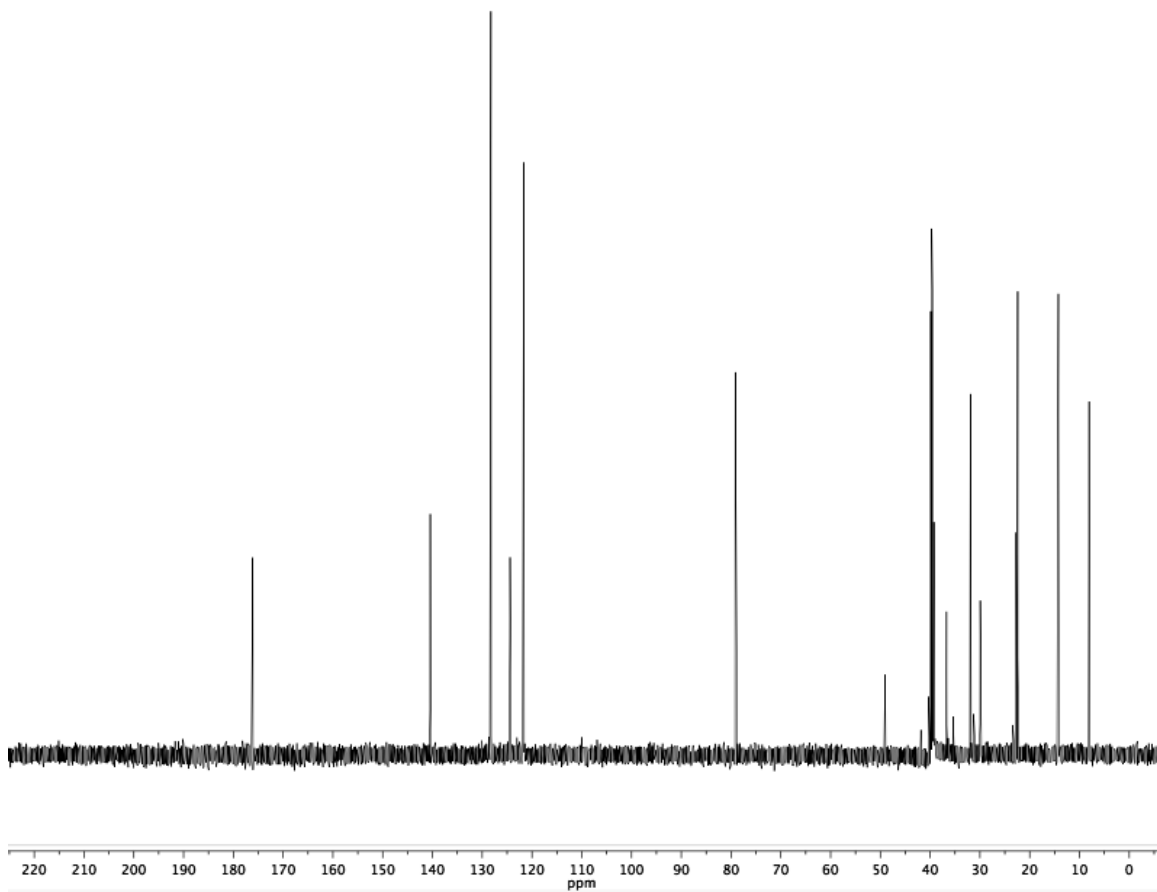
5,5-dimethyl-2-phenyl-1,2,4-triazolidine-3-thione, 1.



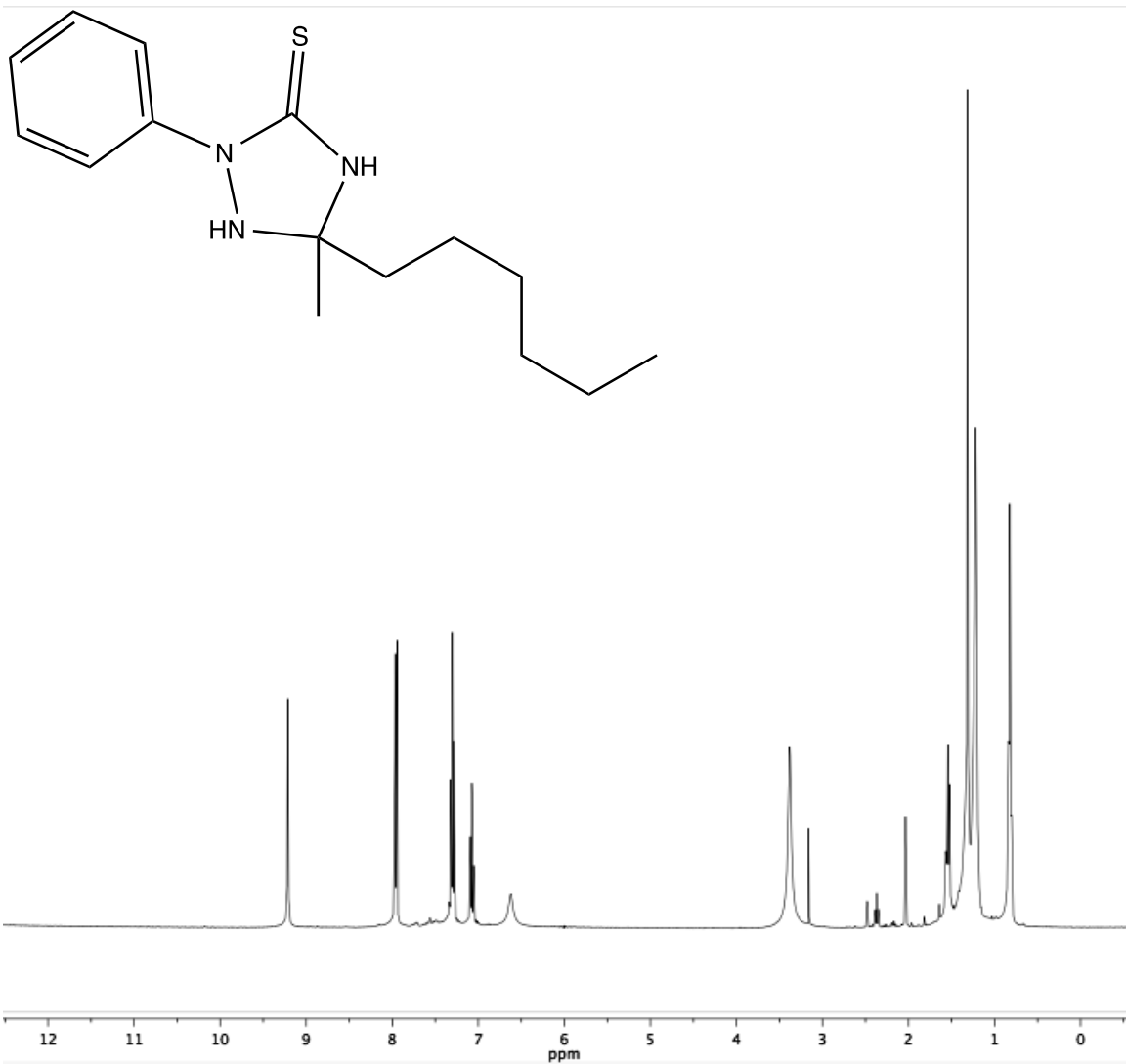


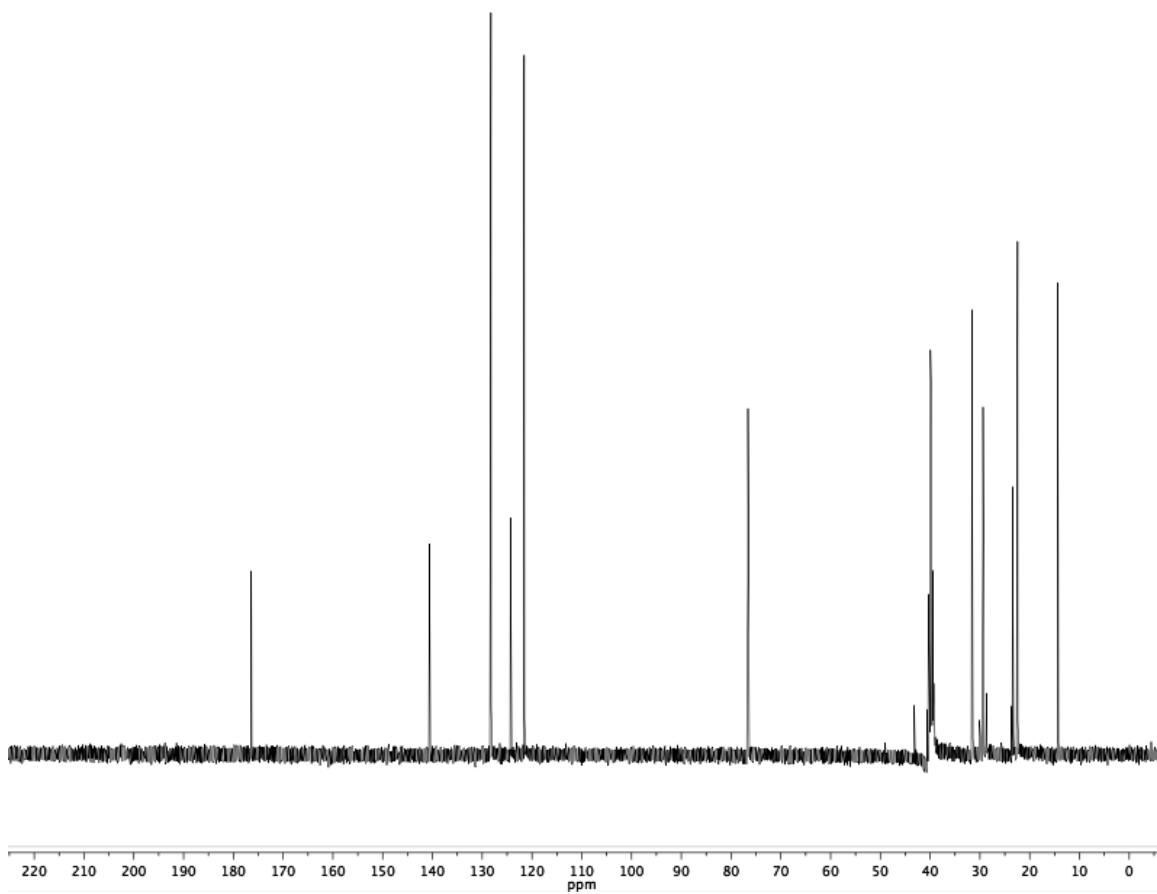
5-ethyl-5-pentyl-2-phenyl-1,2,4-triazolidine-3-thione, 8.



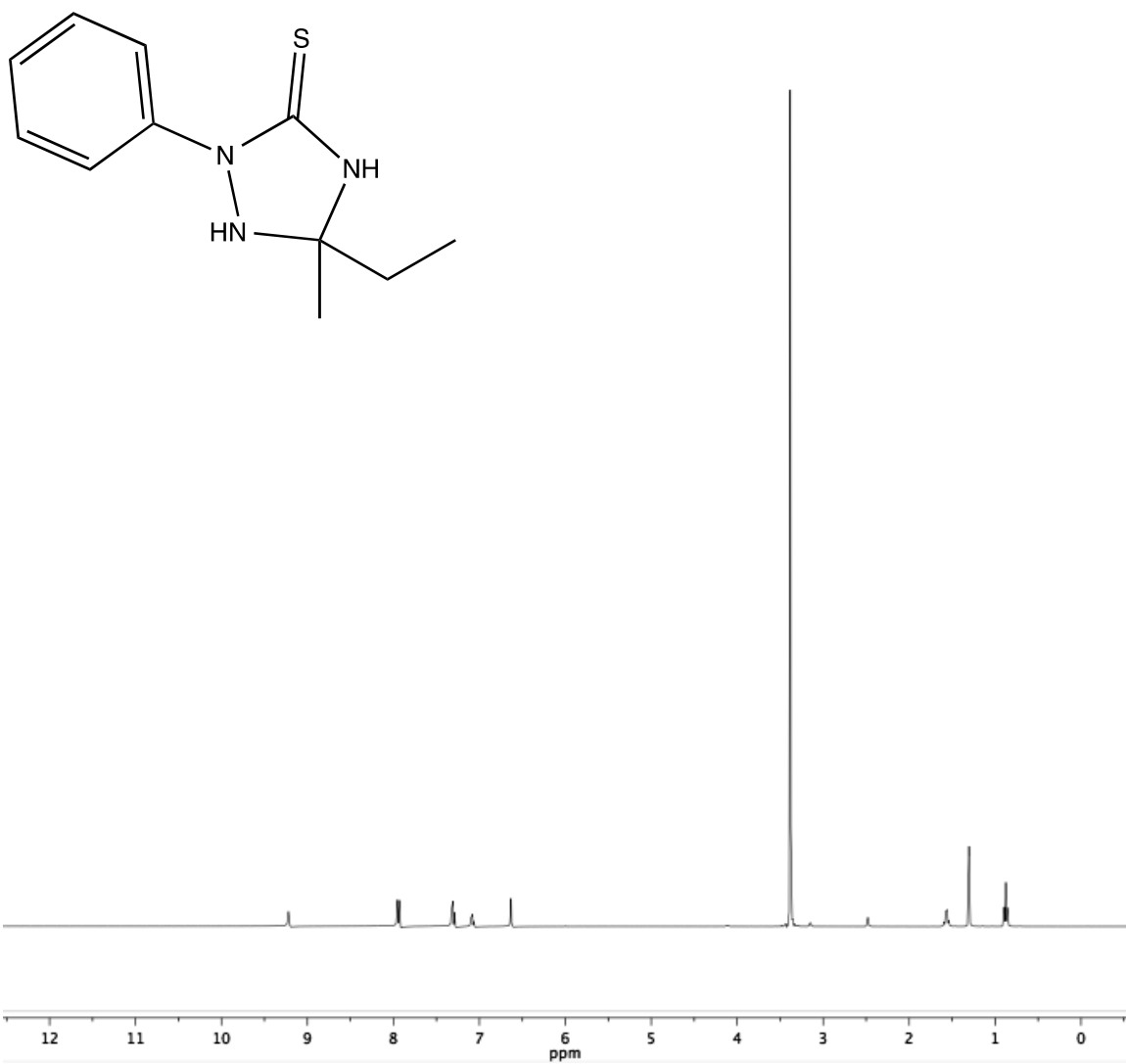


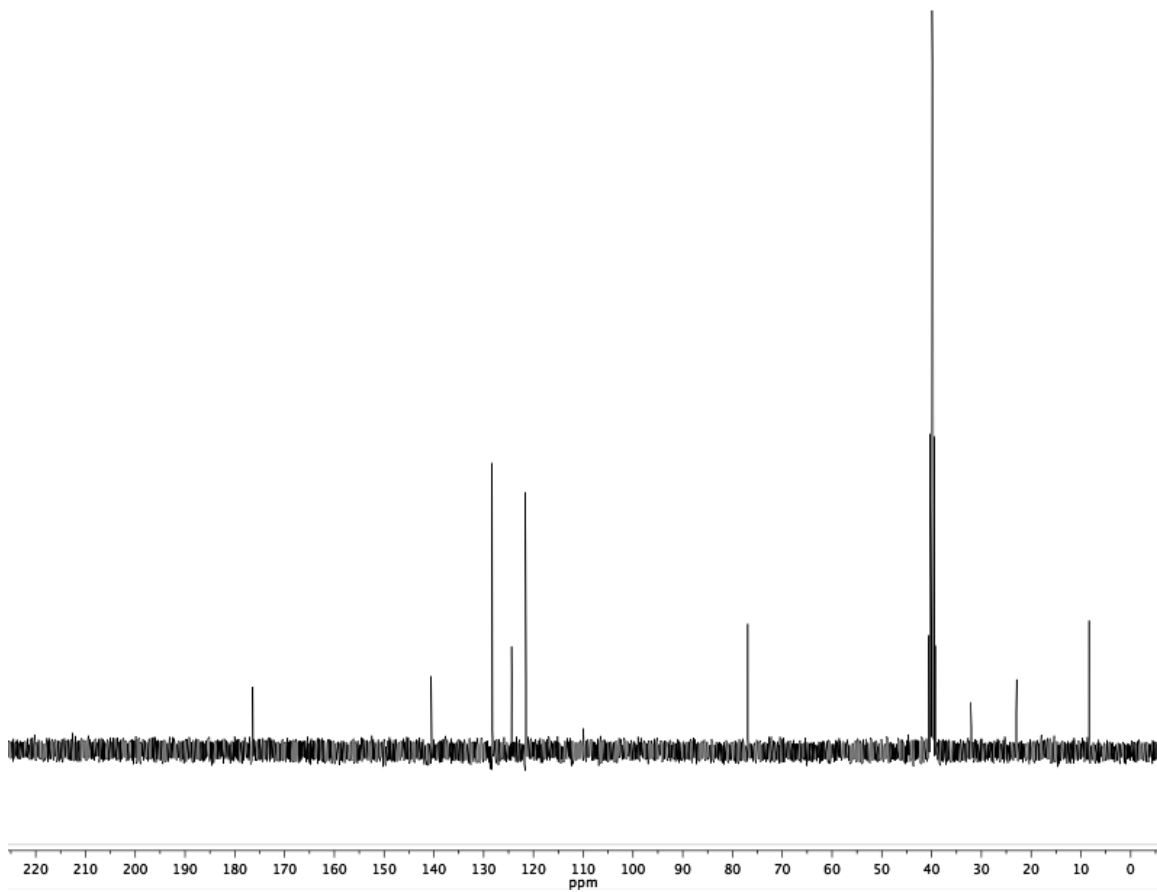
5-hexyl-5-methyl-2-phenyl-1,2,4-triazolidine-3-thione, 7.





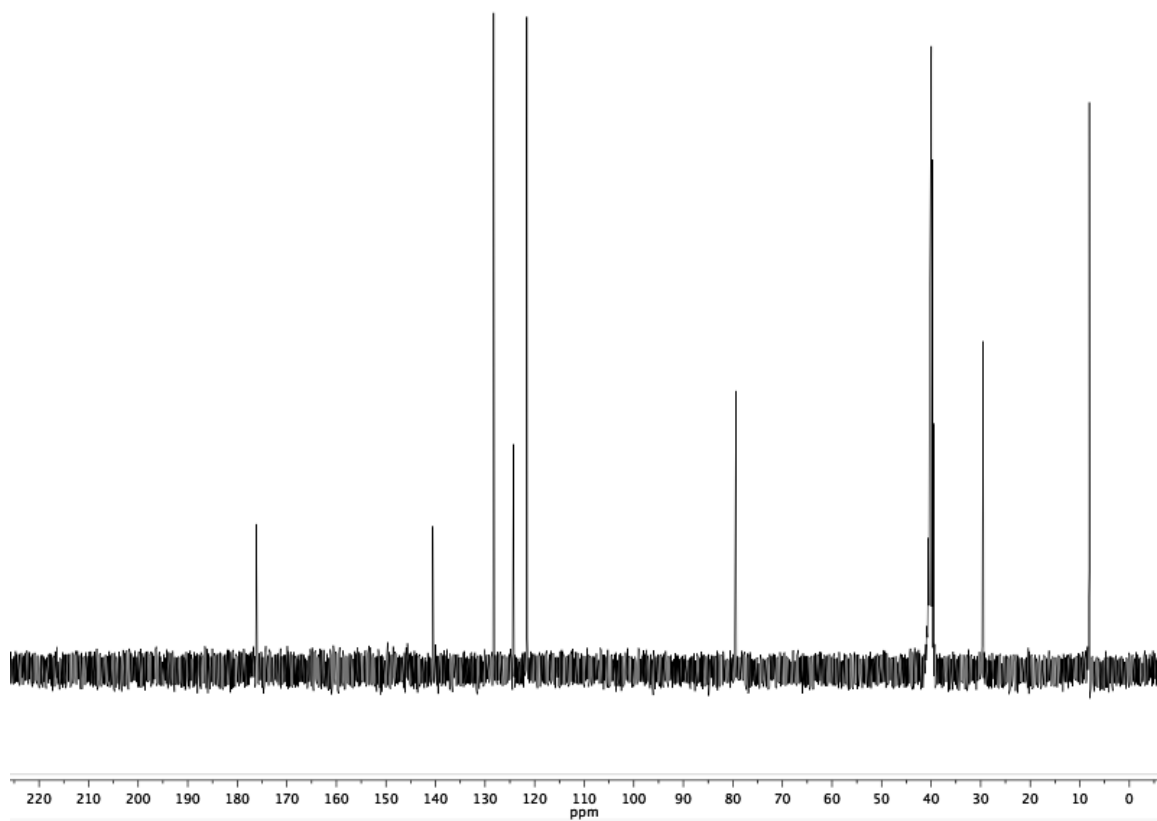
5-ethyl-5-methyl-2-phenyl-1,2,4-triazolidine-3-thione, 2.



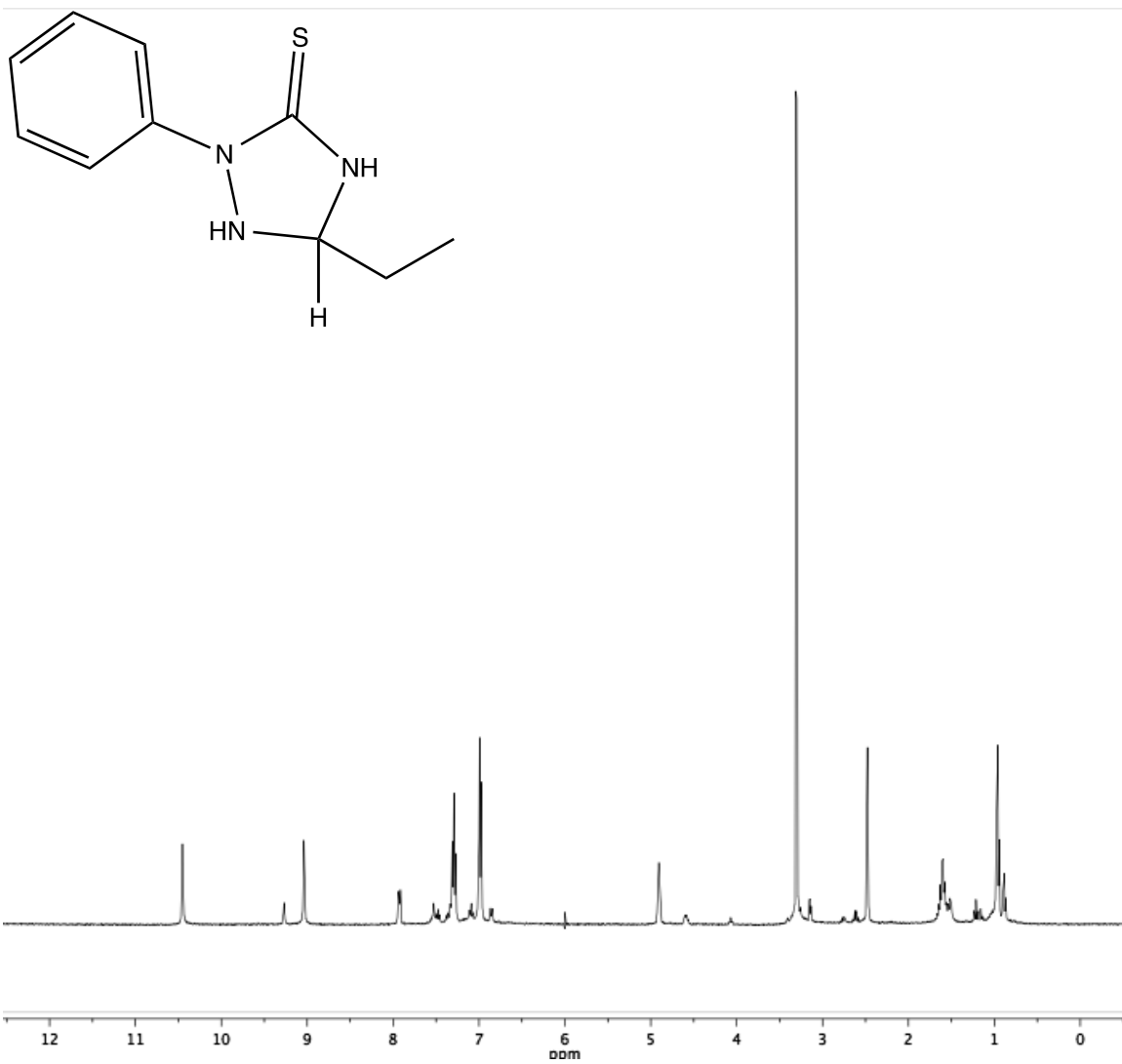


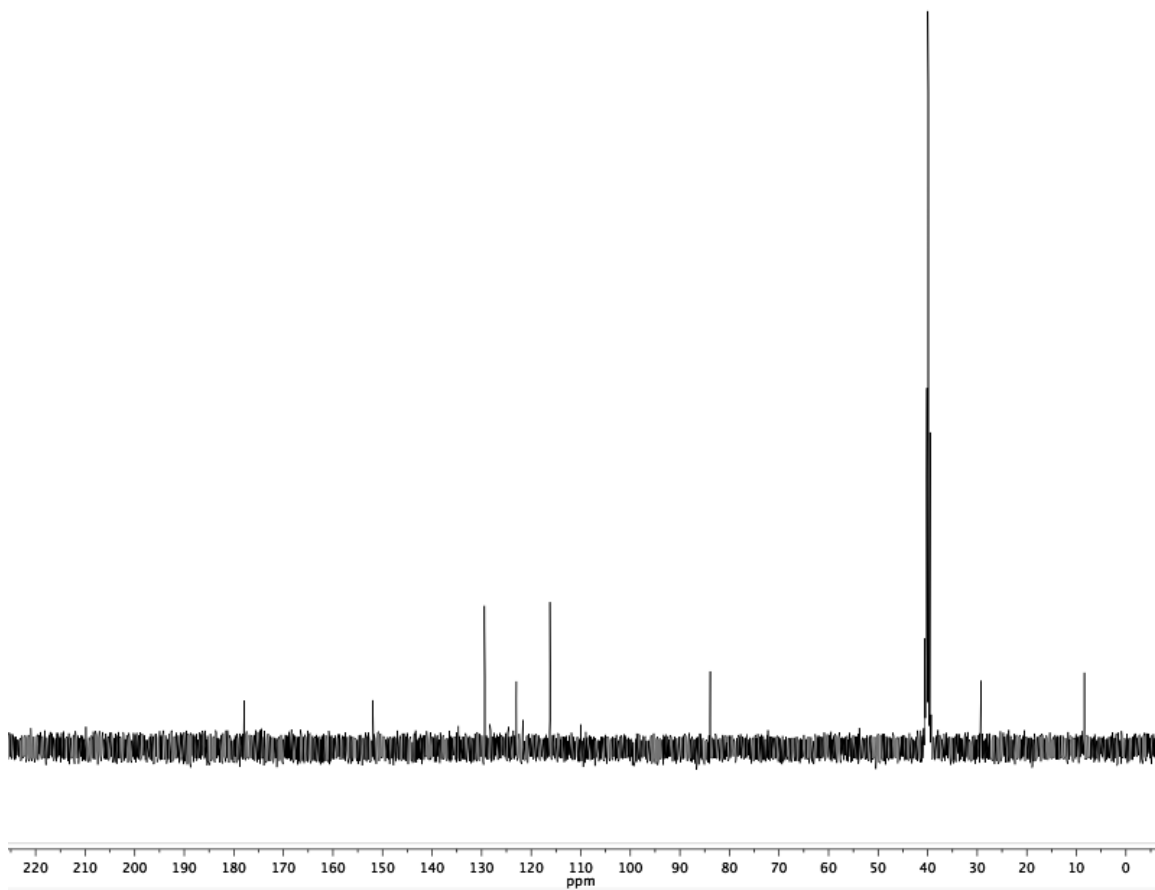
5,5-diethyl-2-phenyl-1,2,4-triazolidine-3-thione, 3.



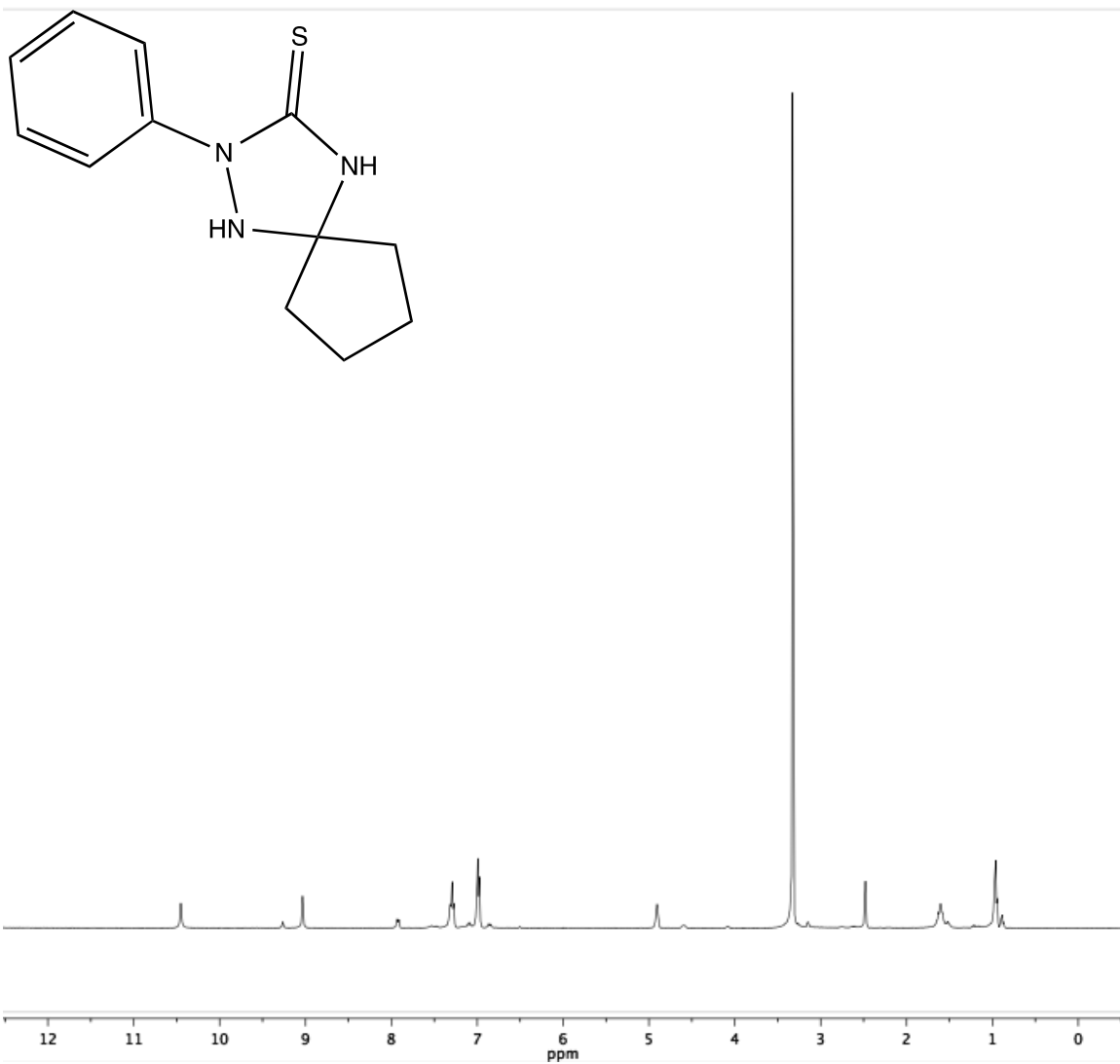


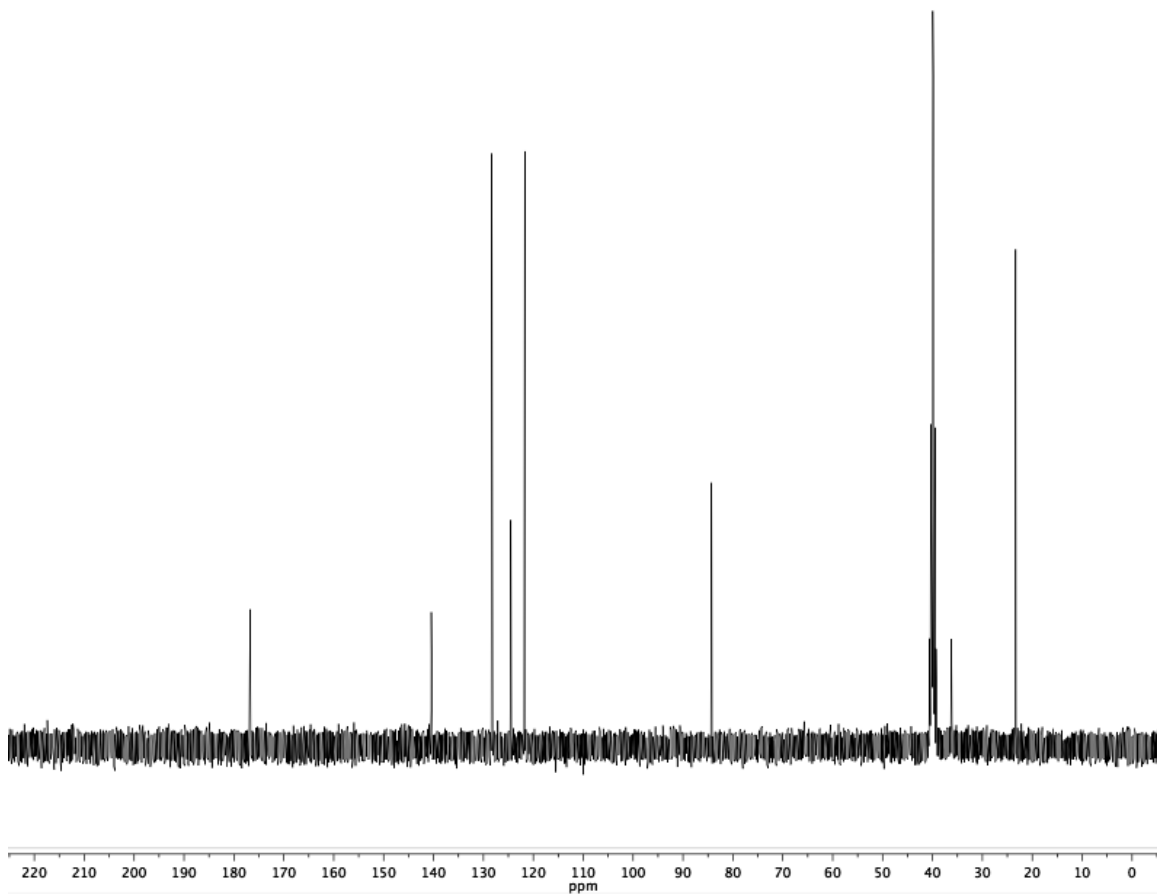
5-ethyl-2-phenyl-1,2,4-triazolidine-3-thione, 5.



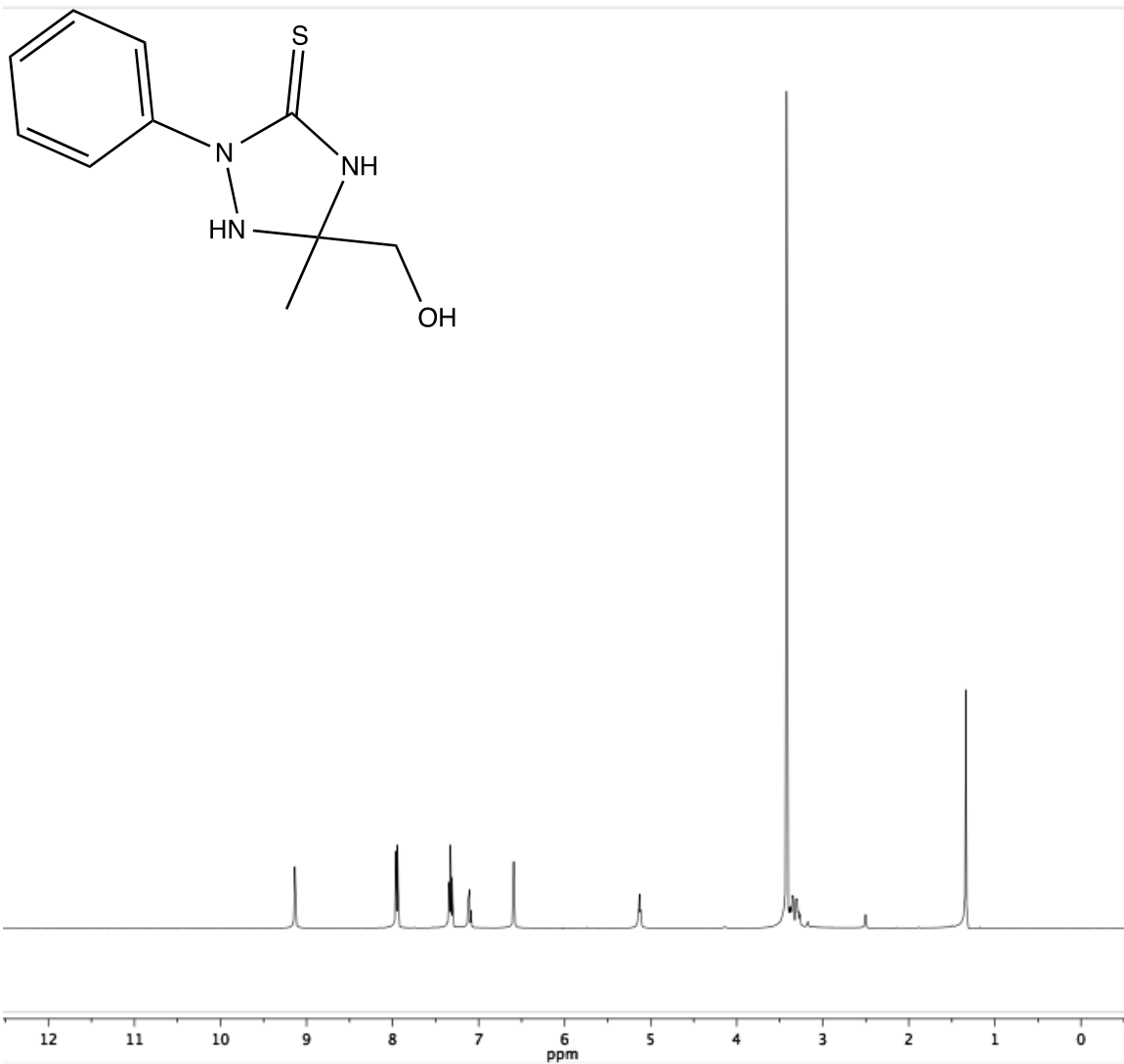


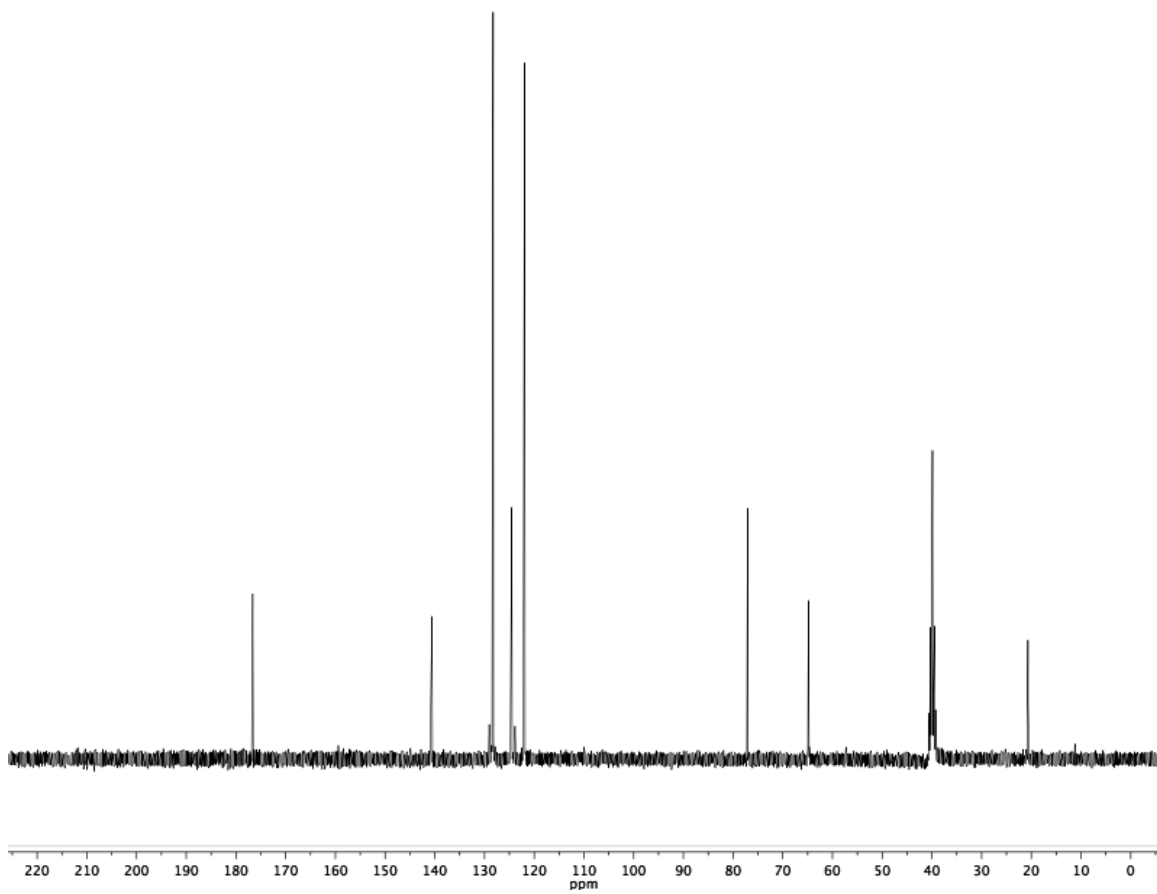
2-phenyl-1,2,4-triazaspiro[4.4]nonane-3-thione, 6.





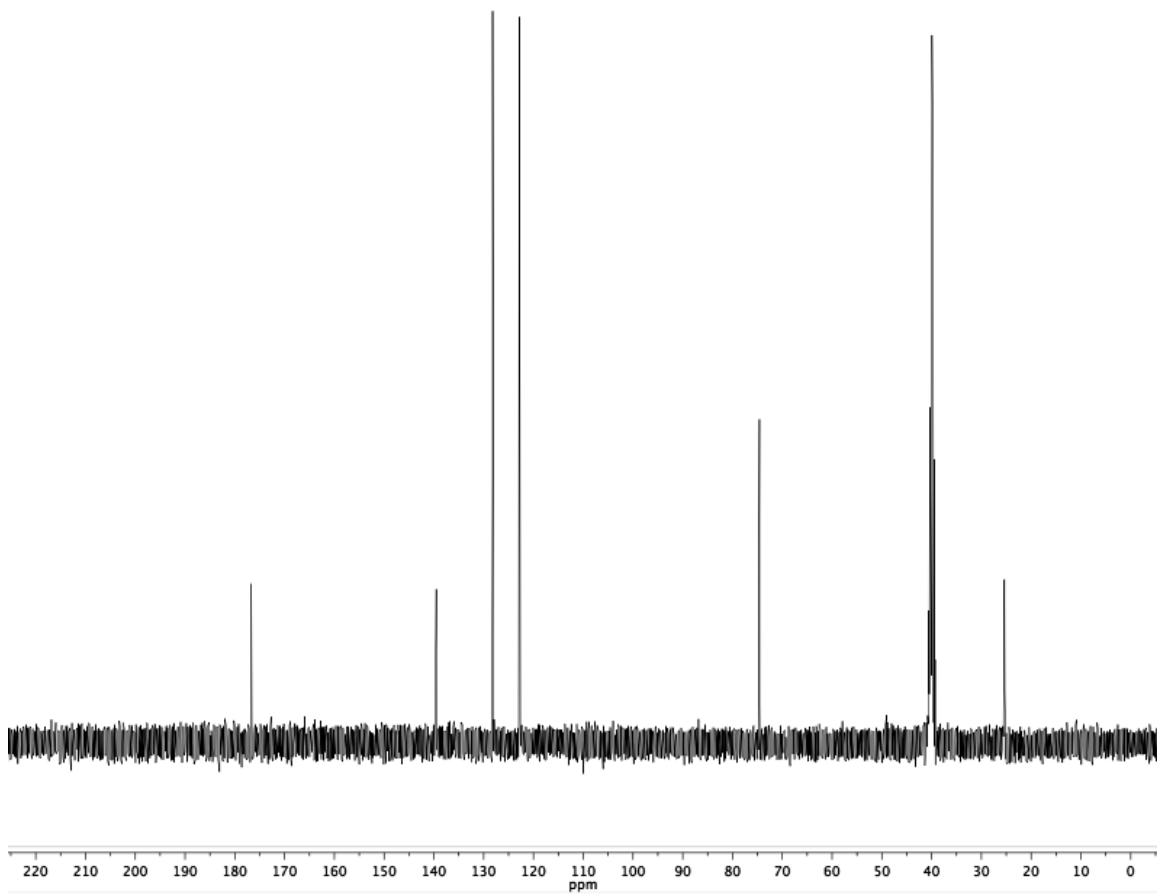
5-(hydroxymethyl)-5-methyl-2-phenyl-1,2,4-triazolidine-3-thione, 4.



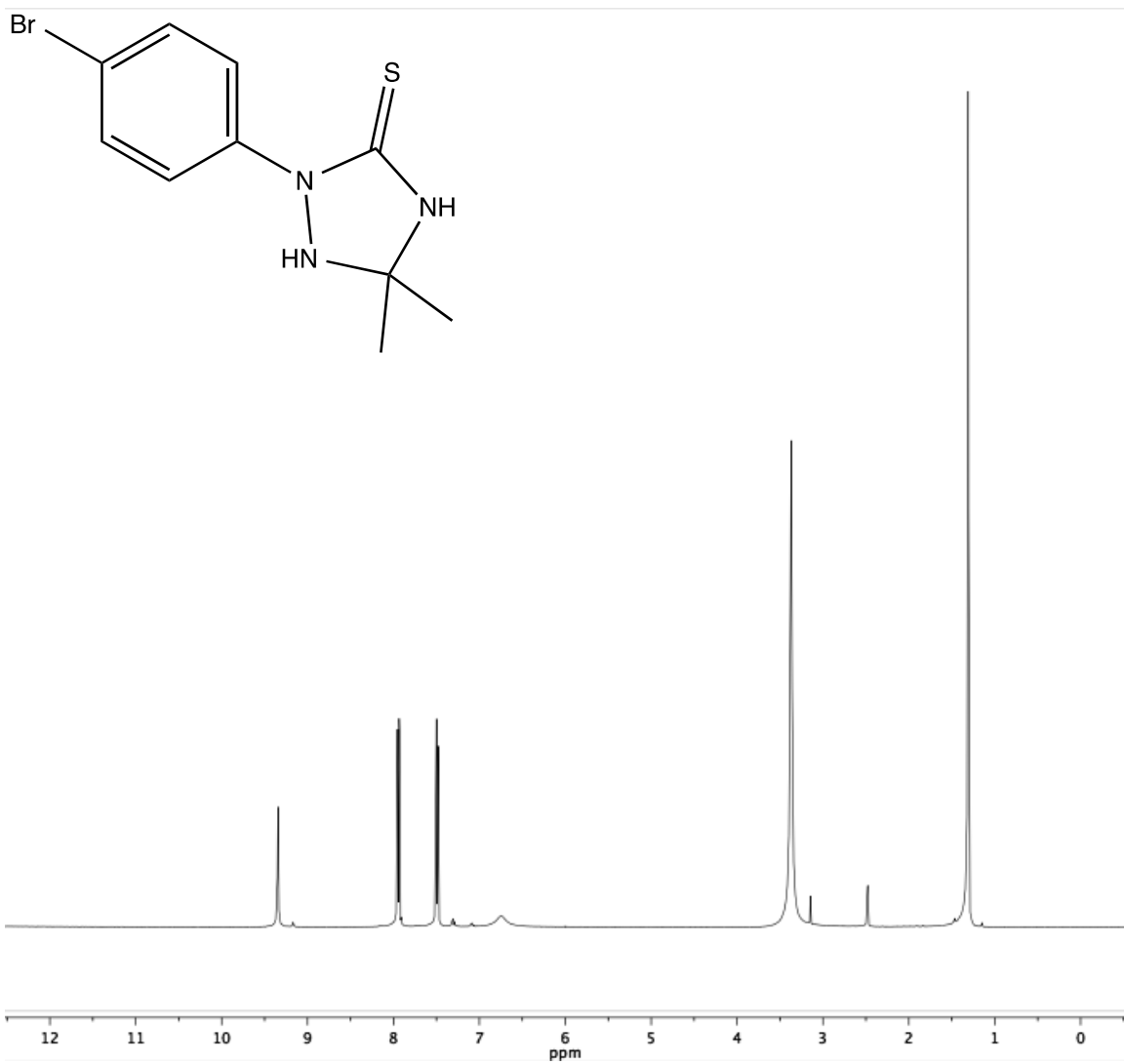


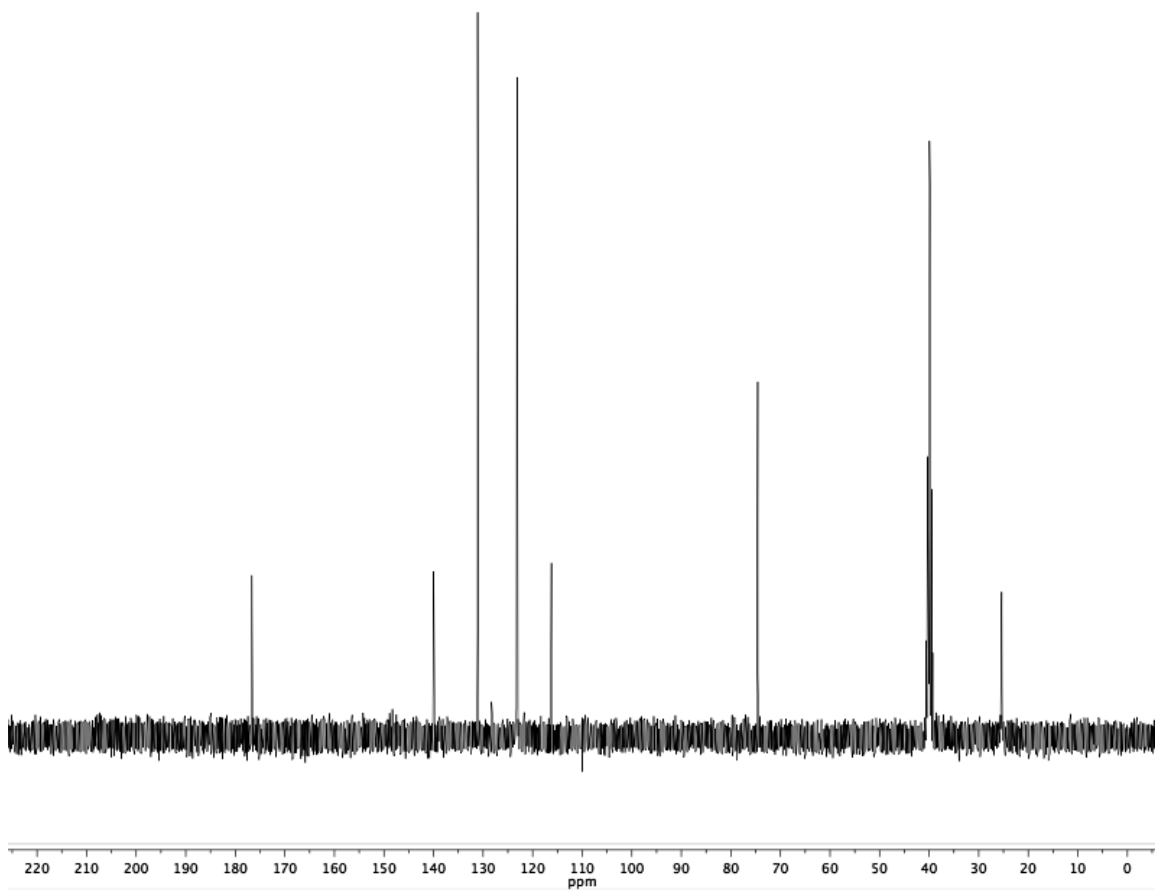
2-(4-chlorophenyl)-5,5-dimethyl-1,2,4-triazolidine-3-thione, 10.



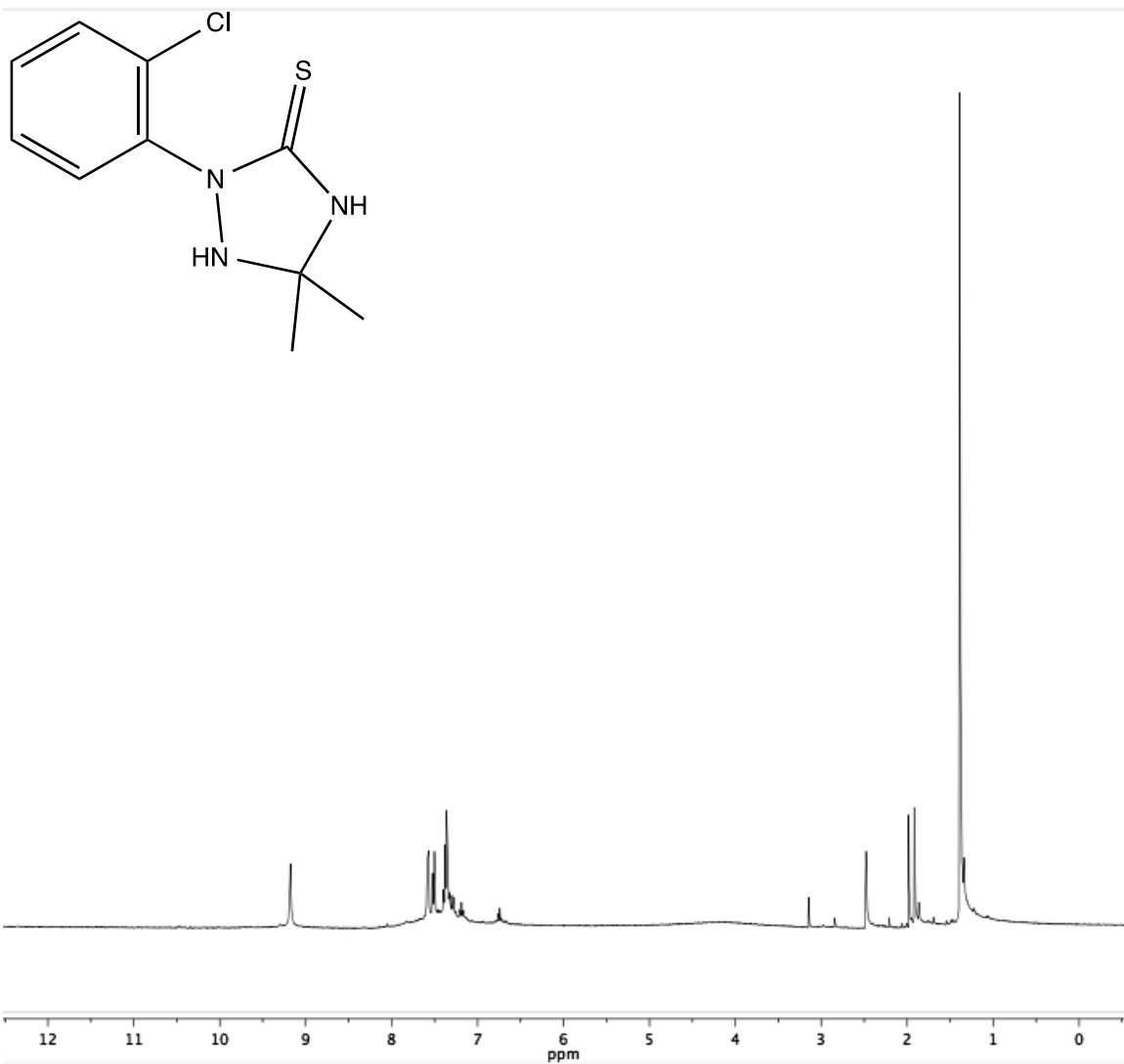


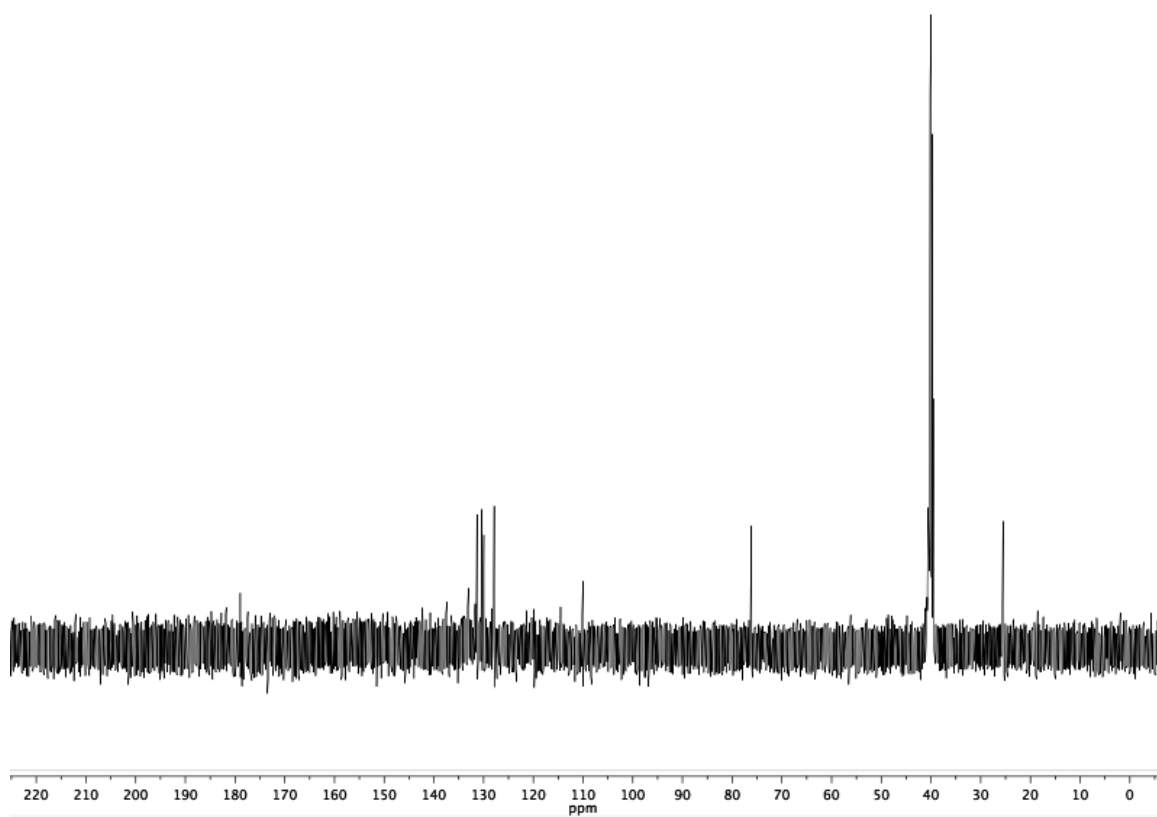
2-(4-bromophenyl)-5,5-dimethyl-1,2,4-triazolidine-3-thione, 15.





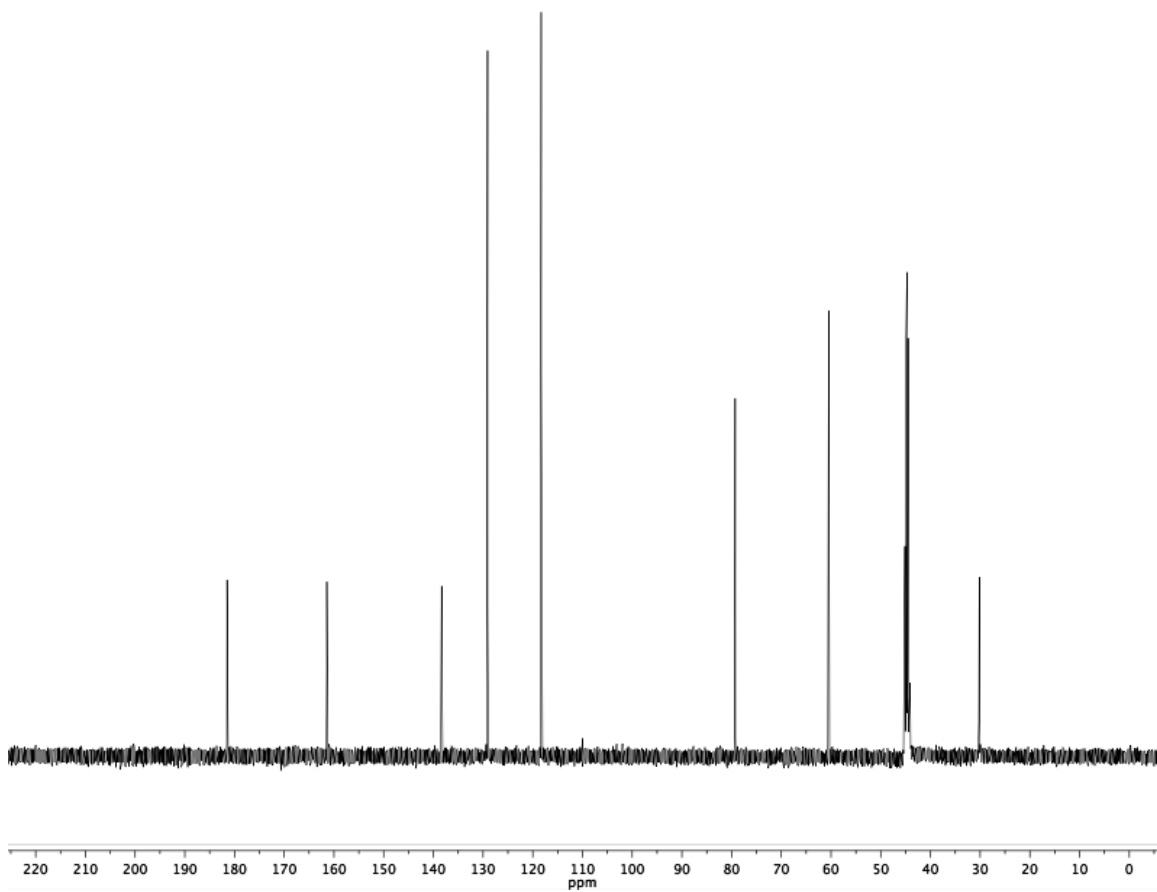
2-(2-chlorophenyl)-5,5-dimethyl-1,2,4-triazolidine-3-thione, 12.



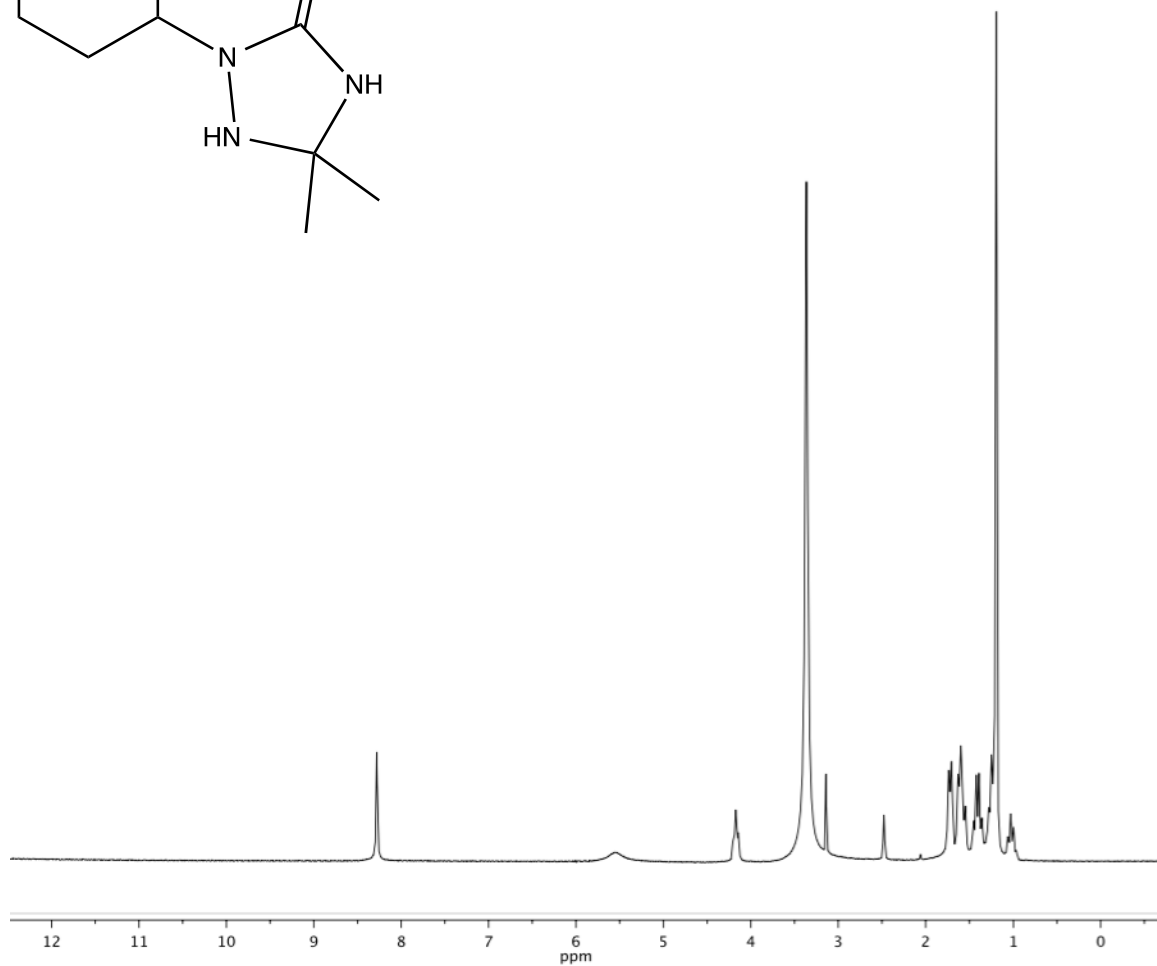
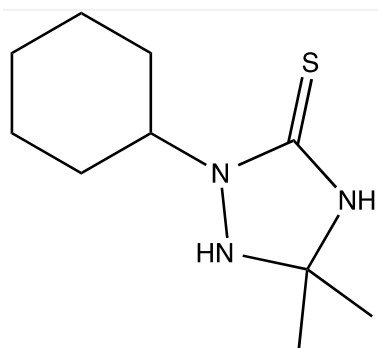


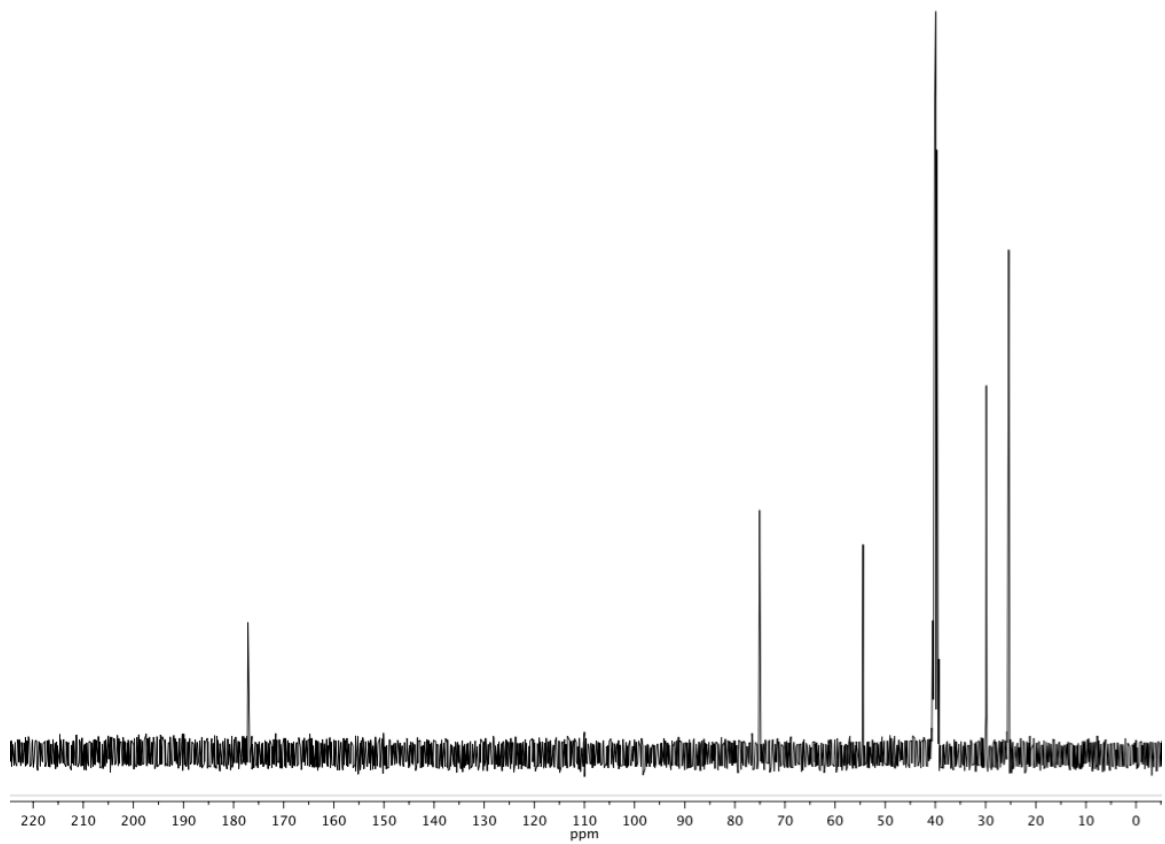
2-(4-methoxyphenyl)-5,5-dimethyl-1,2,4-triazoline-3-thione, 13.



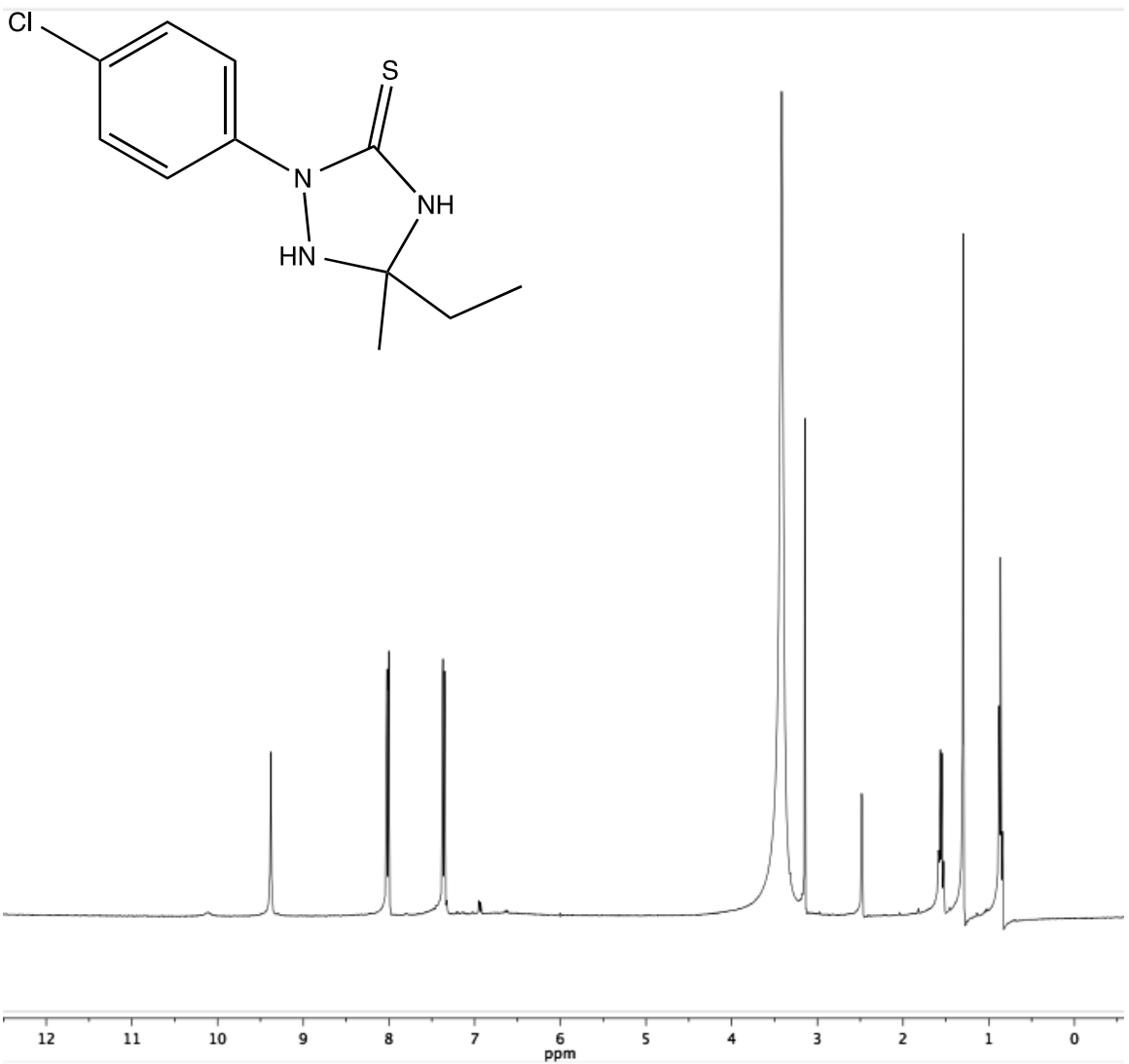


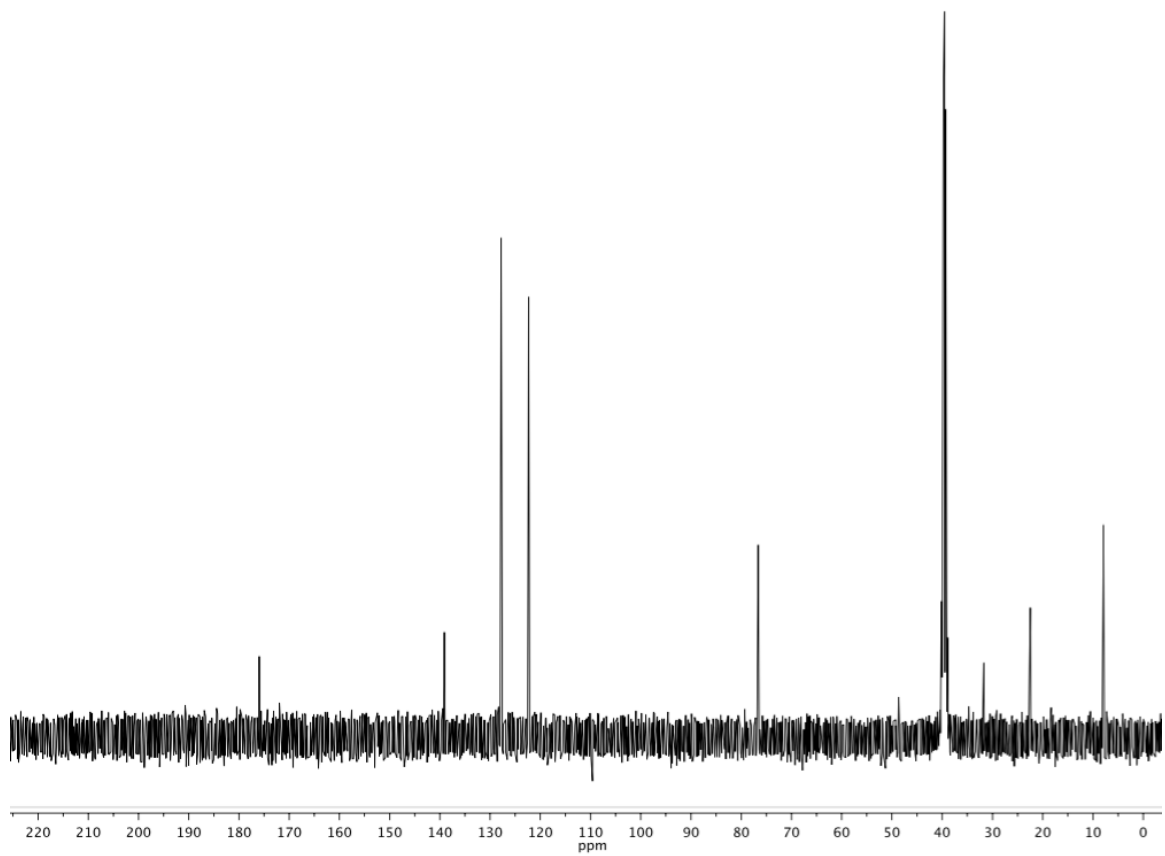
2-(4-cyclohexylphenyl)-5,5-dimethyl-1,2,4-triazolidine-3-thione, 16.



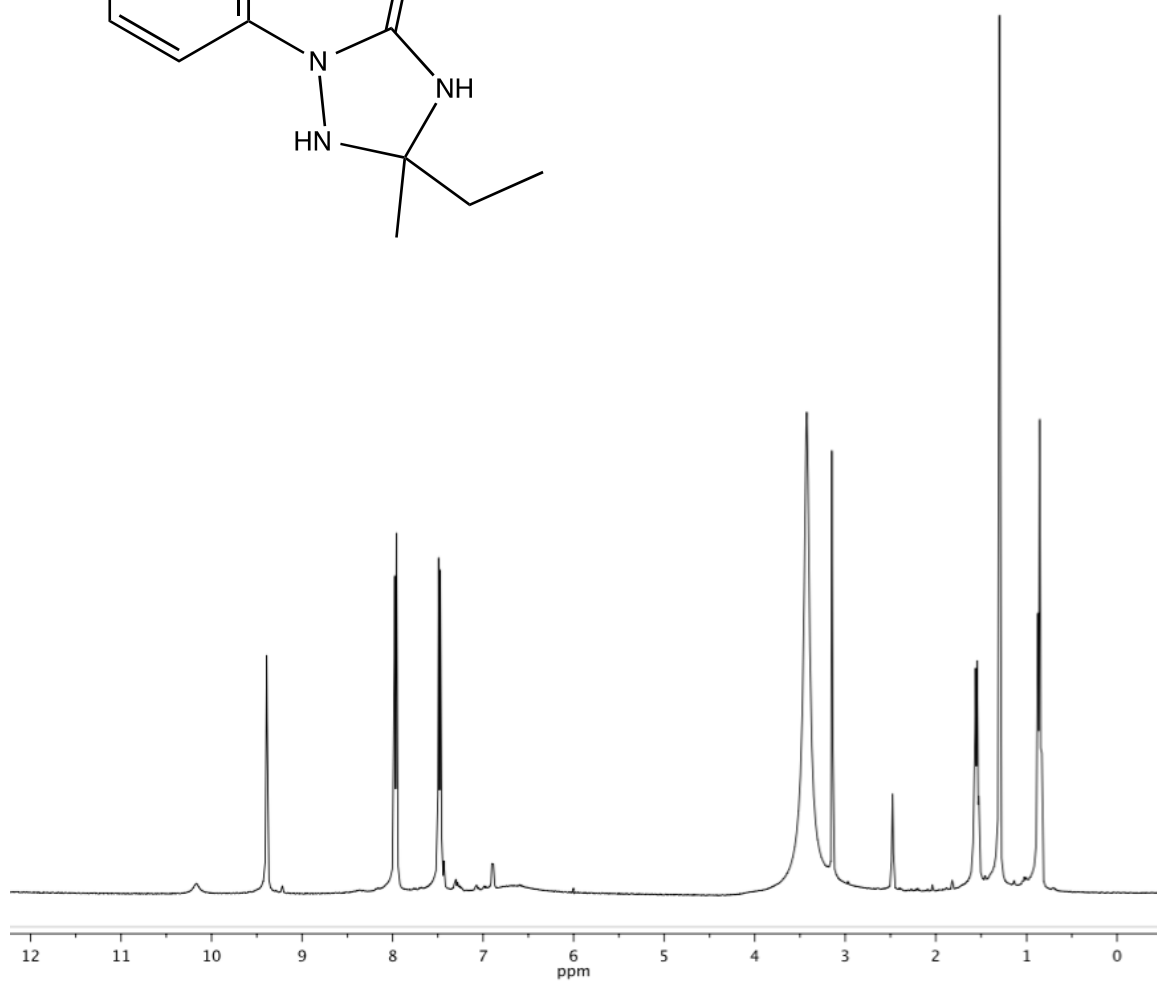
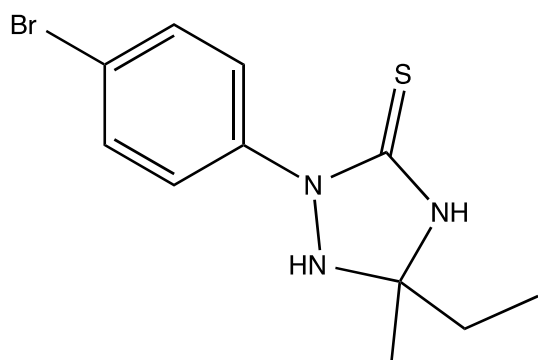


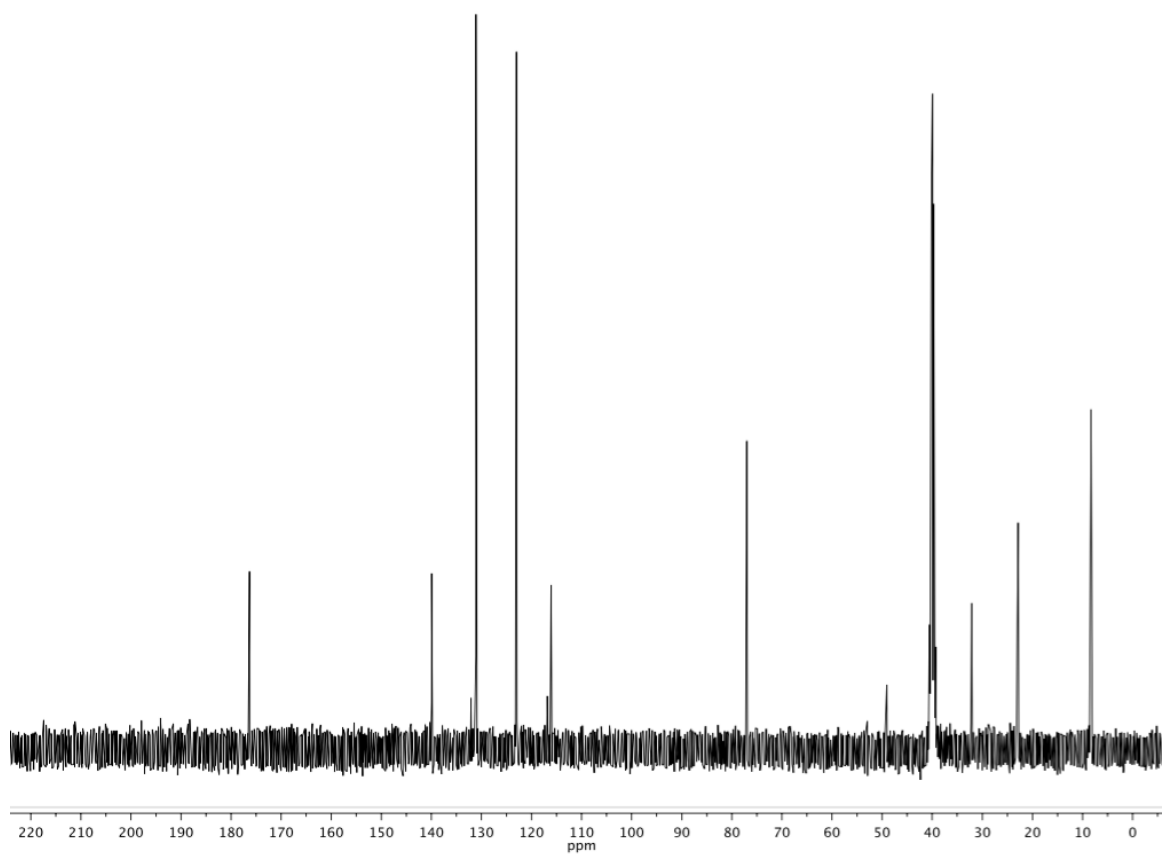
2-(4-chlorophenyl)-5-ethyl-5-methyl-1,2,4-triazolidine-3-thione, 17.



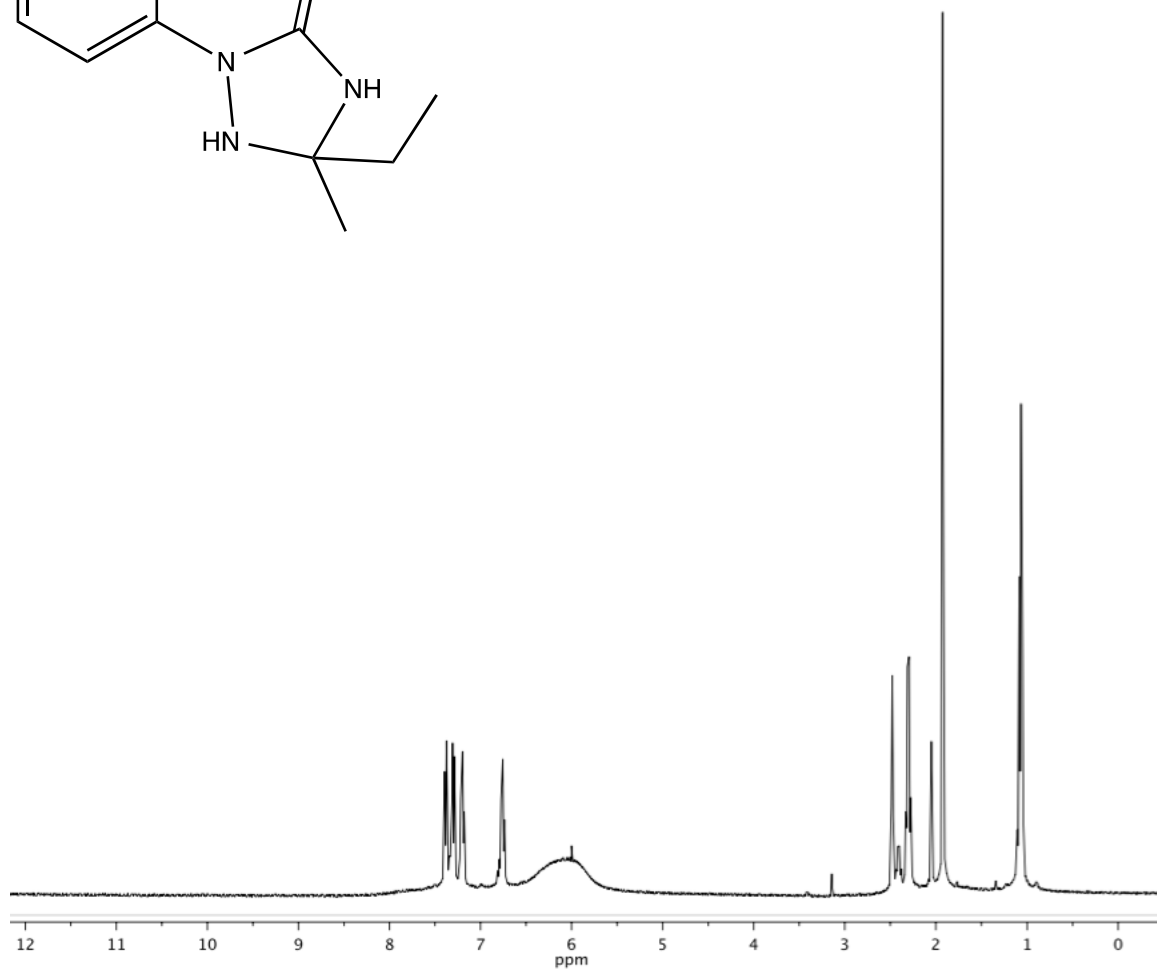
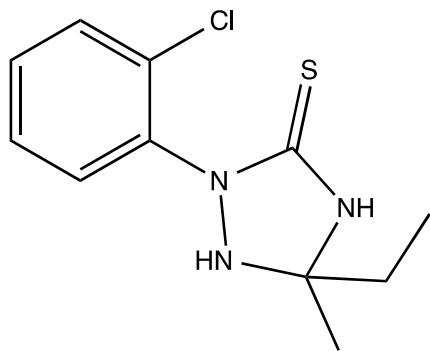


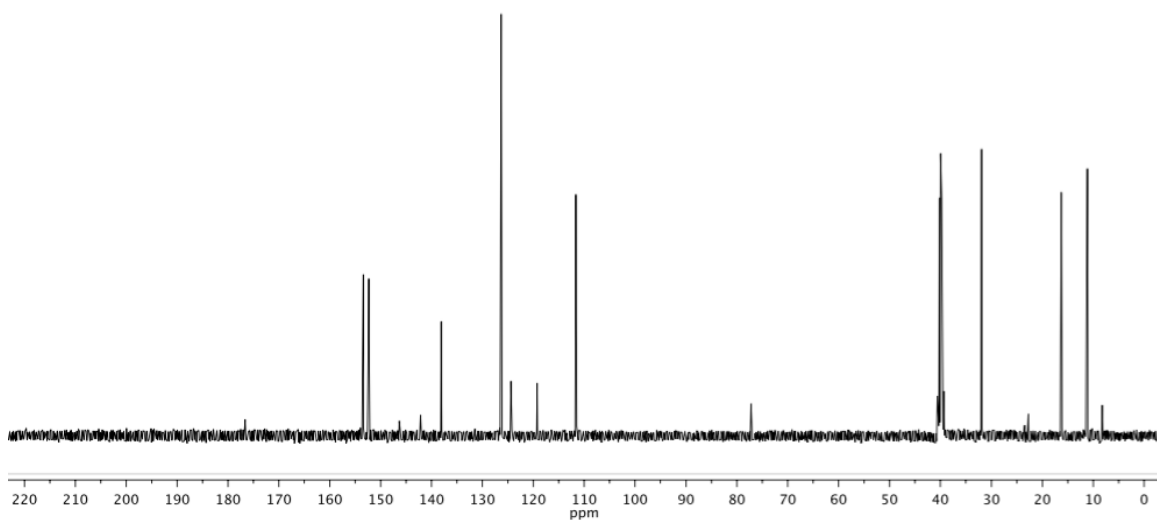
2-(4-bromophenyl)-5-ethyl-5-methyl-1,2,4-triazolidine-3-thione, 22.



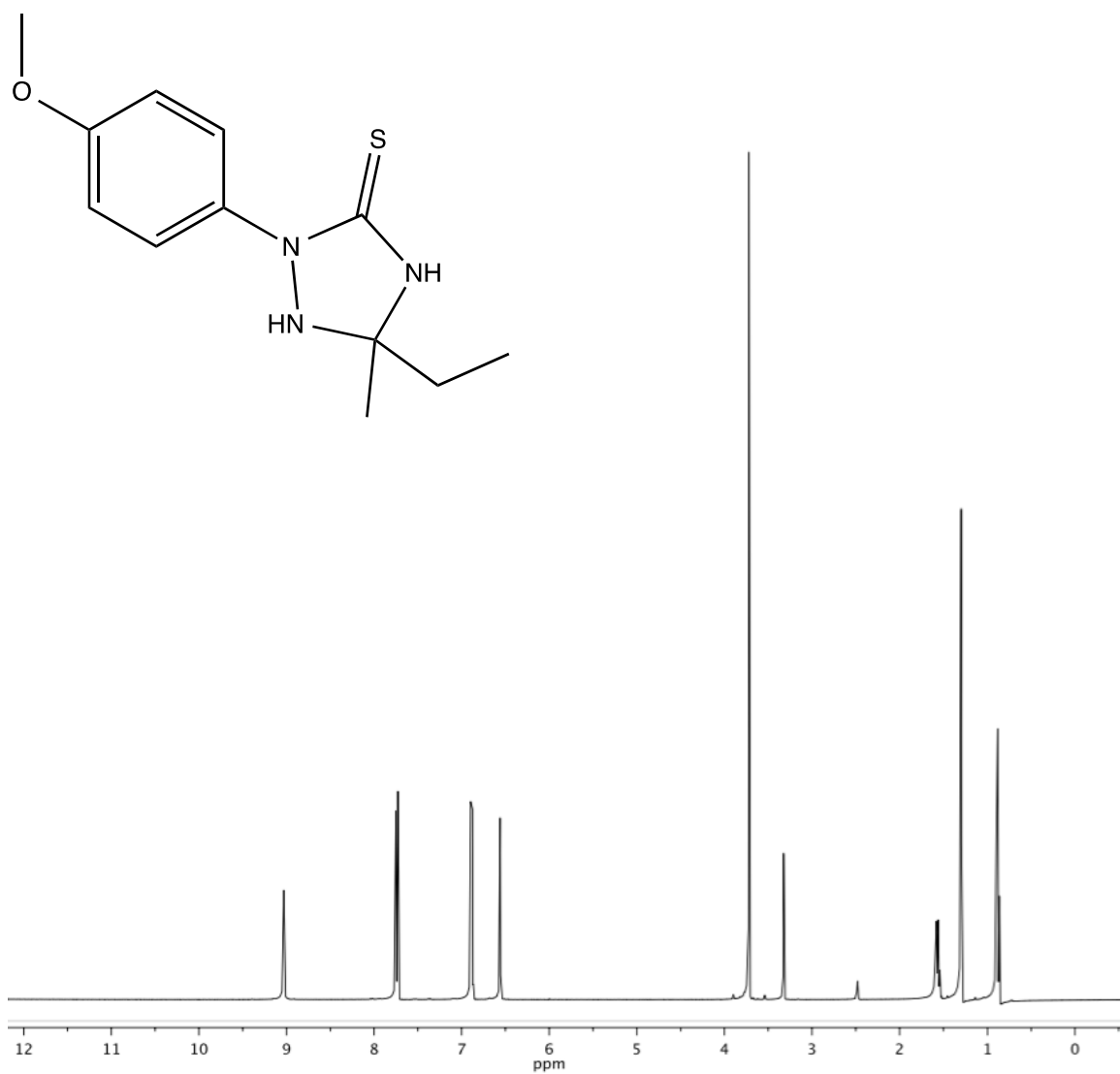


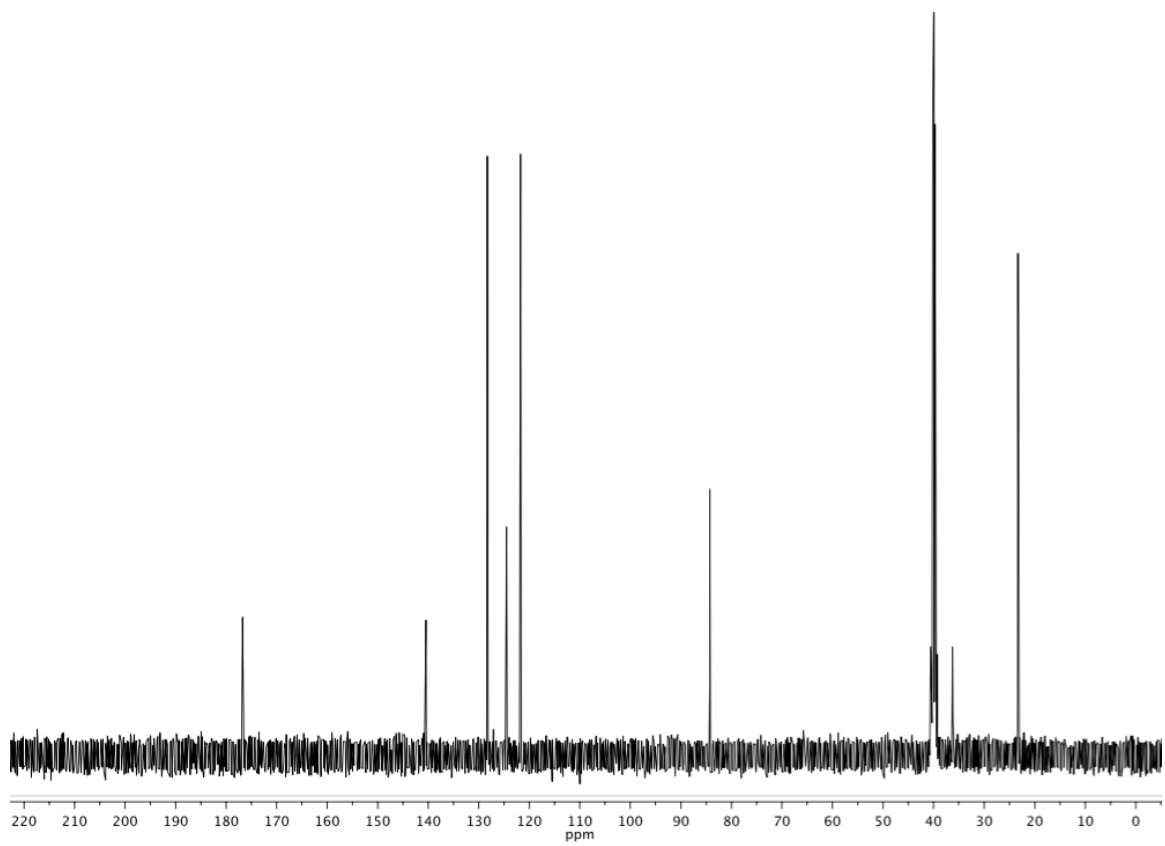
2-(2-chlorophenyl)-5-ethyl-5-methyl-1,2,4-triazolidine-3-thione, 19.



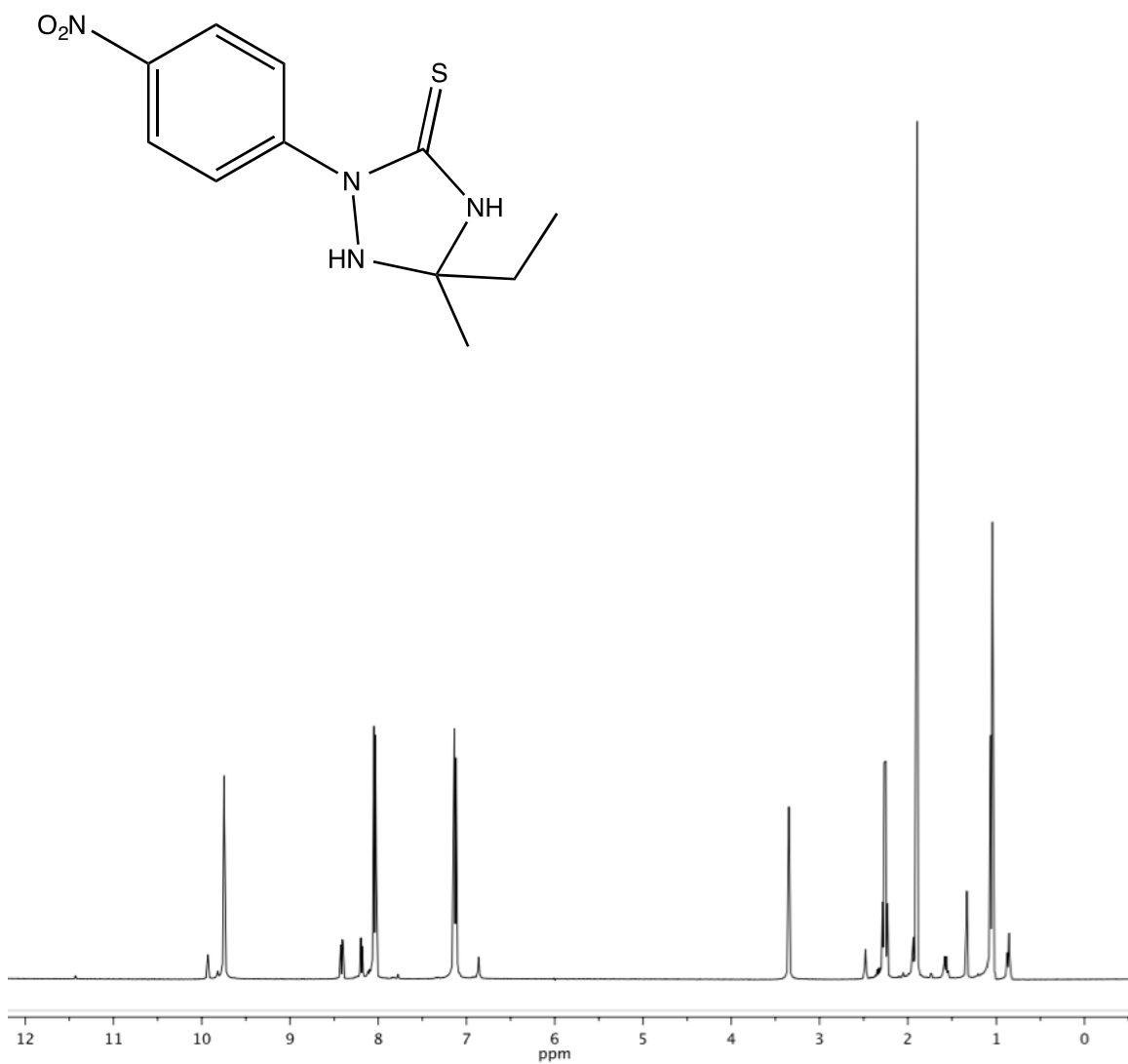


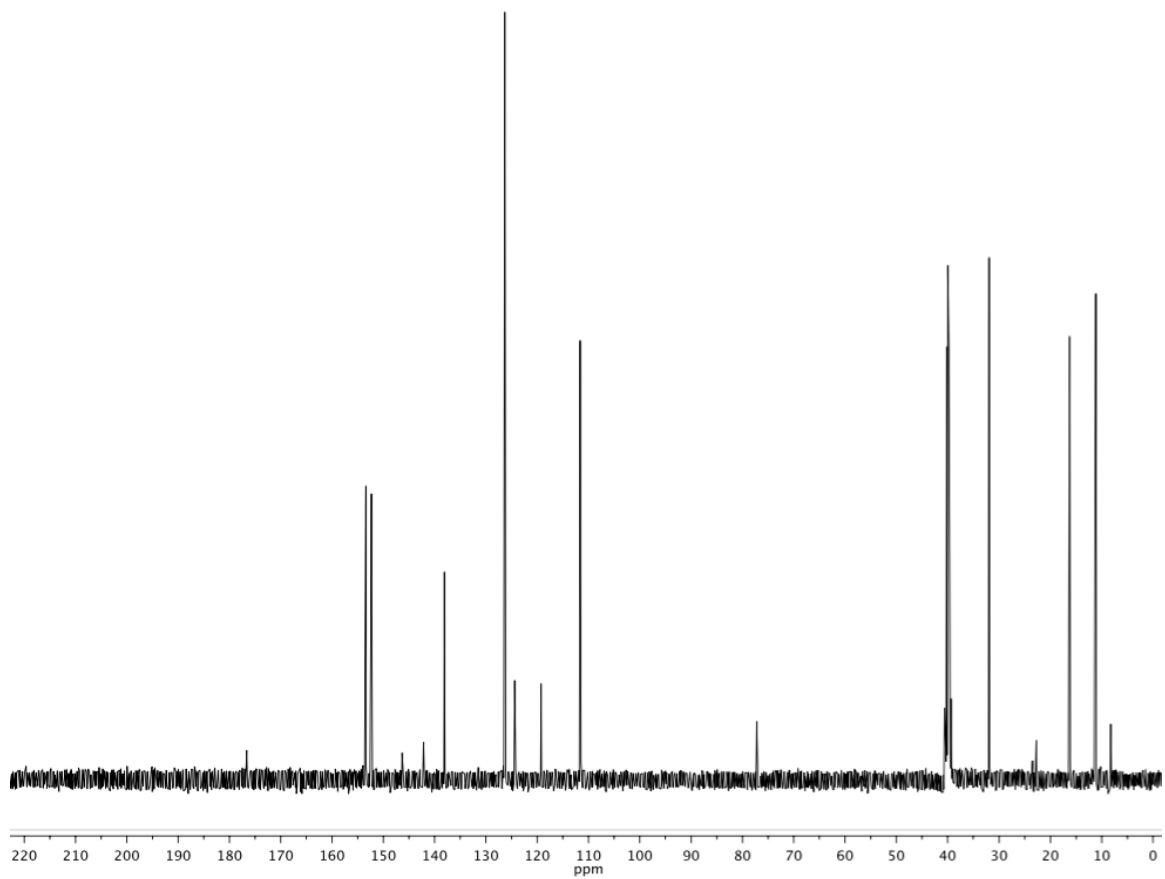
5-ethyl-2-(4-methoxyphenyl)-5-methyl-1,2,4-triazolidine-3-thione, 20.



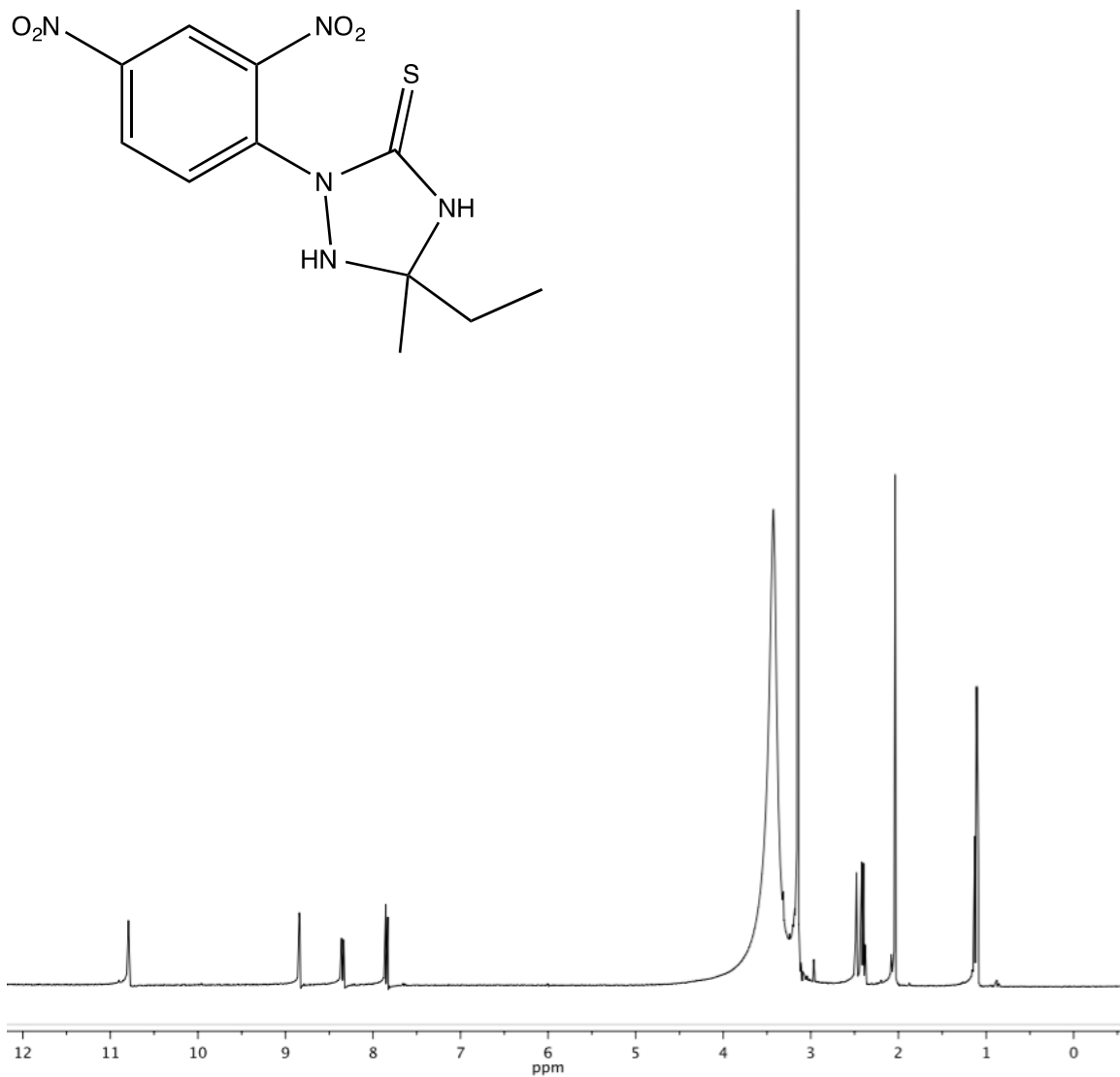


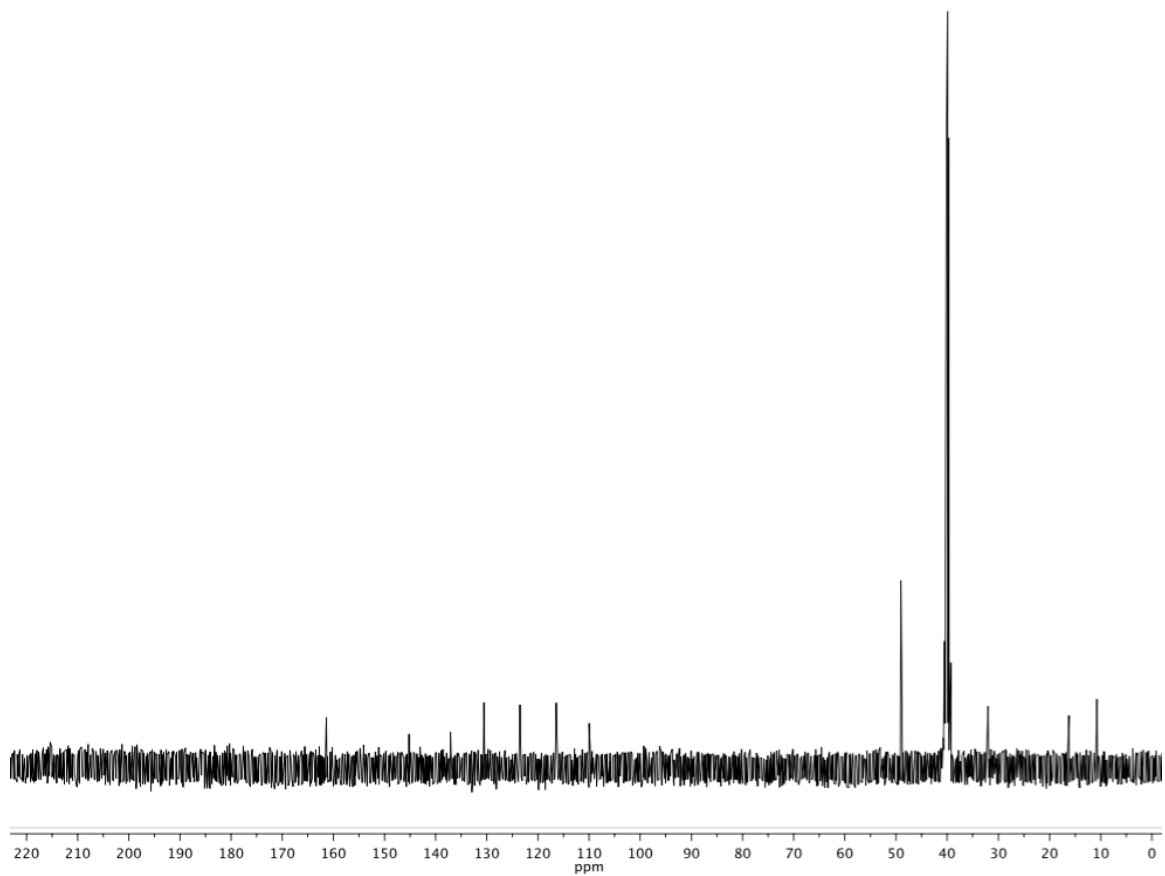
5-ethyl-5-methyl-2-(4-nitrophenyl)-1,2,4-triazolidine-3-thione, 23.



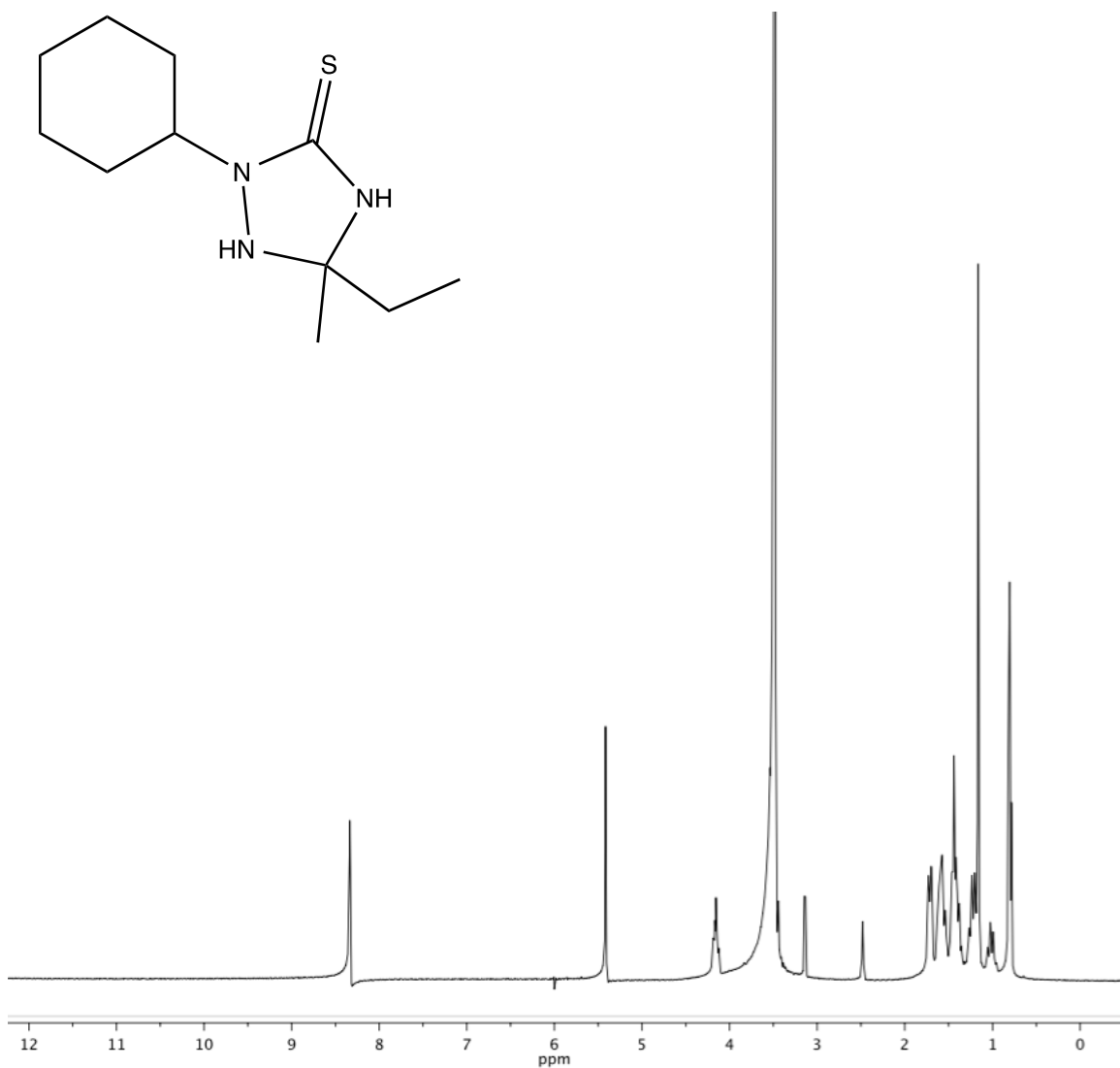
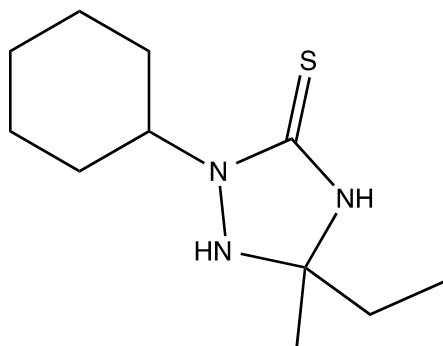


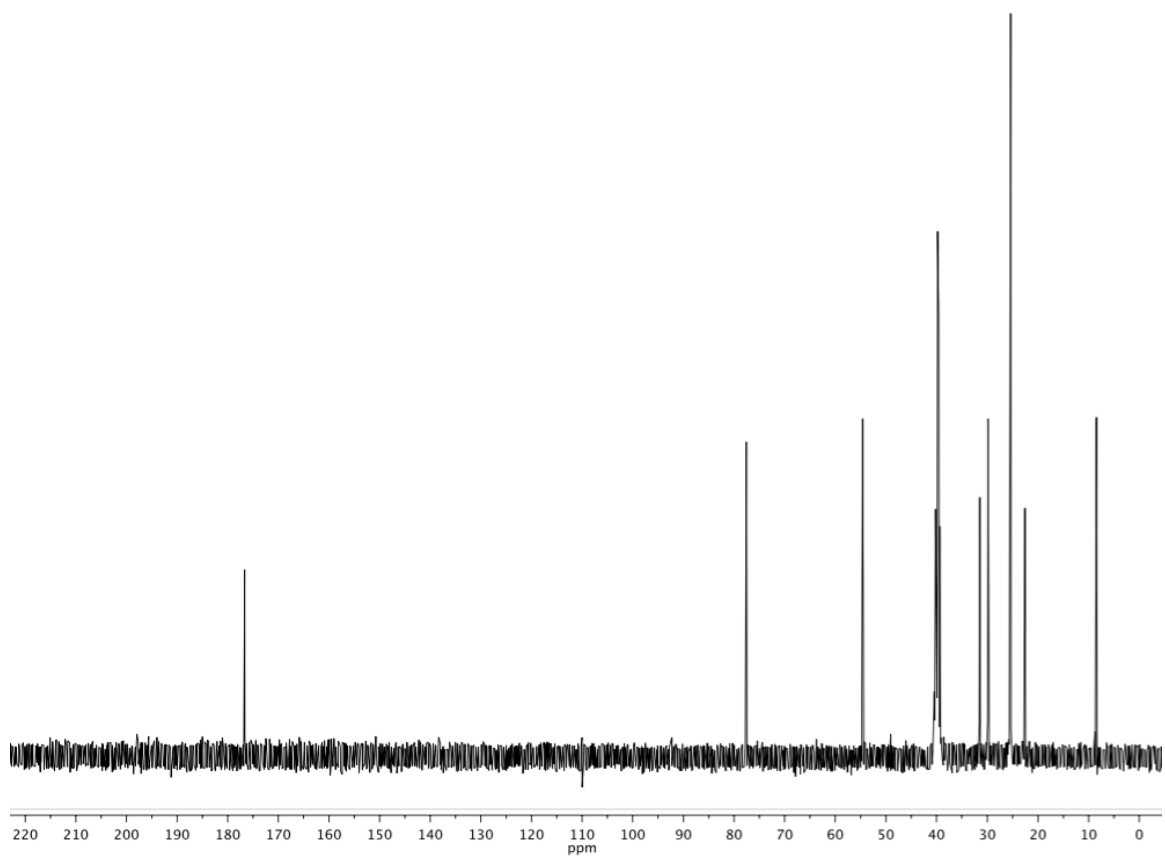
2-(2,4-dinitrophenyl)-5-ethyl-5-methyl-1,2,4-triazolidine-3-thione, 24.



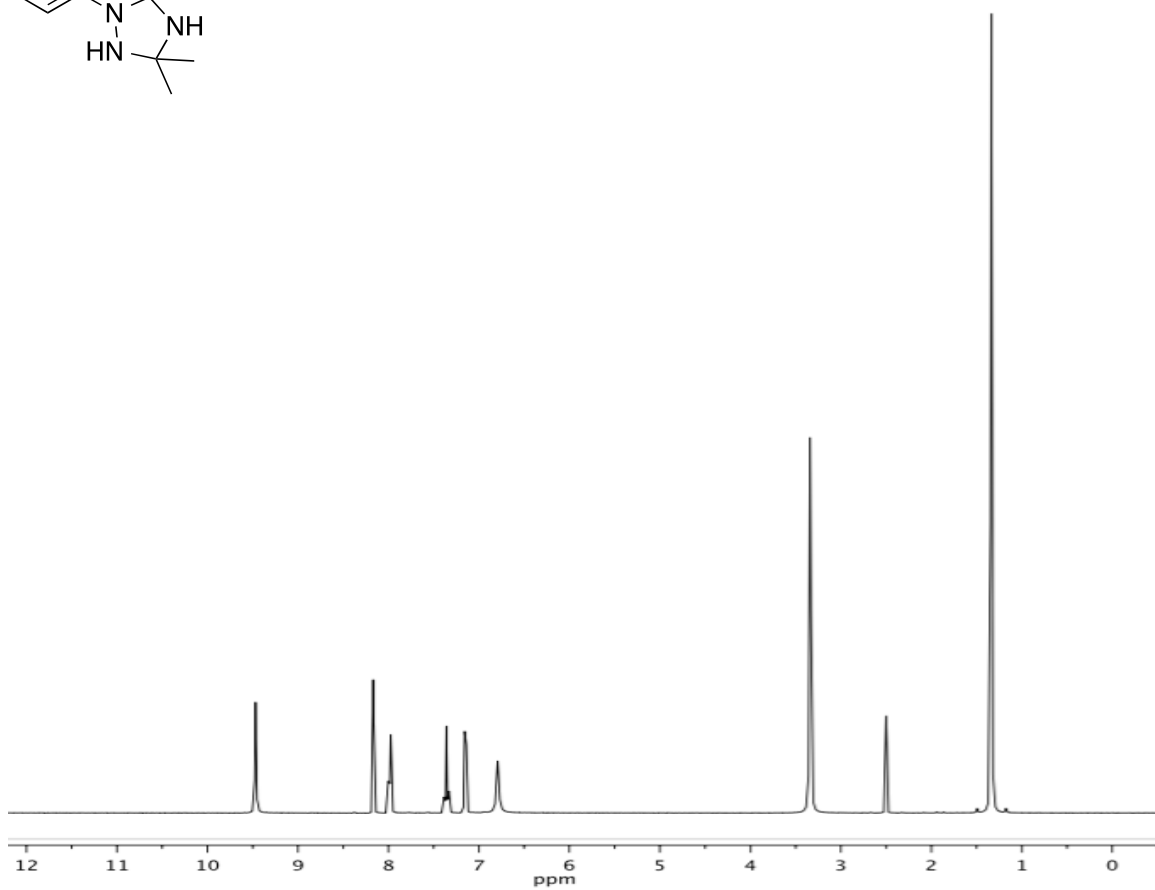
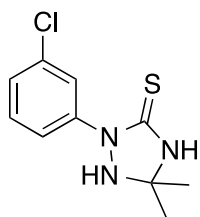


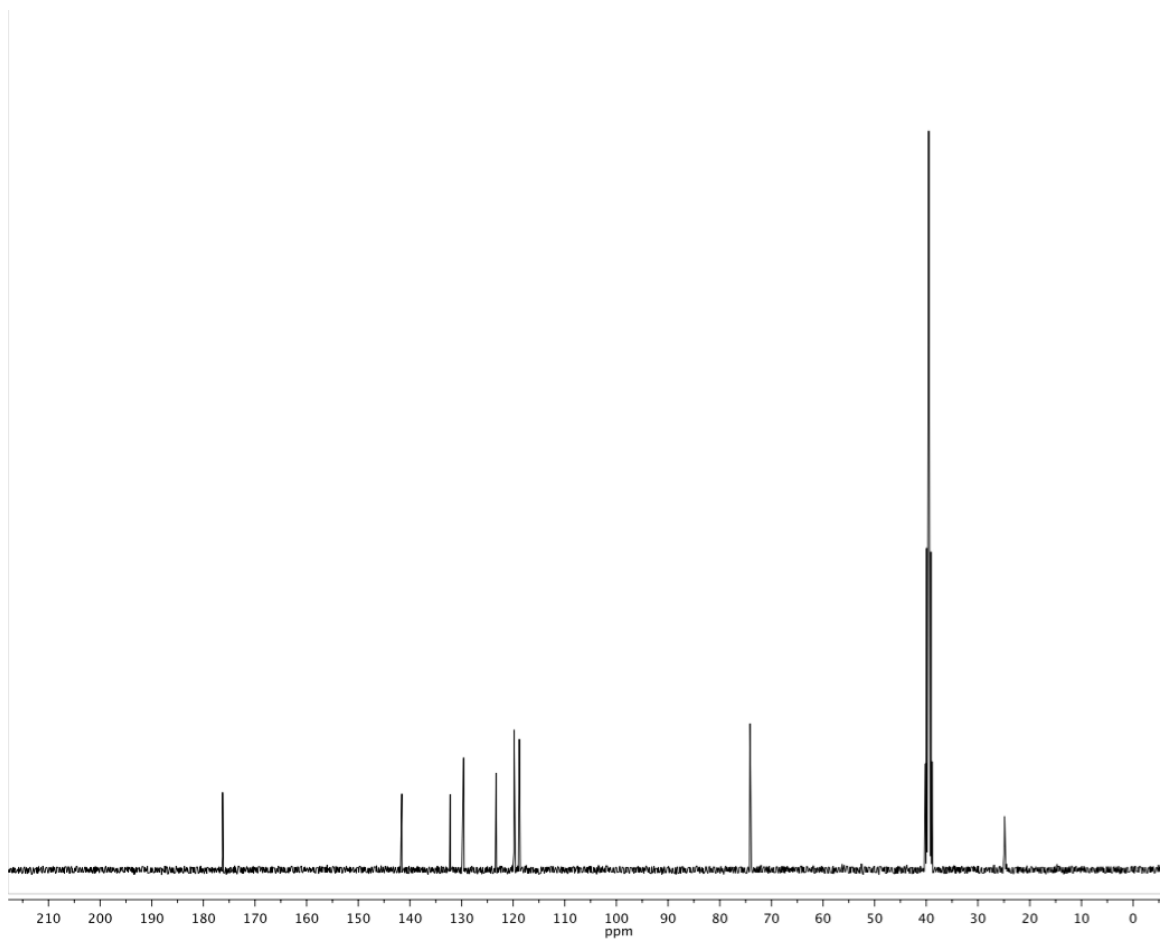
2-(4-cyclohexylphenyl)-5-ethyl-5-methyl-1,2,4-triazolidine-3-thione, 25.



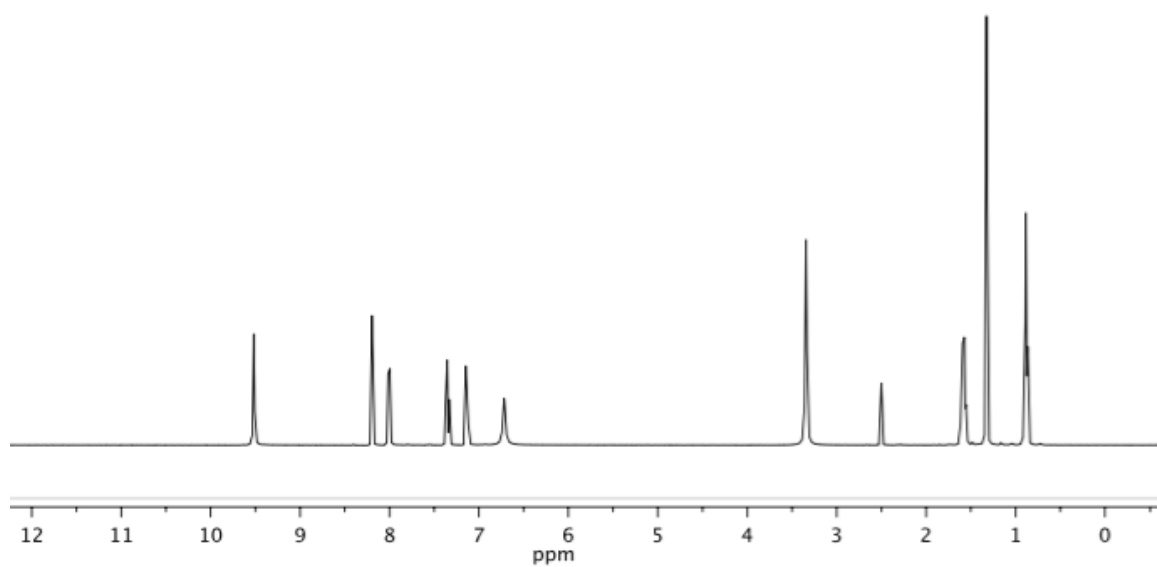
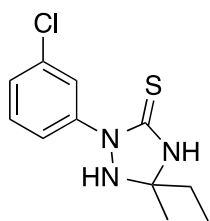


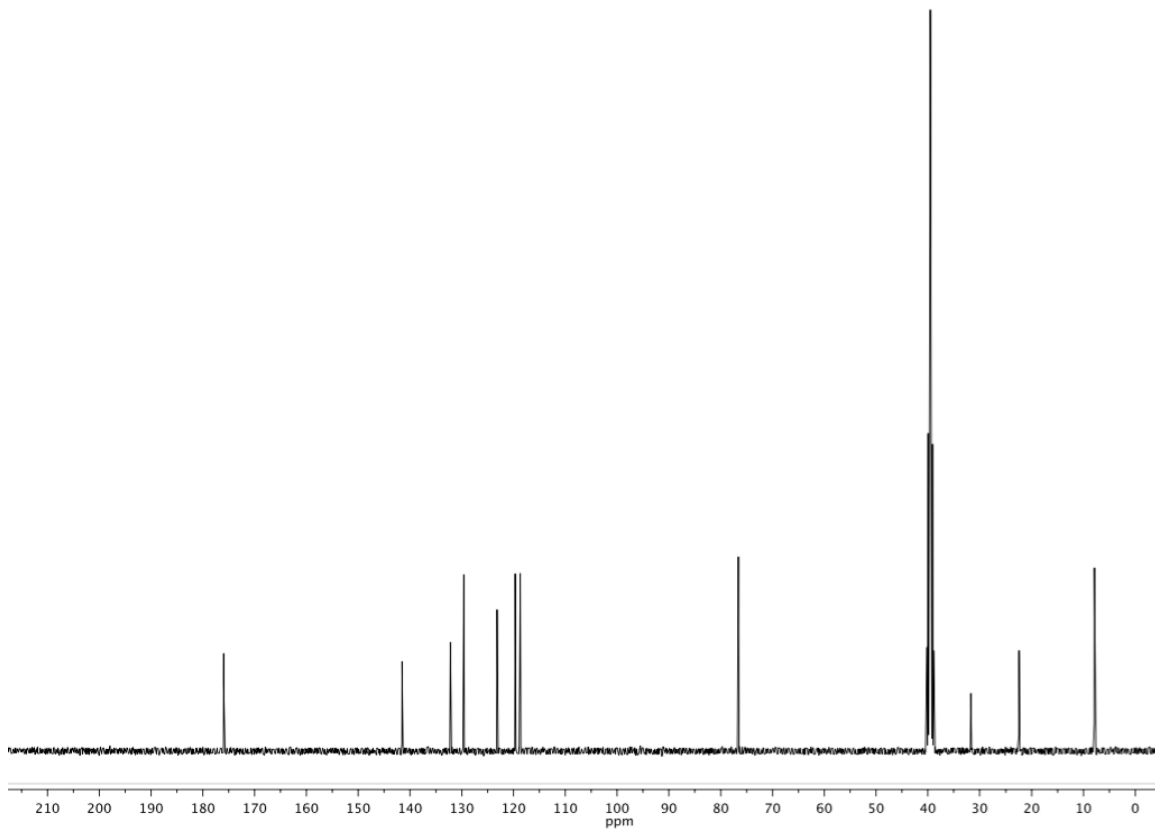
2-(3-chlorophenyl)-5,5-dimethyl-1,2,4-triazolidine-3-thione, 11.



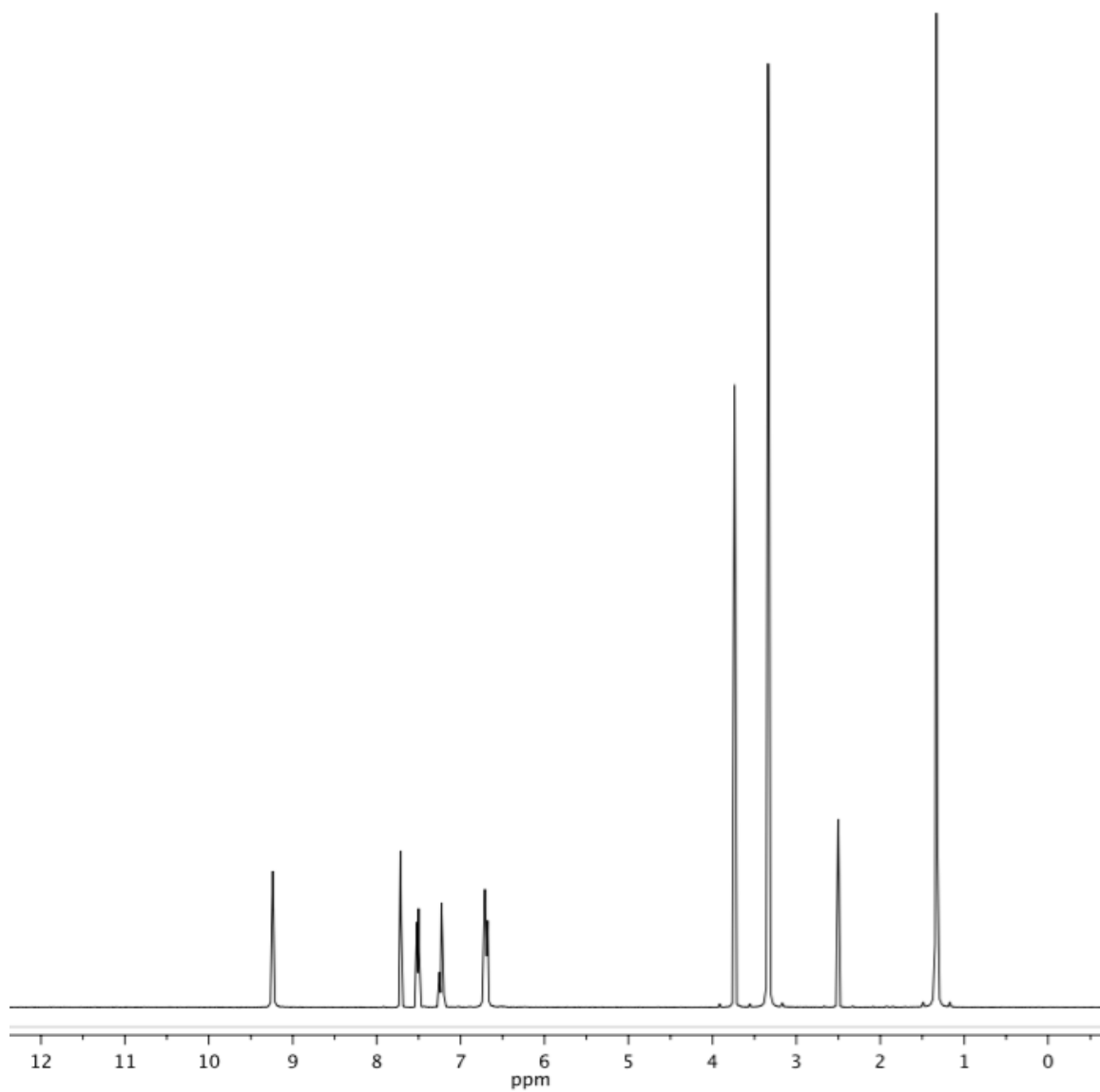
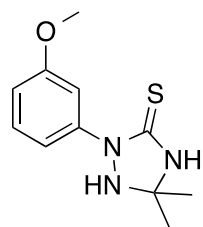


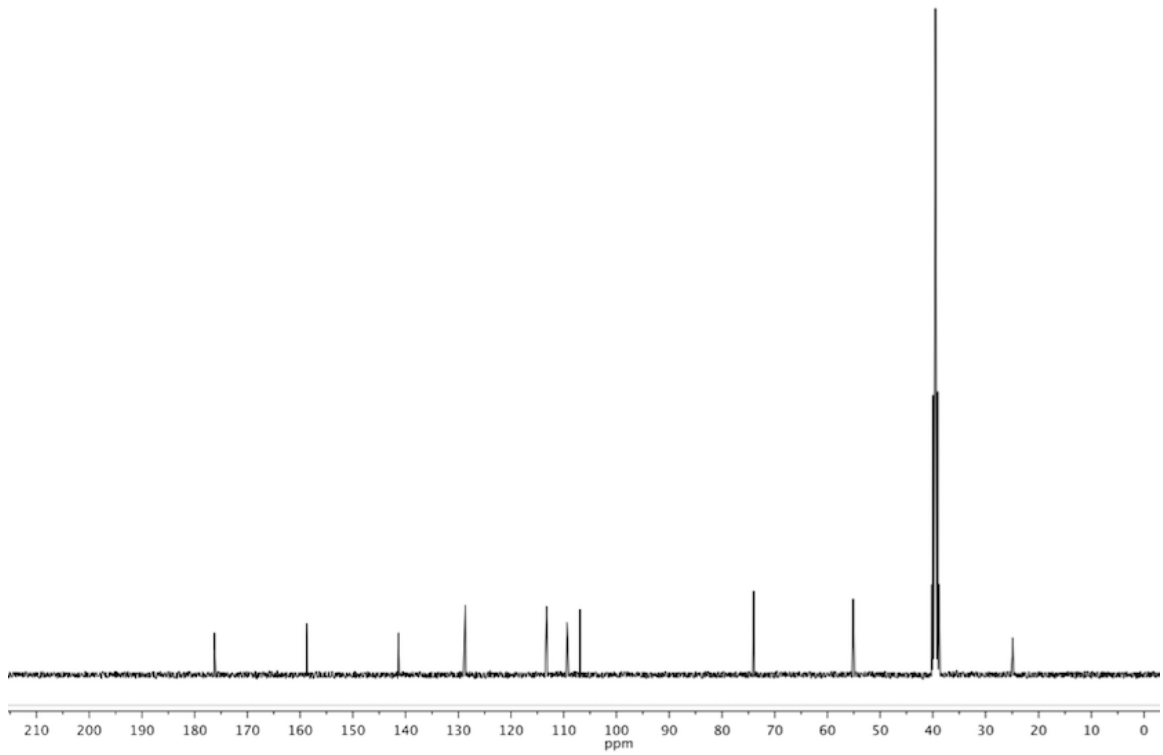
2-(3-chlorophenyl)-5-ethyl-5-methyl-1,2,4-triazolidine-3-thione, 18.



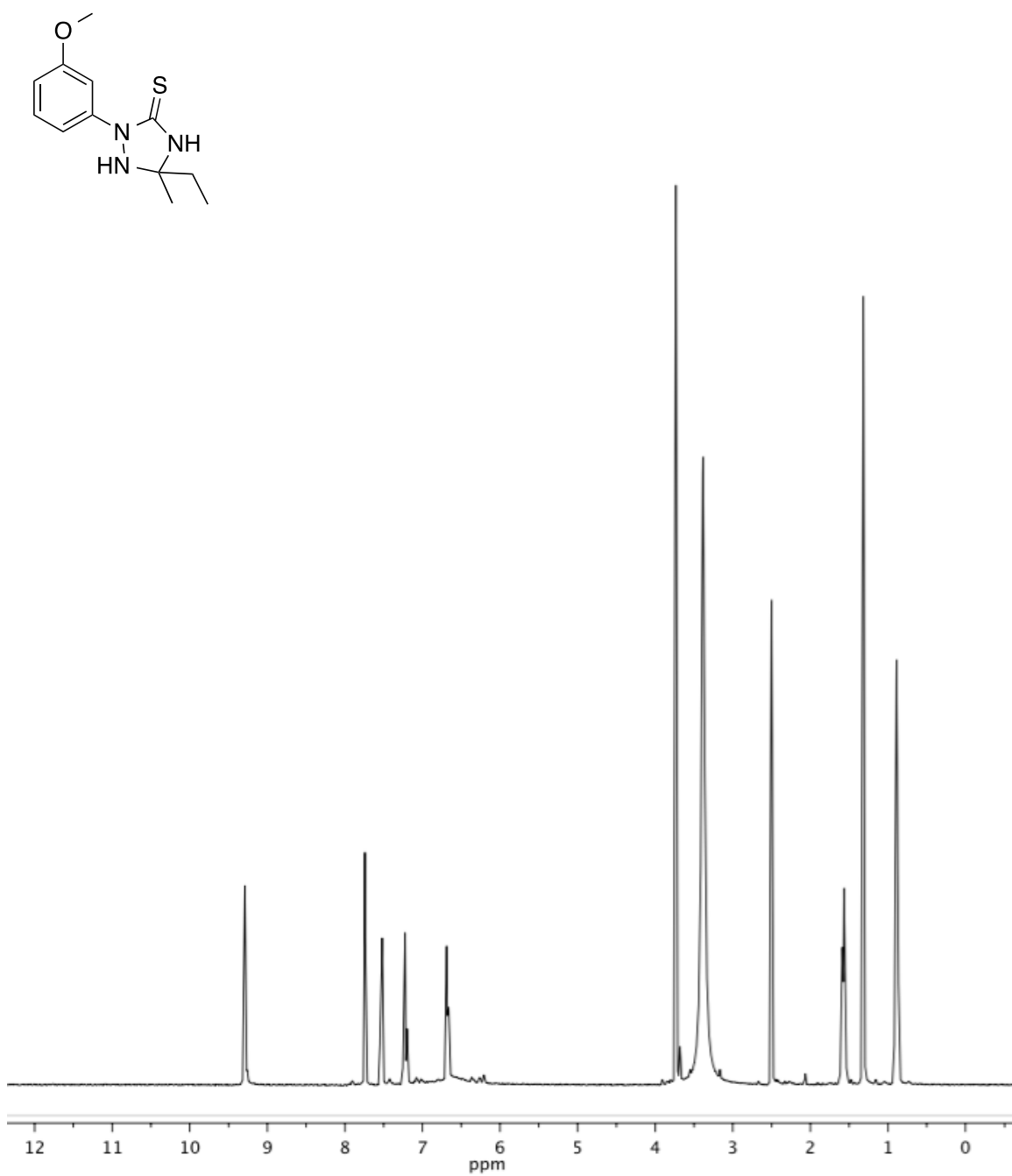


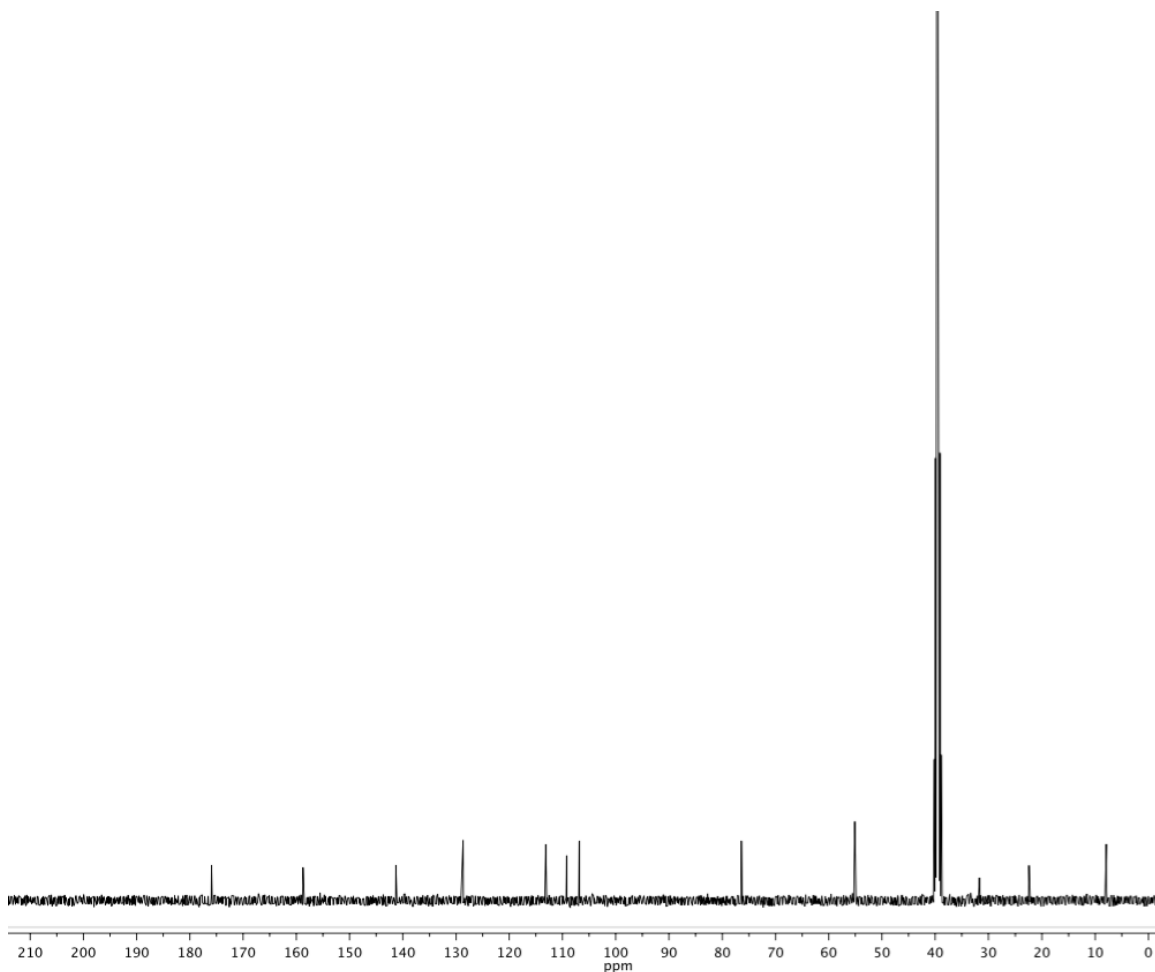
2-(3-methoxyphenyl)-5,5-dimethyl-1,2,4-triazolidine-3-thione, 14.





5-ethyl-2-(3-methoxyphenyl)-5-methyl-1,2,4-triazolidine-3-thione, 21.





Bioassay Procedure

Overnight cultures of *Pseudomonas aeruginosa* or *Staphylococcus aureus* were prepared by inoculating 5mL of LB broth from freezer stocks stored at -80° C that consisted of 40% glycerol. The cultures were prepared in sterile 14mL culture tubes and placed in a shaking incubator at 30° C and 120 rpm's for 24 hrs with the lids in the open position. Following overnight incubation, each culture was diluted 40:1 in LB broth and vortexed. The diluted overnight cultures were then dispensed into clear bottom 96-well microplates at a volume of 150µL per well. The first row then received an additional

30 μ L of the diluted overnight culture, and 20 μ L of 20mg/mL of each compound dissolved in DMSO. This step yielded a final volume of 200 μ L with a 2mg/mL concentration of each compound throughout the first row of the plate in order to prepare for a serial dilution. A 4:1 serial dilution was then performed using a 12-channel micropipette by removing 50 μ L of the first row and dispensing into the 150 μ L of diluted overnight culture in the row below. The wells were then thoroughly mixed and this step was repeated from rows A through G. 50 μ L of the culture were then removed from row G following the dilution in order to maintain a consistent volume of 150 μ L per well. Row H of the 96 well plate was used for a control and a blank. Wells H1 through H6 were subject to the same 4:1 serial dilution as mentioned above using 20 μ L of DMSO without any compound. Wells H7 through H12 were used as blanks containing only 150 μ L of the diluted overnight culture. 50 μ L of mineral oil were then dispensed into each of the 96 wells to yield a final volume of 200 μ L and to prevent evaporation of the LB broth during the following 24 hour incubation. The 96 well plate was then placed into a Molecular Devices Spectramax i3x multimode microplate reader. The plate reader was set to 37°C and recorded the absorption of each well at 420 nm at 15 minute intervals for 24 hours. The plate was subject to shaking at 120 rpm for 15 minutes in between each absorption reading. The values obtained were used to generate growth curves of each well to investigate antimicrobial activity of each compound and analyzed using Prism Graphpad software. Samples were run in duplicate by using two rows on the same plate for each compound and averaging the absorption values.

References

1. Lesic, B.; Lépine, F.; Déziel, E.; Zhang, J.; Zhang, Q.; Padfield, K.; Castonguay, M.-H.; Milot, S.; Stachel, S.; Tzika, A. A.; Tompkins, R. G.; Rahme, L. G. *PLoS Pathog.* **2007**, *3*, 1229–1239.
2. Rasmussen, T. B.; Givskov, M. *Int. J. Med. Microbiol.* **2006**, *296*, 149–161.
3. Lyon, G. J.; Muir, T. W. *Chemistry & Biology* **2003**, *10*, 1007–1021.
4. Manefield, M.; de Nys, R.; Kumar, N.; Read, R.; Givskov, M.; Steinberg, P.; Kjelleberg, S. *Microbiology (Reading, Engl.)* **1999**, *145* (Pt 2), 283–291.
5. Müh, U.; Hare, B. J.; Duerkop, B. A.; Schuster, M.; Hanzelka, B. L.; Heim, R.; Olson, E. R.; Greenberg, E. P. *Proc. Natl. Acad. Sci. U.S.A.* **2006**, *103*, 16948–16952.
6. Müh, U.; Schuster, M.; Heim, R.; Singh, A.; Olson, E. R.; Greenberg, E. P. *Antimicrobial Agents and Chemotherapy* **2006**, *50*, 3674–3679.
7. Geske, G. D.; O’Neill, J. C.; Miller, D. M.; Wezeman, R. J.; Mattmann, M. E.; Lin, Q.; Blackwell, H. E. *ChemBioChem* **2008**, *9*, 389–400.
8. Geske, G. D.; O’Neill, J. C.; Miller, D. M.; Mattmann, M. E.; Blackwell, H. E. *J. Am. Chem. Soc.* **2007**, *129*, 13613–13625.
9. Mattmann, M. E.; Blackwell, H. E. *J. Org. Chem.* **2010**, *75*, 6737–6746.
10. Moore, J. D.; Rossi, F. M.; Welsh, M. A.; Nyffeler, K. E.; Blackwell, H. E. *J. Am. Chem. Soc.* **2015**, *137*, 14626–14639.

11. Lambert, P. A. *Journal of the Royal Society of Medicine* **2002**, *95*, 22.
12. Kollef, M. H.; Golan, Y.; Micek, S. T.; Shorr, A. F.; Restrepo, M. I. *CLIN INFECT DIS* **2011**, *53*, S33–S55.
13. Defoirdt, T.; Boon, N.; Bossier, P. *PLoS Pathog.* **2010**, *6*, e1000989.
14. Khmel, I. A.; Metlitskaya, A. Z. *Mol Biol* **2006**, *40*, 169–182.
15. Clatworthy, A. E.; Pierson, E.; Hung, D. T. *Nat Chem Biol* **2007**, *3*, 541–548.
16. Rasko, D. A.; Sperandio, V. *Nature Reviews Drug Discovery* **2010**, *9*, 117–128.
17. Hentzer, M.; Wu, H.; Andersen, J. B.; Riedel, K.; Rasmussen, T. B.; Bagge, N.; Kumar, N.; Schembri, M. A.; Song, Z.; Kristoffersen, P.; Manfield, M.; Costerton, J. W.; Molin, S.; Eberl, L.; Steinberg, P.; Kjelleberg, S.; Høiby, N.; Givskov, M. *EMBO J.* **2003**, *22*, 3803–3815.
18. O'Reilly, M. C.; Blackwell, H. E. *ACS Infect Dis* **2016**, *2*, 32–38.
19. Zakhari, J. S.; Kinoyama, I.; Struss, A. K.; Pullanikat, P.; Lowery, C. A.; Lardy, M.; Janda, K. D. *J. Am. Chem. Soc.* **2011**, *133*, 3840–3842.
20. Zou, Y.; Nair, S. K. *Chemistry & Biology* **2009**, *16*, 961–970.
21. Meanwell, N. A. *J. Med. Chem.* **2011**, *54*, 2529–2591.
22. O'Brien, K. T.; Noto, J. G.; Nichols-O'Neill, L.; Perez, L. J. *ACS Med Chem Lett* **2015**, *6*, 162–167.

23. O'Loughlin, C. T.; Miller, L. C.; Siryaporn, A.; Drescher, K.; Semmelhack, M. F.; Bassler, B. L. *Proc. Natl. Acad. Sci. U.S.A.* **2013**, *110*, 17981–17986.
24. Sastry, G. M.; Adzhigirey, M.; Day, T.; Annabhimoju, R.; Sherman, W. J. *Comput. Aided Mol. Des.* **2013**, *27*, 221–234.
25. Harder, E.; Damm, W.; Maple, J.; Wu, C.; Reboul, M.; Xiang, J. Y.; Wang, L.; Lupyán, D.; Dahlgren, M. K.; Knight, J. L.; Kaus, J. W.; Cerutti, D. S.; Krilov, G.; Jorgensen, W. L.; Abel, R.; Friesner, R. A. *J Chem Theory Comput* **2016**, *12*, 281–296.
26. Friesner, R. A.; Murphy, R. B.; Repasky, M. P.; Frye, L. L.; Greenwood, J. R.; Halgren, T. A.; Sanschagrin, P. C.; Mainz, D. T. *J. Med. Chem.* **2006**, *49*, 6177–6196.
27. Friesner, R. A.; Banks, J. L.; Murphy, R. B.; Halgren, T. A.; Klicic, J. J.; Mainz, D. T.; Repasky, M. P.; Knoll, E. H.; Shelley, M.; Perry, J. K.; Shaw, D. E.; Francis, P.; Shenkin, P. S. *J. Med. Chem.* **2004**, *47*, 1739–1749.
28. Li, J.; Abel, R.; Zhu, K.; Cao, Y.; Zhao, S.; Friesner, R. A. *Proteins* **2011**, *79*, 2794–2812.
29. Kongsted, J.; Söderhjelm, P.; Ryde, U. *J. Comput. Aided Mol. Des.* **2009**, *23*, 395–409.
30. 1,2,4-Triazolidine-3-thiones as Narrow Spectrum Antibiotics against Multidrug-Resistant *Acinetobacter baumannii*. William M. Huggins, Bradly M. Minrovic, Brendan W. Corey, Anna C. Jacobs, Roberta J. Melander, Roger D. Sommer, Daniel V. Zurawski, and Christian Melander, *ACS Medicinal Chemistry Letters* 2017 8 (1), 27-31